UNIVERSITY OF CALIFORNIA SAN DIEGO

Using experimental evolution to elucidate the genomic drivers of antimicrobial resistance in eukaryotic pathogens

A dissertation submitted in partial satisfaction of the requirements
for the degree Doctor of Philosophy

in

Biomedical Sciences

by

Madeline Rose Luth

Committee in charge:

Professor Elizabeth Winzeler, Chair
Professor Nathan Lewis
Professor Jill Mesirov
Professor Victor Nizet
Professor Larissa Podust

2022

The Dissertation of Madeline Rose Luth is approved, and it is acceptable in quality and form for publication on microfilm and electronically.

University of California San Diego

2022

TABLE OF CONTENTS

LIST OF SUPPLEMENTAL FILES

Chapter 2

Supplemental_Table_2-1_Luth.xlsx – Summary of all variants identified across *in vitro* and *in vivo* selections.

Supplemental_Table_2-2_Luth.xlsx – Copy number variation in the *in vitro* and *in vivo* selected samples.

Chapter 3

Supplemental_Table_3-1_Luth.xlsx – Summary of compounds used in selection.

Supplemental_Table_3-2_Luth.xlsx – Summary of resistant samples sequenced for the study..

Supplemental_Table_3-3_Luth.xlsx – Aggregate SNV and INDEL calls in resistant samples.

Supplemental_Table_3-4_Luth.xlsx – Aggregate CNV calls across the dataset.

Chapter 4

Supplemental_Table_4-1_Luth.xlsx – Mutation rate analysis for clones derived from the unselected 12B line.

Supplemental_Table_4-2_Luth.xlsx – Mutation rate analysis for clones derived from the unselected 5D line.

Supplemental_Table_4-3_Luth.xlsx – Mutational analysis of clones derived from the 100 uM ART selection from the B2 line.

Supplemental_Table_4-4_Luth.xlsx – Mutational analysis of clones derived from the 100 uM ART selection from the F4 line.

Chapter 5

Supplemental_Table_5-1_Luth.xlsx – Compound library description and enriched clusters.

Supplemental_Table_5-2_Luth.xlsx – IC50 values for each resistant clone and relative fold-shift compared to the affiliated parent clone.

Supplemental_Table_5-3_Luth.xlsx – Sequencing statistics for the parents and drug-resistant yeast clones generated for this study.

Supplemental_Table_5-4_Luth.xlsx – Aggregate list of the 1,405 high-quality mutations (1,286 SNVs and 119 INDELs) that arose over the course of compound selection in each of the 355 compound-resistant clones.

Supplemental_Table_5-5_Luth.xlsx – List of 24 Copy Number Variant (CNV) events observed in compound-resistant clones.

Supplemental_Table_5-6_Luth.xlsx – Annotations of the intergenic mutations identified in compound-resistant clones.

Supplemental_Table_5-7_Luth.xlsx – CRISPR/Cas9 confirmation IC50s.

Supplemental_Table_5-8_Luth.xlsx – RT-qPCR of YRR1 and associated genes in wild-type (GM) and mutant yeast strains conferring resistance.

Supplemental_Table_5-9_Luth.xlsx – Oligos used to knock in putative resistance-conferring mutations.

LIST OF FIGURES

Chapter 1

Chapter 2

Chapter 3

Chapter 4

Chapter 5

LIST OF TABLES

Chapter 1

Chapter 2

Chapter 3

Chapter 4

Chapter 5

ACKNOWLEDGEMENTS

I would first like to acknowledge my thesis advisor Elizabeth Winzeler, who has provided me with numerous opportunities for growth and enrichment over the course of my graduate studies. Thanks to her, I have been able to be involved in high-impact projects, engage in extracurricular career development, and represent the lab across multiple national- and international-level conferences and scientific venues.

I next would like to thank the members of my doctoral dissertation committee, who have each provided invaluable feedback on my research and professional goals. I am grateful to Larissa Podust and her team at the Center for Discovery and Innovation in Parasitic Diseases (CDIPD), who introduced me to the field of antiparasitic drug discovery and development as part of my first laboratory rotation as a graduate student. Victor Nizet is a champion of the infectious diseases field who has contributed immensely to my understanding of diverse microbes through coursework and program development at UCSD. Jill Mesirov has provided me with indispensable guidance in bioinformatics and genomic data analysis since she participated on the committee for my Minor Proposition Exam back in 2017. Lastly, Nathan Lewis has provided incredibly constructive feedback through intensive knowledge and expertise in systems biology and interpreting large omics datasets. I would like to thank each of them for giving me their time and energy as I progressed through my graduate work.

My scientific progress in the malaria field would absolutely not be possible without each of my extraordinary mentors and colleagues in the Malaria Drug Accelerator (MalDA) Consortium. I am eternally grateful for the support of Dyann Wirth, David Fidock, Daniel Goldberg, Marcus Lee, Nobutaka Kato, Francisco Javier Gamo-

Beto, Case McNamara, and all other MalDA group leaders. I am especially fortunate to have worked closely with Eva Istvan, Rebecca Mandt, Amanda Lukens, Manu Vanaerschot, James Murithi, John Okombo, Krittikorn Kumpornsin, and Robert Summers, all of whom have given me tremendous personal and scientific support through the challenges of working in malaria and parasitology. Funding for all MalDA work was provided by the Bill and Melinda Gates Foundation and facilitated by our program officer Gang Liu.

I would like to acknowledge funding support provided by a Ruth L. Kirschstein Institutional National Research Award from the National Institute for General Medical Sciences (T32 GM008666). This training grant was awarded by the Genetics Training Program at UCSD under the guidance of program director Professor Bruce Hamilton. I am very grateful to have been able to participate in GTP journal club, coursework, and annual retreats and cannot thank Bruce enough for his enthusiastic dedication to GTP trainees and their development as scientists.

I am grateful for all Winzeler Lab members past and present. I want to especially thank Sabine Ottilie, who perfected the art of being a mentor, coworker, and friend; her tireless work and support of my personal and professional life cannot be understated. Jan Economy helped me navigate every issue under the sun as it pertained to UCSD bureaucracy and remains an integral part of making sure the lab operates smoothly day-to-day. Matthew Abraham, Karla Macias-Godinez, and Krypton Carolino supplied scientific and moral support as fellow graduate students. It has also been a tremendous pleasure working with and getting to know Nimisha Mittal, Tuo Yang, and Abigail Pfantsiel inside and outside of the lab. I am also thankful for Korina Eribez, Jaeson

Calla, Jenya Antonova-Kovich, Purva Gupta, Pamela Orjuela-Sanchez, Francisco Guerra, and Annie Cowell. Together, their support, guidance, and commiseration have made me a better scientist and person.

Certain individuals specifically made BRF2 5th Floor Bay A into a second home for me, and I will cherish the memories made here for the rest of my life. Colleen “Coco” Boyle was the best desk mate and work wife I could possibly ask for and remains one of my dearest friends and co-conspirators. Frances Rocamora, simply put, is a treasure to all of humankind and I would not have survived grad school without her. Gregory LaMonte’s warmth and sense of humor brought light to even the gloomiest of days. As an honorary member of Bay A, David Rios-Covian brought boundless laughter and moral support. I am so lucky to have met each one of them and cannot express my gratitude to them deeply enough.

The BRF2 5th Floor extended family has stood by me through thick and thin. Mario Manresa, Philipp Spahn, Kevin Okamoto, and Maria Lodela especially will always hold a special place in my heart as dear friends, coworkers, and travel partners. Amanda Wu, Paul Tan, and others also contributed to making the 5th floor one of the tightest knit research and social communities on campus. From borrowing lab instruments, to holding happy hours, foodie excursions, parties, and more, this group of people transformed the workplace into something truly special.

I would also like to thank my cohort in the UCSD Biomedical Sciences Graduate Program for their friendship and support over the last several years. The Class of 2016 is something else entirely and I am grateful to have been a part of this simultaneously raucous and incredibly talented group of grad students. Program staff Leanne

Nordeman, Pat Luetmer, and Chris Watson worked relentlessly to support us as cohort and made sure we had everything we needed to succeed at each stage.

Lastly, I would not be where I am today without the love and support of my family. My parents, Randy and Doris Luth, have worked tirelessly and at times thanklessly to support all of my hopes and dreams. At each step of the way, they have provided me with unconditional love, comfort, and guidance. I also would like to thank my brother Corey; future sister-in-law Rita; my grandparents Hannelore Peterie and John and Carolyn Luth; my aunts Theresa and Antje; and uncle Steve, who have all given me endless support, laughter, and encouragement throughout this process.

Chapter 1 includes a full reprint of the material as it appears in ACS Infectious Diseases, 2018. Madeline R. Luth, Purva Gupta, Sabine Ottilie, and Elizabeth A. Winzeler, “Using *in vitro* evolution and whole genome analysis to discover next generation targets for antimalarial drug discovery.” The dissertation author was a co-first author of this paper.

Chapter 2 is a partial, modified reprint of the material as it appears in Science Translational Medicine, 2019. Rebecca E. K. Mandt, Maria Jose Lafuente-Monasterio, Tomoyo Sakata-Kato, Madeline R. Luth, Delfina Segura, Alba Pablos-Tanarro, Sara Viera, Noemi Magan, Sabine Ottilie, Elizabeth A. Winzeler, Amanda K. Lukens, Francisco Javier Gamo, Dyann F. Wirth, “*In vitro* selection predicts malaria parasite resistance to dihydroorotate dehydrogenase inhibitors in a mouse infection model.” The dissertation author was a co-author of the publication and performed all sequencing and analysis, which is the focus of this dissertation.

Chapter 3 contains unpublished material co-authored with Elizabeth A. Winzeler. The dissertation author was the primary author of this chapter.

Chapter 4 is a partial, modified reprint of the material as it appears in Proceedings of the National Academy of Sciences, 2019. Alex Rosenberg, Madeline R. Luth, Elizabeth A. Winzeler, Michael Behnke, and L. David Sibley, "Evolution of resistance *in vitro* reveals mechanisms of artemisinin activity in *Toxoplasma gondii*". The dissertation author was second author on this paper and performed all sequencing analysis. Additional unpublished analyses of ART-resistant *Plasmodium falciparum* parasites are also included and were performed by the dissertation author.

Chapter 5, in full, is a reprint of the material as it appears in Communications Biology, 2022. Sabine Ottilie, Madeline R. Luth, Erich Hellemann, Gregory M. Goldgof, Eddy Vigil, Prianka Kumar, Andrea L. Cheung, Miranda Song, Karla P. Godinez-Macias, Krypton Carolino, Jennifer Yang, Gisel Lopez, Matthew Abraham, Maureen Tarsio, Emmanuelle LeBlanc, Luke Whitesell, Jake Schenken, Felicia Gunawan, Reysha Patel, Joshua Smith, Melissa S. Love, Roy M. Williams, Case W. McNamara, William H. Gerwick, Trey Ideker, Yo Suzuki, Dyann F. Wirth, Amanda K. Lukens, Patricia M. Kane, Leah E. Cowen, Jacob D. Durrant, and Elizabeth A. Winzeler, "Adaptive laboratory evolution in *S. cerevisiae* highlights role of transcription factors in fungal xenobiotic resistance." The dissertation author was a co-first author of this paper.

VITA

2016 Bachelor of Science, University of California Riverside

2016-2022 Research Assistant, University of California San Diego

2022 Doctor of Philosophy, University of California San Diego

PUBLICATIONS

Xie, S. C., Metcalfe, R. D., Dunn, E., Morton, C. J., Huang, S.-C., Puhalovich, T., Du, Y., Wittlin, S., Nie, S., **Luth, M. R.**, et al. Hijacking of tyrosine tRNA synthetase as a new whole-of-life-cycle antimalarial strategy. Science, 376(6597), 1074–1079.

Ottilie, S., **Luth, M. R.**, et al. (2022). Adaptive laboratory evolution in *S. cerevisiae* highlights role of transcription factors in fungal xenobiotic resistance. Communications Biology, 5(1), 128.

Ellis, K. M., Lucantoni, L., Chavchich, M., Abraham, M., De Paoli, A., **Luth, M. R.**, et al. (2021). The novel bis-1,2,4-triazine mips-0004373 demonstrates rapid and potent activity against all blood stages of the malaria parasite. Antimicrobial Agents and Chemotherapy, 65(11).

Summers, R. L., Pasaje, C. F. A., Pisco, J. P., Striepen, J., **Luth, M. R.**, et al. (2021). Chemogenomics identifies acetyl-coenzyme A synthetase as a target for malaria treatment and prevention. Cell Chemical Biology, S2451945621003500.

Rocamora, F., Gupta, P., Istvan, E. S., **Luth, M. R.**, et al. (2021). Pfmfr3: A multidrug-resistant modulator in *Plasmodium falciparum*. ACS Infectious Diseases, 7(4), 811–825.

Luth, M. R., & Winzeler, E. A. (2020). Snapshot: Antimalarial drugs. Cell, 183(2), 554-554.e1.

LaMonte, G. M., Rocamora, F., Marapana, D. S., Gnädig, N. F., Ottilie, S., **Luth, M. R.**, et al. (2020). Pan-active imidazolopiperazine antimalarials target the *Plasmodium falciparum* intracellular secretory pathway. Nature Communications, 11(1), 1780.

Abraham, M., Gagaring, K., Martino, M. L., Vanaerschot, M., Plouffe, D. M., Calla, J., Godinez-Macias, K. P., Du, A. Y., Wree, M., Antonova-Koch, Y., Eribez, K., **Luth, M. R.**, et al. (2020). Probing the open global health chemical diversity library for multistage-active starting points for next-generation antimalarials. ACS Infectious Diseases, 6(4), 613–628.

Rosenberg, A., **Luth, M. R.**, Winzeler, E. A., Behnke, M., & Sibley, L. D. (2019). Evolution of resistance in vitro reveals mechanisms of artemisinin activity in *Toxoplasma gondii*. Proceedings of the National Academy of Sciences, 116(52), 26881–26891.

Mandt, R. E. K., Lafuente-Monasterio, M. J., Sakata-Kato, T., **Luth, M. R.**, et al. (2019). In vitro selection predicts malaria parasite resistance to dihydroorotate dehydrogenase inhibitors in a mouse infection model. Science Translational Medicine, 11(521).

Stokes, B. H., Yoo, E., Murithi, J. M., **Luth, M. R.**, et al. (2019). Covalent *Plasmodium falciparum*-selective proteasome inhibitors exhibit a low propensity for generating resistance in vitro and synergize with multiple antimalarial agents. PLOS Pathogens, 15(6).

Xie, S. C., Gillett, D. L., Spillman, N. J., Tsu, C., **Luth, M. R.**, et al. (2018). Target validation and identification of novel boronate inhibitors of the *Plasmodium falciparu*m proteasome. Journal of Medicinal Chemistry, 61(22).

Antonova-Koch, Y., Meister, S., Abraham, M., **Luth, M. R.**, et al. (2018). Open-source discovery of chemical leads for next-generation chemoprotective antimalarials. Science, 362(6419).

Luth, M. R., Gupta, P., Ottilie, S., & Winzeler, E. A. (2018). Using *in vitro* evolution and whole genome analysis to discover next generation targets for antimalarial drug discovery. ACS Infectious Diseases, 4(3), 301–314.

Kinsinger, N. M., Mayton, H. M., **Luth, M. R.**, & Walker, S. L. (2017). Efficacy of post-harvest rinsing and bleach disinfection of *E. coli O157:H7* on spinach leaf surfaces. Food Microbiology, 62, 212–220.

Debnath, A., Calvet, C. M., Jennings, G., Zhou, W., Aksenov, A., **Luth, M. R.**, Abagyan, R., Nes, W. D., McKerrow, J. H., & Podust, L. M. (2017). CYP51 is an essential drug target for the treatment of primary amoebic meningoencephalitis (PAM). PLOS Neglected Tropical Diseases, 11(12).

Hale, L., **Luth, M.**, & Crowley, D. (2015). Biochar characteristics relate to its utility as an alternative soil inoculum carrier to peat and vermiculite. Soil Biology and Biochemistry, 81, 228–235.

Hale, L., **Luth, M.**, Kenney, R., & Crowley, D. (2014). Evaluation of pinewood biochar as a carrier of bacterial strain *Enterobacter cloacae* UW5 for soil inoculation. Applied Soil Ecology, 84, 192–199.

FIELDS OF STUDY

Major Field: Biomedical Sciences (Genetics)

Professor Elizabeth Winzeler

ABSTRACT OF THE DISSERTATION

Using experimental evolution to define the genomic determinants of drug resistance in eukaryotic pathogens

by

Madeline Rose Luth

Doctor of Philosophy in Biomedical Sciences

University of California San Diego, 2022

Professor Elizabeth Winzeler, Chair

The emergence of drug resistance in an ever-present threat to the successful treatment of infectious diseases. Microorganisms have an almost unparalleled ability

to divide rapidly to achieve large population numbers, introducing a potentially large number of random mutations into the population over time which can confer a distinct advantage (or disadvantage) depending on the environment and selection conditions. *In vitro* evolution combined with whole genome analysis is a powerful forward genetics tool used to study the development of antimicrobial resistance within a tightly controlled experimental environment (i.e. a tissue culture flask). This dissertation explores the use of this method to begin to collectively understand the genomic drivers of drug resistance across multiple eukaryotic microbes: the human malaria parasite *Plasmodium falciparum*, the toxoplasmosis-causing parasite *Toxoplasma gondii*, and the fungus and "model organism" *Saccharomyces cerevisiae*. We find that multidrug resistance mechanisms are major drivers of resistance for both *P. falciparum* and *S. cerevisiae*.

In Chapter 2, *in vitro* evolution of resistance to the antimalarial clinical candidate DSM265 is shown to mirror the results of *in vivo* resistance development both in a murine model and in Phase 2a clinical trial data, thus supporting its value as a method toward understanding the mechanics of *P. falciparum* resistance development. Then in Chapter 3, the method is expanded to 113 different compound selections either performed within the Malaria Drug Accelerator Consortium or by other groups which have made their data publicly available. Here, we show that half of all compounds taken into selection yield parasites with mutations in multidrug resistance mechanisms.

In Chapter 4, we explore how selections performed in *T. gondii* with the antimalarial drug Artemisinin differ from those performed in the malaria parasite. Both organisms are Apicomplexan parasites but parasitize their hosts in distinctly different

ways. While the selections do not yield any homologous resistance genes, both yield mutations that are believed to be involved in each respective parasite's stress response. Moreover, we find that a key shared feature is the multigenic nature of resistance to Artemisinin, which is likely tied to it mode of action.

Finally, in Chapter 5, experimental evolution is applied at scale in *S. cerevisiae* to model resistance development in fungi. Selections with 80 different compounds yielded 355 compound-resistant clones and once again we identify a multidrug resistance mechanism that is strongly overrepresented across the dataset. The two Zn_2C_6 transcription factors *YRR1* and *YRM1*, which are known to induce the pleiotropic drug response, were mutated 100 different times and conferred resistance to 19 structurally distinct compounds.

Chapter 1

Introduction: Using *in vitro* evolution and whole genome analysis to advance drug discovery and development in malaria

1.1 Target discovery: On the road to malaria eradication

Although many new anti-infectives have been discovered and developed solely using phenotypic cellular screening and assay optimization, most researchers recognize that structure-guided drug design is more practical and less costly. In addition, a greater chemical space can be interrogated with structure-guided drug design. The practicality of structure-guided drug design has launched a search for the targets of compounds discovered in phenotypic screens. One method that has been used extensively in malaria parasites for target discovery and chemical validation is *in vitro* evolution and whole genome analysis (IVIEWGA). Here, small molecules from phenotypic screens with demonstrated anti-parasitic activity are used in genome-based target discovery methods. Here we discuss the newest, most promising drug-able targets discovered or further validated by evolution-based methods, as well as some exceptions.

Malaria is the most prevalent parasitic disease in man. The World Health Organization (WHO) estimated 216 million cases and 445,000 deaths in 2016 globally, out of which 91% were in Africa alone and 99% were due to *Plasmodium falciparum* infections (WHO, World Malaria Report 2017). Most deaths occur in children under the age of five. Malaria in humans is caused by 6 different species of *Plasmodium*, where *P. falciparum* causes the deadliest form of infection and *P. vivax* is the most widespread (WHO, World Malaria Report 2017). *Plasmodium* infection of the human host begins with the transmission of the parasite through the bite of an infected mosquito (**Figure 1.1**). Parasites immediately travel through the bloodstream, invade hepatocytes, and replicate asexually, resulting in thousands of merozoites. In *P. vivax* and *P. ovale*, sporozoites might form “hypnozoites”, a dormant form, which can be activated weeks to months later

and cause relapse of infection. The exo-erythrocytic cycle in liver transcends into the intra-erythrocytic stage with asexual replication in red blood cells. The lysis of red blood cells to release more parasites causes the symptomatic disease and can be fatal[1]. Some intra-erythrocytic stage parasites can develop into “gametocytes”, the sexual stage, that can subsequently be transmitted into the mosquito to perpetuate the infection cycle.

Artemisinin combination therapy (ACT) is the first line of treatment for uncomplicated falciparum malaria. Due to their short half-lives, artemisinin (ART) derivatives are administered with partner drugs such as amodiaquine, piperaquine, lumefantrine, mefloquine, sulphadoxine-pyrimethamine, and pyronaridine which have separate mechanisms of action and potentially different half-lives. The emergence of parasites showing resistance to ACTs in the Greater Mekong region could bring about a reversal in malaria control and undermine the feasibility of elimination, as has been reviewed previously[2,3]. For this reason, the consensus in the medical and scientific community is that there is a great need for the development of new classes of antimalarial medicines if malaria elimination is to be achieved[4]. The ideal drug would target multiple stages of the parasite's life cycle, block or prevent transmission, or act against *Plasmodium vivax* liver hypnozoites. Because there are very few known drug targets, a major focus of the last decade has been the search for novel, chemically validated targets that can be starting points for development of next-generation antimalarials.

A method that has been used with great success to find new drug targets is *In Vitro* Evolution and Whole Genome Analysis (IVIEWGA). In this method (**Figure 1.2**), parasites are exposed to sublethal concentrations of compounds that have shown antiparasitic activity. These compounds typically are identified in phenotypic screens and

some are active throughout the parasite lifecycle. To identify the genetic basis of their resistance, the genomes of the resistant clones are analyzed using tiling microarrays or more typically using whole genome sequencing and are compared to the sensitive parent clone. In many cases, newly emerged genomic lesions are found in genes that are predicted to encode the targets. Modeling, crystallography, and further functional studies can confirm that the gene product is the actual target and resistance is not conferred nonspecifically by a multi-drug resistance gene (e.g. a transporter that is frequently observed). The advantage of targets discovered through this method is that they are, by default, chemically validated and drug-able. This review discusses some of the many new drug targets that have been discovered or reconfirmed using this method (**Table 1.1**).

1.2 P-Type Cation ATPase

One of the first novel targets that was discovered with IVIEWGA is PfATP4, a P-type cation ATPase. It was first identified as the target of the spiroindolone compound, KAE609 (also called NITD609), which is now commercially called Cipargamin[5]. KAE609 is highly active against both *P. falciparum* and *P. vivax* field isolates and culture-adapted isolates with single-digit nanomolar IC50s[6]. It is also active against the gametocyte and oocyst development in mosquitoes which would enable this compound to block transmission. Parasites generated from *in vitro* resistance evolution using KAE609 and analyzed with microarrays display both CNVs and SNVs in various positions of PfATP4 (**Table 1.2**). These mutations were later proven to confer resistance in *P. falciparum* and result in at least a 10-fold increase in IC50 values[6,7]. KAE609 has progressed through

Phase I and IIa clinical trials[5] and it remains to be seen how far it will advance in drug development.

Although there are concerns that PfATP4 could be involved in multi-drug resistance[8], it is generally accepted to be a good drug target. All cells must maintain low cytosolic Na+ concentration to survive, and PfATP4 mediates active extrusion of Na+ from the parasite to maintain low-[Na+]/high-[K+] in the host cell cytosol upon infection[9]. PfATP4 is found in the *Plasmodium* plasma membrane and the gene is expressed in all asexual blood stages of *Plasmodium*[7]. PfATP4 has been suggested to be the mechanism of action for multiple potential antimalarial candidates which have been shown to disturb Na+ regulation and homeostasis in the parasite[7,10].

Shortly after the discovery that PfATP4 was the target of the spiroindolones, evolution studies showed that it was involved in resistance to several other compound classes, including the aminopyrazoles, pyrazoleamides, and dihydroisoquinolones, all compounds identified by phenotypic screening[8,11,12]. Like spiroindolones, aminopyrazoles target both the asexual blood stages of the parasite and the oocyst formation in mosquitoes, thus preventing transmission of the parasite. Mutations in PfATP4 acquired after treatment with the aminopyrazole GNF-Pf-4492 also confer resistance to spiroindolones. PfATP4 mutations found in resistant parasite lines treated with either small molecules are present in the region of the predicted transmembrane (TM) domain, suggesting they might exhibit a shared structure-function relationship. An additional point mutation in the putative ADP/ATP transporter protein (PF3D7_1037300) localized to the inner mitochondrial membrane may be a compensatory mutation[5].

Like all other PfATP4 inhibitors, pyrazoleamides kill both *P. falciparum* asexual laboratory isolates and *P. falciparum* and *P. vivax* field isolates, at very low nanomolar IC50 values. In addition, the lead compound PA21A092 inhibits gametocyte development similar to KAE609[12]. PA21A092 enables rapid increase in cytosolic Na^+ and since it does not affect resting cytosolic Ca^{2+} levels, the parasites swell due to the osmotic uptake of water[12].

The dihydroisoquinolone SJ733 also originated with a cellular screen. Selections with SJ733 resulted in resistant parasite lines that displayed an IC50 increase of 2 to 750-fold, and WGS detected mutations in PfATP4 not seen previously in KAE609-resistant lines. Despite the different location of the mutations, SJ733-resistant lines are cross-resistant to spiroindolones[11]. SJ733 causes an increase in the parasite's cytosolic Na+ level and concurrent alkalinization of the cytosol which seems in line with the loss of PfATP4 activity. The overrepresentation of PfATP4 inhibitors in many phenotypic screens may be because PfATP4 is a high-value target whose inhibition results in rapid death, even at higher inhibitor concentrations. Despite its significance, no crystal structure of PfATP4 or biochemical assay is available, and thus there are still many open questions about how these compounds act and whether *pfatp4* may also function as a resistance gene.

1.3 Aminoacyl-tRNA Synthetases

A well-known class of targets in other species, which has become increasing relevant due to multiple discoveries using IVIEWGA in *Plasmodium*, is the tRNA synthetase family. During protein synthesis, aminoacyl-tRNA synthetases (aaRS)

accurately pair the cognate tRNAs with their corresponding amino acids hence defining the genetic code[13]. Translation fidelity is attained by two events: correct pairing of an amino acid with the matching tRNA and the accurate selection of the charged aminoacyl-tRNAs on the ribosome. Functional aspects of aaRSs and their role in keeping translational errors in check have been reviewed previously[14,15].

Apicomplexan parasites have three genomes viz. nuclear, apicoplast, and mitochondria that require charged tRNAs for translation. To synthesize its proteome, the malaria parasite utilizes a combined array of 36 aaRSs (instead of the theoretical 60 aaRSs for the three compartments)[16]. Of these, 16 aaRSs are present exclusively for cytoplasm and 15 nuclear-encoded aaRSs are present exclusively for the apicoplast. The mitochondria is speculated to import charged tRNAs from the cytoplasmic tRNA pool and only harbors an enzymatically active mitochondrial phenylalanyl-tRNA synthetase, a feature unique to *Plasmodium*[17]. There are multiple sites that can provide binding sites for small molecule inhibitors, including the editing site, aminoacylation pocket, and the tRNA binding region[13,18,19].

1.3.1 Isoleucyl-tRNA Synthetase

The first hints that aaRS's might be important drug targets for antimalarials came from IVIEWGA studies with two known inhibitors of isoleucyl-tRNA synthetase, thiaisoleucine and mupirocin[18]. *P. falciparum* contains two isoleucyl-tRNA synthetases, one in the cytoplasm and the other in the apicoplast[20]. Mupirocin, a natural product that is clinically used as an antibiotic, was found to inhibit the *P. falciparum* apicoplastic isoleucyl-tRNA synthetase, and the isoleucine analog, thiaisoleucine, was shown to target

cytoplasmic isoleucyl-tRNA synthetase. Both compounds kill asexual blood stage parasites at mid-nanomolar and low-micromolar concentrations, respectively[18].

1.3.2 Lysyl-tRNA Synthetase

Lysyl-tRNA synthetase was discovered as another potential important target using array-based IVIEWGA. The *P. falciparum* cytosolic lysyl-tRNA synthetase is selectively and specifically inhibited by a fungal secondary metabolite, cladosporin, which has potent, nanomolar activity against both blood and liver stages of the parasite[21]. Cladosporin has >100-fold more potency against the parasite's lysyl-tRNA synthetase as compared to the human ortholog. This was corroborated by other studies that observed the dissociation constant for *P. falciparum* lysyl-tRNA synthetase with cladosporin to be ~14nM, while the human lysyl-tRNA synthetase was ~4μM[22,23]. Another study designed and tested inhibitors against apicoplast lysyl-tRNA synthetase and confirmed that the *Plasmodium* apicoplastic lysyl-tRNA synthetase can be specifically inhibited with compounds that show antimalarial activity in the micromolar range[24].

1.3.3 Prolyl-tRNA synthetase

Cytoplasmic glutamyl-prolyl tRNA synthetase activity in mammalian cells is inhibited by febrifugine, a compound derived from a Chinese herb, and its synthetic derivative halofuginone[25]. However, these inhibitors could not be developed clinically because of their high toxicity. Herman and co-workers developed an analog called halofuginol that is active against both liver and asexual blood stages of the rodent malaria parasite *P. berghei* and is much better tolerated[26]. IVIEWGA was used with halofuginone

to identify prolyl-tRNA synthetase as the target[26]. The group also showed that febrifugine analogs induce eukaryotic initiation factor 2α phosphorylation in both *Plasmodium* and transgenic yeast that express cytoplasmic prolyl-tRNA synthetase, making them important chemical tools to study the amino acid starvation pathway in both species. The importance of prolyl-tRNA synthetases as targets in multiple human eukaryotic pathogens (*Plasmodium*, *Leishmania*, *Toxoplasma*, *Cryptosporidium*, and *Eimeria*) is supported by the development of quinazolinone-inhibitors using structure-guided drug design[27].

1.3.4 Phenylalanyl-tRNA synthetase

Three phenylalanyl-tRNA synthetases are present in the malaria parasite, each essential to the parasite's translational machinery in each of its compartments[16,17]. The three phenylalanyl-tRNA synthetases show functional and structural differences, viz. the cytoplasmic enzyme is an $(\alpha\beta)_2$ hetrotetramer while its apicoplast and mitochondrial counterparts are monomeric. Kato *et al*. screened ~100,000 compounds from the diversity-oriented synthesis (DOS) library against *P. falciparum* and identified a series of bicyclic azetidines, which were then shown to inhibit the phenylalanyl-tRNA synthetase following *in vitro* evolution. These compounds showed activity at a single low-concentration dose in mice against all life cycle stages of the parasite[19]. This seems to be a very promising new drug target due to its presence in all three translational compartments in the parasite.

1.3.5 Dual tRNA Synthetase Targets

Although *in vitro* evolution has been often used to assign specific inhibitors to tRNA synthetase targets in an unbiased manner, data from other species can create testable hypotheses about which tRNA synthetase might be inhibited. Biochemical evidence from *E. coli* has indicated that indolmycin inhibits tryptophanyl-tRNA synthetase[28], leading to the testable hypothesis that it behaves similarly in *P. falciparum*[29]. Likewise, borrelidin is a bacterial secondary metabolite with known antimalarial properties[30]. Characterization of borrelidin-resistant mutants in *Escherichia coli* showed that tolerance resulted from ThrRS (encoding Threonyl-tRNA synthetase) overexpression[31]. Threonyl-tRNA (as with alanyl-, glycyl-, cysteinyl-) synthetase is a very interesting potential target due to its dual localization in both cytosol and apicoplast. Targeting this enzyme would theoretically stall translation in all three compartments[20,32,33]. On the other hand, borrelidin also inhibits human threonyl-tRNA synthetase, making it highly toxic. To overcome this, a library of borrelidin analogs was synthesized and tested for toxicity and antimalarial activity. Some analogs lost their toxicity to human cells and still maintained antiparasitic activity both *in vitro* and *in vivo* when tested in mice against *P. yoelii*[34]. Although several of these analogs inhibited *P. falciparum* threonyl-tRNA synthetase in aminoacylation assays, it is theoretically feasible that these compounds exert their antiparasitic activity through interaction with a different target. The use of *in vitro* evolution studies can provide unbiased confirmation of on-target activity for threonyl and tryptophanyl tRNA synthetase.

1.4 Translation Elongation Factor 2

Previous studies have implicated translation elongation factor 2 (eEF2) as an important drug target in *Saccharomyces cerevisiae* for the antifungal compound

Sordarin[35,36]. Eukaryotic protein synthesis requires several elongation factors and eEF2 is responsible for the translocation of the ribosome along the mRNA. Yeast studies have demonstrated that selective inhibitors for eEF2 can be synthesized that would not inhibit protein synthesis in human cells[36,37].

IVIEWGA was used to show that *P. falciparum* eEF2 is inhibited by compound DDD107498. This compound has high potency, and like the tRNA synthetase inhibitors, antimalarial activity against multiple stages of the parasite's life cycle[38]. In a recent study, DDD107498 was confirmed to have transmission-blocking activity in experimental mosquito models using parasite densities observed in natural infections, supporting the decision to move this compound into early-stage clinical trials[39]. The identification of inhibitors for tRNA synthetases and translation elongation factors clearly demonstrate that targeting protein synthesis in *Plasmodium* is a very effective way for attaining multistage antiparasitic activity.

1.5 Dihydroorate Dehydrogenase

DHODH was already known to be a promising target for the development of antimalarial chemotherapy but has been rediscovered using evolution-based methods. Dihydroorate dehydrogenase (DHODH) is an enzyme localized to the mitochondrial electron transport chain (mETC), which provides oxidized ubiquinone as an electron acceptor for DHODH to synthesize pyrimidines *de novo* [40,41]. The parasite cannot salvage pyrimidines from its host, so the activity of the mETC is essential[42]. DHODH can be considered a good potential drug target with low toxicity due to the differences in the

active site across species. Selective inhibitor binding with triazolopyrimidines in *Plasmodium* was first shown by Phillips and Rathod[42].

A later triazolopyrimidine derivative, DSM265 has now advanced to phase-II clinical trials and is active against both liver and asexual blood stages of the parasite[43]. It has promising efficacy with single-dose regimens in human trials[44]. A secondary derivative, DSM421, has a similar selectivity and potent antimalarial activity[45]. In addition, 5-benzimidazolyl-theophene-2-carboxamides[46] and 7-arylaminopyrazolo [1,5-α] pyrimidines[47] have also been shown to inhibit DHODH. *In vitro* evolution with DSM1, a scaffold related to DSM265, has shown that *P. falciparum* acquires copy number variants that encompass the DHODH loci, providing further *in vivo* validation of the target[48].

Growth inhibition phenotypic screening identified many compounds with multistage activity against *Plasmodium* using diversity-oriented synthesis[19]. BRD7539, an azetidine-2-carbonitrile, has been shown to inhibit DHODH in *P. falciparum* selectively over human DHODH and is potent against the parasite's asexual blood and liver stages. An optimized compound, BRD9185, has *in vitro* activity against blood and liver stage parasites and can clear infection in mouse models in just three doses[49]. This class of compounds is another promising group of potential new antimalarials that target DHODH.

Ross and coworkers showed that resistance to PfDHODH inhibitors is primarily due to mutations and amplifications of the target gene DHODH. Several point mutations were found along with gene amplification that contributed to resistance. They also showed that the mutant parasites were sensitive to other PfDHODH inhibitors (Genz-669178, Genz-666136, and DSM74) which suggests a novel combination therapy approach to prevent resistance[50].

1.6 Cytochrome bc1 Complex

The cytochrome bc1 complex (ubiquinol: cytochrome c oxidoreductase; complex III) is another target localized in the mETC previously known to be inhibited by drugs used in the treatment of malaria and toxoplasmosis. The dimeric cytochrome bc1 protein is comprised of three catalytic subunits: cytochrome b, cytochrome c1, and the Rieske iron-sulphur protein. The cytochrome bc1 complex catalyzes the transfer of electrons from ubiquinol to cytochrome c, and in *P. falciparum*, plays a very important role in pyrimidine biosynthesis by providing oxidized ubiquinone to DHODH[40]. Cytochrome bc1 is the target of atovaquone (which is combined with proguanil in the antimalarial drug, Malarone), a hydroxynapthoquinone which is a competitive inhibitor of the Q_o site.

The importance of cytochrome bc1 as an antimalarial target was first reconfirmed using IVIEWGA and decoquinate, a compound with low nanomolar activity against *P. yoelii* liver stage and *P. falciparum* blood stages[51]. Analysis of decoquinate-resistant lines revealed two new cytochrome bc1 mutations, A122T and Y126C, were present in the evolved lines and that these mutations mapped to the Q_o binding pocket of cytochrome bc1[51]. Although both atovaquone and decoquinate interact in the ubiquinol binding site of the cytochrome bc1 complex, each compound adopts a different mode of binding as has been shown by molecular docking studies and identification of different mutations in the respective resistant lines[52]. There is very limited cross-resistance with decoquinate in atovaquone resistant lines. At about the same time, a G131S mutation in the Q_o quinol binding site in resistant evolved lines was detected after selection with tetracyclic

benzothiazepines, a compound class discovered in a phenotypic screen. In this case, however, only the cytochrome bc1-encoding gene was amplified and sequenced[53].

Not much is known about the Qi binding site of cytochrome bc1 with respect to the interaction of its inhibitors. Recent studies have suggested that antimalarial compounds like 1-hydroxy-2-dodecyl-4(1H)quinolone bind to this site and are even effective against atovaquone-resistant strains with known Q_o mutations[54]. X-ray crystallography studies later provided evidence that 4(1H)-pyridone compounds GW844520 and GSK932121 bind to the Qi site of cytochrome bc1 complex and overcome atovaquone resistance[55]. IVIEWGA also established that the quinolone reduction site (Qi site) of cytochrome bc1 is a drug-able target using an antimalarial probe from the DOS library that lacks cross-resistance with Q_o site inhibitors like atovaquone[56]. The presence of two different active sites in the same enzyme indicates that cytochrome bc1 is a very promising drug target. Furthermore, the absence of cross-resistance between inhibitors targeting these two sites can be harnessed for development of effective combination therapies.

1.7 Thymidylate synthase portion of Bifunctional DHFR-TS

Dihydrofolate reductase-thymidylate synthase (DHFR-TS) is a very well-established drug target in *P. falciparum* for antifolates such as pyrimethamine and cycloguanil. This bifunctional enzyme is essential in the production of folates and thymidylate, which are crucial for DNA synthesis[57]. Although many antimalarials inhibit the DHFR portion of this bifunctional enzyme, a recent study evolved resistant parasites against the benzoquinazolinone MMV027634 and identified 3 non-synonymous mutations in the TS portion. A previously published crystal structure allowed the mapping

of these novel mutations to the active TS binding site of the protein, revealing that each mutation occurs on the fringe of the 2'-deoxyuridylic acid (dUMP) binding site[58].

Understanding the role of the junctional region of DHFR-TS could prove useful in antimalarial drug development, since it has been shown that a critical length of this junctional region (at least 44 amino acids) is essential for the *P. falciparum* TS domain to be catalytically active[59]. Exploiting the junctional region of this multi-faced enzyme would simultaneously inhibit other portions of DHFR-TS enzyme to overcome drug resistance.

1.8 Phosphatidylinositol 4-kinase

Another target discovered using IVIEWGA is phosphatidylinositol 4-kinase (PI4K). This important new antimalarial drug target operates in all stages of the *Plasmodium* life cycle. PI4K is an essential cellular regulatory molecule, conserved in all eukaryotes that phosphorylate lipids (phosphatidylinositol to PI4-phosphate) to regulate intracellular signaling and trafficking[60]. In *Plasmodium*, PI4-P recruits lipid-binding effector proteins that are driven by Rab11A for the late-stage membrane ingression during merozoite biogenesis[61].

PI4K was first discovered as the target of imidazopyrazines, a new class of antimalarial molecule that shows potency against blood-stage field isolates of *P. falciparum* and *P. vivax*. Imidazopyrazines such as KDU691 demonstrate therapeutic, preventive, and transmission-blocking activity in the malaria parasite by altering PI4-phosphate levels and membrane trafficking[61]. Selections with analogs of KDU691 (KAI407, KAI715, and BQR695) yielded both CNVs and SNVs in PI4K, confirming it as the target of this compound class[58].

Subsequent phenotypic screens have identified other PI4K inhibitors. MMV390048, a 2-aminopyridine, also inhibits the PI4K enzyme, although this was discovered using affinity chromatography. Strains resistant to other antimalarials are sensitive to MMV390048 and it has activity against all stages of the parasite life cycle except hypnozoites[62]. Another compound, BRD73842 has activity in all stages of the parasite life cycle and was discovered in the DOS library discussed above[19]. It is notable that all three are structurally quite different from one another (**Figure 1.3**).

1.9 Cleavage and polyadenylation specificity factor (CPSF) subunit 3

CPSF is a multi-protein complex present in all eukaryotic cells that plays an important role in processing pre-mRNA to mRNA by cleavage and polyadenylation at the 3' end of pre-mRNA[63]. CPSF was discovered to be a promising antimalarial drug target when point mutations were found in *P. falciparum* lines resistant to the small molecule AN3661, a benzoxaborole. Homology modeling studies showed the mutations were located in the active site where AN3661 binds to the protein. This compound was found to be highly potent against multiple stages of the parasite's life cycle *in vitro*, indicating further efforts should be made to design inhibitors that target CPSF[63].

1.10 Isoprenoid Pathway

The isoprenoid biosynthesis pathway is essential in *Plasmodium* and occurs via the methylerythritol phosphate (MEP) (methyl-D-erythritol-4-phosphate) pathway. Isoprenoids are essential for protein prenylation and the synthesis of ubiquinone, dolichols, carotenoid, and vitamin E; tRNA prenylation has also been shown to be

dependent on the isoprenoid pathway, making this pathway an attractive target for the development of new antimalarial therapies[64,65]. The first successful application of the IVIEWGA method to identify an antimalarial target attributed acquired fosmidomycin resistance to copy number variation in the *pfdxr* gene, which is involved in the isoprenoid biosynthesis pathway[66]. More recently, IVIEWGA using small molecules from the MMV Malaria Box, a library of 400 diverse drug- and probe-like molecules[67], has identified multiple targets of this pathway, which will be discussed below.

1.10.1 2-C Methyl-D- Erythritol 4-Phosphate Cytidylyltransferase

PfIspD (2-C methyl-D- erythritol 4-phosphate cytidylyltransferase), is a key enzyme in the MEP isoprenoid biosynthesis pathway and was identified as the target of MMV008138 from the MMV Malaria Box. *In vitro* selections with MMV008138 followed by whole-genome sequencing of drug-resistant parasites identified E688Q and L244I mutations to confer resistance[68]. The MEP pathway is not functionally conserved in humans, but an orthologous enzyme is expressed. The human ISPD shows only very weak sequence similarity to PfIspD, so antimalarials developed for this target should display low toxicity.

1.10.2 Bifunctional Farnesyl/Geranylgeranyl Diphosphate Synthase

IVIEWGA using MMV019313 from the MMV Malaria Box[67] identified a SNV, S228T, in the bifunctional farnesyl and geranylgeranyl diphosphate synthase (PfFPPS/GGPPS) that conferred resistance[69]. PfFPPS/GGPPS synthesizes C15 and C20 prenyl chains for multiple downstream enzymes in the isoprenoid biosynthesis

pathway. Bisphosphonates used for the treatment of osteoporosis also target PfFPPS/GGPPS and were shown previously to clear *Plasmodium* parasites in a mouse model, validating this enzyme as an antimalarial drug target. MMV019313 represents the first non-bisphosphonate inhibitor of PfFPPS/GGPPS and demonstrates superior physicochemical properties. It is highly selective for the *Plasmodium* FPPS/GGPPS and showed no activity against human FPPS or GGPPS.

Notably, Gisselberg *et al*. had to employ chemical mutagenesis with the alkylating agent ethyl methanesulfonate (EMS) in their selections to facilitate resistance evolution after multiple unsuccessful attempts to identify resistant strains using a standard protocol[69]. This represents a useful alternative strategy for resistance evolution when traditional IVIEWGA methods fail.

1.11 Farnesyltransferase

An important post-translational event in eukaryotic organisms is the prenylation of proteins, which allows for protein-protein interactions and binding of intracellular proteins to membranes. One key process is the farnesylation of proteins, driven by farnesyltransferase. This enzyme catalyzes the transfer of the farnesyl group, a 15-carbon isoprenoid lipid unit, from farnesyl pyrophosphate to the C-terminus of proteins containing the CaaX motif[70]. Farnesyltransferase is an interesting known potential drug target in *P. falciparum* since the inhibition of this enzyme is fatal to the parasite[71,72]. Inhibitors of the protein have also been developed into anticancer therapeutics[73,74].

Previously, resistance evolution of the parasite with the farnesyltransferase inhibitor BMS-388891, a tetrahydroquinoline, showed mutations in the protein at the

peptide substrate binding domain. In selections with BMS-339941, another tetrahydroquinoline, a mutation was identified in the farnesyl pyrophosphate binding pocket[75].

In a very recent IVIEWGA study, two different mutations in amino acid 515 viz. A515V and A515T were found in the beta subunit of the farnesyltransferase in *P. falciparum* strains resistant to MMV019066, a pyrimidinedione from the MMV Malaria Box. Modeling studies revealed that the mutations distort the critical interaction site of the small molecule with the farnesylation active site, thereby conferring resistance[58].

1.12 Using IVIEWGA in other species to inform antimalarial drug development and target identification

IVIEWGA data from other species can also be used to confirm likely on-target activity or to suggest new targets. *In vitro* evolution with *Saccharomyces cerevisiae* has shown that cladosporin, mentioned above, also inhibits yeast lysyl-tRNA synthase, just as it inhibits *P. falciparum* lysyl-tRNA synthetase[21]. IVIEWGA using KAE609 showed that mutations in the orthologous yeast protein PMA1 confer resistance[76]. In addition, yeast selections have been used to confirm on-target activity of proteasome inhibitors.

The proteasome is a well-known drug target important in the treatment of both pathogenic infectious diseases[77] and cancer[78]. For example, the boronic acid inhibitor bortezomib has cytotoxic activity and is very effective in treating hematopoietic malignancies by targeting the β5 subunit[79,80]. On the basis of its success in cancer drug development, researchers suspected that proteasome inhibitors could also be antimalarials if problems with specificity could be overcome. A study using affinity probes

showed that when the β2 and β5 activities are inhibited in the *P. falciparum* proteasome, parasite growth is inhibited in all asexual blood stages even after short treatment[81]. Carfilzomib is an α', β'-epoxyketone inhibitor used to treat refractory or relapsed multiple myeloma that also kills *P. falciparum*, including artemisinin-resistant strains[81,82]. Later work identified WLL-vs (Trp-Leu-Leu-vinylsulfone) as a molecule that inhibits multiple subunits of the *Plasmodium* proteasome simultaneously while having lower activity against the human proteasome[83]. When tested in a *P. chabaudi* infection model, WLL-vs caused a drastic reduction in the parasite burden and was well-tolerated by host cells. Carmaphycin B is a natural product derived from cyanobacterium *Symploca spp.* that targets the β5 subunit of the proteasome but exerts a cytotoxic effect on human lung adenocarcinoma and a colon cancer cell line[83]. Analogs have been designed that display high antimalarial activity against both asexual blood stages and gametocytes, but also low human cytotoxicity[84].

Although proteasome inhibitors bind to the proteasome in *in vitro* assays, questions remain as to whether the proteasome is their primary target. Employing IVIEWGA in *S. cerevisiae* has shown that Carmaphycin B targets the β5 subunit as predicted, confirming affinity profiling data and the usefulness of IVIEWGA studies across species to identify the mechanism of action of small molecule compounds.

1.13 Protease inhibition

Although many important targets have been discovered or confirmed with IVIEWGA, several new targets have been identified using conventional reverse genetic approaches. The best example are the proteases. Malaria parasites utilize highly evolved

and specific proteolytic pathways to invade and replicate in host cells while simultaneously avoiding the host immune response. Proteases play both regulatory and effector roles in parasite egress and invasion of RBCs. Proteases have well-characterized active site structures and are considered good drug targets. Protease inhibitors are already used to treat various human diseases like cancer, cardiovascular disorders viz. hypertension and congestive heart failure, HIV, diabetes, and osteoporosis[85,86].

In malaria parasites, serine proteases are implicated in RBC deformability and cytoadhesion[87] as well as in egress and RBC/hepatocyte invasion[88,89]). Aspartyl proteases (plasmepsins I-V)[90], cysteine proteases (falcipains 2, 2' and 3; DPAP1)[90,91,92,93,94] and the metalloprotease falcilysin[95,96] all play an important role in hemoglobin degradation. Plasmepsin V is an essential aspartyl protease with a major role in the export of effector proteins to parasite-infected erythrocytes by cleaving proteins within the *Plasmodium* export element (PEXEL) in the parasite's endoplasmic reticulum[97,98]. Recent studies have shown that plasmepsin V might be an important drug target for both *P. falciparum* and *P. vivax*. Plasmepsin V is inhibited by WEHI-842, a compound designed to mimic the parasite PEXEL motif[98], and by WEHI-916, which blocks PEXEL cleavage and kills the parasite at the ring-trophozoite transition[99].

Plasmepsins IX and X are another class of aspartyl proteases that have remained unexplored until recently. Plasmepsin IX is functionally involved in erythrocyte invasion, targeting the biogenesis of the rhoptry secretory organelle. Plasmepsin X is paramount in both invasion and egress, and for the final processing step carried out by subtilisin-like serine protease (SUB1) in the exoneme secretory vesicles[100]. Treatment with inhibitors in the aminohydantoin class resulted in an accumulation of schizonts and loss of SUB1

and SERA5 (a cysteine protease) maturation. Because inhibitors of plasmepsin X impair egress events downstream, aspartyl protease is a very promising antimalarial target.

The membrane metalloprotease FtsH1 was recently discovered as the target of the antibiotic actinonin using resistance evolution in Toxoplasma gondii after attempts to generate resistance in P. falciparum failed[101]. Treatment of *P. falciparum* with actinonin resulted in apicoplast biogenesis defects, establishing it as a promising target for a couple of reasons. Because apicoplast biogenesis is essential in proliferative stages of the *Plasmodium* life cycle, inhibitors of FtsH1 may have multistage efficacy. Additionally, there may be a decreased risk of host–cell toxicity since the organelle is unique to apicomplexan parasites[102,103].

The attention that proteases have received leads to questions about why they have not been identified frequently using IVIEWGA. One possibility is that protease inhibitors lack specificity and/or there is genetic redundancy in the protease family. If a compound inhibits multiple proteases simultaneously, it is possible that specific mutations would not be identified.

1.14 Challenges and outlook for experimental evolution approach

The recent dramatic increase in novel drug-able pathways in *Plasmodium* parasites has been facilitated largely by the utilization of *in vitro* resistance evolution combined with mutation identification through a variety of genomic techniques. The increased efficiency and declining cost of WGS has only accelerated the rate of target discovery by this approach. Nonetheless, certain challenges remain in WGS analysis. The extreme A-T richness of the *P. falciparum* genome presents a unique problem for

standard bioinformatic analysis protocols, for example, especially within intergenic regions where PCR amplification bias can severely distort depth of coverage. Additionally, alignment confidences decrease across the highly variable *Plasmodium* genes involved in antigenic variation. Lack of complete functional annotation across the genome is another challenge for IVIEWGA studies because potentially interesting mutations may occur in uncharacterized genes. One example of this was the identification of mutations in the uncharacterized *P. falciparum* cyclic amine resistance locus (PfCARL) in selections with the clinical candidate KAF156[104]. As next-generation sequencing technology advances and methods of SNV and CNV detection become more sensitive, however, target discovery will become a more streamlined process. To date, the IVIEWGA method has been successfully applied to identify a number of novel antimalarial targets to expedite drug discovery. This review highlights core drug-able targets identified or further confirmed via IVIEWGA that should be given priority in the antimalarial drug development pipeline.

Genes that are identified using IVIEWGA are already chemically validated but must be further validated through structural docking studies and reverse genetics to prove their direct role in resistance. When a compound lacks strong on-target activity, mutation calls may be inconclusive, or resistance may be conferred by generalized resistance mechanisms rather than a mutation in the target itself. Additionally, background and compensatory mutations that play an indirect role in resistance acquisition must be filtered out from genes that are truly relevant and drug-able. While sequencing of resistant clones leads to more robust results, deep-coverage sequencing of bulk populations instead could make IVIEWGA more efficient. In a sample sequenced to 500X coverage, alleles with 1%

frequency might be robustly detected and the additional time required to generate clones would be unnecessary. Nevertheless, if there is ambiguity, whole genome sequencing of singular parasite clones may be needed. The most promising mutations are ones that occur in multiple, independently-derived resistant lines using the same compound. Even in cases where IVIEWGA identifies resistance genes rather than drug-able targets, those genes are valuable for epidemiological tracking of antimalarial resistance when compounds enter clinical use. For example, presence of the Kelch13 C580Y mutation is used to track resistance to artemisinin and its derivatives in field isolates.

At present, no intergenic alleles have led to the identification of a target, although in theory mutations in promoter sequences could yield transcriptional upregulation of a target. Better annotations of promoter regions in *Plasmodium*, which has been accomplished for the human ENCODE projects, could be useful for defining regulatory regions.

Occasionally, IVIEWGA methods fail during the *in vitro* resistance evolution process. Chemical mutagenesis has been shown to assist in resistance generation[69], but alternative methods may still need to be developed. Despite several challenges, IVIEWGA has proven to be a very successful and robust method for target identification studies. The discovery of these drug-able pathways will facilitate the creation of an ideal antimalarial that will be orally bioavailable, cheap to synthesize, easily stored at room temperature, and demonstrate low host cytotoxicity. It remains to be seen whether this same method will be adopted successfully for target identification in other pathogens.

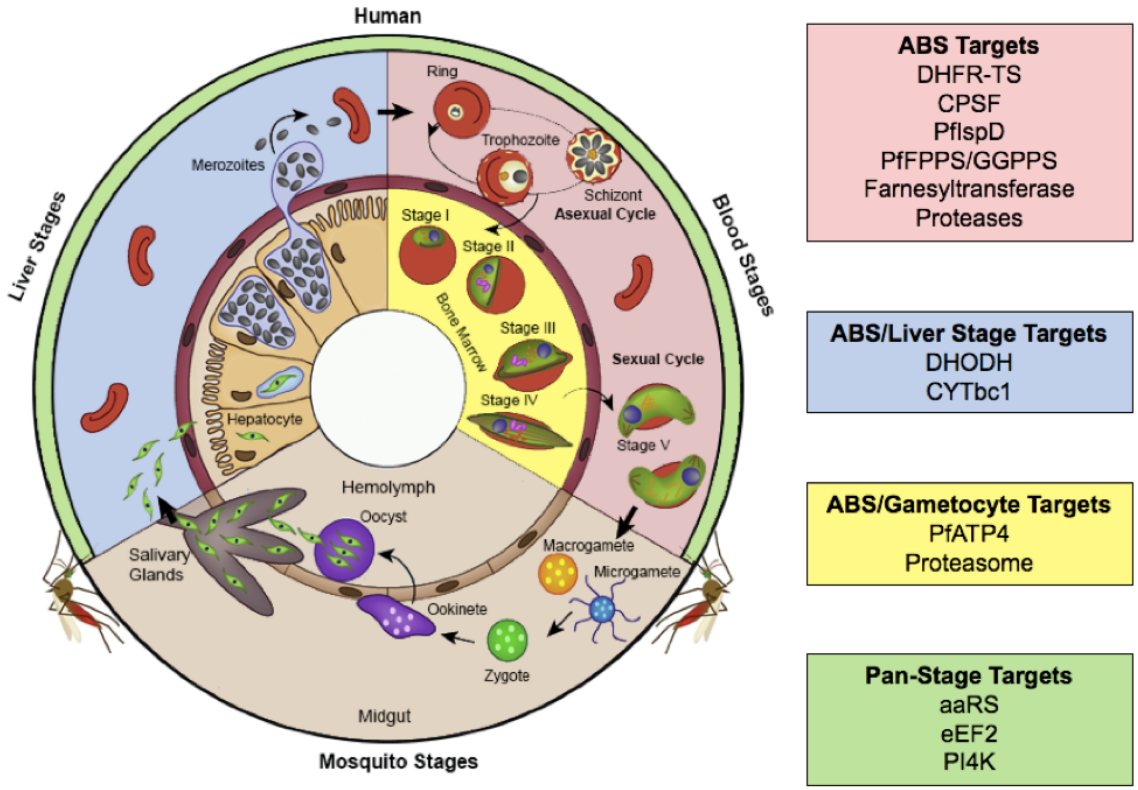

Figure 1.1. ***Plasmodium*** **life cycle with chemically validated targets** for chemotherapeutic intervention divided by the stages in which they are active. Reproduced and modified under the terms of the Creative Commons Attribution License CC BY 4.0.

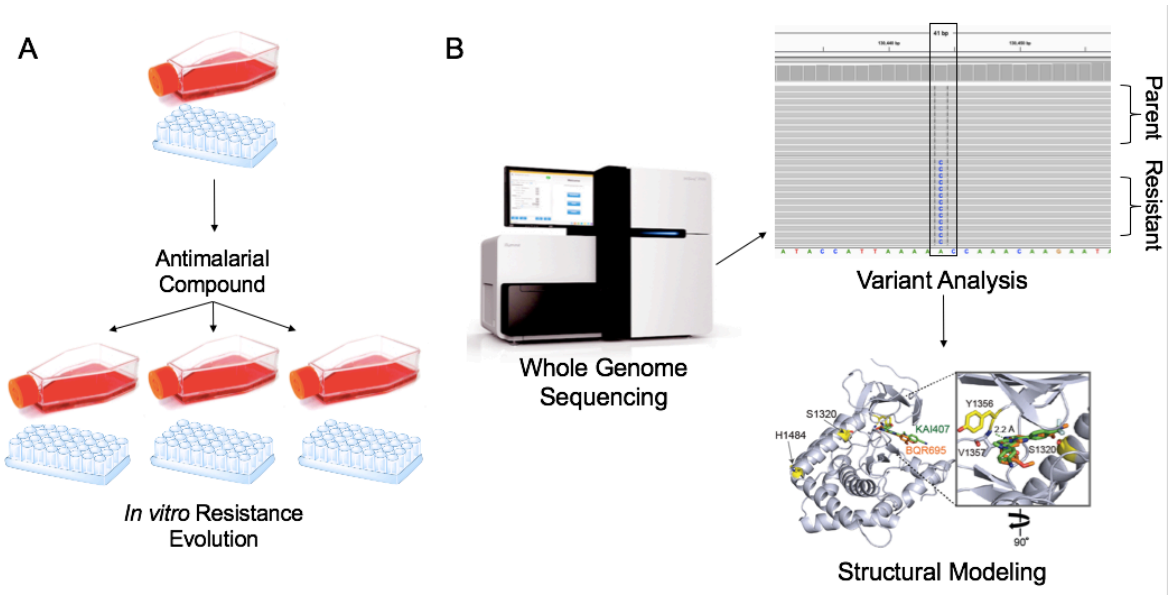

Figure 1.2. Overview of IVIEWGA process. (A) A clonal aliquot (obtained by limiting dilution in a microtiter plate) of a sensitive parent *P. falciparum* strain is cultured in triplicate and subjected to the selective pressure of an antimalarial compound using a slow ramping or pulse method. Upon successful generation of resistant parasite bulk cultures, clones are isolated using limiting dilution and retested for resistance. (B) Whole genome sequencing is performed using gDNA extracted from the parent and resistant clones. Bioinformatic analysis calls variants between the parent and resistant lines to determine which mutations confer resistance. Generally, mutations that arise in multiple, independently-derived clones are prioritized for further validation, which may include structural modeling, molecular docking simulations, and/or reverse genetics techniques.

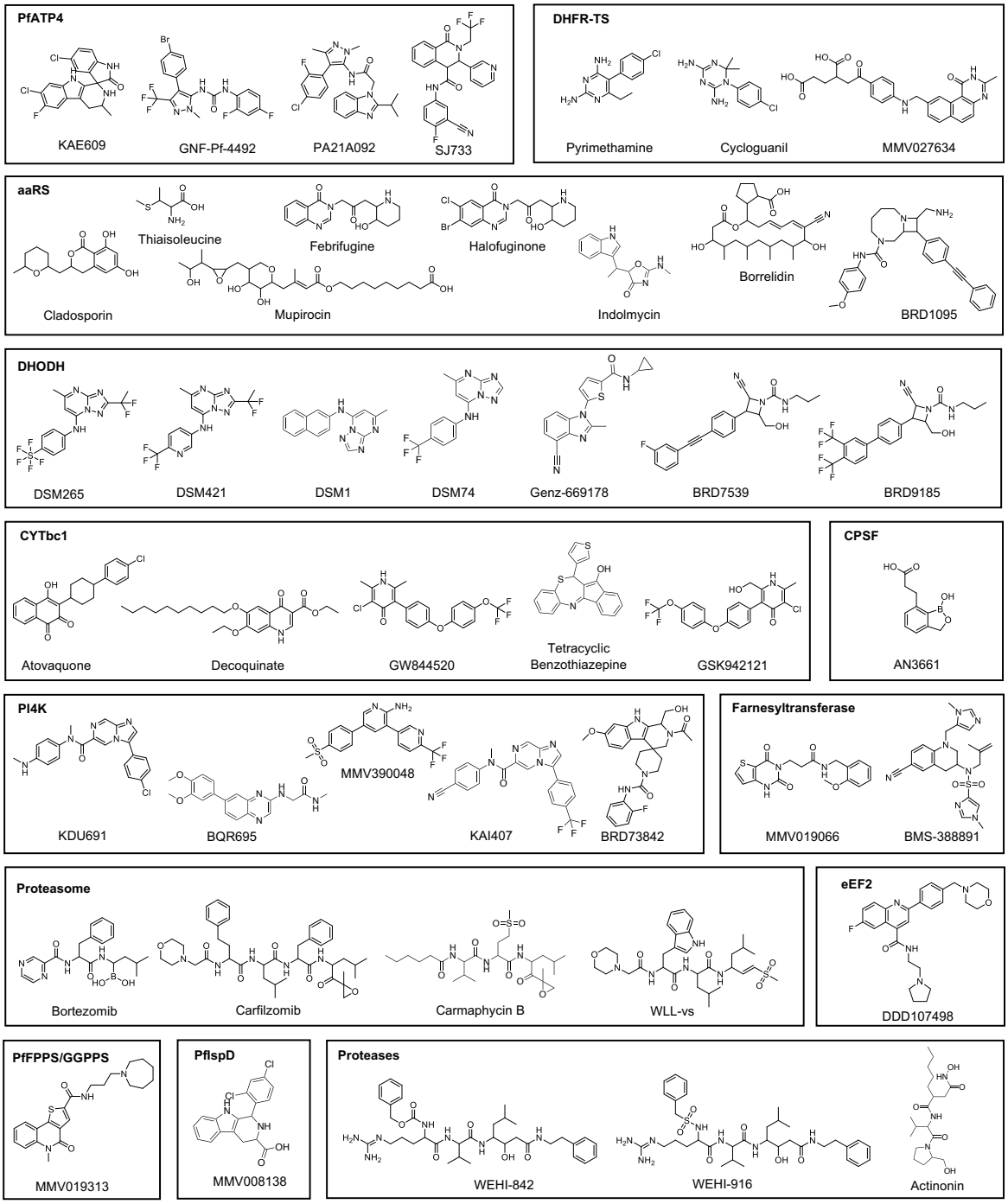

Figure 1.3. Antimalarial compounds grouped by targets as determined or supported by IVIEWGA studies.

Table 1.1. Chemically validated targets for *Plasmodium falciparum*.

Drug Target	Inhibitor
PfATP4	KAE609 (Cipargamin), GNF-Pf-4492, PA21A092, SJ733
Aminoacyl-tRNA sythetases	
Prolyl-tRNA synthetase	Febrifugine, Halofuginone
Lysyl-tRNA sythetase	Cladosporin
Isoleucyl-tRNA synthetase	Mupirocin, Thiaisoleucine
Phenylalynyl-tRNA sythetase	BRD1095
Threonyl-tRNA sythetase	Borrelidin
Tryptophanyl-tRNA synthetase	Indolmycin
Translation elongation factor 2	DDD107498
Dihydroorotate dehydrogenase	DSM265, DSM421, DSM1, DSM74, Genz-669178, Genz-666136, BRD7539, BRD9185
Cytochrome bc1	Atovaquone, Decoquinate, Tetracyclic Benzothiazepine, GW844520, GSK932121
Dihydrofolate reductase - Thymidylate synthase	Pyrimethamine, Cycloguanil, MMV027634
Phosphatidylinositol 4-kinase	KDU691, MMV390048, KAI407, BQR695, BRD73842
Cleavage and polyadenylation specificity factor	AN3661
Isoprenoid biosynthesis	Fosmidomycin, MMV008138, MMV019313
Farnesyltransferase	BMS-388891, MMV019066
Proteasome inhibition	Bortezomib, Carfilzomib, Carmaphycin B, WLL-vs
Proteases	
Aspartic proteases	
plasmepsin I, II, IV	2-aminoquinazolin-4(3H)-ones
plasmepsin V	Aminohydantoins
Cysteine protease	WEHI-842, WEHI-916
Metalloprotease	Actinonin

Table 1.2. Mutations observed in *P. falciparum* IVIEWGA studies.

Drug Target	Inhibitor	Gene ID	Mutations
PfATP4	KAE609	PF3D7_1211900	Asp1247Tyr; Pro990Arg; Thr418Asn; Ile398Phe
	GNF-Pf-4492		Ala211Thr; Ile203Leu; Pro990Arg; Ala187Val
	PA21A092		Val178Ile
	SJ733		Val415Asp; Leu350His; Pro412Thr; Pro966Ser; Pro966Thr
aaRs	Thiaisoleucine	PF3D7_1332900	Leu810Phe
	Mupirocin	PF3D7_1225100	Pro1233Ser
	Cladosporin	PF3D7_1350100	Amplification
	Halofuginone	PF3D7_1213800	Leu482His; Leu482Phe
	BRD1095	PF3D7_0109800	Leu550Val; Met316Ile; Gly512Glu; Val545Ile
eEF2	DDD107498	PF3D7_1451100	Glu134Gly; Glu134Asp; Tyr186Asn; Ala482Thr; Ile183Thr; Thr185Ile; Pro754Ala; Pro754Ser; Leu755Phe; Ser474Arg
DHODH	DSM1	PF3D7_0603300	Amplification
	DSM74		Glu182Asp; Leu531Phe
	DSM265		Gly181Cys
	Genz-669178		Phe188Ile; Phe188Leu
	Genz-666136		Glu182Asp; Phe227Ile
Cytbc1	Atovaquone	mal_mito_3	Met133Val; Met133Ile; Leu144Ser; Phe267Val
	Decoquinate		Ala122Thr; Tyr126Cys
	Tetracyclic Benzothiazepine		Gly131Ser; Phe264Leu
DHFR-TS	MMV027634	PF3D7_0417200	Gly378Glu; Ile403Leu; His551Asn
PI4K	KAI407	PF3D7_0509800	His1484Tyr
	BQR695		Ser1320Leu; Tyr1356Phe
CPSF	AN3661	PF3D7_1438500	Thr406Ile; Tyr408Ser; Thr409Ala; Asp470Asn; His36Tyr
PfDXR	Fosmidomycin	PF3D7_1467300	Amplification
PfIspD	MMV008138	PF3D7_0106900	Glu688Gln; Leu244Ile
PfFPPS/GGPPS	MMV019313	PF3D7_1128400	Ser228Thr
Farnesyltransferase	BMS-388891	PF3D7_1147500	Asn315Y; Gly612Ala
	MMV019066		Ala515Val; Ala515Thr

Chapter 2

Case Study: *in vitro* resistance development predicts *in vivo* resistance determinants for an antimalarial clinical candidate targeting DHODH

2.1 Introduction

Even for drugs that have never been introduced to parasite populations, resistance can emerge and spread rapidly, limiting their useful lifetime. For example, resistance to the dihydrofolate reductase inhibitor pyrimethamine emerged shortly after clinical introduction[105,106,107]. Even when pyrimethamine was later combined with sulfadoxine, parasites resistant to the sulfadoxine-pyrimethamine combination were identified less than 1 year after its adoption as a frontline therapy[108]. Because of this, use of the sulfadoxine-pyrimethamine combination is primarily limited to intermittent preventive treatment during pregnancy [reviewed in [4,109]]. Resistance to the cytochrome b inhibitor atovaquone was detected in clinical trials before the drug was widely in use[110]. This rapid emergence of drug resistance is thought to be due to selection of *de novo* mutations in malaria parasites that arose during the treatment of *P. falciparum*–infected individuals[4,111]. These examples illustrate the importance of identifying *de novo* mutations in *P. falciparum* and understanding their contributions to development of resistance to drug candidates early in the drug development pipeline.

A powerful tool to study drug resistance is experimental selection of resistance *in vitro* followed by whole genome sequencing of resistant parasites[112]. By exposing malaria parasites to antimalarial drugs *in vitro* and *in vivo*, we have been able to identify or confirm the mechanism of drug resistance in some cases [reviewed in [113]]. For example, treatment of cultured *P. falciparum* parasites with atovaquone *in vitro* led to the development of resistant parasites with single point mutations in the atovaquone-binding pocket of cytochrome b[114]. It was subsequently found that failure of atovaquone-combination

therapy in infected individuals was associated with point mutations in the same binding pocket[113,115,116].

Our work and that of others have demonstrated the usefulness of *in vitro* selection for identifying both targets and mechanisms of resistance in *P. falciparum* against new antimalarial drugs[52,58]. However, there are aspects of the *in vivo* environment, such as pharmacokinetics/pharmacodynamics (PK/PD) and pathophysiology, that are not captured in tissue culture. To further explore the translational relevance of experimental *in vitro* selection to the emergence of resistance *in vivo*, we developed a proof-of-concept study to directly compare the development of resistance of *P. falciparum* in tissue culture to that in a mouse model of *P. falciparum* infection. We focused on antimalarial drugs that inhibit *Plasmodium* dihydroorotate dehydrogenase (DHODH), an essential enzyme that catalyzes the rate-limiting step of pyrimidine biosynthesis[42]. Multiple high-throughput screens have identified a range of structurally diverse molecules that target this protein[117,118,119,120,121]. We and others have previously demonstrated that resistance to DHODH inhibitors can be acquired through point mutations in the inhibitor-binding pocket or copy number variations (CNVs) at the *dhodh* locus[43,48,50,117,122,123,124]. We chose the triazolopyrimidine inhibitor of DHODH, DSM265, for drug resistance studies *in vitro* and *in vivo* because it is a next-generation antimalarial drug candidate with demonstrated efficacy in recent phase 2 clinical trials[125].

2.2 Results

2.2.1 Drug resistance emerges rapidly in *P. falciparum* during *in vitro* selection

We performed four *in vitro* selection experiments with two DHODH inhibitors, DSM265 (**Figure 2.1A**) and DSM267 (**Figure 2.1D**), using two independent *P. falciparum* 3D7 clones. The malaria parasite isolates used were Pf3D7 A10, used previously in large-scale *in vitro* drug selection studies[58], and Pf3D70087/N9[126], which was the same clone used for *in vivo* selection in a mouse model of *P. falciparum* infection. We used two *in vitro* selection procedures: an intermittent pulse of DHODH inhibitor treatment and continuous exposure of parasite to drug (**Figures 2.2 and 2.3**). For pulse selections, *P. falciparum* cultures were treated with the 99% effective concentration (EC99) of the compound DSM265 for 6 to 8 days (selection 1 and selection 3). In addition to DSM265, we also used the chemical analog DSM267 as a tool compound to explore the landscape of resistance development to triazolopyrimidine-based inhibitors of DHODH (selection 2)[127].

During and after drug exposure, the parasitemia of the cultures was monitored by thin-smear microscopy, which allowed for the identification and quantification of replicating parasites. For pulse selection, *P. falciparum* asexual blood-stage parasites were consistently visible in thin smears taken from cultures about 2 weeks after exposure to drug *in vitro* (**Figures 2.2 and 2.3**). In all three pulse selection procedures, at least two independent parasite populations became resistant to drug after either the first or second round of drug exposure (**Figures 2.1, 2.2, and 2.3**). Drug-resistant parasites arising during pulse selection *in vitro* exhibited heterogeneous dose-response phenotypes when exposed to DSM265 or DSM267, with half-maximal effective concentration (EC50) values ranging from 2 to ~400 times that of the wild-type parent strain of *P. falciparum* (**Figures 2.1 and 2.2, Table 2.1**). Whole genome sequencing revealed that 20 of 21 resistant

parasite clones generated during pulse selection had single point mutations in DHODH (**Table 2.1 and Supplemental Table 2.1**). These mutations resulted in the following amino acid changes in DHODH: C276Y, L531F, F227L, G181C, and F227Y. One resistant parasite line had an amplification on chromosome 6, which included the *dhodh* locus (**Supplemental Table 2.2**). CNVs at the *dhodh* locus were additionally verified by quantitative polymerase chain reaction (qPCR) (**Figure 2.4**). Consistent with previous findings, duplication of the *dhodh* locus conferred a ~2-fold increase in drug resistance to DHODH inhibitors in *P. falciparum* parasites *in vitro* (**Table 2.1**)[43,48,50].

We also wanted to explore how *P. falciparum* parasites responded to continuous selective pressure *in vitro*. We treated resistant parasite populations recovered from the first step of selection 2 with 25 nM DSM267 (which was the EC99 of the parental line) for 7 days, followed by an increase to 50 nM DSM267 for 7 to 8 weeks (**Figure 2.2**). Clonal parasite lines from this second selection step had increased EC50 values compared to clones isolated after the first round of drug treatment (**Figure 2.1F, Table 2.1, and Supplemental Table 2.1**). Whole genome sequencing revealed single- and double-point mutations in DHODH, including F227Y and F227L/L531F, as well as one clone showing both *dhodh* amplification and an F227L mutation (**Figure 2.4, Table 2.1, and Supplemental Tables 2.1 and 2.2**). In a separate selection process, we continuously exposed Pf3D70087/N9 parasites to increasing concentrations of DSM265 from 30 to 200 nM over a 2-month period (selection 4) (**Figure 2.3**). Parasites isolated from this selection process showed a stronger drug resistance phenotype compared to those recovered from pulse selection. All four clones characterized from the selection 4 population carried a V532G mutation in DHODH and showed a ~100-fold increase in EC50 (**Figure 2.2, Table**

2.1, and Supplemental Table 2.1). In addition to these *in vitro* selections, we assessed the activity of DSM265 and DSM267 against mutant parasite lines previously isolated from *in vitro* selections using other structural classes of DHODH inhibitors[50,122]. We found that four of these lines (3D7-E182D, Dd2-I263F, Dd2-F227I, and Dd2-F227I/L527I) showed cross-resistance with DSM265 (**Table 2.1**).

2.2.2 *In vivo* drug resistance occurs through the same DHODH mutations identified by *in vitro* selection

We initially infected four SCID mice with 2×10^7 *P. falciparum* parasites of the Pf3D70087/N9 strain (groups A, B, C, and D). Each mouse was orally treated with DSM265 (50 mg/kg) once daily for 4 days. In all mice, the parasite population initially decreased below the LoD but was then detected by flow cytometry about 2 weeks after drug treatment (**Figure 2.5**). Infected red blood cells (iRBCs) from each mouse were then used to infect four naïve mice, two of which were treated with the same dose of DSM265 and two of which received vehicle. The parasite populations from each of the original four mice (A, B, C, and D) were maintained as separate lineages in each of the rounds of selection and were labeled groups A, B, C, and D. This process was repeated until a resistant parasite population emerged in treated animals. Resistant parasites emerged in group A (**Figure 2.5A**) and also in groups B and D but not group C (**Figure 2.5B**).

Similar to the *in vitro* results, a stable resistance phenotype was generated after a short period of time in three of the four groups of mice. For selection group A, reduced efficacy of the drug was observed after only one round of treatment, and treatment was completely ineffective by round 3 (**Figure 2.5A**). For selection groups B and D, treatment

was ineffective by rounds four and five, respectively, of drug treatment (**Figure 2.5B**). Drug resistance was never observed for selection group C, and the assay was terminated after six rounds of treatment. The drug resistance phenotypes of the parasite populations were confirmed by *in vitro* dose-response assays (**Figure 2.6A**), and individual clones were isolated by limiting dilution. As observed in our *in vitro* selections, clonally derived parasites showed heterogeneous dose-response phenotypes, with the EC50 ranging from 16 to 116 times that of the wild-type *P. falciparum* parental strain (**Figure 2.6B and Table 2.2)**.

When comparing the *in vivo* and *in vitro* selections, we found overlap in the amino acid residues of DHODH that were mutated. Whole genome sequencing revealed that two of four clones from group A carried a C276F mutation, which was similar to the C276Y mutation observed *in vitro* (**Table 2.2 and Supplemental Table 2.1**). Both mutations resulted in replacement of the cysteine at position 27 with an amino acid with an aromatic side chain. The other two parasite clones from group A carried an R265G mutation, which was not identified in any of our *in vitro* selection experiments. However, an R265A mutation was identified after *in vitro* selection experiments by another group[124]. All four clones isolated from *in vivo* selection groups B and D carried a G181D mutation similar to the G181C mutation identified during our *in vitro* selection experiments, with the nonpolar glycine being replaced by a charged (G181D) or polar (G181C) amino acid residue (**Table 2.2 and Supplemental Table 2.1**).

In addition to whole genome sequencing of parasite clones from the stably resistant parasite populations, we also collected genomic DNA (gDNA) before each round

of drug treatment and performed whole genome sequencing on the bulk parasite populations (**Supplemental Table 2.1**). We calculated allele frequencies based on read counts (**Table 2.3**). In populations B and D, the G181D mutation predominated before rounds 3 and 4 of selection, respectively, corresponding to when reduced drug efficacy was observed; the G181D mutation reached 100% frequency as drug resistance became stable. In contrast, for population A, the predominant mutation was R265G, which appeared at 97% frequency after round 1 of selection. However, the frequency of this allele decreased over the next two rounds of drug treatment to a frequency of 89%. In contrast, the frequency of the C276F mutation increased from 5 to 12% in the same parasite samples, suggesting that the two parasite lines were engaging in clonal competition in infected SCID mice *in vivo*[128].

2.3 Discussion

The major finding of this study is that *in vitro* resistance of *P. falciparum* asexual blood-stage parasites to the DHODH inhibitor DSM265 can predict drug resistance in infected mice *in vivo*. This approach provides a framework for assessing the potential for emergence of drug resistance in *P. falciparum* during the early stages of drug development. Development of drug resistance may be inevitable, but the rate at which resistance emerges and spreads has implications for public health. An understanding of how parasites develop resistance to new classes of antimalarial drugs both *in vitro* and *in vivo* is therefore an important criterion when evaluating the drug development pipeline.

Our study compared *in vitro* and *in vivo* selection of resistance to the same compound. The *P. falciparum* infection mouse model enabled capture of the dynamics of drug resistance development that were lacking from the *in vitro* experiments[129]. We found

that selection of resistance to the DHODH inhibitors DSM265 and DSM267 *in vitro* mirrored the findings in the mouse model. In both systems, parasites recrudesced roughly 2 weeks after drug treatment. Stable drug resistance occurred in most of the selected parasite populations (seven of nine *in vitro*–selected populations and three of four *in vivo*–selected populations) and emerged after either one or a few cycles of drug treatment. Together, we identified 13 unique mutations that led to drug resistance (**Figure 2.7**). Several of these mutations were also identified in other studies, confirming their contributions to the observed resistance phenotypes[43,50,122,124]. There was also similarity in the mutations that arose *in vitro* compared to *in vivo*. Of the three residues in DHODH that were mutated during *in vivo* selections, all were also identified after *in vitro* selections in our study and in studies by other groups[43,124].

Our findings also correlate with results from the Phase 2a clinical trial with DSM265. In that study, two *P. falciparum*–infected individuals treated with a single dose of DSM265 had recrudescent parasites at day 28 after treatment. Genome sequencing of these recrudescent parasites identified mutations in the *dhodh* locus. One patient had a clonal parasite population carrying the C276Y mutation. Another had a minor population of parasites harboring the C276F mutation, with the G181S mutation also detected in a subset of reads[125]. These DHODH amino acid positions were all mutated in our *in vitro* and *in vivo* selection experiments, demonstrating that our approach may be a good model for predicting clinical resistance to DSM265. We identified several mutations that conferred resistance to DHODH inhibitors and saw both *in vitro* and *in vivo* that within a single parasite population there could be multiple mutational trajectories simultaneously.

Given that there can be 10^{10} to 10^{13} parasites in an infected human host[130], it is expected that drug-resistant parasites emerged during the Phase 2 clinical trial.

2.4 Materials and Methods

2.4.1 Parasite strains and culturing conditions

The 3D7 A10 clone has been used in previous *in vitro* drug selection and sequencing efforts[58]. The Pf3D70087/N9 line was generated by adapting 3D7 to grow in peripheral blood of engrafted NOD-scid/β2 m−/− mice[126]. The Dd2 2D4 clone was derived from MR4 line MRA-156 (MR4, BEI Resources). In addition to the selected lines derived in this study, parasites with point mutations in *pfdhodh* were generated as described previously[50,122]. Parasite strains were cultured in 5% human O+ hematocrit in RPMI 1640 (RPMI) (Life Technologies) supplemented with 28 mM $NaHCO_3$, 25 mM Hepes, and hypoxanthine (50 mg/mL). Depending on the parasite line, the media either contained gentamycin (25 µg/ mL), or no antibiotic and was additionally supplemented with 0.5% AlbuMAX II (Life Technologies) and/or O+ human serum (heat inactivated and pooled). Blood and serum products were obtained from Interstate Blood Bank. Cultures were maintained at 37°C in 1.1% O_2, 4% CO_2, and 95% N_2. Parasite populations were synchronized by 5% sorbitol treatment[131].

2.4.2 Selection of drug resistance *in vitro*

Resistance selections were performed using 100-mL cultures at 3 to 4% starting parasitemia (~10^9 parasites). Intermittent pulse selections were treated with the EC99 of the selecting agent for 6 to 8 days. Compound pressure was then removed, and cultures

were fed with compound-free media daily for the first week and on alternate days thereafter. For continuous selections, cultures were maintained in 25-mL flasks and replenished daily with medium containing the selecting agent. Bulk populations were cloned by limiting dilution in 96-well plates. Pulse treatment selections were cloned in compound-free RPMI. Cultures selected with continuous treatment were cloned at the highest concentration of compound to which they were exposed during the selection.

2.4.3 Selection of drug resistance *in vivo*

Four mice infected with 2×10^7 Pf3D70087/N9 parasites were established as the parent generation. The day of infection was designated day 0. From days 3 to 6, each mouse was orally treated daily with DSM265 at a dose of 50 mg/kg free base (10-fold ED90), until the parasite population decreased below LoD. After a recrudescence period, infected RBCs from mice with detectable parasitemia were donated to four mice for an additional passage. Infected mice in the second passage were randomly divided into two groups, one of which received the previous dose of DSM265, and other was treated with vehicle as a control. Drug concentrations in blood were monitored at the end of treatment in each selection cycle. The process was repeated until the resistance phenotype was observed. In each cycle of selection, additional mice infected with the parental *P. falciparum* Pf3D70087/N9 strain were used as controls. Resistant parasite populations were cryopreserved, cloned in compound-free RPMI, and tested for *in vitro* dose-response phenotype.

2.4.4 Whole genome sequencing and analysis

Genomic DNA (gDNA) was obtained from *P. falciparum* clones by washing iRBCs with 0.1% saponin and extracting gDNA using the DNeasy Blood and Tissue Kit (Qiagen). Sequencing library preparation and analysis were performed as previously described[58]. PCR amplification/Sanger sequencing of the *Pfdhodh* locus was performed as described[50] using BIO-X-ACT Short Mix (Bioline Reagents).

Sequencing libraries were prepared with the Nextera XT kit (cat. no. FC-131-1024, Illumina) using the standard dual index protocol, and whole-genome sequencing was performed on an Illumina HiSeq 2500 in RapidRun mode with 100–base pair paired-end reads. Reads were aligned to the *P. falciparum* 3D7 reference genome (PlasmoDB v. 13.0), and variants were called using a previously established analysis pipeline[58].

2.5 Acknowledgements

Chapter 2 is a partial, modified reprint of the material as it appears in Science Translational Medicine, 2019. Rebecca E. K. Mandt, Maria Jose Lafuente-Monasterio, Tomoyo Sakata-Kato, Madeline R. Luth, Delfina Segura, Alba Pablos-Tanarro, Sara Viera, Noemi Magan, Sabine Ottilie, Elizabeth A. Winzeler, Amanda K. Lukens, Francisco Javier Gamo, Dyann F. Wirth, "*In vitro* selection predicts malaria parasite resistance to dihydroorotate dehydrogenase inhibitors in a mouse infection model." The dissertation author was a co-author of the publication and performed all sequencing and analysis, which is the focus of this dissertation.

Figure 2.1. Emergence of resistance to DSM267 and DSM265 in *P. falciparum in vitro*. (A) Structure of the DHODH inhibitor DSM265 used in *in vitro* resistance selection experiments [selection 1 (S1)]. (B) Representative dose-response curves for bulk-selected parasite populations. Parasite populations in three independent culture flasks containing human blood were exposed to DSM265 at the EC99 and allowed to recrudesce. Cultures recovered after selection were tested in a dose-response assay to determine the resistance phenotype (flask 1, yellow; flask 2, blue; Flask 3, red). (C) Shown is the dose-response phenotype of clones isolated from *in vitro* resistance selection experiments using pulsed treatments with DSM265. Bulk resistant populations were cloned in the absence of compound pressure. Clonal parasite lines from flasks 1 and 3 exhibited heterogeneous resistance phenotypes. Each clonal line is labeled on the x axis with a unique identifier that includes the selection number (S), flask number (F), and clone number (C), for example, S1-F1-C1. Individual replicate EC50 values are shown as a scatter plot, with error bars depicting mean and SD. Statistically significant differences in specific clonal phenotypes relative to the wild-type (WT) 3D7 A10 parental parasite line are indicated on the graph. Significance was calculated using a nonparametric one-way ANOVA (Kruskal-Wallis) with post hoc multiple comparisons (Dunn's test): **P < 0.01, ****P < 0.0001; ns, not significant. (D to F) Increasing continuous drug selection pressure yielded parasites with highly drug-resistant phenotypes. (D) Structure of the DHODH inhibitor DSM267 used in *in vitro* drug resistance selection experiments (selection 2). (E) Parasites were exposed to two steps of selective pressure (steps 1 and 2). In step 1, parasites were exposed to a single pulse of 25 nM DSM267, leading to ~10-fold resistance in two of three flasks (flask 1, yellow; flask 2, blue; flask 3, green). In step 2, the drug-resistant populations from flasks 2 and 3 were continuously exposed to DSM267 at an increased dose (50 nM) for 7 to 8 weeks. Shown are representative dose-response curves for bulk-selected populations from step 1. (F) Shown are dose-response phenotypes of clones isolated from step 1 and step 2 of selection 2 (S2). Each clonal line is labeled on the x axis with a unique identifier that includes the selection number (S), flask number (F), and clone number (C), for example, S2-F2-C1. Individual replicate EC50 values are shown as a scatter plot, with error bars depicting mean and SD. Statistically significant differences in specific clonal phenotypes relative to the wild-type 3D7 A10 parental line are indicated on the graph. Significance was calculated using a nonparametric one-way ANOVA (Kruskal-Wallis) with post hoc multiple comparisons (Dunn's test): *P < 0.05, **P < 0.01; ns, not significant.

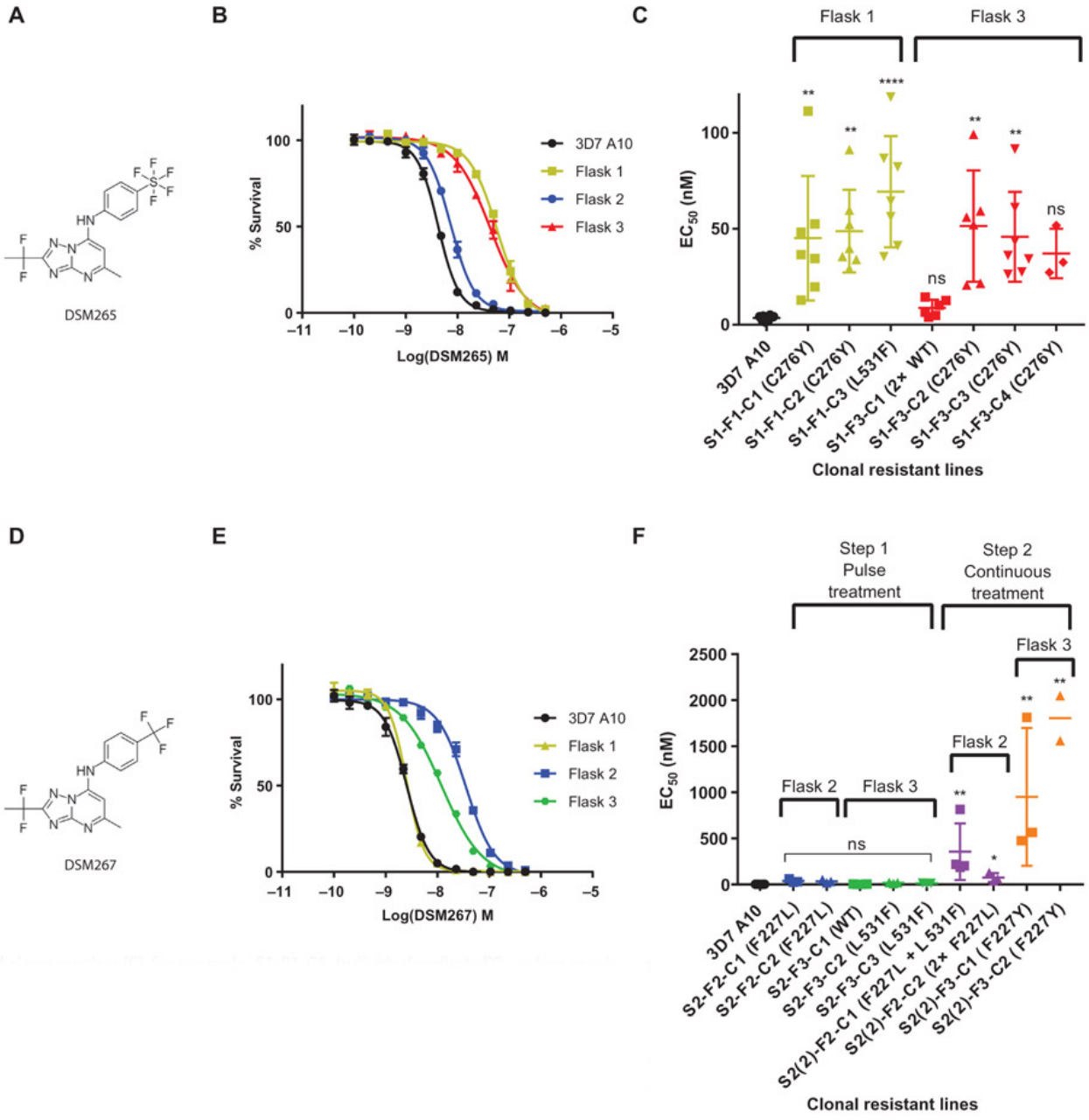
A
DSM265
B
% Survival
Log(DSM265) M
3D7 A10
Flask 1
Flask 2
Flask 3
C
Flask 1
Flask 3
EC50 (nM)
ns
3D7 A10
S1-F1-C1 (C276Y)
S1-F1-C2 (C276Y)
S1-F1-C3 (L531F)
S1-F3-C1 (2× WT)
S1-F3-C2 (C276Y)
S1-F3-C3 (C276Y)
S1-F3-C4 (C276Y)
Clonal resistant lines
D
DSM267
E
% Survival
Log(DSM267) M
3D7 A10
Flask 1
Flask 2
Flask 3
F
Step 1
Pulse
treatment
Step 2
Continuous
treatment
Flask 2
Flask 3
EC50 (nM)
ns
3D7 A10
S2-F2-C1 (F227L)
S2-F2-C2 (F227L)
S2-F3-C1 (WT)
S2-F3-C2 (L531F)
S2-F3-C3 (L531F)
S2(2)-F2-C1 (F227L + L531F)
S2(2)-F2-C2 (2× F227L)
S2(2)-F3-C1 (F227Y)
S2(2)-F3-C2 (F227Y)
Clonal resistant lines

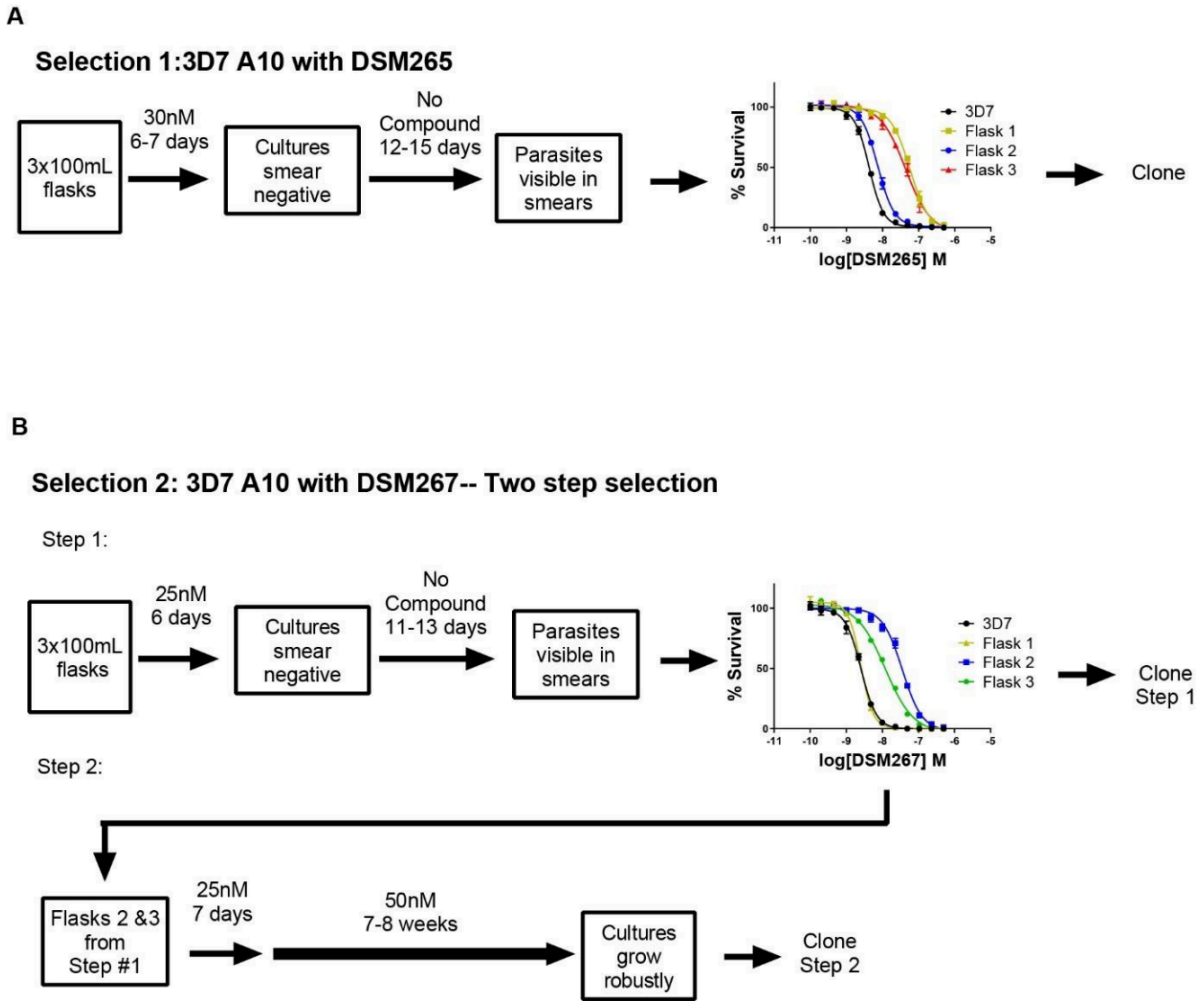

Figure 2.2. Study design for *in vitro* selections. Schematics show the design of in vitro resistance selection experiments for Selections 1 and 2. (A) Pulse selection with DSM265 (Selection 1), with representative dose-response phenotype of selected populations shown (Flask 1 in yellow, Flask 2 in blue, Flask 3 in red). (B) Two-step selection with DSM267 (Selection 2), with representative dose-response phenotype of selected populations shown (Flask 1 in yellow, Flask 2 in blue, Flask 3 in green). Individual clone phenotypes for both selections are displayed in Figure 2.1.

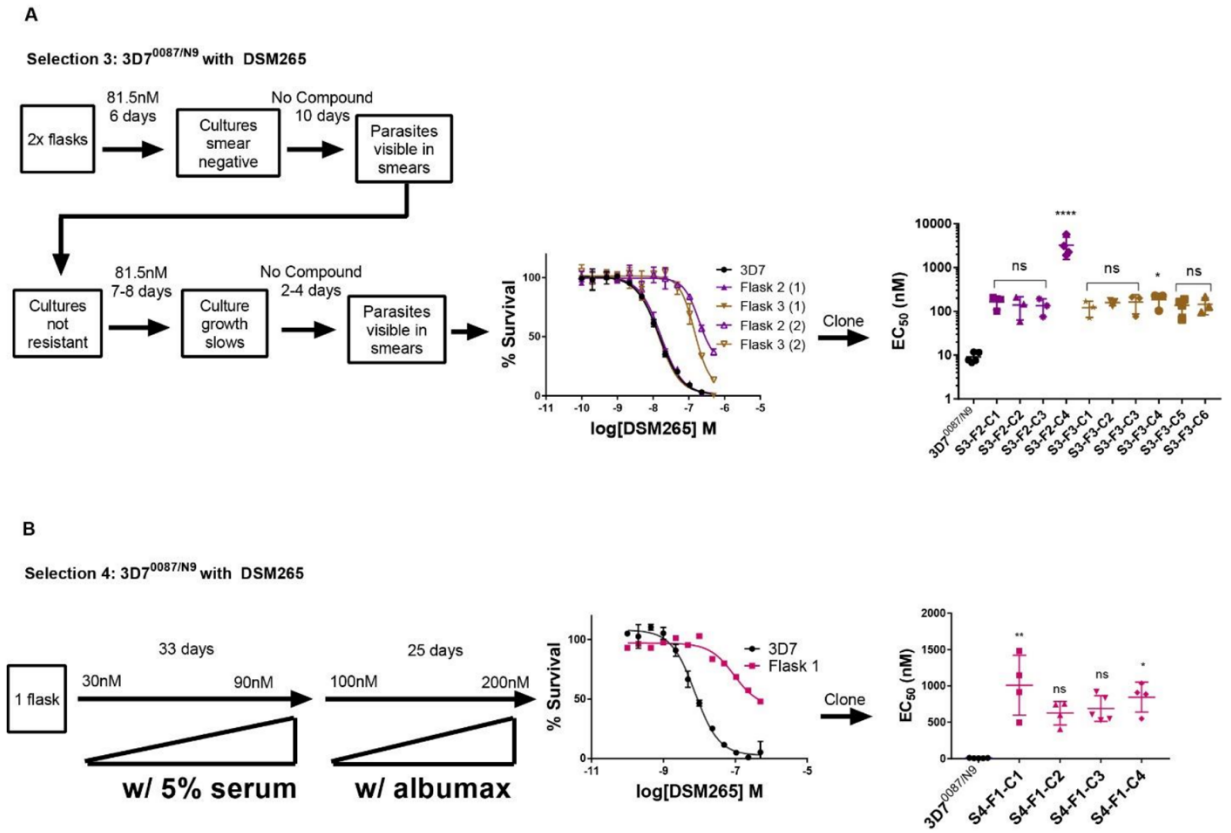

Figure 2.3. Study design for additional *in vitro* selections. (A) Schematic for Selection 3, with representative phenotype of bulk selected populations (Flask 2, purple; Flask 3, brown. Closed triangles, first pulse; open triangles, second pulse of DSM265 treatment). (B) Schematic for Selection 4, with representative phenotype of bulk selected populations (Flask 1, pink). For both selections, resistant bulk cultures were cloned and phenotyped by dose response assay. Individual replicate EC50 values are shown for each clonal line in the right-most graph. Each clonal line is labelled on the x-axis with a unique identifier that includes the selection number (S), flask number (F), and clone number (C), for example S3-F2-C1. Individual replicate EC50 values are shown as a scatter plot, with error bars depicting mean and standard deviation. Note that the y-axis of the graph in panel A is in log-scale to allow for better visualization of the data. Statistically significant differences in specific clonal phenotypes relative to the wild-type 3D7 parental line are indicated on the graph. Significance was calculated using a non-parametric one-way ANOVA (Kruskal-Wallis) test with post-hoc multiple comparisons (Dunn's test) between resistant lines and the 3D7 parent. *p<0.05, **p<0.01, ****p<0.0001. ns= not significant.

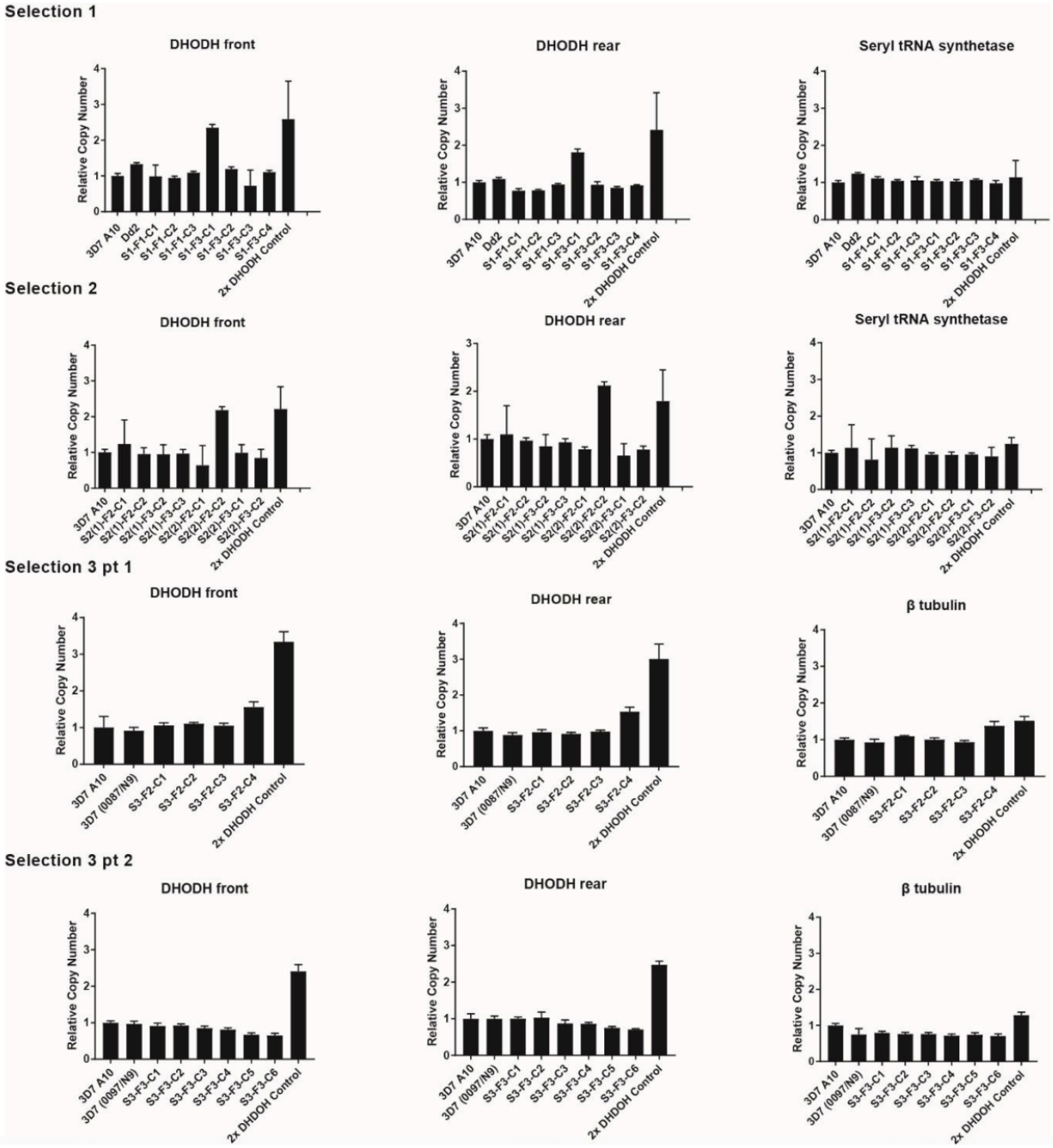

Figure 2.4. Detection of copy number duplication of the *dhodh* locus in *in vitro*-isolated clones by real-time qPCR. Increased copy number of *dhodh* was calculated relative to the 18s rRNA gene and 3D7 A10 wildtype strain. β tubulin or seryl tRNA synthetase genes shown as additional control. Error bars represent min/max values calculated from four technical replicates. Copy number variation was detected in expected clones based on the whole-genome sequence analysis. 2x DHODH control is from a previously-published parasite line confirmed to have *dhodh* copy number duplication[50].

Figure 2.5. Development of DSM265 resistance in SCID mice infected with *P. falciparum*. Four *P. falciparum*–infected SCID mice (experimental animal groups A, B, C, and D) were treated with DSM265 (50 mg/kg), and parasitemia was monitored until recrudescent parasites were observed (round 1). Recrudescent resistant parasites were used to infect naive mice in a second cycle (round 2). Rounds of infection, treatment, and recovery were continued until drug resistance was observed. The parasite populations from groups A to D were maintained as independent lineages starting from the four initially infected mice through each subsequent passage and treatment cycle. (A) Shown are representative results for group A mice for efficacy (top) and parasite recrudescence (bottom). Two of the mice in round 2 were treated orally with the same dose of drug (individual mice M1 and M2, open blue symbols), and the other two mice were treated with vehicle alone as a control (represented as an average, closed blue symbols). Infections with the 3D7 A10 parental line parasites as a control are plotted in red (drug treated, open symbols; vehicle control, closed symbols). In group A, the infected mice were never able to completely clear parasites from round 1 [Resistant population A (RPA)], and the parasites recrudesced faster than did 3D7 A10 wild-type control parasites, indicating that the parasite population had evolved resistance. By round 3, the original dose of DSM265 was completely ineffective. Once resistance to DSM265 was observed, parasites were subjected to an additional round of drug treatment. Genomic DNA then was extracted from the bulk population and subjected to whole-genome sequencing. (B) Shown is a summary of results from all groups of mice (A, B, C, and D) undergoing in vivo resistance selection, with the iterative infection, treatment, and recrudescence periods for each group indicated. The round when resistant parasites were observed (treatment ineffective) and the time to resistance development are also indicated.

A

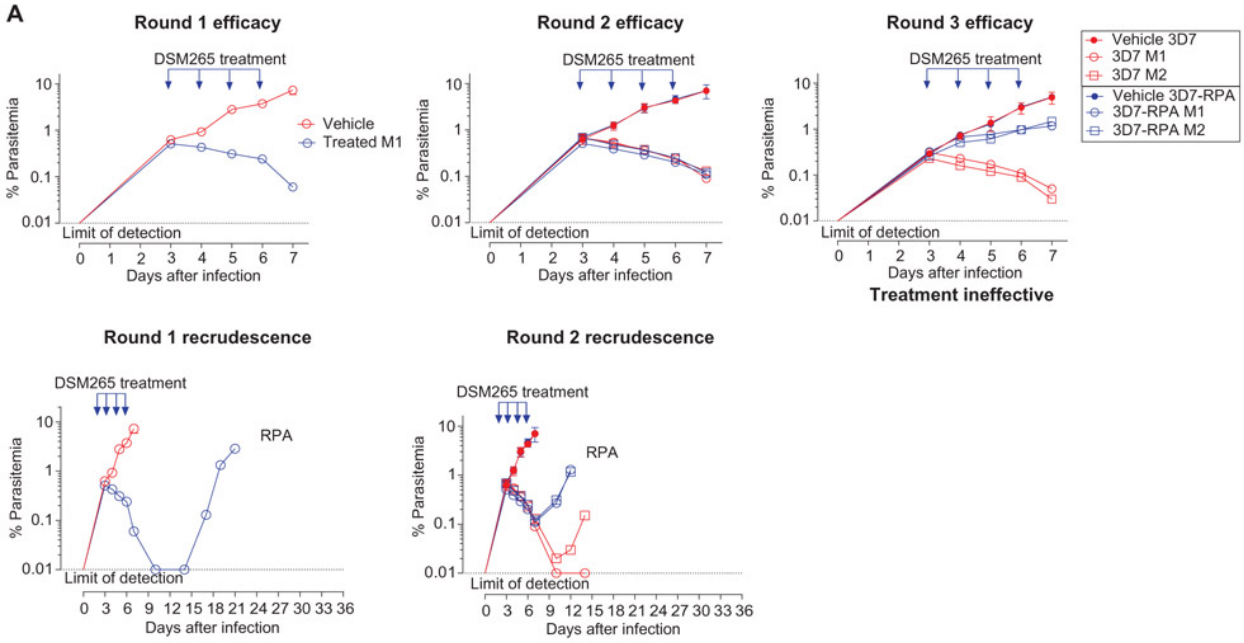

B

	Round 1		Round 2		Round 3		Round 4		Round 5		Round 6		
	Treatment (days)	Recovery (days)	Treatment (days)	Recovery (days)	Treatment (days)	Recovery (days)	Treatment (days)	Recovery (days)	Treatment (days)	Recovery (days)	Treatment (days)	Recovery (days)	Time to resistant population (days)
Group A	4	11	4	1	4	Ineffective	Additional treatment round	Clone recovered parasites					**20**
Group B	4	9	4	10	4	1	4	Ineffective	Additional treatment round	Clone recovered parasites			**32**
Group C	4	11	4	10	4	10	4	9	4	9	4	9	**N/A**
Group D	4	8	4	9	4	9	4	1	4	Ineffective	Additional treatment round	Clone recovered parasites	**38**

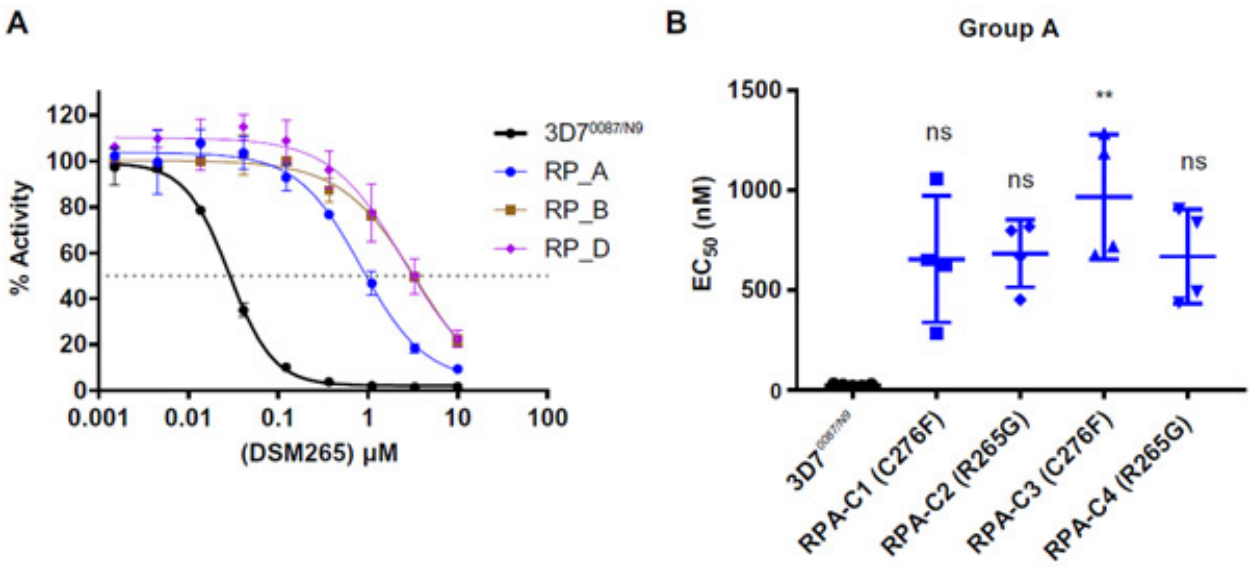

Figure 2.6. Drug resistance phenotypes of parasites in *P. falciparum*–infected SCID mice. (A) Resistant *P. falciparum* parasites (RP) from groups A, B, and D were adapted to in vitro growth and phenotyped using an in vitro dose-response assay. Shown are representative dose-response curves relative to wild-type 3D70087/N9 parasites (wild-type, black symbols; group A parasites, blue symbols; group B parasites, brown symbols; group D parasites, purple symbols). (B) Individual replicate EC50 values are shown for clonal parasite lines isolated from the group A parasite population, with error bars depicting mean and SD. Statistically significant differences in specific drug-resistant phenotypes relative to the wild-type 3D70087/N9 parental line are indicated on the graph. Significance was calculated using a nonparametric one-way ANOVA (Kruskal-Wallis) with post hoc multiple comparisons (Dunn's test): **P < 0.01.

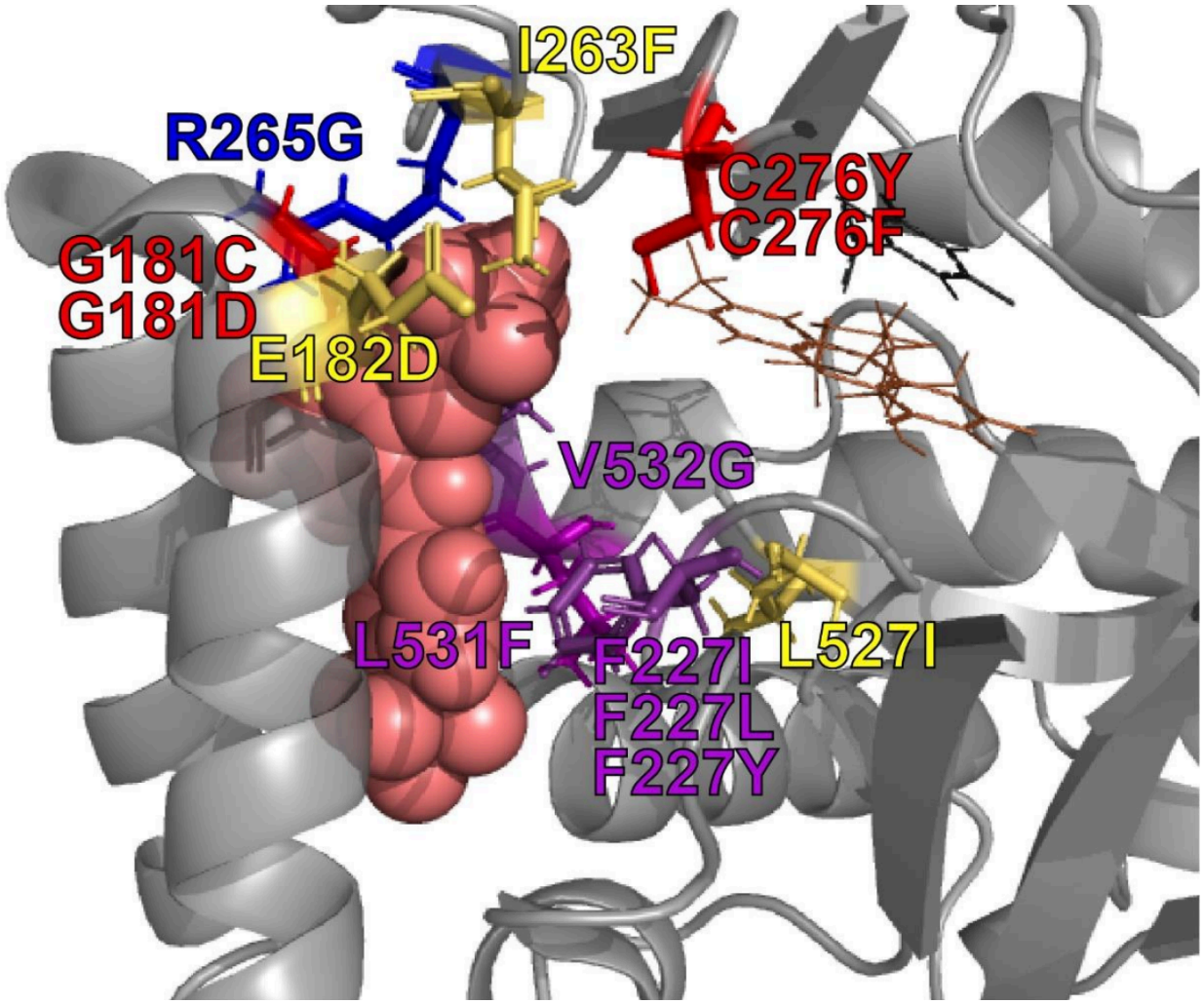

Figure 2.7. Crystal structure of PfDHODH bound to DSM265 (PDB 4RX0) with mutations that confer resistance to DSM265 highlighted. DSM265 is represented by the pink space-filled ligand. Purple residues show location of mutations selected by DSM265/267 *in vitro* in this study. Blue residues were selected by DSM265 *in vivo*. Red residues were selected both *in vivo* and *in vitro*. Yellow residues were selected by other DHODH inhibitors in a previous study[50].

Table 2.1. Point mutations identified in drug-resistant parasite lines arising from *in vitro* selections with resulting EC50s (nM). EC50s (nM) represent average of 3-10 bioreplicates ± SD.
*Whole genome sequencing indicated that S2(1)-F3-C3 was a mixed population with both the L531F (57%) and wildtype (43%) alleles.
**EC50 outside of dose range tested
***Previously-selected DHODH mutant lines

Parent Lines					
	Clone ID:	**DHODH Mutations**	**Copy No.**	**DSM265 EC_{50}**	**DSM267 EC_{50}**
	3D7 A10	N/A	1	3.55±1.28	2.18±0.646
	$3D7^{0087/N9}$	N/A	1	9.08±2.41	4.57±0.873
	Dd2	N/A	1	3.92±2.00	3.46±1.07
Selection 1: 3D7 A10 with DSM265 (Pulse Selection)					
	Clone ID:	**DHODH Mutations**	**Copy No.**	**DSM265 EC_{50}**	**DSM267 EC_{50}**
Flask 1	S1-F1-C1	C276Y	1	45.1±32.5	36.2±23.6
	S1-F1-C2	C276Y	1	48.8±21.6	34.2±15.4
	S1-F1-C3	L531F	1	69.3±29.0	35.0±21.4
Flask 3	S1-F3-C1	WT	2	8.76±4.33	5.99±2.72
	S1-F3-C2	C276Y	1	51.5±29.0	37.0±19.6
	S1-F3-C3	C276Y	1	45.8±23.4	36.8±16.7
	S1-F3-C4	C276Y	1	37.2±12.9	24.0±6.05
Selection 2.1: 3D7 A10 with DSM267 (Pulse Selection)					
	Clone ID:	**DHODH Mutations**	**Copy No.**	**DSM265 EC_{50}**	**DSM267 EC_{50}**
Flask 2	S2(1)-F2-C1	F227L	1	59.7±11.5	45.9±19.1
	S2(1)-F2-C2	F227L	1	71.4±44.4	43.2±21.9
Flask 3	S2(1)-F3-C2	L531F	1	63.9±25.9	17.2±6.06
	S2(1)-F3-C3	L531F*	1	49.1±10.2	12.8±3.19

Table 2.1. Point mutations identified in drug-resistant parasite lines arising from *in vitro* selections with resulting EC50s (nM), Continued.

Selection 2.2: 3D7 A10 with DSM267 (Continuous Selection)					
	Clone ID:	**DHODH Mutations**	**Copy No.**	**DSM265 EC_{50}**	**DSM267 EC_{50}**
Flask 2	S2(2)-F2-C1	F227L+L531F	1	911±864	357±307
Flask 2	S2(2)-F2-C2	F227L	2	91.3±50.9	56.6±43.5
Flask 3	S2(2)-F3-C1	F227Y	1	562±224	952±748
	S2(2)-F3-C2	F227Y	1	1270±257	>500**
Selection 3: $3D7^{0087/N9}$ with DSM265 (Pulse Selection)					
	Clone ID:	**DHODH Mutations**	**Copy No.**	**DSM265 EC_{50}**	**DSM267 EC_{50}**
Flask 2	S3-F2-C1	G181C	1	166±56.8	75.3±5.80
	S3-F2-C2	G181C	1	139±76.2	61.3±21.3
	S3-F2-C3	G181C	1	134±58.6	65.6±25.6
	S3-F2-C4	F227Y	1	3750±1860	6160±2810
Flask 3	S3-F3-C1	L531F	1	122±49.4	39.7±12.3
	S3-F3-C2	L531F	1	159±25.0	42.8±11.7
	S3-F3-C3	L531F	1	163±75.3	39.2±7.50
	S3-F3-C4	L531F	1	186±71.6	50.4±11.6
	S3-F3-C5	L531F	1	139±53.5	34.0±7.78
	S3-F3-C6	L531F	1	146±61.6	45.3±14.5
Selection 4: $3D7^{0087/N9}$ with DSM265 (Continuous Selection)					
	Clone ID:	**DHODH Mutations**	**Copy No.**	**DSM265 EC_{50}**	**DSM267 EC_{50}**
Flask 1	S4-F1-C1	V532G	1	1010±413	495±221
	S4-F1-C2	V532G	1	627±163	317±116
	S4-F1-C3	V532G	1	690±178	363±73.4
	S4-F1-C4	V532G	1	846±207	463±129

Table 2.1. Point mutations identified in drug-resistant parasite lines arising from *in vitro* selections with resulting EC50s (nM), Continued.

Previously-selected *Pf*DHODH mutant lines** (Parental line indicated)				
Clone ID:	**DHODH Mutations**	**Copy No.**	**DSM265 EC_{50}**	**DSM267 EC_{50}**
N/A	3D7-E182D	1	174.4±53.7	97.1±20.9
N/A	Dd2-I263F	1	> 200***	>200***
N/A	Dd2-F188I	1	8.96±4.52	1.30±0.441
N/A	Dd2-F227I	1	51.6±30.3	31.5±10.9
N/A	Dd2- F227I/L527I	1	99.6±51.7	71.0±41.7

Table 2.2. Point mutations identified in drug-resistant parasite lines arising from *in vivo* selections with resulting EC50s (nM). Point mutation and dose-response phenotype listed for each *in vivo* selected clone. EC50s (nM) represent average of 2-5 bioreplicates ± SD. Where 2 bioreplicates were performed, only average is reported.

***in vivo* selections: $3D7^{0087/N9}$ with DSM265**				
	Clone ID:	**DHODH Mutations:**	**Copy No.**	**DSM265 EC_{50}**
	$3D7^{0087/N9}$	N/A	1	25.0±4.73
Group A	RPA-C1	C276F	1	655±317
	RPA-C2	C276F	1	684±169
	RPA-C3	R265G	1	966±314
	RPA-C4	R265G	1	669±238
Group B	RPB-C1	G181D	1	3419
	RPB-C2	G181D	1	3173
	RPB-C3	G181D	1	3346
	RPB-C4	G181D	1	3098
Group D	RPD-C1	G181D	1	3060
	RPD-C2	G181D	1	3360
	RPD-C3	G181D	1	3240
	RPD-C4	G181D	1	1800

Table 2.3. Population-level sequencing of the *Pf*DHODH gene after *in vivo* resistance selections.

Sample Name	Position in *dhodh*	Amino Acid Change	Ref Allele	Alt Allele	Alt Allele Count	Alt Allele %	Total Reads
RPA-Round 1	131246	R265G	T	C	8	3%	288
	131212	C276F	C	A	0	0%	271
RPA-Round 2	131246	R265G	T	C	217	97%	223
	131212	C276F	C	A	10	5%	212
RPA-Round 3	131246	R265G	T	C	409	93%	439
	131212	C276F	C	A	24	6%	412
RPA-Round 4	131246	R265G	T	C	255	89%	286
	131212	C276F	C	A	27	12%	229
RPB-Round 1	131497	G181D	C	T	1	1%	128
RPB-Round 2	131497	G181D	C	T	0	0%	86
RPB-Round 3	131497	G181D	C	T	48	91%	53
RPB-Round 4	131497	G181D	C	T	69	99%	70
RPB-Round 5	131497	G181D	C	T	62	100%	62
RPD-Round 1	131497	G181D	C	T	0	0%	74
RPD-Round 2	131497	G181D	C	T	0	0%	34
RPD-Round 3	131497	G181D	C	T	1	1%	100
RPD-Round 4	131497	G181D	C	T	77	100%	77
RPD-Round 5	131497	G181D	C	T	76	100%	76
RPD-Round 6	131497	G181D	C	T	41	100%	41

Chapter 3

Constructing a genome-wide *in vitro* drug resistance resource for the human malaria parasite with the Malaria Drug Accelerator

3.1 Introduction

The rapid emergence of drug-resistant malaria parasites in the field presents a major challenge to global disease eradication efforts and highlights the need for treatment strategies that retain efficacy long-term[4,132]. In 2012, the Malaria Drug Accelerator (MalDA) Consortium convened with the primary goal of accelerating the early antimalarial drug discovery process by delivering new druggable targets and hit-to-lead programs[133]. MalDA has employed at scale one particularly successful forward genetics strategy for identifying mechanisms of resistance and their relationship to specific drug targets: *in vitro* evolution and whole genome analysis, reviewed in [112]. Often, mutations identified in these evolution experiments affect the compound's ability to bind to its molecular target or localize to its site of action, yielding key insights into mechanism of action (MOA) and facilitating drug development efforts. This method also helps uncover potential resistance liabilities for a given compound or target prior to rigorous clinical development. For example, *in vitro* selections with the clinical candidate DSM265[43] generated highly resistant mutants with the same allelic changes in *dhodh* that were identified in recrudescent parasite samples isolated from Phase 2a clinical trial patients (see **Chapter 2**)[125,134].

One key challenge in these kinds of experimental evolution experiments and most other forward genetics approaches lies in distinguishing variants that drive the observed phenotype from passengers. Genetic validation in the form of CRISPR/Cas9 editing of the mutations into a naïve background can be used to confirm links between genotype and phenotype, but methods remain costly and technically challenging in the *Plasmodium* parasite, especially when applied at scale[135].

In 2018, MalDA published findings from a genome analysis of 235 drug-resistant parasite clones which identified key resistance mediators and several drug target-inhibitor pairs[58]. Here, we present an updated sequencing repository including all drug selections performed to date within the MalDA Consortium as well as the application of our genome analysis pipeline to other publicly available selection datasets. In total, we compiled and assessed the genotypes and phenotypes from 665 compound-selected *P. falciparum* parasite samples, which to our knowledge represents the largest *in vitro* dataset of its kind in the malaria parasite. In addition to analyzing the selections piecemeal for insights into specific compound MOAs and resistance liabilities, we applied systematic and statistical approaches across the entire drug selection dataset to more effectively characterize the main drivers of resistance in malaria at the genomic level. Strikingly, we find that known multidrug resistance mechanisms arise in selections with 50% of the compounds in the dataset, highlighting their importance in drug development efforts.

3.2 Results

3.2.1 The malaria parasite evolves resistance to many different chemotypes

The 113 small molecules used successfully in selection experiments have demonstrated potent antiparasitic activity in at least one human-relevant *Plasmodium* life stage, as determined by phenotypic screening with cell-based assays[136,137,138] (**Supplemental Table 3.1**). Most compounds were sourced by the Medicines for Malaria Venture (MMV) (https://www.mmv.org). Sequencing data from all previously published MalDA selections were also included in the study[58,139,140], and here we present new sequencing information for 29 compounds. Sequencing information for parasite samples

with evolved resistance to 24 additional antimalarial compounds were downloaded from the NCBI Sequence Read Archive (https://www.ncbi.nlm.nih.gov/sra) or acquired through direct correspondence with the senior author(s) of published work. These compounds include the gold-standard antimalarial drug Artemisinin[141]; the benzoxaboroles AN13956, AN13762, AN10248[63,142,143]; the triazolopyrimidine analog series including DSM1[48,119], DSM265, and DSM267[43,134]; the imidazolopiperazine GNF179[104,144,145]; halofuginone, a synthetic derivative of the natural quinazolinone alkaloid febrifugine[146]; the boronate human proteasomal inhibitor Bortezomib[147]; the pantothenamide CXP18.6-052[148]; the dihydroisoquinolones SJ733, SJ247, and SJ279[11]; the 2,6-disubstituted quinoline-4-carboxamide compound DDD107498[38]; the antitubercular clinical candidate SQ109[149,150]; the peptide vinyl sulfones WLL-vs and WLW-vs[151]; the primary sulfonamide glycoside PS-3[152]; the bis-1,2,4-triazine compound MIPS-0004373[153]; MMV019313[69]; the trisubstituted imidazole MMV030084[154]; the 3-Hydroxypropanamidine compound 22[155]; and the pyrazolopyrimidine sulfamate ML901[156].

3.2.2 Building a repository of mutations that constitute the antimalarial resistance landscape

Drug selections with these 113 compounds yielded 665 clones or bulk parasite populations that were subsequently sequenced through next-generation methods (**Supplemental Table 3.2**). To identify the genomic determinants of resistance, we utilized a bioinformatic approach wherein mutations from the drug-sensitive parent line were subtracted from the mutations in the drug-resistant lines. Altogether, we identified 3,129 SNVs and 2,098 INDELs that had evolved over the course of the selection process

(**Supplemental Table 3.3**). We further filtered mutations by whether they occurred in what is considered "core genome," the ~90% of the *P. falciparum* genome which generally sequences to high coverage and produces unambiguous alignments, or the "non-core" genome, which includes more problematic hypervariable and subtelomeric repeat regions that are often involved in antigenic variation and do not contribute to drug resistance[157]. Of the 5,227 original SNVs and INDELs, 2,481 were called within genic regions of the core genome (47%), 714 mutations were in regions of the non-core genome (14%), and 2,032 mutations were intergenic (39%). Copy number variants (CNVs) were also assessed, as they have been previously shown to play a significant role in drug resistance phenotypes[58]. A total of 1,135 CNVs were identified in the dataset, occurring for 75 different compounds and in 325 resistant samples.

To better assess our set of mutations for roles in observed drug resistance phenotypes, we also sought to take advantage of multiple systems-level datasets available for *Plasmodium spp*. First, we imported gene essentiality data from the Plasmodium Genetic Modification (PlasmoGEM) *P. berghei* genetic knockout screen[158,159] as well as the *P. falciparum* genome-wide piggyBAC saturation mutagenesis screen performed by Zhang *et al*.[160]. Essentiality is a requirement for drug target candidates in pathogens[161,162] and can also indicate that the encoded protein plays an important functional role in parasite growth and proliferation. We next imported stage-specific, single-cell transcriptional data from the Malaria Cell Atlas[163,164]. This dataset is complementary to previous MalDA work uncovering stage-specificity of certain antimalarial inhibitors[165]. Finally, we assessed whether mutations fell within annotated

InterPro domains[166,167] and supplied Gene Ontology (GO) terms for each gene[168,169] to yield insights on their involvement in various cellular processes and area of localization.

3.2.3 Mutations in validated targets of the MalDA portfolio can inform drug development efforts

Table 3.2 summarizes mutations in 17 chemically validated *Plasmodium* drug targets under investigation within the MalDA Consortium[170], and for which there are corresponding resistance selections. Of the 69 independent amino acid positions mutated across these 17 target proteins, 67 of them are localized to an annotated InterPro domain[166,167], suggesting that proximity to protein structural features are informative of overall functionality of any given variant. The location of these mutations can inform structure-guided design of next-generation antimalarials by providing insight into key residues in the catalytic domains of target proteins. Notably, all of these target-encoding genes are considered essential by at least one of essentiality screen (with exception to *cytb*, which is mitochondrially encoded and cannot be tested)[158,159,160].

3.2.4 Codifying a computational framework for the prioritization of potential functional variants

To better classify whether variants identified in compound selections were likely or unlikely to drive the resistance phenotype, we utilized a frequency-based statistical approach to identify mutations that were unlikely to have occurred at high frequency purely by chance (**Figure 3.1A**). Using the hypergeometric distribution, we identified 33 core genes that were unlikely to have been observed by chance, with *pi4k*, a well-known

antimalarial drug target[61], achieving the highest level of significance (mutated 48 times, $p = 1.09 \times 10^{-71}$) (**Table 3.1**). Importantly, a large proportion of these 33 genes have been extensively validated as being antimalarial drug targets or resistance mechanisms.

In addition to high-frequency observations, low-frequency events across the dataset – genes that are observed very rarely – are also of potential interest. Variants that are functional with respect to the resistance phenotype but that do not readily occur are promising if the goal is to identify small molecule inhibitors that are unlikely to rapidly generate resistance when under clinical development. It could be that the parasite does not tolerate mutation of certain genes unless under extreme selection conditions such as those applied in the *in vitro* evolution system. There were 424 core genes that were only mutated once across the entire dataset. For these singletons, it is important to consider whether the mutations reside in a conserved protein domain or a known binding site and whether the gene is a transporter/membrane protein or a homolog of a known resistance gene. One such example is the MMV006901-selected singleton E515Q SNV in PF3D7_0527200, which encodes USP14, the de-ubiquinating enzyme (DEB) ubiquitin carboxyl-terminal hydrolase 14. DEBs have long been considered potential therapeutic targets, including in cancer[171]. When mapped into a homology model using SWISS-MODEL[172], E515Q clearly resides in the catalytic domain which has been shown to bind small molecule inhibitors[173,174] (**Figure 3.1B**). Structural considerations are therefore incredibly important when determining whether a mutation is likely functional.

3.2.5 Multidrug resistance mechanisms are a liability for half of the compounds in the dataset and can readily co-occur in single selections

Multidrug resistance (MDR) often involves mutation of transporters, such as those belonging to the ATP-binding cassette (ABC) protein family or the major facilitator superfamily (MFS)[175]. Generally, MDR is associated with an overall decrease in intracellular drug accumulation through increased efflux, decreased uptake, or both[176]. Though less common, MDR can also be caused by loss-of-function mutations in enzymes that activate prodrugs, one example being the prodrug activation and resistance esterase, PfPARE (PF3D7_0709700)[177]. **Table 3.3** summarizes the mutations that were identified in known multidrug mechanisms, as well as the compounds that selected for them. Assessing the entire dataset, we find that these well-validated multidrug resistance mechanisms were observed 288 times in 240 total clones (36%) and arise in selections with 57 compounds (50%).

As expected, multidrug resistance protein 1 (*mdr1*), which confers resistance to multiple drug classes through both SNVs[178,179] and CNVs[180] was the most frequently observed mutated resistance gene across the full sequencing dataset. In total, we observed 29 SNVs (probability of enrichment by chance, $p = 6.81 \times 10^{-35}$) and 122 CNVs (91 amplifications and 31 de-amplification events) across *mdr1*. A total of 36 compounds showed *mdr1* involvement, highlighting the importance of this single resistance gene.

In the case of MMV006901, a small molecule containing the quinoline scaffold, 4 known multidrug resistance mechanisms were observed in a single selection (*mdr1*, *abci3*, *aat1*, and *mrp2*) (**Figure 3.2A**). 3 of these mutated genes have been previously implicated in resistance to certain quinolines[181,182,183,184], with the exception of *abci3*[165,185]. Interestingly, MMV084864, which also contains the quinoline scaffold, yielded resistant parasites with some combination of *abci3* amplification, *mdr1* deamplification, an INDEL

in a putative magnesium transporter (PF3D7_0827700), and a Ser94Phe mutation in *crt* (**Figure 3.2B**). Together, these data highlight the ability of the parasite to utilize a number of strategies of multidrug resistance even in the context of a single compound and selection.

3.3 Discussion

Here, we present the collated sequencing information of 665 compound-resistant parasite lines in database format, representing the largest interactive *in vitro* selection dataset of its kind for the malaria parasite, and likely all eukaryotic pathogens. We provide the individual resistance profiles of 113 structurally distinct compounds in the antimalarial drug development pipeline, spanning a large subset of the entire chemical space currently being investigated for the treatment of this deadly disease. In addition to identifying potential drug targets and resistance mediators for single selections, we identified patterns that emerged across the entire dataset.

One key finding was that almost all mutations that have been identified in chemically validated antimalarial drug targets were localized to important functional domains of the protein. These mutations and their resulting protein conformational effects could prove useful for the structure-guided design of novel inhibitors that can (1) more selectively bind to the target molecule or (2) neutralize the effect of commonly-selected resistance mutations altogether. Moreover, the knowledge that these variants occur in defined, well-structured protein domains can also inform the prioritization of potential functional variants that do not reach statistical significance across the dataset by frequency-based calculations. A singleton mutation occurring in the catalytic domain of a protein is of high interest for follow-up experiments with CRISPR-Cas9. Given the

resource-intensive nature of genetic manipulation techniques in *Plasmodium*, it is imperative that there exists a strong justification for pursuing any given variant in a list of hundreds of candidate genes/variants.

Another striking finding across the dataset is the prevalence of multidrug resistance mechanisms. Given the relative ease at which the parasite can acquire these types of mutations, it is alarming indeed that half of the compounds tested in our study resulted in multidrug resistance mechanism involvement. This suggests that cross-resistance testing against these major resistance mediators should be an early step of the antimalarial drug development pipeline in order to ensure that only compounds with low resistance propensities are developed further.

3.4 Materials and Methods

3.4.1 Parasite strain information

P. falciparum 3D7 is a mostly drug-sensitive line, although it is resistant to sulfadoxine and contains an amplification of GTP cyclohydrolase[186]. The 3D7-A10 clone has been used by MalDA in previous drug selection and sequencing efforts[58]. Dd2 is a multi-drug resistant line originating from an Indochina III/CDC isolate which contains a mutant pfcrt sequence and amplifications in pfmdr1 and GTP cyclohydrolase that confer resistance to mefloquine, lumefantrine, and pyrimethamine[187]. Dd2-B2 is a genetically homogenous line that was cloned from Dd2 by limiting dilution[188] in the Fidock Lab. The Dd2-polδ line is a Dd2 strain that was genetically modified at the DNA polymerase δ subunit (Asp308Ala and Glu310Ala) to knock out proofreading function and increase

accumulation of mutations over successive replication events[189,190]. W2 is an Indochinese chloroquine-resistant line and 7G8 is a line resistant to chloroquine, amodiaquine, and pyrimethamine[191,192,193].

3.4.2 *In vitro* evolution of compound-resistant parasites

P. falciparum parasites were cultured in RPMI1640 media supplemented with 0.5% Albumax II, 4.3% human serum, 25 mM Hepes, 25 mM NaHCO3, 0.36 mM hypoxanthine, and 100 ug/mL gentamicin. Cultures were maintained in leukocyte-depleted red blood cells at 2.5% hematocrit and incubated at 37°C in an atmosphere of 3% O2, 4% CO2, and 93% N2. Resistant parasites were generated using either a high-pressure pulse, step-wise, or constant method of compound exposure as previously described[58]. Cultures were maintained under selection conditions until they demonstrated a reproducible EC50 fold-shift of at least 3x, at which point parasites were cloned in 96-well plates by limiting dilution[188].

Compound EC_{50} was assessed in dose-response format using a SYBR Green-I based cell-proliferation assay as previously described[136]. Parasites were incubated for 72 hours in 96-well plates with exposure to the compound of interest in a 12-point dilution series. An artemisinin dilution series was conducted in parallel as a positive control. Following the incubation, parasites were lysed, DNA was stained using SYBR Green fluorescence and I was measured at 535 nm on an Envision plate reader (Perkin Elmer, Waltham, MA) after excitation at 485 nm. Dose-response curves were fitted and log(EC_{50}) values calculated using Prism (Graphpad Prism, La Jolla, CA). EC_{50}

fold-shift changes were calculated by comparing EC_{50} of the resistant clones to that of the corresponding compound-sensitive parent line.

3.4.3 Next-generation sequencing and analysis

Genomic DNA (gDNA) was obtained from parasite samples by washing infected RBCs with 0.05% saponin and isolating using the DNeasy Blood and Tissue Kit (Qiagen) following standard protocols. Sequencing libraries were prepared by the UCSD Institute for Genomic Medicine (IGM) Genomics Center using the Nextera XT kit (Cat. No FC-131-1024, Illumina) with 2ng input gDNA and standard dual indexing. Libraries were sequenced on the Illumina HiSeq 2500 (PE100, RapidRun mode) or the Illumina NovaSeq6000 (S4 200, PE100).

Sequencing reads were aligned to the *P. falciparum* 3D7 reference genome (PlasmoDB v13.0) and pre-processed following standard GATK version 3.5 protocols[194,195]. SNVs and INDELs were called with GATK HaplotypeCaller and filtered to retain high-quality variants. SNV calls were retained if they met the following criteria: ReadPosRankSum >8.0 or <-8.0, QUAL<500, Quality by Depth (QD) <2.0, Mapping Quality Rank Sum <-12.5, and filtered depth (DP) <7. INDELs were retained if they met the following criteria: ReadPosRankSum <-20, QUAL<500, QD<2, and DP<7. Allele fraction cutoffs for alternate alleles were ≥0.35 for bulk samples and ≥0.90 for clonal samples. Functional annotation of variants was carried out using SnpEff[196] and a custom database built with the 3D7 GFF downloaded from PlasmoDB (https://plasmodb.org/plasmo/app). Mutations that were considered background (native

to the drug-sensitive parent) were removed, leaving a list of only high-quality mutations that had evolved over the course of the drug selection process.

CNVs were detected by calculating denoised log2 copy ratios across gene intervals through the GATK 4.0 CNV pipeline. We constructed two separate panels of normals for Dd2 and 3D7, using 30 independently derived and sequenced parent clones of each genetic background. Read counts for each sample were calculated across a predefined gene interval list where intergenic regions and the highly variable antigenic var, rifin, stevor, and surfin genes[197,198,199] were removed. Following denoising against the strain-matched panel of normals, log2 copy ratios were calculated for each gene interval. CNVs were retained if at least 4 sequential genes showed a denoised log2 copy ratio of at least 0.6. In the case of *mdr1* in Dd2 samples, we retained CNVs with a copy ratio of at least 0.4, indicating acquisition of at least one additional copy on top of the two *mdr1* copies already native to the strain.

3.4.4 CNV detection by quantitative real-time PCR

For relative copy number quantification by real-time PCR, assays were performed in a CFX96 Touch Deep Well Real-Time PCR System (Bio-Rad Laboratories) with PowerUp SYBR Green master mix (2X) (ThermoFisher). Triplicate samples were run in parallel in 96-well plates with a total reaction volume of 20µl comprised of 0.25ng/µl genomic DNA and 0.3µM of each primer. The qPCR conditions were: 2 min at 50°C, 5 min at 95°C, followed by 40 cycles of 15s at 95°C, and 1 min at 60°C. Target gene copy number for each of the test genes was assessed relative to the control gene, ß-tubulin (PF3D7_1008700). Ct values for each gene of interest were averaged and normalized

against ß-tubulin within each clone (ΔCt), then each gene of interest was normalized against corresponding genes in the non-selected parent background (ΔΔCt). Fold expression was calculated using the formula: $2^{-\Delta\Delta Ct\ 200}$.

3.5 Acknowledgements

Chapter 3 contains unpublished material co-authored with Elizabeth A. Winzeler. The dissertation author was the primary author of this chapter.

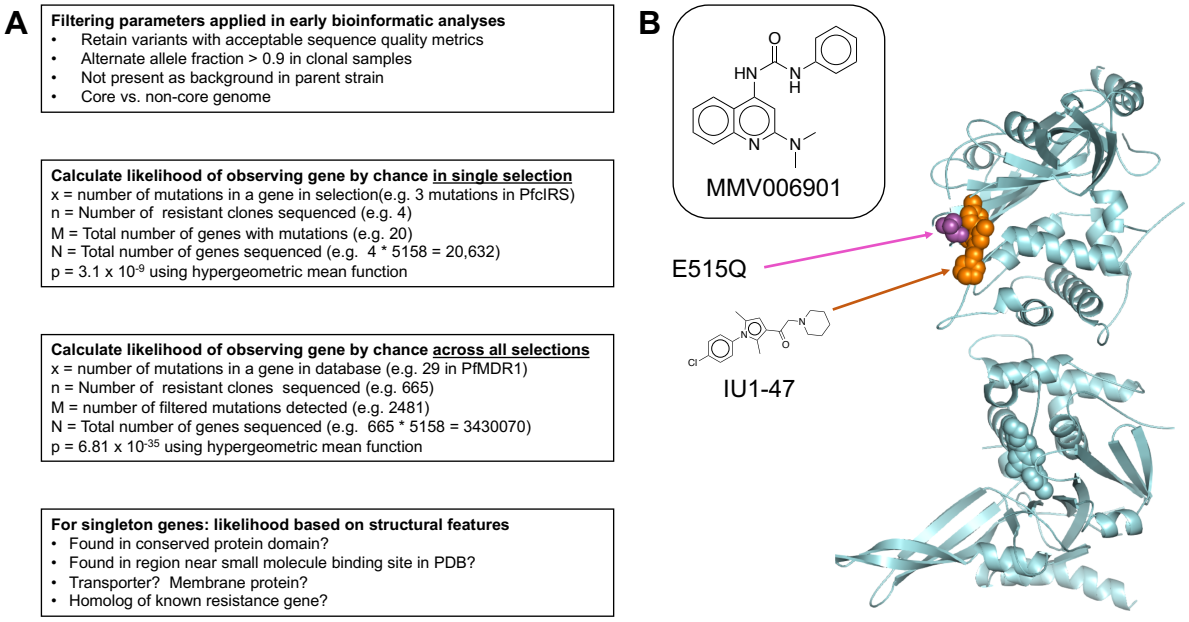

Figure 3.1. Schematic of framework for prioritizing potential functional variants. (A) Variants are first filtered according to quality and genome characteristics. The remaining variants are then assessed by high-frequency and low-frequency events. High-frequency events are those that are not expected to have occurred purely by chance, as calculated by the hypergeometric mean function. Singleton events, which would not be considered significant by this metric but may still be functionally important, are further assessed by structural characteristics. (B) Example of a singleton mutation located in a structurally important region of the protein. The E515Q SNV in ubiquitin carboxyl-terminal hydrolase 14 (PF3D7_0527200), found in a single clone selected with MMV006901, is mapped onto a homology model of the USP14 catalytic domain bound to the inhibitor IU1-47[174], and is shown to reside within the binding pocket.

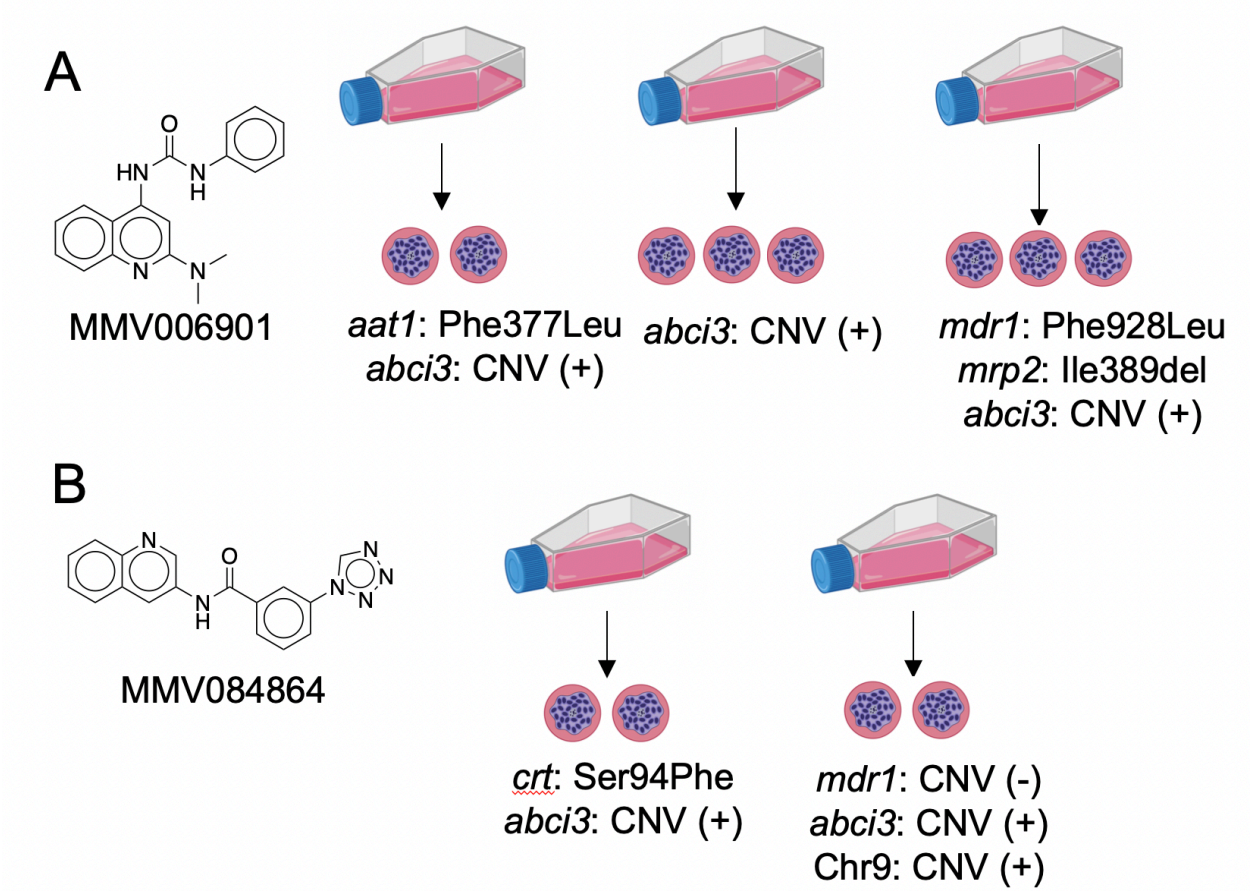

Figure 3.2. Examples of multidrug resistance mechanisms co-occurring in selections with the same small molecule. (A) Selections with the quinoline-scaffold-bearing molecule MMV006901 yielded parasite clones that harbored mutations in 4 well-validated multidrug resistance genes: *aat1*, *abci3*, *mdr1*, and *mrp2*. (B) The quinoline compound MMV084864 generated resistant parasites with co-occurring mutations in *crt*, *abci3*, and *mdr1*.

Table 3.1. Mutations identified in select genetically and chemically validated *Plasmodium* falciparum drug targets. Previously unpublished compounds and/or mutations are shown in **bold**. (**) This mutation was discovered during reanalysis of previously published results.

Target Gene	Compound(s)	Mutation(s)
ncr1	MMV019662 MMV028038 MMV009108	F1436I; S490L A1208E; M398I; A1208V; I402T A1108T
cphers	BRD1095 BRD3444	L550V; M316I; G512E; V545I L550V; M316I; G512E; V545I
asnrs	**OSM-S-106**	**R487S; CNV**
dhfr-ts	MMV027634	G378E; I403L; H551N
pi4k	MMV024038 MMV673482 **MMV010545** KAI407 Sapanisertib	CNV Y1356N; L1418F **I1354M** H1484Y; S743F; S743Y E1236D; Y1356C
dhodh	DSM1 DSM265 DSM267 MMV1454442	CNV C276Y; L531F; CNV F227Leu; F531Phe F188I; CNV
acs	CXP18.6-052 MMV019721 MMV084978	T627A A597V A652; Y607C; A597V
pfk9	PS-3	R860G; L513Q
dpap1	MMV029272	L437S; L415P; N62H
fpps/ggpps	MMV019313	**M259I****, S228T
ftb	MMV019066	A515V; A515T; Y837N
atp4	KAE609 GNF-Pf-4492 MMV020623 SJ733	D1247Y; P990R; T418N; I398F A211T; I203L; P990R; A187V L369F; A187V V415D; L350H; P412T; P966S; P966T
rfc4	ACT-451840	S42T
vapA	SQ109	Q225K; R353K
cyto-irs	**MMV1091186** **TCMDC-124553** **MMV1081413**	**N269K; E180Q** **C502Y; V500A; S288I; E180D** **W395L**
krs2	**cladosporin**	**CNV**
cytb	Atovaquone DDD01061024 MMV008149 MMV1427995 MMV1432711	M133V; L144S; F267V V259L Y126C; G131S R95K Y126C; V259L

Table 3.2. Genes that achieve statistical significance across the dataset. The Bonferroni-corrected p-value was calculated from the hypergeometric mean function and indicates the probability that the number of mutations observed occurred by chance.

Gene Name	Gene Description	# of Mutations	Bonferroni-corrected *p*-value
PF3D7_0509800	phosphatidylinositol 4-kinase	48	1.09843E-71
PF3D7_1211900	non-SERCA-type Ca2+ -transporting P-ATPase	46	1.28362E-67
PF3D7_1222600	AP2 domain transcription factor AP2-G	31	1.5133E-38
PF3D7_0523000	multidrug resistance protein 1	29	6.80972E-35
PF3D7_0709700	prodrug activation and resistance esterase	28	4.3311E-33
PF3D7_0109800	phenylalanine--tRNA ligase alpha subunit	20	2.70631E-19
PF3D7_0603300	dihydroorotate dehydrogenase	18	4.76525E-16
PF3D7_0627800	acetyl-CoA synthetase	18	4.76525E-16
PF3D7_1332900	isoleucine--tRNA ligase	18	4.76525E-16
PF3D7_0312500	major facilitator superfamily-related transporter	17	1.84098E-14
PF3D7_0321900	cyclic amine resistance locus protein	17	1.84098E-14
PF3D7_0709000	chloroquine resistance transporter	17	1.84098E-14
PF3D7_1036800	acetyl-CoA transporter	17	1.84098E-14
PF3D7_0107500	Niemann-Pick type C1-related protein	16	6.70414E-13
PF3D7_1238800	acyl-CoA synthetase	16	6.70414E-13
PF3D7_1447900	multidrug resistance protein 2	14	7.34024E-10
PF3D7_1451100	elongation factor 2	14	7.34024E-10
PF3D7_0404600	conserved *Plasmodium* membrane protein, unknown function	12	6.04738E-07
PF3D7_0613800	AP2 domain transcription factor	12	6.04738E-07
PF3D7_0609100	zinc transporter ZIP1	11	1.5395E-05
PF3D7_0909700	FHA domain protein	11	1.5395E-05
PF3D7_1008700	tubulin beta chain	11	1.5395E-05
PF3D7_1417400	rap guanine nucleotide exchange factor, pseudogene	11	1.5395E-05
PF3D7_0914700	major facilitator superfamily-related transporter	10	0.000358562
PF3D7_1131400	conserved *Plasmodium* protein, unknown function	10	0.000358562
PF3D7_1229100	multidrug resistance-associated protein 2	10	0.000358562
PF3D7_0211500	GAF domain-related protein	9	0.007577354
PF3D7_0629500	amino acid transporter AAT1	9	0.007577354
PF3D7_0804500	conserved *Plasmodium* membrane protein, unknown function	9	0.007577354
PF3D7_0908800	mitochondrial carrier protein	9	0.007577354
PF3D7_0915000	type II NADH:ubiquinone oxidoreductase	9	0.007577354
PF3D7_1011400	proteasome subunit beta type-5	9	0.007577354
PF3D7_1250200	CSC1-like protein	9	0.007577354

Table 3.3. Mutations in genetically validated multidrug resistance mediators. Previously unpublished compounds and/or mutations are shown in **bold.**

Multidrug Resistance Gene	Compound(s)	Mutation(s)
mfr3	GNF-Pf-3600	G146R; S16R; D150V
	MMV085203	C401Y; S519*; Q487E; N279fs
abci3	**BI-2536**	**CNV**
	MMV006767	CNV
	MMV020746	R2180P/G; L690I
	MMV023367	CNV
	MMV029272	CNV
	MMV024114	CNV
	MMV407834	**H2181L; CNV**
	MMV665939	R2180P; Y2079C; CNV
	MMV675939	CNV
	MMV006901	**CNV**
	MMV084864	CNV
carl	GNF179	E834K
	GNF452	M81I; L830V
	GNF707	L830V; E834D
	MMV007564	L1136P; L833I; L1073Q
	MMV907364	**Q821H; E1066V; S1076N; S1134R; L1142I**
aat1	**MMV006901**	**F377L**
	MMV007224	N134dup
	MMV011895	F230L
	MMV668399	V185L; K238N; P380S
crt	MMV006767	A138V; S65R
	MMV011895	K76Q
	MMV023388	**Ter425S_ext***
	MMV024114	S90N
	MMV084864	**S94F**
	MMV665928	**Q352R**
pare	AN13762	L82*; S94R; M1?; G58C; G206E; P223fs
	AN13956	S195*; H304Y
	MMV011438	N346Y; Y91fs; I353S; L323H; L357P; I353fs; Q139*
	MMV023949	**N200dup**
	Pepstatin n-butyl ester	L323H; L357P; I353fs; Q139*
mrp2	Atovaquone	A403P; N1974fs
	GNF707	D976N
	MMV006901	**I389del**
mdr2	MMV665789	K840Asn
	PS-3	L183*
	Suloctidil	**S451F**

Table 3.3. Mutations in genetically validated multidrug resistance mediators, Continued.

mdr1	ACT-451840	M841I; A807T; G316R
	BCH070	CNV
	BI-2536	**F78L; G293C; N1042I; CNV**
	GNF452	CNV
	GNF707	CNV
	GNF-Pf-5310	Y290F
	GNF-Pf-5611	**CNV**
	GNF-Pf-5660	CNV
	GNF-Pf-5668	Y290F
	Lopinavir	**I205F; G293V; CNV**
	MIPS-0004373	CNV
	MMV006901	**F928L**
	MMV023367	CNV
	MMV026596	F806L
	MMV000570	**CNV**
	MMV007181	**CNV**
	MMV008149	CNV
	MMV009108	CNV
	MMV009063	CNV
	MMV019017	CNV
	MMV084864	CNV
	MMV1427995	CNV
	MMV665785	**CNV**
	MMV665789	CNV
	MMV665882	CNV
	MMV665928	**CNV**
	MMV982556	**L917F**
	NEU1029	**CNV**
	NITD609	CNV
	OSM-S-106	**CNV**
	Pepstatin n-butyl ester	CNV
	Sapanisertib	CNV
	Suloctidil	**CNV**

Chapter 4

Artemisinin selections in *T. gondii* identify alternative mechanisms of drug activity compared to *Plasmodium*

4.1 Introduction

Toxoplasma gondii is a widespread parasite of animals that also frequently causes zoonotic infections in people. Serological testing suggests that approximately one-third of the world's human population is chronically infected[201], although such infections are typically well controlled by the immune response following mild clinical symptoms in the acute phase[202]. Chronic infections are characterized by semi-dormant tissue cysts containing a stage of the life cycle called the bradyzoite, which divides asynchronously and sporadically[203]. Current therapies, and induction of a potent immune response, are insufficient to clear these stages and instead they undergo slow turnover to sustain infection over time. Reemergence of chronic infection in patients that are immunocompromised results in serious disease[204,205], especially when this occurs in the central nervous system where tissue cysts most often occur in neurons[206]. Toxoplasmosis is also a threat due to risk of congenital infection, especially in resource-limited regions[207]. More severe disease has been reported in some regions of South America, where infections are associated with ocular disease in otherwise healthy individuals[208]. Treatment of toxoplasmosis is typically provided by antifolates using a combination of pyrimethamine-sulfadiazine or trimethoprim-sulfamethoxazole, although pyrimethamine has also been used in combination with clindamycin, azithromycin, and atovaquone (also used as monotherapy)[209]. Because infections are not commonly transferred from human to human, with the exception of congenital infections that do not occur serially, emergence of drug resistance is rarely a problem, although several examples of clinical failure have been reported such as in patients given atovaquone as a monotherapy[210,211].

Combination therapies including artemisinin (ART) are the first line of treatment against malaria[212]. Since their original discovery, a wide variety of analogs have been made to improve solubility and other drug-like properties, including artemether, artesunate, and dihydroartemsinsin[213]. ARTs are fast acting and effective across multiple life cycle stages; however, they have short half-lives *in vivo* and hence must be coupled with longer-lasting partner drugs, which reduces the risk of resistance arising[212]. ART derivatives share an endoperoxide bond that is essential for activity, as shown by the fact that the deoxyartemisinin derivative loses antimalarial activity[214]. More recently, completely synthetic analogs containing a similar ozonide group have been developed and some of these have increased half-lives *in vivo*[215]. ART analogs are also effective in blocking growth of *T. gondii in vitro*[216,217,218] and controlling infection *in vivo* in murine models of toxoplasmosis[219,220]. Although analogs show similar potency ranking, they are effective against *T. gondii* at~50-fold higher concentrations when compared to *Plasmodium falciparum*[218,221]. This major difference in sensitivity may result from the fact that *P. falciparum* digests hemoglobulin in the food vacuole, thus releasing heme in high concentrations[222]. Although most of the heme is detoxified into a crystalline form called hemozoin, the presumption is that elevated reduced iron (Fe^{2+}) is present in the food vacuole. Although the exact mechanism is unknown, it is thought that free Fe^{2+} activates the endoperoxide bond[223], resulting in formation of adducts to a variety of protein and lipid targets that result in parasite death[224,225]. There is no analogous process to hemoglobin digestion in *T. gondii*, which may thus explain its lower sensitivity to ART. Instead, it is possible that heme derived from sources such as the mitochondria plays an important role in activating ART in *T. gondii*, similar to yeast and tumor cell models.

Treatment failure in *P. falciparum* patients treated with ART in Southeast Asia is associated with delayed clearance rather than a shift in EC50, and this phenotype is monitored using a ring-stage survival assay (RSA)[226]. Laboratory selection of ART-resistant *P. falciparum* lines lead to identification of mutations in a Kelch13 (K13) ortholog, which can confer resistance when expressed in a wild-type background, and similar mutations are found in high abundance in Southeast Asia[227,228]. Several mechanisms have been proposed to explain the role of K13 in ART resistance, including an enhanced cell stress response leading to upregulation of the unfolded protein response, decreased ubiquitination, and increased cell survival[3]. Consistent with this model, inhibitors of the proteasome synergize with ART[82,229]. However, other studies have reported the development of delayed clearance or dormancy phenotypes in *P. falciparum*-infected patients without associated K13 mutations[230,231]. Furthermore, genetic crosses between parasite lines bearing sensitive vs. resistant K13 mutations demonstrated a correlation with the RSA assay *in vitro* but not with clearance of blood infection following treatment of infected *Aotus* monkeys, suggesting other mechanisms are responsible *in vivo*[232]. It has also been proposed that ART inhibits phosphoinositol 3-kinase (PI3K), and that K13 mutations that confer resistance lead to increased PI3K activity and increased inositol triphosphate and membrane vesicles that may confer protection to ring stages[233]. In a separate study of *in vitro* selection for evolved resistance, mutations were identified in a number of genes, including the actin-binding protein coronin, changes that were shown to confer ART resistance[234]. In summary, it seems evident that a number of distinct mechanisms can lead to decreased sensitivity of *P. falciparum* to ART, thus complicating tracking of the development of resistance in the field.

ART derivatives have also been promoted as potential treatment for cancer as they are active against a wide variety of tumor cells *in vitro* and a number of specialized analogs have been synthesized[235]. The activities of the common ART derivatives against tumor cell lines are in the low micromolar range, comparable to *T. gondii* but much higher than what is typically observed against *P. falciparum*. The mechanism of action of ART against tumor cells is also uncertain, but it has been linked to oxidative stress, DNA damage, decreased cell replication, and activation of cell death pathways, including apoptosis[236,237]. Studies in Baker's yeast (*Saccharomyces cerevisiae*) implicate the mitochondria as a target of ART, and consistent with this model, growth on fermentable carbon sources results in insensitivity as the mitochondria is dispensable under these conditions[238]. Treatment of yeast with ART results in mitochondrial membrane depolarization, leading to the suggestion that ART is activated by the electron transport system, thus leading to oxidative stress and membrane damage[239]. Inhibition of mitochondrial function in tumor cells treated with ART derivatives has also been shown to promote cell death due to apoptosis[240]. In human tumor cells, it is proposed that mitochondrial heme activates the endoperoxide group of ART and interaction with the electron transport chain generates reactive oxygen species leading to cell death[241].

Here we sought to use the versatility of *T. gondii* as a genetic system to explore potential mechanisms of resistance to ART. Previous studies have shown that ART resistance can be selected in chemically mutagenized *T. gondii* parasites[242], although the molecular mechanism for the modest shift in EC50 observed in these resistant clones has not been defined. Chemical mutation introduces numerous changes in the genome, confounding analysis of those that might confer resistance. Consequently, we used a

natural evolution process to select for mutations that would confer increased survival in ART, while monitoring the background mutation rate in the absence of selection in parallel. Whole genome sequencing identified several single nucleotide variants (SNVs) that arose in the resistant populations and reached fixation over time. Reverse genetic approaches based on CRISPR/Cas9 gene editing were used to show that these mutations confer increased survival, despite the fact that they do not alter EC50 values. These findings define molecular changes associated with ART resistance in *T. gondii*, which may be informative for understanding mechanism of action of this important class of compounds.

4.2 Results

4.2.1 Estimating the background mutation rate in *T. gondii*

Prior to selecting for resistant parasites, we wanted first to establish the background mutation rate of *T. gondii* during a continuous *in vitro* passage under standard laboratory conditions. Because lines that have been passed for years in the laboratory are likely a mixture of genotypes that contain both private and shared SNVs, as well as potential copy number variations (CNVs), we first cloned the starting population by limiting dilution on monolayers of human foreskin fibroblasts (HFF cells). We obtained clones from the common laboratory RH strain, referred to as 5D and 12B lines, and grew them by sequential passage in HFF cells for the duration of 365 days, subculturing them every 2 to 3 days (**Figure 4.1A**). During *in vitro* passage in this format, the total population parasite size of a given culture expands to ~2×10^7 over a timeframe of 2 to 3 days. The

population is then reduced by 1:10 or 1:20 when a fraction of the growing culture is used to inoculate a new flask of previously uninfected HFF cells. At the time points of 182 and 365 days, separate subclones from the growing populations were isolated by limiting dilution, and these were named with the prefix of the parental line followed by a clone designation (**Figure 4.1A**). Genomic DNA was extracted from all 12 of these clones and subjected to whole genome sequencing using Illumina technology. In parallel, we also sequenced the genomic DNA of the parental strains. The short reads obtained by Illumina sequencing were mapped with high stringency to the reference genome of the ME49 strain of *T. gondii* (https://toxodb.org/toxo/) using a specially developed pipeline. We then compared the frequency of reads that identified SNVs between the reference parental clones (i.e., 5D and 12B) from the subclones that were obtained from these lines following passage. Overall the number of mutations detected in the clones were quite low, with a range from 0 to 8 SNVs seen in each clone (**Supplemental Tables 4.1 and 4.2**).

Analysis of the frequency of SNVs was used to derive approximate rates of mutation based on the assumption that the parasite doubles approximately every 6 hours (4 generations per day)[243] and that the composite genome is roughly 6.5×10^6 bp[244]. We calculated the rates for mutation in individual clones assuming that the mutants arose spontaneously, and that the rates of mutation and growth were constant during the course of the experiment. Based on these calculations, the average rates over the course of the 365-day culture period was 6.62×10^{-11} mutations per base pair per generation for the 5D clones and 4.71×10^{-11} mutations per base pair per generation for the 12B clones. We also estimated the composite mutation rate for both sets of clones by treating the frequency of SNVs as mutants in a classic fluctuation analysis yielding a combined rate

of 5.79×10^{-11}. Since both methods give highly similar rates, we used the latter value of 5.8×10^{-11} for subsequent analysis.

In comparing the types of mutations found in each of the lines, there was approximately an equal number of variants found in coding and noncoding regions (19 coding vs. 13 noncoding in 5D and 10 coding vs. 13 noncoding in 12B). However, within coding regions, there was a marked increase in nonsynonymous mutations vs. synonymous mutations with a nonsynonymous/synonymous (dN/dS) ratio of 2.8 for all of the clones derived from 5D and dN/dS ratio of 9 for all of the clones derived from 12B. These high dN/dS ratios suggest strong selective pressure during the culture, although these clones were grown under standard laboratory conditions. In addition, there were some mutations that had apparently reached fixation as they were common to multiple clones from a particular line. For example, in clones from the 12B line, there was a missense mutation in a hypothetical protein that was found in all 6 clones. Similarly, in clones from line 5D, there were 2 frameshift mutations in hypothetical proteins, 1 missense mutation in a hypothetical protein, and 1 intronic mutation that occurred in multiple clones.

4.2.2 Establishment of ART-resistant mutants of *T. gondii*

Based on the background mutation rate, we designed an experimental protocol using sequential *in vitro* culture of relatively large parasite populations in combination with stepwise increases in drug concentrations to derive parasites with elevated ART tolerance. To initiate this trial, we re-cloned the 5D line to derive 2 parental lines, designated as B2 and F4 (**Figure 4.1B**), and cultured them in HFF cells supplemented

with 8μM ART as a starting point for selecting parasite populations (**Figure 4.1A**). Although growth was initially delayed, as evident from the time required to lyse the host cell monolayer, after 122 days of sequential passage at 8μM ART both lineages exhibited reproducible growth and rapidly lead to lysis of the monolayer within 2 to 3 days of inoculation. At this time point, we cryopreserved each line for future study; these lines are referred to as F4_ART8 and B2_ART8 (**Figure 4.1B**). We then increased the ART concentration by 2-fold to 16μM and continued to passage both lines with drug until attaining the phenotype of reproducible growth and infectivity, which took ~120 days. At this time point, we cryopreserved each line for future study; these lines are referred to as F4_ART16 and B2_ART816 (**Figure 4.1B**). We then increased the concentration of ART to 100μM and passaged the lines for an additional 100 days, after which they showed normal growth. At this stage, we generated subclones from each of the F4 and B2 lines by limiting dilution (**Figure 4.1B**).

4.2.3 Identification of candidate genes associated with ART resistance

To determine the extent of resistance that had developed during selection, we tested the 8-μM and 16-μM populations from both the F4 and B2 lines across a dilution series of ART and calculated their EC50 for growth inhibition. The evolved populations showed an~3- and~6-fold increase in EC50 in the 8-μM and 16-μM resistant populations, respectively (**Figure 4.1C**). To analyze genetic changes that might have conferred enhanced ART resistance, genomic DNA from all 3 of the selected populations (i.e., 8, 16, and 100μM from both clones) was extracted and subjected to whole genome sequencing. Mapping of the reads to the reference genome was used to identify changes

from the parental lines that showed altered alleles due to nonsynonymous mutations in the selected populations. Several of the changes were only detected in 1 of the 2 selected lines. For example, mutations were identified in 2 candidate genes in selected lines derived only from the B2 line and in 4 candidate genes derived only from the F4 line (**Table 4.1**). The majority of these changes were also only found at the highest level of selection (i.e., 100μM ART), where they were present with allele frequencies of >90% (**Table 4.1**). However, because they were not common to both lines, we did not pursue them further, although it is possible that they contributed to the observed ART-resistance phenotypes observed here.

In addition, we detected nonsynonymous changes in 2 genes that were common to the ART-resistant populations derived from both lines. The first of these was in the gene TGME49_290840, which is annotated in ToxoDB as a serine protease (**Table 4.1**). It has high similarity to DegP in *P. falciparum* and is referred to here as a DegP2 ortholog. The DegP2 ortholog studied here is different from a previously named DegP-like serine protease that is localized in the rhoptry of *T. gondii*[245]. We consider TGME49_290840 to be the more likely mitochondrial DegP2 ortholog based on the presence of a DegP-htrA superfamily motif and detection in the mitochondrial proteome[246]. Moreover, a recent study in *T. gondii* reported that this gene is localized to the mitochondrion and it can be deleted without major loss of fitness[247]. The *T. gondii* DegP2 ortholog was mutated in a different position in each of the F4 and B2 lines, although both non-conservative mutations resided in the PDZ2 domain (DegP2-F4-E821Q and DegP2-B2-G806E) (**Table 4.1**). The frequency of the mutated DegP2 alleles was 50% and 68.08% in F4 and B2 8-μM populations, respectively, and these rose to 84% and 98.61% in the 16-μM

populations, respectively (**Table 4.1**). The second gene identified in both clones is TGME49_239420, which is annotated in ToxoDB as a serine/threonine protein kinase with similarity to calmodulin-dependent and myosin light-chain kinases. Because its function is unknown in *T. gondii*, it is referred to here as ART resistance kinase 1 (Ark1). The mutations in Ark1 occurred at the same site, which resides in the hinge region of the ATP binding pocket, with a different non-conservative substitution in each lineage (Ark1-F4-C274R and Ark1-B2-C274F). Mutations appeared in Ark1 in 70.58% of the reads in the B2 8-μM population but 4.1% mutant allele reads in the 8-μM population from the F4 line (**Table 4.1**). However, in the 16-μM populations Ark1 mutated alleles reached 90% and 100% abundance in F4 and B2 16-μM populations, respectively. The frequency of mutations in both genes increased to 100% in the 100-μM ART-selected populations from both the B2 and F4 lines.

4.2.4 Validation of the DegP and Ark1 mutations in conferring ART tolerance

To establish a functional link between the identified mutations and ART resistance, we used a CRISPR/Cas9-based marker-less genome editing strategy to introduce nonsynonymous SNVs into the endogenous loci of the wild-type parental line[248] (**Figure 4.2A**). Two pairs of mutations were created to simulate mutations identified in the B2 and F4 resistant lines, respectively. Each set consisted of clones with single mutants in DegP2, single mutants in Ark1, and double mutants of both DegP2 and Ark1. Initially, we combined the DegP2 G806E and Ark1 C274F mutations seen in the F4 line, either alone or together. We then constructed similar mutants based on the DegP2 E821Q and Ark1 C274R mutations seen in B2. The point mutations were introduced into a wild-type

RHΔku80 line expressing firefly luciferase (FLUC), so that we could use a luciferase-based growth assay to monitor growth more precisely. The correct mutations were confirmed by restriction enzyme digestion followed by Sanger sequencing of an amplicon flanking the mutated residue. Surprisingly, introduction of any single- or double-point mutation combinations from either lineage resulted only in a slight increase in EC50, ranging from 1.2- to 1.6-fold (**Figure 4.2B and C**). Hence, introduction of the single- or double-point mutations seen in the original resistant populations does not recapitulate their phenotypes shown in **Figure 4.1C**. One explanation for these results could be the existence of additional mutations that are needed to confer the full level of ART resistance seen in the original populations. However, there were no other mutations found in common (**Table 4.1**). Additionally, when we analyzed the genomic sequences of B2 and F4 lines grown at 100μM ART and their respective clones, we also did not detect any additional novel mutations in coding regions that were common to both lineages (**Table 4.1 and Supplemental Tables 4.3 and 4.4**). It is also evident from analysis of the SNVs in these selected lines that the background rate of mutation is 2- to 3-fold higher, and a number of these are found in a majority of clones, albeit typically not in coding regions (**Supplemental Tables 4.3 and 4.4**). Analysis of the mutation frequency in these clones, including those mutations in DegP2 or Ark1, gave a rate of 1.39×10^{-10} for the B2 clones (**Supplemental Table 4.3**) and 9.77×10^{-11} for the F4 clones (**Supplemental Table 4.3**).

To further characterize the role of these mutations in ART resistance, we performed a growth competition assay *in vitro* under pressure of ART. In these assays an equal number of wild-type and mutant parasites were co-cultured in the presence of 16μM ART or in vehicle DMSO as a control. When grown in the presence of ART, the mixture

of parasites exhibited a slight delay before lysing the monolayer at day 3 vs. the normal day 2 time period. When these parasites were passed onto a fresh HFF monolayer in the presence of ART, they exhibited a growth crash, with variable times of recovery that were dependent on the strains present in culture. Cultures containing DegP2 mutant parasites were the slowest, with a recovery time of ~11 days. Cultures containing Ark1 mutants exhibited shorter recovery times, ranging between 6 and 8 days. The double mutants in both lineages consistently showed the fastest recovery time, ranging between 5 and 6 days.

To analyze the proportion of the wild-type vs. mutant strains at the initial inoculation and after the recovery from the ART-induced growth crash, genomic DNA was extracted at both timepoints and the respective loci were PCR-amplified and analyzed by Sanger sequencing (**Figure 4.3A**). Remarkably, all single-point mutants and their double-mutant combinations reproducibly out-competed the wild-type parental strain by the end of the culture period in the presence of ART (**Figure 4.3B and C**). Of note, while both DegP2 point mutants showed fitness defect when co-cultured with the wild-type strain under control conditions, they were superior to the wild-type in the presence of ART. Furthermore, this growth defect was rescued in the double mutant containing Ark1 mutations in addition to DegP2 mutations (**Figure 4.3B and C**).

4.2.5 Analysis of *in vitro* ART selections in *P. falciparum*

To understand the genetic basis of the ART resistance phenotype in *Plasmodium* and how it differs from that of *T. gondii*, we acquired the raw sequencing information for 2 clonal parasite lines, termed 6A-R and 11C-R, which had been selected at the clinically

relevant concentration of 900nM ART[249] for a period of 474 days[141]. Compared to their corresponding parental lines, 6A-R and 11C-R demonstrated up to a 398- and 69-fold increase in $IC50_{10hpi/4hr}$, respectively, in a ring-stage survival assay (RSA)[226]. We next applied our whole genome sequencing analysis pipeline for *Plasmodium* (see **Section 3.4.3**) to identify mutations that were present in the ART-selected lines that were not present in the non-selected parent lines, which might explain the ART resistance phenotype.

A total of 5 core genome mutations were identified in 6A-R, while 11C-R contained 7 core genome mutations, with no commonly mutated genes shared between either of the two independently derived lines (**Table 4.2**). Of the 11 genes, only one has been previously implicated in ART resistance *in vitro*, the hemoglobinase cysteine proteinase falcipain 2a (PF3D7_1115700)[227,250]. 5 additional genes have been observed at least once in our other *in vitro* drug selections in *Plasmodium* (see **Chapter 3**): a conserved protein with unknown function (PF3D7_1345400); a putative lipase (PF3D7_1427100); an AP2 domain transcription factor (PF3D7_0420300); a TBC-domain containing protein (PF3D7_1230000); and a conserved membrane protein of unknown function (PF3D7_1324300), meaning a total of 6 genes are unique to ART selections only (**Table 4.2**). CNV analysis reconfirmed the reported amplified genomic segments in 6A-R on chromosome 14 which spanned 40 contiguous genes (PF3D7_1454000-PF3D7_1458000) 6A-R and in 11C-R on chromosome 12 which spanned 9 contiguous genes (PF3D7_1228000-PF3D7_1228800)[141].

Of potential note, the conserved protein of unknown function (PF3D7_0528300), which acquired a P249H mutation, is classified by PANTHER[251] as a BTB-domain-

containing protein. The BTB/POZ domain is primarily found at the N terminus of zinc finger proteins[252], and interestingly, is also one of the three highly conserved protein domains found in Kelch13[228,253]. While most of the mutations previously identified in Kelch13 are localized to the Kelch-repeat beta-propeller domain, a recent study identified a single mutation in the BTB/POZ domain which was then confirmed to drive the observed ART resistance phenotype[254]. While the precise functional contribution of each of the 11 genes to the ART resistance phenotype remains unclear, what is striking is the diversity of genes that were mutated; this includes genes involved in membrane composition/function, transcriptional and translational regulation, and response to oxidative stress. There was no obvious overlap in the genes identified in *P. falciparum* versus those identified in *T. gondii*, but what does appear to be similar is that both ART resistance phenotypes appear to be multigenic in nature and largely tied to how each parasite mounts a stress response when exposed to the drug.

4.3 Discussion

We took advantage of flexible *in vitro* culture systems and genetic tools available in *T. gondii* to evolve lines that were resistant to ART and compared the results to an ART selection performed in *P. falciparum*. In parallel, we determined the background mutation rate after long-term passage in the absence of intentional selection. Surprisingly, spontaneous mutations showed a strong bias for nonsynonymous changes that in some cases were present at a very high frequency among separate clones, suggesting strong positive selection during normal culture. Passage in ART led to enhanced resistance at the population level and whole genome sequencing of the ART-resistant lines identified

several non-conserved SNVs in the coding sequences of DegP2, a serine protease, and Ark1, a serine/threonine kinase of unknown function. We engineered these point mutations into a wild-type background using CRISPR/Cas9 and confirmed that they confer a competitive advantage in the presence of ART, despite not altering the EC50 value for growth inhibition. In contrast, the ART-resistant lines, which had a shift in EC50, also showed up-regulation of heme-containing cytochromes encoded in the mitochondrial genome, consistent with previous studies suggesting a mitochondrial target for ART. Collectively, our studies define mechanisms of mutation that lead to ART resistance, including point mutations in specific genes and alterations in mitochondrial function.

Analysis of the frequency of mutations in clones of *T. gondii* that were grown under standard laboratory conditions led to several surprising findings. First, the rate of apparent mutation in *T. gondii* was relatively low, at ~5.8×10^{-11} mutations per base pair per generation, which is ~30-fold lower than that estimated for *P. falciparu*m (1.7×10^{-9})[255]. Second, we observed a high level of nonsynonymous relative to synonymous mutations in coding regions, indicating that strong selection is operating under these conditions. Previous studies examining SNVs between different lineages of the RH strain that were passaged for an unknown number of doublings in different laboratories also reported elevated dN/dS ratios that ranged from 2 to 10[256]. Studies conducted on the model organism *Escherichia coli* have shown that strong selective pressures exist even under homogeneous conditions and that spontaneous mutations often contribute to fitness advantage and reach fixation[257]. In the present study, we did not evaluate the fitness of the mutations that reached fixation in non-selected lines, although the high dN/dS ratio is

more consistent with improved growth characteristics vs. potential bottlenecks during passage.

To test the importance of mutations in DegP2 and Ark1, we engineered point mutations into a wild-type background using CRISPR/Cas9. Somewhat surprisingly, these introduced point mutations did not shift the EC50 to a similar extent, as seen in the original evolved resistant clones. However, both point mutations did enhance fitness over the wild-type background in a competition assay. This outcome is similar to the phenotype seen in *P. falciparum* K13 mutations, where "resistant" lines show improved survival in the RSA but do not exhibit a shift in the EC50[226]. The differences in EC50 shift between the evolved lines and the engineered clones may relate to additional background mutations in each of the lines or differences in transcription that were not examined here. In this regard, it would be informative to revert these mutations in the evolved resistant mutants to determine to what extent they are required for the enhanced resistance. The mechanisms by which point mutations in DegP2 and Ark1 confer enhanced survival to ART in *T. gondii* are unclear, as previous mutations have not been observed in similar targets in other systems. The mutations seen in *T. gondii* Ark1 occur in the hinge region of the kinase, a critical spot for ATP binding, suggesting they might affect catalytic activity. The substrates of Ark1 are presently unknown and its role in the biology of the parasite has not previously been explored, although it has a fitness score in a genome-wide CRISPR screen that would suggest it is essential (−3.77)[258]. DegP2 is a member of the high-temperature requirement A family (HtrA) and it is a periplasmic protease in *E. coli*[259]. In bacteria, DegP is involved in protective stress responses to aid survival at high temperatures[259], a phenotype also reported in yeast[260]. Htr orthologs in eukaryotes are

typically found in the mitochondria where they function in quality control[261]. Given the role of DegP in stress responses, it may play a similar to K13 in ART resistance in malaria, where mutations in K13 propeller domains have been linked to altered stress responses[3].

Our findings provide support for several previously suggested mechanisms of ART resistance and also make several new predictions about the frequency and consequences of mutation in *T. gondii*. First, we identify point mutations that confer enhanced survival in the presence of ART without shifting the EC50 in a classic resistance phenotype. Second, similar to *P. falciparum*, the mechanism of resistance to ART in *T. gondii* appears to be multigenic and may have a link to altered stress responses. Third, although the low intrinsic mutation rate in *T. gondii* may limit the potential for drug resistance to arise in the clinic, our finding that mutational drift occurs readily in the absence of purposefully applied selection predicts that mutations that may alter phenotypes are likely to accumulate during normal laboratory passage. Collectively, these processes may also drive evolution and affect the occurrence of drug resistance and other biological traits *in vivo*.

4.4 Materials and Methods

4.4.1 Parasite and Cell Culture

The type I *T. gondii* strain RH-88, transgenic lines were reported previously RHΔhxgprtΔku80[262] or were developed here. *T. gondii* tachyzoites were maintained in HFF monolayers cultured and purified, as described previously[248]. All strains and host

cell lines were determined to be mycoplasma negative using the e-Myco pluskit (Intron Biotechnology).

4.4.2 Parasite Transfection

Following natural egress, freshly harvested parasites were transfected with plasmids, using protocols previously described[263]. In brief, ~2×10^7 extracellular parasites were resuspended in 370µL cytomix buffer were mixed with ~30µL purified plasmid or amplicon DNA in a 4-mm gap BTX cuvette and electroporated using a BTX ECM 830 electroporator (Harvard Apparatus) using the following parameters: 1,700 V, 176-µs pulse length, 2 pulses, 100-ms interval between pulses. Transgenic parasites were isolated using a FACS Aria II (BD Biosciences) FACS on the basis of Cas9-GFP fluorescence or by outgrowth under selection with pyrimethamine (3µM) or 5-fluorodeoxyuracil (10µM), as needed. Stable clones were isolated by limiting dilution on HFF monolayers grown in 96-well plates.

4.4.3 Plasmid Construction and Genome Editing

All CRISPR/Cas9 plasmids used in this study were derived from the single-guide RNA (sgRNA) plasmid pSAG1:CAS9-GFP, U6:sgUPRT[264] by Q5 site-directed mutagenesis (New England Biolabs) to alter the 20-nt sgRNA sequence, as described previously[265]. Separate sgRNA plasmids were made for editing mutations in DegP2 (i.e., pSAG1:CAS9-GFP, U6:sgDegP2G806E; pSAG1:CAS9-GFP, U6:sgDegP2[G821Q]) and Ark1 (i.e., pSAG1:CAS9-GFP, U6:sgArk1). To introduce point mutations into endogenous

genes, we used a marker-less genome editing strategy: CRISPR/Cas9 combined with a repair template.

4.4.4 *In Vitro* Growth Assays

Lactate dehydrogenase release. To assess ART sensitivity of the original resistant mutant clones, growth was monitored over a 10-point dose–response curve based on lactate dehydrogenase (LDH) release from the HFF monolayer. Briefly, parasites (100μL per well) were added to HFF cells grown in a 96-well plate that contained 100μL of 2×ART concentration (to achieve 1× final ART concentration in 200μL total well volume containing 0.1% DMSO) and allowed to replicate for 48 hours. Parasite growth was quantified by measuring LDH release from host cells as a consequence of rupture, as described previously[266]. Supernatants were collected after 48 hours and LDH measured using the CytoTox 96 assay (Promega) according to the manufacturer's instructions. Values were normalized to total lysis (100%) and uninfected (0%).

Luciferase assay. To assess the ART sensitivity of the engineered point mutant strains, growth was monitored over a 10-point dose–response curve using luciferase activity. Briefly, luciferase-expressing parasites (100μL per well) were added to HFF cells grown in a 96-well plate that contained 100μL of 2×ART concentration (to achieve 1× final ART concentration in 200μL total well volume containing 0.1% DMSO) and allowed to replicate for 72 hours prior to measuring luciferase activity. Briefly, culture medium was aspirated and replaced with 40μL of 1× passive lysis buffer (1×PLB, Promega, E1531) and incubated for 5 min at room temperature. Luciferase activity was measured on a

Cytation 3 (BioTek) multimode plate imager using the following protocol: Inject 100μL of luciferase assay reagent, shake 1 s, and read 10 s post-injection.

Data were analyzed using Prism (GraphPad) to determine EC50 values by plotting normalized, log-transformed data (x-axis), using nonlinear regression analysis as a sigmoidal dose–response curve with variable slope. The EC50 data are presented as the average of 3 biological replicates (i.e., separate EC50 titrations) each with 3 technical replicates (i.e., separate wells).

4.4.5 Growth Competition Assays

Parental and point-mutant parasites were inoculated at 1:1 ratio into T25 flasks of confluent HFFs with or without ART (16μM). Following growth for several days and natural egress, cultures were passed into a fresh T25 flask at a dilution of 1:10 or 1:20. Parasite cultures growing in the presence of ART exhibited growth crash upon second passage. Parallel cultures of the mixture of wild-type and mutant lines were serially passaged with no drug treatment. Parasite genomic DNA was extracted at the starting time point and after the recovery from the ART-induced growth crash. The target loci were amplified by PCR and analyzed by Sanger sequencing. QSVanalyser[267] was used for the analysis of DNA sequence traces for estimation of the relative proportions of the wild-type and mutant variants.

4.4.6 Genome Sequence Analysis, Variants, and Mutation Rates

Sequencing. Parasite DNA was extracted from *in vitro* cultures using QIAamp DNA blood kits (Qiagen). Integrity of genomic DNA was determined on an Agilent Tapestation. An aliquot of 1 μg of gDNA as determined by Qubit assay was sonicated to an average

size of 175 bp. Fragments were blunt ended using T4 DNA Polymerase, Klenow DNA Polymerase, and T4 polynucleotide kinase. Then, the fragments were modified to contain an "A" base to 3' end with Klenow (3′→ 5′ exo-) and ligated to Illumina's sequencing adapters with T4 DNA ligase. Half of the ligated fragments underwent amplification for 8 cycles incorporating a unique indexing sequence tag with VeraSeq DNA Polymerase. All enzymes were purchased from QIAGEN. The resulting libraries were normalized and sequenced using the Illumina HiSeq-3000 as paired end reads extending 150 bases from both ends of the fragments. Illumina's bcl2fastq utility was used to demultiplex the samples. Sequencing reads were deposited in the Sequence Read Archive repository at NCBI, SRA accession: PRJNA575881.

*SNV analysis***.** Reads were aligned to the *T. gondii* ME49 reference genome (ToxoDB release 41) using BWA-mem[268] and further processed using Picard Tools (http://broadinstitute.github.io/picard/). SNVs and INDELs were called using GATK HaplotypeCaller, then filtered based on GATK recommendations[194]. Briefly, SNV calls were retained if they met the following criteria: ReadPosRankSum >8.0 or <-8.0, QUAL<500, Quality by Depth (QD) <2.0, Mapping Quality Rank Sum <-12.5, and filtered depth (DP) <7. INDELs were retained if they met the following criteria: ReadPosRankSum <-20, QUAL<500, QD<2, and DP<7. Mutations were annotated with a custom SnpEff[196] database built from a GFF file. Variants were further filtered by removing mutations that were present in the both parent strain and evolved strains, such that mutations were only retained if they arose during the course of long-term culturing for neutral mutation rate experiments or the drug selection process for artemisinin-pressured lines. Manual inspection of the resulting SNVs was used to remove polymorphisms where the read

depth for a majority of clones was below the cutoffs stated above, since correct assignment of genotypes was ambiguous in many of these cases.

*Statistical analysis of mutation rate by whole genome sequencing***.** The mutation rate was calculated based on the number of SNVs identified in each of the subclones from the unselected 5D and 12B lines sampled at 182 or 365 days. For these calculations, we assumed that the growth rate and mutation rate are constant across the experiment. We also assumed that the observed mutations (SNVs) are an accurate measure of the mutation rate across the experiment. The equation used for calculating the mutation rate μ was:

$$\mu = m / (N*t/g)$$

where m = the number of SNVs, N = the genome size of 65,464,221 bp[244], t = time of growth in days and g = the number of doubling per day (assumed to be 4 here[243]). Identical mutation that were observed in more than one clone were only counted once. We calculated the average mutation rate for the 365-day clones from the individual clones for the two separate lines. We also estimated the mutation rate by treating the whole genome sequencing results for all unselected clones from the 56D and 12B series as a fluctuation analysis scoring the number of SNVs (mutations) for each of the clones over 728 doublings equal to 182 days of culture (for clones sampled at 365 days the number of SNVs was halved to allow direct comparison), under the assumption that the mutants have equal fitness to the wild type. Mutation rates were calculated using bz-rates[269] based on equations that have been described previously[270].

4.5 Acknowledgements

Chapter 4 is a partial, modified reprint of the material as it appears in Proceedings of the National Academy of Sciences, 2019. Alex Rosenberg, Madeline R. Luth, Elizabeth A. Winzeler, Michael Behnke, and L. David Sibley, “Evolution of resistance *in vitro* reveals mechanisms of artemisinin activity in *Toxoplasma gondii*”. The dissertation author was second author on this paper and performed all sequencing analysis. Additional unpublished analyses of ART-resistant *Plasmodium falciparum* parasites are also included and were performed by the dissertation author.

Figure 4.1. Generation of ART-resistant parasite populations. (A) Schematic for growth of parasites used to determine the background mutation rate. Two initial RH88 strain clones (5D and 12B) were sequentially passed in T25 flasks containing HFF monolayers every 48 h. The clones were subcloned by limiting dilution at 182- and 365-day time points. The genomes of the parental strain clones (5D and 12B) and the various subclones were sequenced using Illumina technology. (B) Schematic for selection of ART-resistant parasites. The parasite clone (5D) was further subcloned into 2 lines (F4 and B2) and subjected to 8 μM ART during sequential in vitro passages. The ART concentration was increased to 16 μM and 100 μM at the intervals shown. Populations were frozen for further analysis at the 8- and 16-μM levels and clones (a–e) were made after passage in 100 μM. (C) Dose–response curves for inhibition of *T. gondii* parental and ART adapted B2 and F4 lines growth in response to increasing concentration of ART. Parasite was monitored by measurement of LDH release from host cells as a consequence of rupture. Data presented as percent LDH release (% LDH) normalized to growth in naïve (untreated) HFF cells. Shown are 3 biological replicates each with technical replicates (n = 9) ±SE. EC50 values were determined using non-linear regression analysis as a sigmoidal dose–response curve with variable slope. The EC50 data are presented as the average of 3 biological replicates (i.e., separate EC50 titrations), each with 3 technical replicates.

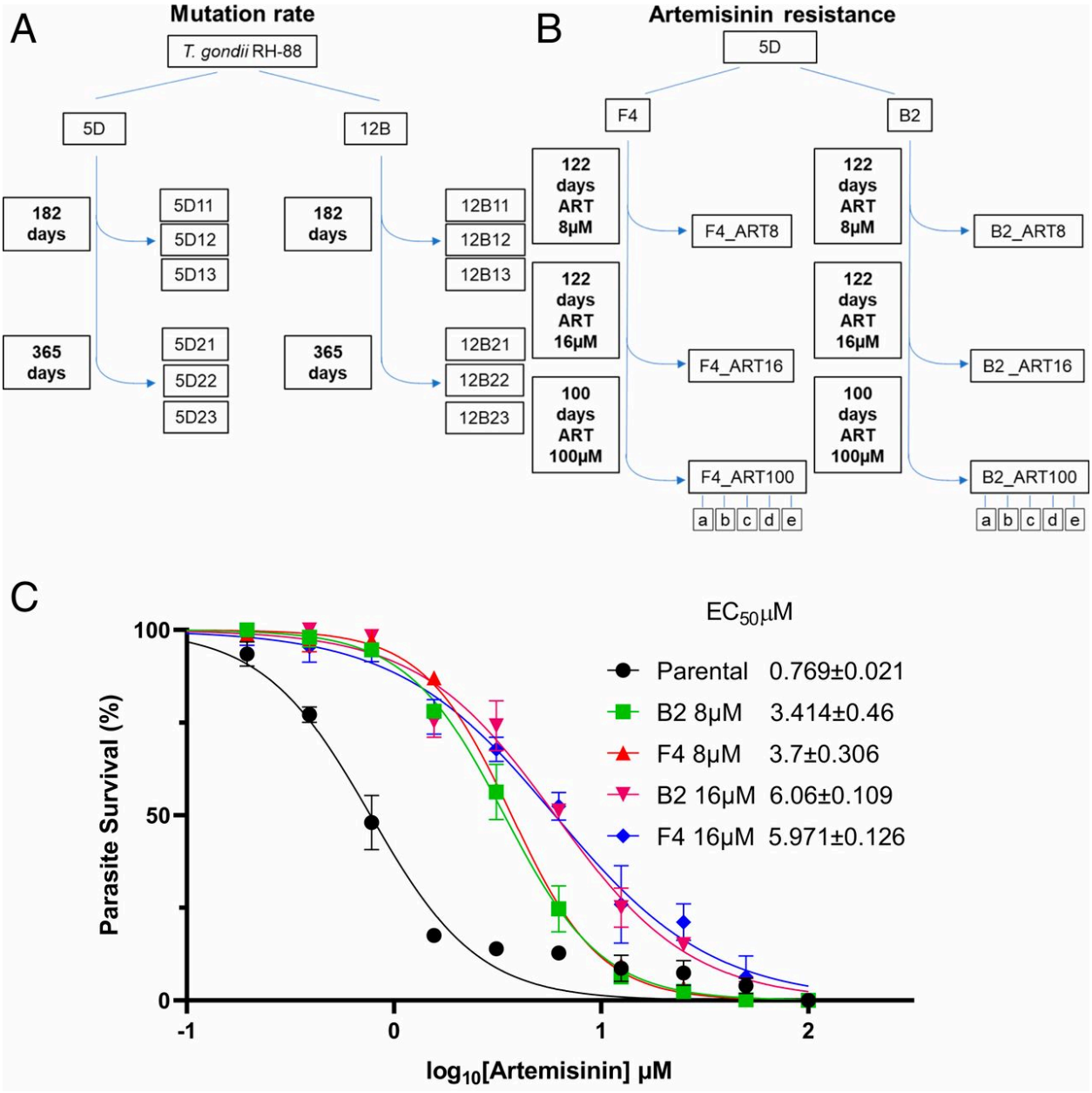
A
Mutation rate
T. gondii RH-88
5D
12B
182 days
365 days
5D11
5D12
5D13
5D21
5D22
5D23
12B11
12B12
12B13
12B21
12B22
12B23
B
Artemisinin resistance
5D
F4
B2
122 days ART 8μM
122 days ART 16μM
100 days ART 100μM
F4_ART8
F4_ART16
F4_ART100
B2_ART8
B2 _ART16
B2_ART100
a b c d e
C
EC50μM
Parental 0.769±0.021
B2 8μM 3.414±0.46
F4 8μM 3.7±0.306
B2 16μM 6.06±0.109
F4 16μM 5.971±0.126
Parasite Survival (%)
100
50
0
-1
0
1
2
log10[Artemisinin] μM

Figure 4.2. Effect of ART on growth of wild-type *T. gondii* and engineered lines containing point mutations in candidate genes. (A) Schematic illustration of the marker-less CRISPR/Cas9 genome-editing strategy used to introduce mutations into the T. gondii chromosome for candidate genes. The scheme depicts introduction of the C274R mutation into the Ark1 gene. The wild-type allele is C274, while the mutant is C274R. CRISPR DSB, targeted Cas9 double-stranded break; HR, homologous recombination. Transformants were isolated by FACS for GFP expression followed by single-cell cloning and confirmation of the editing by diagnostic PCR and sequencing. (B and C) A dose–response curves for inhibition of T. gondii wild-type and point mutant tachyzoites growth in response to increasing concentration of ART. Parasite clones were inoculated in 96-well plates containing HFF cells and growth was monitored by measurement of luciferase activity after 72 h of incubation with different concentrations ART. Data presented as percent relative light units (% RLU) normalized to growth in naïve (untreated) HFF cells. Shown are 3 biological replicates each with technical replicates (n = 9) mean ± SE. EC50 values were determined using nonlinear regression analysis as a sigmoidal dose–response curve with variable slope. The EC50 data are presented as the average of 3 biological replicates (i.e., separate EC50 titrations), each with 3 technical replicates.

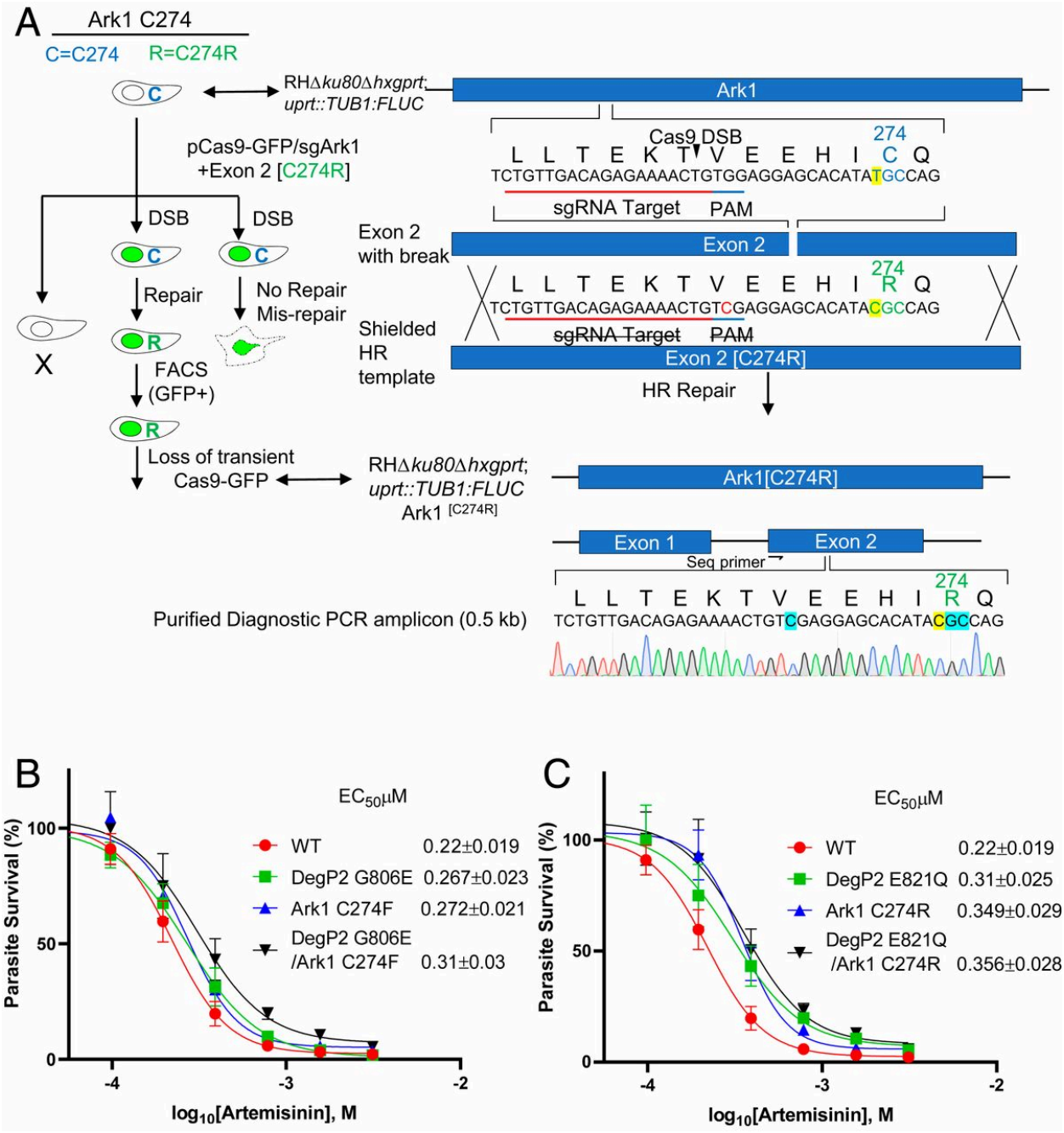
A
Ark1 C274
C=C274 R=C274R
RHΔku80Δhxgprt;
uprt::TUB1:FLUC
Ark1
pCas9-GFP/sgArk1
+Exon 2 [C274R]
Cas9 DSB
274
L L T E K T V E E H I C Q
TCTGTTGACAGAGAAAACTGTGGAGGAGCACATATGCCAG
sgRNA Target
PAM
DSB
DSB
Exon 2
with break
Repair
No Repair
Mis-repair
274
L L T E K T V E E H I R Q
TCTGTTGACAGAGAAAACTGTCGAGGAGCACATACGCCAG
Shielded
HR
template
sgRNA Target
PAM
Exon 2 [C274R]
X
FACS
(GFP+)
HR Repair
Loss of transient
Cas9-GFP
RHΔku80Δhxgprt;
uprt::TUB1:FLUC
Ark1 [C274R]
Ark1[C274R]
Exon 1
Exon 2
Seq primer
274
L L T E K T V E E H I R Q
TCTGTTGACAGAGAAAACTGTCGAGGAGCACATACGCCAG
Purified Diagnostic PCR amplicon (0.5 kb)
B
EC50μM
WT 0.22±0.019
DegP2 G806E 0.267±0.023
Ark1 C274F 0.272±0.021
DegP2 G806E
/Ark1 C274F 0.31±0.03
Parasite Survival (%)
100
50
0
-4
-3
-2
log10[Artemisinin], M
C
EC50μM
WT 0.22±0.019
DegP2 E821Q 0.31±0.025
Ark1 C274R 0.349±0.029
DegP2 E821Q
/Ark1 C274R 0.356±0.028
Parasite Survival (%)
100
50
0
-4
-3
-2
log10[Artemisinin], M

Figure 4.3. Growth competition assays between wild-type and the point mutant strains. (A) Schematic for growth competition assay. Parental and point-mutant parasites were inoculated at 1:1 ratio (5×10^5 parasites of each strain) into T25 flasks of confluent HFFs with or without ART 16 μM. After natural egress, parasites were passed by a dilution of 1:10 to 1:20 into a fresh T25 flasks containing confluent HFF cells. Parallel cultures without drug treatment were serially passaged throughout the duration of the experiment. Toxoplasma genomic DNA was extracted at the starting time point and after the recovery from the ART induced growth crash. The mutated loci were amplified by PCR and analyzed by Sanger sequencing. DNA sequence traces were used to estimate the relative proportions of sequence variants for wild-type and mutant alleles. (B and C) DNA sequence trace results for analysis of the ratio of wild-type and the point mutants. Two different competition assays are shown: (B) DegP2 G806E or Ark1 C274F vs. the combined double mutant and DegP2 G821Q or (C) Ark1 C274R vs. the combined double mutant.

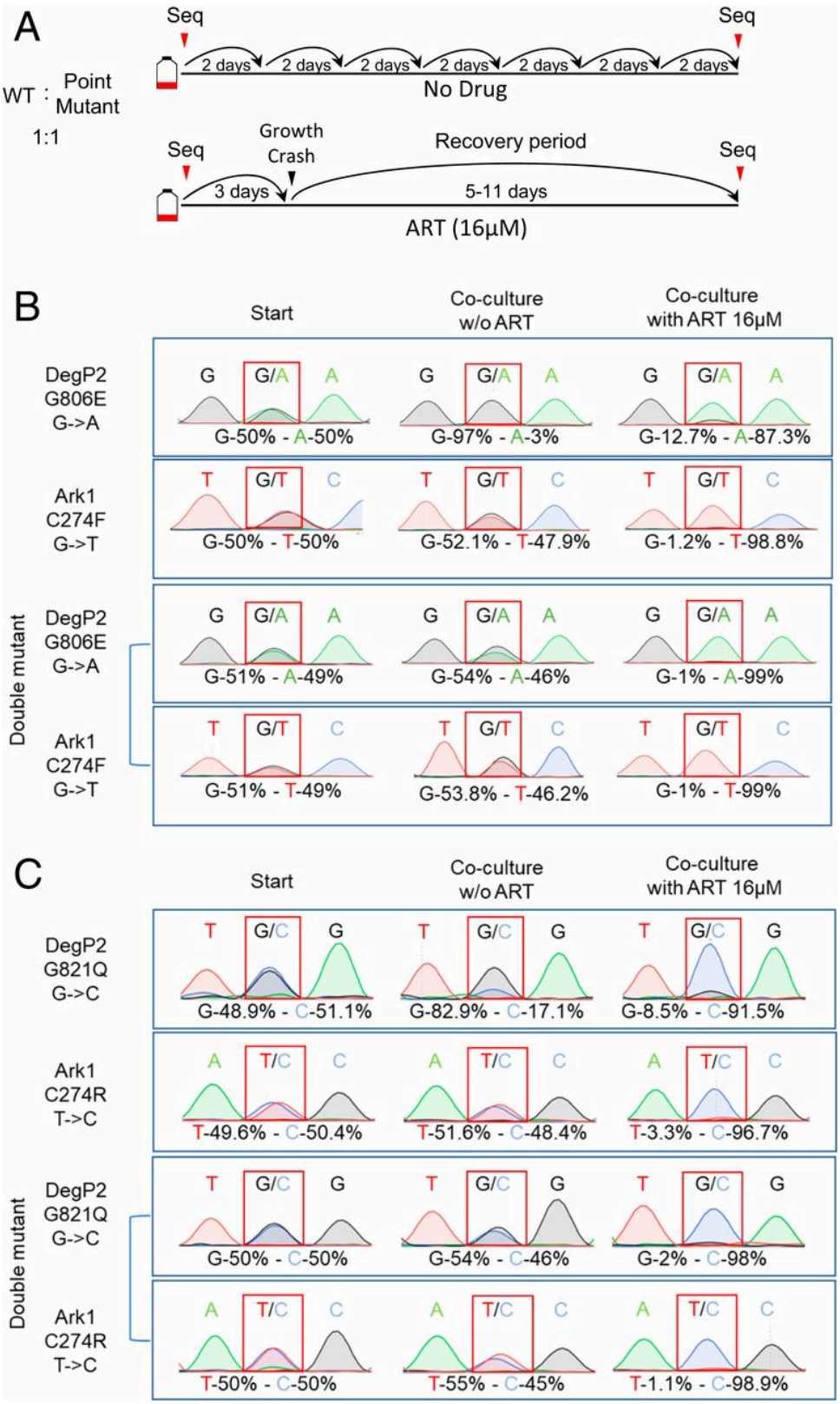
A
WT : Point Mutant
1:1
Seq
2 days
2 days
2 days
2 days
2 days
2 days
2 days
Seq
No Drug
Seq
Growth Crash
3 days
Recovery period
5-11 days
Seq
ART (16μM)
B
Start
Co-culture w/o ART
Co-culture with ART 16μM
DegP2 G806E G->A
G G/A A
G-50% - A-50%
G-97% - A-3%
G-12.7% - A-87.3%
Ark1 C274F G->T
T G/T C
G-50% - T-50%
G-52.1% - T-47.9%
G-1.2% - T-98.8%
Double mutant
DegP2 G806E G->A
G-51% - A-49%
G-54% - A-46%
G-1% - A-99%
Ark1 C274F G->T
G-51% - T-49%
G-53.8% - T-46.2%
G-1% - T-99%
C
Start
Co-culture w/o ART
Co-culture with ART 16μM
DegP2 G821Q G->C
T G/C G
G-48.9% - C-51.1%
G-82.9% - C-17.1%
G-8.5% - C-91.5%
Ark1 C274R T->C
A T/C C
T-49.6% - C-50.4%
T-51.6% - C-48.4%
T-3.3% - C-96.7%
Double mutant
DegP2 G821Q G->C
G-50% - C-50%
G-54% - C-46%
G-2% - C-98%
Ark1 C274R T->C
T-50% - C-50%
T-55% - C-45%
T-1.1% - C-98.9%

Table 4.1. Mutations found in candidate genes identified by whole genome sequencing that were shared in both ART selected lines.

Clone	Gene	Frequency % (ART 8μM)	Frequency % (ART 16μM)	Frequency % (ART 100μM)	Coding Region Change	Amino Acid Change
F4	TGME49_290840-Degp-erine protease-	50	84	100	2461G>C	E821Q
F4	TGME49_239420-Ark1-protein kinase	4.1	90	100	820T>C	C274R
B2	TGME49_290840-serine protease	68.08	98.61	100	2417G>A	G806E
B2	TGME49_239420-Ark1-protein kinase	70.58	100	100	821G>T	C274F

Table 4.2. Mutation analysis of ART-selected *Plasmodium* parasites. Core genome mutations acquired in 2 independent parasite clones ("6A-R" and "11C-R") selected with 900nM ART over 474 days. Raw sequencing data acquired from Rocamora *et al.* 2018[141].

Sample	Chromosome	Position	Gene Name	Gene Description	Amino Acid Change	Other Compounds with Same Gene Mutated
6A-R	Pf3D7_07_v3	241086	PF3D7_0704800	protein phosphatase PPM12	I323V	None
	Pf3D7_08_v3	225894	PF3D7_0803600	conserved Plasmodium protein, unknown function	V514del	None
	Pf3D7_11_v3	593481	PF3D7_1115700	cysteine proteinase falcipain 2a	S35*	MMV023367 MMV665794
	Pf3D7_13_v3	1816526	PF3D7_1345400	conserved Plasmodium protein, unknown function	K1414fs	OSM-S-106
	Pf3D7_14_v3	1059278	PF3D7_1427100	lipase	W1039C	MMV668311
11C-R	Pf3D7_02_v3	513860	PF3D7_0212500	conserved Plasmodium protein, unknown function	N1464-Y1467del	None
	Pf3D7_04_v3	923966	PF3D7_0420300	AP2 domain transcription factor	T1993A	GNF179 Desoxy B
	Pf3D7_05_v3	1167265	PF3D7_0528300	conserved protein, unknown function	P249H	None
	Pf3D7_08_v3	543210	PF3D7_0810600	ATP-dependent RNA helicase DBP1	A414S	None
	Pf3D7_12_v3	1237510	PF3D7_1230000	TBC domain-containing protein	S816*	AN13762 MMV665794
	Pf3D7_13_v3	1006429	PF3D7_1324300	conserved Plasmodium membrane protein, unknown function	R4286-N4291dup	MMV009063 PS-3
	Pf3D7_13_v3	2720248	PF3D7_1368400	ribosomal protein L1	F202Y	None

Chapter 5

Adaptive laboratory evolution in *S. cerevisiae* highlights role of transcription factors in fungal xenobiotic resistance

5.1 Introduction

Experimental evolution is an important method for studying evolutionary processes and is especially amenable to microorganisms given their short generation times, large population sizes, and ability to cryopreserve at distinct timepoints[271]. The longest-running and largest-scale laboratory evolution experiment to date utilizes *E. coli*[257,272,273], though the approach has been used successfully in additional microbes, including the eukaryote *S. cerevisiae*[274,275,276]. While many laboratory evolution experiments focus on changing nutrient availability or culturing conditions, another application of *in vitro* evolution involves studying an organism's evolutionary response to drug pressure. For example, many antibiotic resistance mechanisms have been identified and characterized through this method[277,278,279]. A key challenge lies in identifying functional variants that contribute to the evolved phenotypes given the sheer number of mutation events; for example, a recent sequencing study of 1,011 yeast isolates identified 1,625,809 SNVs[280].

Systematic functional genomic studies are also used to understand drug-target interactions, but most rely on strain libraries in which the entire coding region is modified. For example, a set of homozygous and heterozygous knockout yeast strains was constructed which bear deletions in all genes in the genome[281,282]. This set has been used to repeatedly and systematically identify knockout/knockdown lines that show sensitivity or resistance to a wide variety of different compounds[283] and remains important[284]. CRISPR-based, genome-wide knockout and knockdown studies and novel genome editing systems like base editors are also used in many organisms to identify drug targets[285,286,287,288] or study processes such as the emergence of cancer drug resistance. A key limitation of such studies is that they will miss gain-of-function SNVs, which often drive natural adaptive evolution[289]. Some examples of gain-of-function antibiotic resistance mechanisms include mutations that activate global transcription factors[290] and mutations within the promoter region of resistance genes that result in their hyperproduction[291,292,293].

Here, we perform *in vitro* evolution and whole genome analysis (IVIEWGA) in *S. cerevisiae* to delineate drug-target interactions with a large set of compounds and in the process, extensively characterize key features of the yeast resistome. Whole genome sequencing of 355 evolved, compound-resistant clones showed only a few new coding

variants per clone and that statistical approaches can be used to readily identify variants that modify phenotypes. As proof-of-concept, we confirmed targets that were previously reported and identified additional resistance-conferring mutations for molecules with unknown mechanisms of action (MOA). We also observed an enrichment for gain-of-function variants that affect transcription and confer resistance to multiple compounds.

5.2 Results

5.2.1 Building a library of compounds that are active against a drug-sensitive yeast

To understand how yeast evolves to evade the action of small molecules, identify genes contributing to resistance to uncharacterized small molecules, and hone in on domains that might contribute to compound-target interaction, we tested a collection of molecules for activity against *S. cerevisiae*. Since wild-type *S. cerevisiae* (strain S288C) requires higher compound concentrations to inhibit growth due to an abundance of drug export pumps (ABC transporters), *in vitro* selection would be impossible for many compounds. Therefore, to find compounds with activity against yeast at physiologically-relevant concentrations, we used a modified *S. cerevisiae* strain, termed the "ABC_{16}-Green Monster" (GM), in which 16 ABC transporters have been replaced with green fluorescent protein (GFP)[294]. This has proven an excellent platform for *in vitro* drug selection and target identification experiments because of lower compound requirements[76,84,145,295,296].

Specifically, we evaluated compound libraries comprised of (1) drugs approved for human use with characterized MOAs, (2) well-known tool compounds, and (3) compounds from open-source libraries with demonstrated activity against eukaryotic pathogens, viruses, or tuberculosis[138,297] (**Supplemental Table 5.1**). Commercially available compounds were tested in dose response, while other libraries were initially tested at a single point concentration (in biological duplicates) of up to 150μM, the maximum concentration possible to avoid in-assay DMSO toxicity. Compounds that showed at least 70% growth inhibition were subsequently tested in dose response. Overall, the compounds of the assembled collection had drug-like physiochemical properties in terms of molecular weight and the number of hydrogen bond donors and

acceptors (**Figure 5.1A**). Maximum Common Substructure (MCS) clustering identified 307 clusters with a Tanimoto similarity coefficient of 0.64 (**Figure 5.1B and Supplemental Table 5.1**). Cluster enrichment was observed at rates greater than expected by chance. For example, there were 12 members of a benzothiazepine family (cluster 185, **Figure 5.1B**) of which six had an IC_{50} of less than 10 μM in the yeast model ($p = 2.46 \times 10^{-5}$).

5.2.2 *In vitro* resistance evolution and whole genome analysis link compound structures to phenotype

Based on potency and compound availability, we selected 100 active compounds for follow-up *in vitro* evolution experiments to verify known MOAs, validate the use of this modified yeast strain in target deconvolution studies, and characterize crucial amino acids that disrupt compound binding when mutated. For each independent selection, ~500,000 cells derived from an ABC_{16}-Green Monster single colony were grown to saturation (OD_{600}=1.0 - 1.5) in 20mL YPD media in the presence of sublethal compound concentrations equal to the previously determined IC_{50} (**Figure 5.2**). After any of the independent cultures reached saturation (OD_{600}=1.0 - 1.5), ~500,000 cells were transferred to a new 20mL culture containing increasing concentration of the compound until resistance was observed as measured by an increase in IC_{50} compared to the parental strain. Although growth rates of individual clones in a culture could be variable, each dilution series (1×10^9 cells) was nevertheless grown to saturation (on average ~14 generations amounting to a selection time of 5-20 days before plating on solid media). Cultures were considered resistant if they (1) continued to grow at compound concentrations 2-3-fold above the IC_{50} value of the untreated culture, and (2) had at least a 1.5-fold shift in IC_{50} value compared to the drug-naïve parental line (**Supplemental Table 5.2**). After a variable number of resistance cycles (R average = 2.93, range = 1 to 9), these resistant cultures were plated on drug-containing plates with compound concentration of at least 2-fold IC_{50} to isolate single clones. We picked two independent colonies from the drug-containing plates to verify the resistance phenotype before submitting DNA for whole genome sequencing. We attempted up to 12 independent selections per compound and obtained 1 to 12 resistant clones. Using this strategy, we

isolated 355 clones selected against 80 compounds. The IC_{50} values of the resistant clones increased 1.5- to 5-fold for 121 clones, 5- to 10-fold for 101 clones, and >10-fold for 98 resistant clones (**Supplemental Table 5.2**). Some selections were performed in a modified ABC_{16}-Green Monster clone with *YRR1* deleted (see below). Culture contamination or poor compound availability accounted for most failed selections (20 compounds).

Next, resistant clones were sequenced to 55-fold average coverage (**Supplemental Table 5.3**) using short-read methodology. To detect mutations that arose during compound selection, we designed a custom whole genome analysis pipeline and filtering method. In total, we discovered 1,405 mutations (1,286 SNVs and 119 INDELs) that met the filtering criteria, with an average of 3.96 mutations per clone (**Supplemental Table 5.4).** 1,117 mutations occurred in coding regions while 288 mutations were intergenic, intronic, or splice region variants. 781 unique genes were mutated across the dataset. We typically observed between 1 to 8 coding mutations per evolved clone per compound (**Figure 5.1C**) with some variation. For 53 of the 80 compounds, we observed statistically significant (p<0.05) reproducibility with respect to genes that were mutated, with enrichment considerably over that expected by chance (**Figure 5.1D**). For example, we obtained 13 independent TCMDC-124263-resistant clones with 52 mutations (38 coding), of which ten were in a single gene, *YRM1*. Given that yeast has roughly 6,000 genes, the Bonferroni-corrected probability of this enrichment by chance is 1.53×10^{-25}. For this example, 9 of the 10 nucleotide changes in *YRM1* were clearly independent (**Supplemental Table 5.4**).

To further assess how our evolved mutations were driving the observed resistance phenotypes, we considered the types of mutations that arose during selection and compared them to a published set of 3,137 mutations in yeast strains grown long-term in the absence of compound selection[298]. We observed significantly different distributions in our compound-selected set than in the non-compound-selected set (χ^2, $p < 0.0001$). For example, 39% of the nucleotide base transitions for 1,286 SNVs in our compound-selected dataset were C to A or G to T, while for the 3,137 transitions in the non-selected set, 40% were for A to G or T to C (**Figure 5.3A**). Likewise, we observed a noteworthy difference in the coding changes. Among exonic selected mutations, 941 were

nonsynonymous and 127 were synonymous. The estimated ratio of divergence at nonsynonymous and synonymous sites (dN/dS) was 2.62 across the dataset, indicating that drug treatment applied positive selection. In contrast, the neutral SNVs had a strong bias toward synonymous mutations (**Figure 5.3B**). These data suggest that the observed mutations in our dataset are likely functional and could provide a selective advantage to the evolved clones.

We also assessed our large mutational dataset to identify broad insights into the functional impacts of different variant types. Synonymous and missense variants emerged in essential genes in approximately 20% of cases. This finding agrees with the literature, which suggests that only 20% of the yeast genome encodes essential genes[299]. By this same metric, mutation types with more disruptive impacts, such as premature stop codons and frameshift variants, deviate strikingly from the expected genome-wide value of 20%. These mutations occur in essential genes only 4.9% and 7.0% of the time, respectively (**Figure 5.3C**).

Copy number variants (CNVs) were detected through a coverage-based algorithm using the output from GATK DiagnoseTargets to identify contiguous genic regions with increased read coverage relative to the parent. We observed 24 CNVs including apparent aneuploidy (11 times, occurring in 10 clones) and small, intrachromosomal amplifications (13 times, occurring in 13 clones) (**Supplemental Table 5.5**). Altogether, we observed aneuploidy with eight compounds, including BMS-983970, doxorubicin, etoposide, GNF-Pf-3582, GNF-Pf-4739, hygromycin B, CBR110, and wortmannin (**Figure 5.3D**). This is perhaps not surprising given that aneuploidies arise in *S. cerevisiae* as a short-term stress response[300]. We observed an amplification on chromosome XVI that involved the bZIP transcription factor, *ARR1,* for clones resistant to GNF-Pf-1618 and GNF-Pf-2740, as well as with four strains resistant to MMV665794. The strains Wortmannin-13R3a and CBR113-7R4a, both had chromosome XV CNVs that involved the transcription factors *YRR1* and *YRM1* (discussed below).

5.2.3 Resistance-conferring intergenic mutations are rare

Although intergenic mutations are frequently found in cells not subject to selection, mutations in promoters or 3' UTRs could confer resistance by increasing or decreasing transcript levels. To assess examples where this might be the case, we mapped the 271 intergenic mutations identified across the sequencing dataset to their nearest-neighbor coding genes and other genomic features (**Supplemental Table 5.6**). This analysis showed little enrichment, though we did observe several repeated mutations located in the intergenic promoter regions of a few genes that showed significance in our enrichment analysis. For example, we discovered three mutations upstream of the ergosterol biosynthesis and azole resistance gene *ERG9*[301,302] in addition to seven *ERG9* coding region mutations. One of the *ERG9* intergenic mutations falls in its putative promoter region and was also observed in selections with compound AN7973 (**Figure 5.3E**). Four coding and one non-coding mutation upstream of the start codon in the endoplasmic reticulum membrane protein and caspofungin resistance protein[303], *CSG2,* were also observed. All five mutations are associated with selections to compound GNF-Pf-1618 and its close analog, KAAA725 (**Figure 5.3F**). We also identified five mutations in the coding region of *PDR3*[304]*,* a Zn_2C_6 transcriptional regulator of the multidrug efflux, and an additional mutation was found downstream of the open reading frame (**Figure 5.3G**). These examples demonstrate that intergenic mutations should not be entirely dismissed when considering the effects of variant types on observed phenotypes.

5.2.4 CRISPR/Cas9 validation shows that most genes identified more than once confer resistance, but singleton mutations may not

Because many mutations can co-occur and be non-adaptive[305], the presence of one SNV in a resistant clone is not proof that the specific mutation is resistance-conferring. To confirm that some of these mutations directly contribute to the resistance phenotype and rule out the possibility of them being merely passenger mutations, we used CRISPR/Cas9 technology to introduce 61 altered alleles from the evolved mutants back into the original (unevolved) ABC_{16}-Green Monster strain. Mutations were chosen for validation based on frequency of mutation and/or whether the gene product was

implicated as a potential target for the compound based on literature searches. Successfully reverse-engineered strains were tested in liquid-growth assays using the same compounds from the corresponding IVIEWGA experiments. Using a combination of fold change and p-value in comparing the IC_{50} values of these edited clones to those of the parental ABC_{16}-Green Monster strain, we verified that 45 genetic changes across 37 unique genes contributed to the observed resistance (**Supplemental Table 5.7**). Independent mutations that were repeatedly identified for a specific gene tended to have a high probability of confirming at least a partial resistance phenotype and these gene products were likely to be the direct target of the small molecule. The only exception was *RPO21*, a subunit of RNA polymerase, which was mutated four separate times with four compounds (two nonsynonymous and two synonymous mutations) but failed to confirm a resistance phenotype after CRISPR/Cas9 editing. However, it is known that mutations in *RPO21* result in transcriptional slippage, which may allow cells to better survive cytotoxic drugs that alter nucleotide pools[306]. For the 15 alleles that did not show a statistically significant IC_{50} shift (**Supplemental Table 5.7**), we noted that 11 of the resistant clones also carried additional resistance alleles in a highly represented gene such as *YRR1* or *YRM1* (**Supplemental Table 5.4**), two transcription factors involved in multi-drug resistance.

5.2.5 Using *in vitro* evolution for drug target and mechanism of action studies

For compounds with known targets, we frequently identified mutations clustering in the active site of the proposed target molecule. For example, we isolated six clones resistant to flucytosine (**Table 5.1 and Supplemental Table 5.4**). Of the nine identified missense or nonsense mutations, six were in the uracil phosphoribosyltransferase domain of *FUR1* (probability of enrichment by chance = 1.2×10^{-26} using hypergeometric mean function). Resistance to 5-flucytosine has been reported in multiple clinical isolates of *Candida* and is typically caused by mutations in genes that encode the enzymes involved in the metabolic transformation of the prodrug. In a study of flucytosine-resistant clinical isolates of *C. albicans*, mutations in *Fur1* were identified[307]. A homology model (**Figure 5.4A**) revealed that the amino acid changes identified in our *in vitro* selections

are all located near the 5-FUMP binding pocket, suggesting that these changes confer resistance by disrupting 5-FUMP binding.

We obtained four benzoxaborole-resistant clones using the antifungal drug tavaborole. They were highly resistant and contained six SNVs, four of which (R316T, V400F, V400D, and M493R) were mutations in the 145 amino acid aminoacyl-tRNA synthetase editing domain of *CDC60* ($p = 1.11 \times 10^{-18}$, hypergeometric mean function), the gene that encodes leucyl-tRNA-synthetase in yeast. Wild-type yeast can evolve benzoxaborole resistance via amino acid changes both within the ligase editing site of the leucyl-tRNA synthetase and outside the active site[308,309,310], indicating the relevance of the GM model. A LeuRS homology model (**Figure 5.4B**) with a tavaborole ligand docked using QuickVina2[311] suggests that the observed *CDC60* mutations could confer resistance by directly interfering with tavaborole binding to Cdc60.

We also examined compounds used in chemotherapy. Camptothecin is a specific topoisomerase (Top1) inhibitor that binds the DNA/Top1 cleavage complex, preventing DNA relegation[312]. We isolated two camptothecin-resistant yeast clones with three missense mutations, two of which were in *TOP1* (G297C and E669*) (**Supplemental Table 5.4**). *TOP1* mutations can lead to camptothecin resistance in the human HCT116 colon adenocarcinoma cell line when exposed to SN38, a water-soluble camptothecin derivative[313,314]. A homology model was constructed[315] by aligning a partial yeast Top1 crystal structure to a crystal structure of human TOP1 with camptothecin bound (PDB: 1T8I)[316] (**Figure 5.4C**). This model showed that G297 is located in the core domain of the enzyme near the binding pocket, suggesting that it confers drug resistance by directly impeding compound binding. E669* truncates the entire C-terminal domain, which contains the DNA-binding site[317] (**Figure 5.4C**), thus eliminating many protein/DNA contacts and likely impeding the formation of the drug-DNA-protein complex.

Rapamycin, a macrocyclic lactone, and its analog everolimus potently inhibit mTOR, a protein kinase component of both the mTORC1 and mTORC2 complexes that controls cell growth and proliferation in many species. Two rapamycin-resistant and three everolimus-resistant clones were isolated in our study. One carried a S1975I mutation in the FKBP12-rapamycin binding domain of mTOR, *TOR2*, and three carried a mutation in the FKBP-type peptidyl-prolyl cis-trans isomerase Pfam domain of FPR1, a small

peptidylprolyl isomerase that interacts with mTOR (**Supplemental Table 5.4**). Recently, a selection with rapamycin in a *pdr1* deletion strain of *S. cerevisiae* BY4741 identified mutations in TOR1, TOR2, and FPR1 that confer resistance to rapamycin[318]. One of the reported TOR2 mutations produced a S1975R amino acid change, the same residue we identified as being mutated in our study. A model of the yeast Tor2/Fpr1/rapamycin tertiary complex shows that residue S1975 is near the bound rapamycin molecule (**Figure 5.4D**), suggesting that changes at this location might disrupt the formation of the tertiary complex. The model suggests that the two *FPR1* truncation mutations (Y33* and Q61fs) (**Figure 5.4E and Supplemental Table 5.4**) likely confer resistance by interfering with everolimus binding.

Our collection also contained compounds active against other pathogens. For example, mebendazole, a benzimidazole compound, is among the few effective drugs available for treating soil-transmitted helminths (worms) in both humans and animals. It binds to tubulin, thereby disrupting worm motility[319]. We confirmed the antifungal activity of mebendazole[320] and obtained two independent resistant clones with nine missense mutations, two of which were in the GTPase domain of the *TUB2* gene (R241S and L250F) (**Supplemental Table 5.4**), near or at the same residues (R241H and R241C) that confer resistance to the related antimitotic drug, benomyl, which also binds tubulin[318,321]. Modeling studies (**Figure 5.4F**) confirm that the binding mode is similar to that of benomyl, which binds with high affinity to the beta subunit of tubulin, thereby disrupting the structure and function of microtubules[322]. Despite sharing a common target with yeast, helminths and nematodes have benzimidazole-resistance mutations in codons 167, 198, and 200, suggesting conservation of structure and function across phyla.

Alkylphosphocholines such as miltefosine and edelfosine were originally developed as anticancer agents, but recent work has shown that they are also effective against trypanosomatid parasites such as *Leishmania* and *Trypanosoma*[323,324,325,326]. The specific target of these drugs remains uncertain. Compound uptake in yeast is known to depend on the membrane transporter Lem3[327], which facilitates phospholipid translocation by interacting with the flippase Dnf1[328] and *DNF1* is closely related to the gene associated with miltefosine resistance in *Leishmania* (Ldmt (AY321297), BLASTP

e = 2 x 10^{-125}). We identified two independent *LEM3* mutations that confer resistance to miltefosine (K134* and Y107*) (**Supplemental Table 5.4**). Editing Y107* into the drug naïve parent reconfirmed resistance to both miltefosine and edelfosine (**Supplemental Table 5.7**). Both mutations truncate the protein, functionally mimicking a deletion strain. *LEM3* is a yeast ortholog of LdROS (ABB05176.1, BLASTP 5x10^{-13}), also related to *Leishmania* miltefosine resistance[329].

5.2.6 Revealing the putative target for an uncharacterized antimalarial natural product

Hectochlorin is a natural product from the marine cyanobacterium *Lyngbya majuscul*e[330] that has strong antimalarial blood stage activity (IC_{50} = 85.60 nM ± 0.96) as well as activity against the ABC_{16}-Green Monster strain (IC_{50} = 0.25 μM). We identified six independent disruptive mutations, three of which were in the actin Pfam domain of Act1 (p = 1.9 x10^{-13}, **Supplemental Table 5.4**). We confirmed by CRISPR-Cas9 editing that a mutation in *ACT1* confers resistance to hectochlorin in yeast (**Supplemental Table 5.7**). When mapped onto a crystal structure of Act1 (PDB: 1YAG)[331], the altered amino acids line a distinct protein pocket (**Figure 5.4G**), suggesting they confer resistance by directly disrupting compound binding. To assess whether hectochlorin resistance in *Plasmodium* might occur through a similar mechanism, we also mapped the mutations onto a synthetic construct of *P. berghei* Act1 protein (PDB: 4CBW), which shares 97% sequence identity with *Pf*Act1. The altered amino acids again line a well-defined protein pocket, and the hectochlorin docked pose is also similar. This work supports published experiments that suggest actin is the target of hectochlorin[332]. To provide further support for this hypothesis, we determined if hectochlorin produces the same cell-invasion inhibition phenotype in malaria liver stage parasites as cytochalasin D, another actin polymerization inhibitor, which reduces *Plasmodium* sporozoite motility[333]. Treatment with 1μM hectochlorin blocked parasite invasion as efficiently as 10μM cytochalasin D (**Figure 5.4H**).

5.2.7 Mutations in the transcription factors YRR1 and YRM1 are associated with multidrug resistance in the ABC_{16}-Green Monster yeast

SNVs in some genes appeared repeatedly across different compound sets. The set of 25 highest confidence genes (mutated five or more times across the dataset) was enriched for DNA-binding transcription factor activity (seven genes, Holm-Bonferroni-corrected $p = 0.035$). Altogether we observed 140 coding mutations in 24 genes affecting transcription (**Figure 5.5A**). The greatest number of unique allelic exchanges was found in the two transcription factors, *YRR1* (27x) and *YRM1* (23x) (**Figure 5.5B and C**). In addition, multiple unique missense mutations were observed in *PDR1* (7x), *PDR3* (5x) *YAP1* (5x), *AFT1* (5x), *TUP1* (3x) *HAL9* (2x), *AZF1* (2x) (**Table 5.1** and **Supplemental Table 5.4)**. With the exception of *TUP1*, *AFT1*, and *YAP1*, all of these transcription factors contain the Zn_2C_6 fungal-type DNA-binding domain. In fact, we discovered 124 different mutations in 15 different Zn_2C_6 transcription factors. This Zn_2C_6 domain family (Pf00172) is only found in fungi: *S. cerevisiae* has 52 genes with this domain, and *C. albicans* has 225. In this human pathogen, members include *FCR1, MRR2, TAC1, PDR1* and *PDR3*, all genes involved in drug resistance. *YRR1 (PDR2), YRM1, PDR1* and *PDR3* are all known to be involved in the pleiotropic drug response in *S. cerevisiae*[334,335], activating transcription of drug transporters such as *PDR5, PDR10, PDR15, YOR1* and *SNQ2* (reviewed in [336]). Although the GM strain has some of these multidrug efflux pumps deleted, the GM genome retains many other genes that could contribute multidrug resistance that are under transcriptional control of *YRR1*[334]. In addition to statistical enrichment strongly suggesting a driving role in resistance, reverse gene editing by CRISPR/Cas9 of some of the mutations identified in *YRR1*, *AFT1,* and *TUP1* fully recapitulated the observed resistance phenotype (**Supplemental Table 5.7**).

Because the two Zn_2C_6 transcription factors *YRR1* and *YRM1* were mutated 100 times for 19 structurally diverse compounds (**Figure 5.5B-D**), we conducted a focused investigation of the mutations and their spatial localization. Remarkably, all resistance-conferring *YRR1* and *YRM1* mutations were clustered in a ~170 amino acid domain in the C-terminal half of the protein (**Figure 5.5B and C**) which is distal to the DNA binding domain. We found no mutations in the DNA binding domain and no mutations in the predicted activation domain at the far C-terminus. Notably, it has been shown that the C-terminal activation domain of Gal4 (activation domain 9aaTAD (857–871 aa), which interacts with Tra1 protein of the SAGA complex, can be substituted for the activation

domain of Yrr1[334]. Yrr1 binds to the sequence (T/A)CCG(C/T)(G/T)(G/T)(A/T)(A/T), found upstream of genes involved in multidrug resistance such as *AZR1, FLR1, SNG1, SNQ2, APD1,* and *PLB1*[334,337,338].

YRR1 and *YRM1* are nonessential genes, and we hypothesized that our evolved resistant strains possessed *YRR1* and *YRM1* gain-of-function mutations that result in constitutive expression of transcriptional target genes encoding proteins with roles in drug resistance. This hypothesis is motivated in part by the fact that others have reported multidrug resistance-conferring gain-of-function mutations in the related genes *PDR1* and *PDR3*[339,340,341]. To expand on this previous work, we exposed a *YRR1* L611F strain (generated using CRISPR/Cas9) to a set of compounds and observed cross-resistance to almost all compounds tested (**Supplemental Table 5.7**). Others have found that deleting the *YRR1* gene entirely does not significantly increase sensitivity to cytotoxic compounds[339], providing further evidence that the *YRR1* and *YRM1* mutations identified in our selections—which were all single amino acid changes—represent gain-of-function mutations. We confirmed this finding by testing a small set of cytotoxic compounds against a *yrr1* deletion strain[76]. With very few exceptions, we also noted no significant differences in growth inhibition over the wild-type-allele strain. Only compounds MMV6685852, GNF-PF-4739, and MMV668507 had different IC_{50s} against the *yrr1* deletion strain and the fold IC_{50} differences were very modest.

To further test the hypothesis that the *YRM1* and *YRR1* SNVs are gain-of-function mutations resulting in constitutive expression of additional transporters and other potential resistance genes (including *AZR1, FLR1, SNG1, YLR046L, YLL046C, YPL088W,* and *YLR179C*), we used qPCR to directly evaluate the expression of three such target genes (*AZR1*, *FLR1,* and *SNG1*). To this set we added the *YRR1* gene itself, since *YRR1* activates its own expression via an auto-feedback loop[340] (**Figure 5.5E**). We examined gene expression in *YRR1*-mutant strains, in the ABC_{16}-Green Monster strain with a wild-type *YRR1* allele, and in the *yrr1* deletion clone (**Supplemental Table 5.8**). Relative RNA expression levels of the putative target genes *AZR1*, *FLR1, SNG1* and *YRR1* are 1.5 to 140-fold higher in all *YRR1* evolved mutant clones tested compared to the parental GM strain; mutant clones also display elevated levels relative to the *yrr1* deletion clone

(**Figure 5.5E**). This data is further corroborated when using *TDH3* or *TAF10* as alternative housekeeping genes to *ACT1* **(Supplemental Table 5.8)**.

To assess whether *YRR1* mutations confer resistance to specific compounds or elicit a more general resistance response, we evaluated seven different *YRR1* mutant clones derived from our resistance selections for resistance to a set of five structurally unrelated compounds. All tested cultures showed strong cross-resistance to all tested compounds (**Supplemental Table 5.7**). Taken together, these results strongly support our hypothesis that the identified *YRR1* SNVs lead to constitutive transcriptional activation of its target genes involved in the pleiotropic drug response, thereby conferring general resistance to many compounds.

5.3 Discussion

To our knowledge, this is one of the most comprehensive and systematic studies of the drug-selected mutational landscape in a model system like yeast. Although genome-wide sets of knockout strains have been used to discover drug targets and to study drug resistance[342,343,344,345,346,347], our approach is different in that we identify SNVs in specific domains that might play a crucial role in compound-target interaction. Since these mutations confer resistance, we hypothesize that many of the SNVs are gain-of-function mutations. This difference in approach allows IVIEWGA to complement other genome-wide knockdown approaches, including those that rely on measures of haploinsufficiency in the presence of compound (HIPHOP)[342]. Few genetic tools are needed, and the approach can be applied to any organism that can be subjected to drug pressure and sequencing.

One potential disadvantage of whole genome evolutionary approaches is that background passenger mutations can accumulate during the prolonged culturing of a fast-dividing organism and some may not contribute to resistance[305]. However, given the enrichment for nonsynonymous mutations in our study, most mutations likely do offer some advantage to the cell even when they are not the primary drivers of resistance. A large dataset like ours can provide clarity and statistical confidence regarding an allele's importance even in the absence of CRISPR-Cas9 reconfirmation. The examples that are discussed in the manuscript did, in almost all cases, achieve strong statistical significance, with mutations in the same genes or with compounds that are structurally

closely related appearing at rates much greater than expected by chance. It should be mentioned that many other mutations were found at rates not expected by chance and were not discussed here for the sake of brevity. For example, we found a strong association between *BUL1* and *BAP2* mutations and inhibitors of mitochondrial function as well as vacuolar ATPase mutations that were associated with other scaffold families.

The reproducibility of the results for genes and compound families indicates that the approach could be powerful in other fungal species that lack the genetic tools available for *S. cerevisiae*. Although others have identified targets of antifungal compounds through deep sequencing of drug-resistant mutants in other fungi[348], *S. cerevisiae* is an excellent model for studying antifungal drug-resistance in part because it is haploid. IVIEWGA may be more difficult to apply in diploid species such as *Candida albicans* since complete loss-of-function mutations may be difficult to evolve and heterozygous gain-of-function mutations may be hard to identify in whole genome sequencing data.

Another notable finding is the enrichment for Zn_2C_6 transcription factors *YRR1* and *YRM1* in the set of resistance genes. Though this may be specific to *Saccharomyces* or even the ABC_{16}-Green Monster strain that was used, smaller-scale studies with specific compounds strongly support our findings (reviewed in [349]). Evolution experiments with unmodified *S. cerevisiae* and fluconazole gave mutations in *PDR1*[350]. Gallagher *et al.* mapped the ability of wild-type yeast to resist 4-nitroquinoline 1-oxide to *YRR1*[351]. In addition, *YRR1* was originally identified with selections in unmodified yeast[352]. Zn_2C_6 transcription factors are known to play a major role in the pathogenesis and pleiotropic drug response of pathogenic fungi such as *Candida* spp., the most common clinically relevant fungal pathogens[353,354,355]. Examples include *TAC1*, *STB5,* and many others (reviewed in [356]). Nevertheless, it is plausible that the abundance of *YRR1* and *YRM1* mutations that we identified only emerges when multiple other drug pumps are deleted, as in the GM strain.

A major unanswered question is how the cell senses increased compound pressure and translates this to increased transcription. A cofactor could bind to the drug resistance domain in Yrr1 and Yrm1. Alternatively, the observed amino acid changes could increase either the strength of the dimerization of Yrr1 and/or its binding to DNA,

causing an increase in the transcription of drug pumps, which would lead to resistance to many compounds irrespective of their MOA. This hypothesis is supported by the fact that (1) the RNA expression levels of the Yrr1 target genes *AZR1*, *FLR1, SNG1,* and *YRR1* are 2 to 70-fold higher in all of the tested *YRR1* mutant clones when compared to the parental GM strain or the *yrr1* deletion lineage and (2) clones with *YRR1* mutations confer resistance even to compounds that were not used in selections or that did not yield *YRR1* mutations.

The World Health Organization has declared antimicrobial resistance one of the top 10 public health concerns currently facing humanity. While understanding resistance profiles and the rate at which resistance emerges are already key components of drug development pipelines for eukaryotic pathogens like the human malaria parasite *Plasmodium falciparum*[357], studies of drug resistance in fungal pathogens remain extremely limited. Adaptive laboratory evolution has proven a useful tool for cataloging resistance variants across multiple microbes, enabling strategic drug design efforts and more. If the goal is to create better drugs for fungal pathogens, more studies like these are urgently needed.

5.4 Material and Methods

5.4.1 Statistics and Reproducibility

To calculate probabilities of enrichment chance for specific allele sets a high accuracy hypergeometric mean function (Excel) was used:

$$P(X \geq x) = \frac{\binom{k}{x}\binom{N-k}{n-x}}{\binom{N}{n}}$$

n is the number of different observed alleles in a particular domain or gene for a compound in n selections.

x is the number of independent selections that were performed for a compound.

N is the number of nucleotides in the gene or domain of interest (e.g., 300 bases), or the number of genes in the genome multiplied by the number of n selections.

K is the number of nucleotides in the yeast genome (12.1 Mb), or the number of genes (6,000) multiplied by the number of n selections.

A Bonferroni adjustment using the yeast genome size ($12.1x10^6$) or number of genes (6,000) was made to correct for multiple hypothesis testing.

5.4.2 *S. cerevisiae* susceptibility and dose-response assays

To measure compound activity against whole-cell yeast, single colonies of the ABC_{16}-Green Monster strain were inoculated into 2mL of YPD media and cultured overnight at 250RPM in a shaking incubator at 30°C. Cultures were diluted the following day and 200µl of log-phase cultures, (OD_{600}nm readings between 0.1 and 0.2) were added to the wells of a 96-well plate. Eight 1:2 serial dilutions of compound were subsequently performed, in biological duplicates, with final compound concentrations ranging from 0.1 - 150µM. After an initial reading of OD_{600} (time 0 hours), the plate was placed in an incubator at 30°C for 18 hours, and OD_{600} nm determined. IC_{50} values were calculated by subtracting OD_{600} nm values at time 0 hours from time 18 hours. Nonlinear regression on log([inhibitor]) vs. response with variable slope was performed using GraphPad Prism. As a negative control, cultures not treated with any compounds were run in parallel.

5.4.3 GM Growth inhibition *evaluation for the MMV Malaria Box, Pathogen Box, and Charles River libraries*

96-well plates containing 10µl 10mM compounds were provided. We first tested these compounds for cytotoxicity of the ABC_{16}-Green Monster clone in single-dose measurements (150µM, in biological duplicates). Compounds that inhibited GM growth by at least 70% after 18 hours (in either replicate) were further characterized using an eight-point dose-response assay (**Supplemental Table 5.1**).

5.4.4 *In vitro* resistance evolution

In vitro selections were performed as outlined in **Figure 5.2**. At least five independent selections were initiated with a single colony of the ABC_{16}-Green Monster strain. Assorted drug concentrations (corresponding to 1-fold to 3-fold IC_{50}) of diverse

compounds were added to 50mL conical tubes containing 50µL of saturated (OD_{600}=1.0 - 1.5; 1-5x10^7/mL cells) ABC_{16}-Monster cells in 20 mL of YPD medium. The tubes were then cultured at 250RPM in a shaking incubator at 30°C. Cultures that achieved OD_{600} values between OD_{600}=1.0-1.5; ~14 generations) were diluted 1: 400 into fresh media with the inhibitors, and multiple rounds of dilutions (about of 2-6 rounds of dilutions) were performed at increasingly higher concentrations. After a culture was able to grow at a compound concentration that was at least equal to 2-3x IC_{50} compared to the parental IC_{50}, cells from this polyclonal culture were plated onto agar plates containing the inhibitor. Single colonies were isolated, and an eight-point dose-response assay (in biological duplicates) with two-fold dilutions steps and final compound concentrations ranging from 0.1 – 150µM (depending on the original parental IC_{50}) was performed to determine the IC_{50} values of the evolved versus parental clones. Genomic DNA from clones that had at least an IC_{50} shift of 1.5-fold was extracted using the YeaStar Genomic DNA kit (cat. No D2002, ZYMO Research).

5.4.5 Whole genome sequencing and analysis

Sequencing libraries using 200ng genomic DNA were prepared using the Illumina Nextera XT kit (Cat. No FC-131-1024, Illumina) following the standard dual indexing protocol, and sequenced on the Illumina HiSeq 2500 in RapidRun mode to generate paired-end reads at least 100bp in length. Reads from the paired-end FASTQ files were aligned to the *S. cerevisiae* 288C reference genome (assembly R64-1-1) using BWA-mem and further processed using Picard Tools (http://broadinstitute.github.io/picard/). Quality control, alignment, and preprocessing workflows were automated using the computational platform Omics Pipe[358] to ensure scalable and parallelized analysis. A total of 363 clones were sequenced to an average coverage of 54.6x with an average of 99.7% reads mapping to the reference genome. Additional sequencing quality statistics are given in **Supplemental Table 5.3**. SNVs and INDELs were first called against the 288C reference genome using GATK HaplotypeCaller, filtered based on GATK recommendations[194], and annotated with a SnpEff[196] database built from the *S. cerevisiae* 288C (assembly R64-1-1) GFF to leave only high-quality variants with high allelic depth. Variants that were present in both the drug-sensitive parent clone and resistant clones

were then subtracted using a custom shell script so that mutations were only retained if they arose during the compound selection process. To standardize and streamline the analysis, only one of the eight parent clones was used for the subtraction of variants (NODRUG--GM2). However, all 7 parent clones were analyzed for their own background mutations against NODRUG--GM2 first so that any background mutations could be removed following the first subtraction against NODRUG--GM2.

In total, 1,405 mutations (1,286 SNVs and 119 INDELs) met these criteria and were collated into a single list for subsequent analyses (**Supplemental Table 5.4**). Mutations were visually inspected using the Integrative Genomics Viewer (IGV)[359]. Manual annotation of variants was required in some cases to resolve issues with SnpEff outputs. Raw sequencing data files were uploaded to NCBI Sequence Read Archive under accession PRJNA590203. To increase the depth of our analysis, we also reanalyzed FASTQ files from several resistance selections that were previously published (https://escholarship.org/uc/item/42b8231t) and deposited in the NCBI Short Read Archive with the following accession numbers: SRX1745463, SRX1745464, SRX1745465, SRX1745466, SRX1751863, SRX1751950, SRX1751953, SRX1751954, SRX1805319, SRX1805320, SRX1805321, SRX1805322, SRX1805323, SRX1868845, SRX1869272, SRX1869274, SRX1869275, SRX1869276, SRX1869277, SRX1869278, SRX1869279, SRX1869280, SRX1869282). These include selections with the following compounds: KAE609, MMV001239, cycloheximide, MMV000570, MMV007181, MMV019017 and MMV396736.

5.4.6 CNV Analysis

Read coverage values across defined gene intervals in each alignment file were calculated using GATK DiagnoseTargets (input parameters: -max 2000 -ins 1500 -MQ 50). Coverage values were log-transformed then mean-centered across and within arrays in Cluster (http://bonsai.ims.u-tokyo.ac.jp/~mdehoon/software/cluster). Copy number variants were filtered so that they would only be retained if there was at least 2-3x fold

coverage change relative to the parent strain and if they spanned four or more genes (**Supplemental Table 5.5**). CNVs were visually confirmed in IGV.

5.4.7 Intergenic mutation analysis

A Python script was written to map the 271 intergenic mutations to the coordinates of known chromosomal features based on the GFF supplied on SGD for the *S. cerevisiae* S288C genome version R64-2-1. For each intergenic mutation position, we determined whether it was located within a feature and/or if it was located within 500bp either upstream or downstream of a known coding gene. All possible annotations for each intergenic mutation position are listed in **Supplemental Table 5.6**.

5.4.8 CRISPR-Cas9 allelic exchange in *S. cerevisiae*

CRISPR-Cas9 genome engineering was performed using the *S. cerevisiae* ABC_{16}-Green Monster strain. gRNA plasmids were generated with specific oligonucleotides (**Supplemental Table 5.9**) for the desired allelic exchange (Integrated DNA Technologies) containing a 24bp overlap with the p426 vector backbone. Subsequently, target-specific gRNAs were PCR amplified/transformed into competent *E. coli* cells and selected on LB-Ampicillin plates. ABC_{16}-Monster cells expressing Cas9 were simultaneously transformed with 300-500ng of gene-specific gRNA vector and 1-2 nmole of synthesized donor template (IDT) via a standard lithium acetate method. Transformed cells were plated and selected on methionine and leucine deficient CM-glucose plates. Each engineered mutation was confirmed by Sanger sequencing (Eton Bioscience).

5.4.9 qPCR

S. cerevisiae strains were grown in YPD (1% yeast extract, 2% bacto peptone, 2% dextrose) overnight at 30°C. 1 OD_{600} log-phase cells were harvested and subject to total RNA extraction using Qiagen RNeasy kit, following the manufacturer's protocol. cDNA was generated using ThermoFisher SuperScript IV First-Strand Synthesis System, following the manufacturer's protocol using oligo(dT). qPCR was performed with oligonucleotides) in technical triplicate with Quanta PerfeCTa SYBR Green FastMix. Analysis was done using Prism 8. Ct values for each gene of interest were averaged and normalized against *ACT1* within each clone (ΔCt). Then each gene of interest was normalized against corresponding genes in the wild-type GM background (ΔΔCt). Fold expression was calculated using the formula: $2^{-\Delta\Delta Ct}$ [200]. This analysis was done for each of the four biological replicates (**Supplemental Table 5.8**).

5.4.10 *Plasmodium* invasion assay

The impact of hectochlorin on hepatocellular traversal and invasion by *Plasmodium berghei* (Pb) sporozoites was measured using a flow cytometry-based assay[333]. *Anopheles stephensi* mosquitoes infected with GFP expressing Pb sporozoites (Pb-GFP)[61] were purchased from the New York University (NYU) Insectary Core Facility. Approximately 24h before infection, 1.75 x 10^5 Huh7.5.1 cells were seeded in 24-well plates using DMEM (Invitrogen cat# 11965-092) supplemented with 10% FBS (Corning cat# 35-011-CV) and 1x Pen Strep Glutamine (100 Units/mL Penicillin, 100µg/mL Streptomycin, and 0.292 mg/mL L-glutamine) (Invitrogen cat# 10378-016) for a final volume of 1mL. On the day of infection, hectochlorin was added to test wells (final

concentration 1μM) with cytochalasin D (final concentration 10μM) acting as a positive control for invasion inhibition. A non-infected control and DMSO (final concentration 0.5%) negative control was also utilized to mimic the treated well conditions. Sporozoites were freshly dissected and prepared 2-4 hours before infection[137]. Immediately prior to infection, rhodamine-dextran was added to each test well (final concentration 1 mg/mL) followed by 3.5 x 10^4 Pb-GFP sporozoites. The plates were then incubated at 37°C and 5% CO_2 for 2 h. Following this incubation, the cells were washed and the presence of GFP and rhodamine-dextran signals were evaluated using flow cytometry.

5.4.11 Model building

We used I-TASSER[315] to model proteins without acceptable structures in the Protein Data Bank[360]. To visually inspect the homology models, we aligned them to the structural templates used for model construction[361]. We discarded models that had poor I-TASSER C-scores or that we judged to be improbable (e.g., excessively disordered). Where there were no homologous crystal structures with bound ligands for reference, we used docking to predict ligand binding poses. Specifically, we converted the SMILES strings of the ligands to 3D structures using a beta version of Gypsum-DL[362] and docked the 3D models using QuickVina2[311] (exhaustiveness = 15). The AutoDock forcefield does not include parameters for boron. To dock tavaborole, we substituted the boron atom with a carbon atom, as recommended on the AutoDock webpage (http://autodock.scripps.edu). We tested both the “C” and “A” atom types as boron substitutes to determine which gave predicted tavaborole poses with the best binding

affinities. For heme groups, we manually added a charge of +2 to the iron atom. All protein-structure images were generated using BlendMol[363].

5.4.12 Data Availability

Raw DNA sequences for all 363 yeast clones have been deposited in the Sequence Read Archive (www.ncbi.nlm.nih.gov/sra) under BioProject accession PRJNA590203. All other data are available in the manuscript or the supplemental materials.

5.5 Acknowledgements

Chapter 4, in full, is a reprint of the material as it appears in Communications Biology, 2022. Sabine Ottilie, Madeline R. Luth, Erich Hellemann, Gregory M. Goldgof, Eddy Vigil, Prianka Kumar, Andrea L. Cheung, Miranda Song, Karla P. Godinez-Macias, Krypton Carolino, Jennifer Yang, Gisel Lopez, Matthew Abraham, Maureen Tarsio, Emmanuelle LeBlanc, Luke Whitesell, Jake Schenken, Felicia Gunawan, Reysha Patel, Joshua Smith, Melissa S. Love, Roy M. Williams, Case W. McNamara, William H. Gerwick, Trey Ideker, Yo Suzuki, Dyann F. Wirth, Amanda K. Lukens, Patricia M. Kane,

Leah E. Cowen, Jacob D. Durrant, and Elizabeth A. Winzeler, “Adaptive laboratory evolution in *S. cerevisiae* highlights role of transcription factors in fungal xenobiotic resistance.” The dissertation author was a co-first author of this paper.

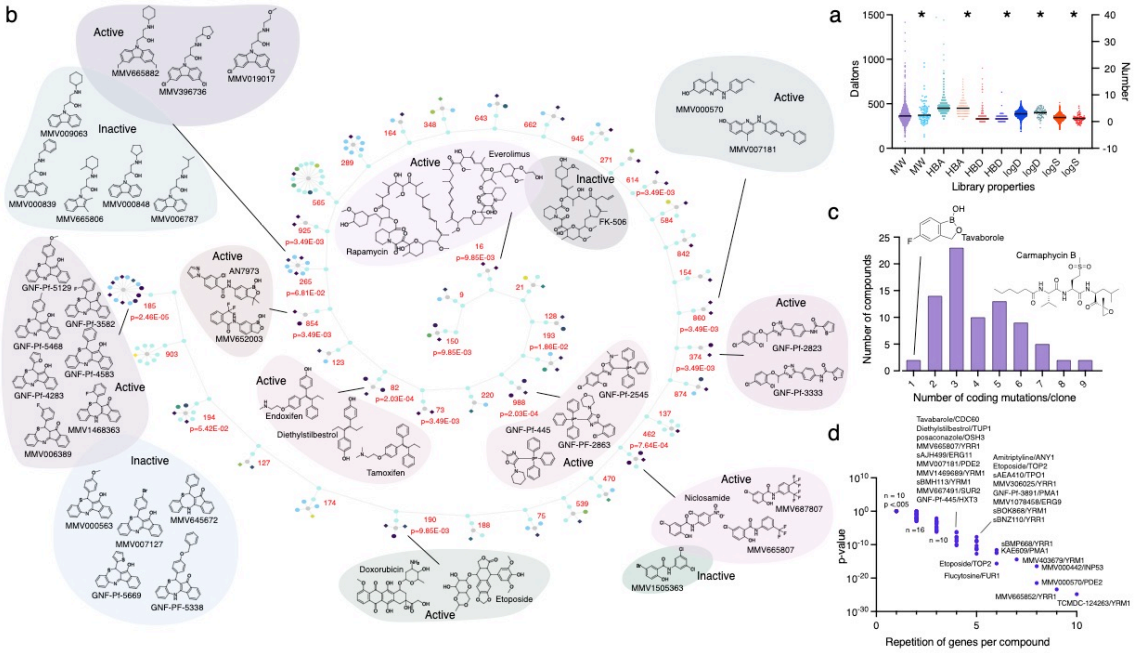

Figure 5.1. Compound Summary. (A) Lipinski properties. Lipinski's properties of compounds used in this study calculated using StarDrop version 6.6.4. Left Y axis: MW, molecular weight: Right Y axis: HBD, hydrogen bond donor, HBA, hydrogen bond acceptor, logD, logS. * indicates 80 compounds that yielded resistant clones. (B) Maximum Common Substructure (MCS). Structure similarity clustering analysis for 80 compounds yielding resistant clones and larger library of 1600, using Tanimoto as similarity metric. The diagram shows 41 clusters sharing an MCS from which at least one compound was selected for drug response (indicated by diamonds). Circles represent compounds that were not selected, or inactive. The strength of cytotoxicity against the *S. cerevisiae* GM strain of tested compounds is indicated by the node's color intensity from purple (higher potency) to yellow (lower potency). Probability values were calculated using the hypergeometric mean function showing that enrichment for clusters was greater than expected by chance. Compounds from clusters with a p-value of less than 0.05 and which had multiple members active against GM are shown. (C) Coding region mutations for selected compounds. Histogram showing the distribution of the number of coding mutations (e.g., missense, start-lost) per clone for the set of 80 compounds used in selections. (D) Gene enrichment for selected compounds. The p-value is the probability of repeatedly discovering the same gene for a given compound, calculated using Bonferroni-corrected hypergeometric mean function as described in Methods. Compound/gene pairs for n = 1, 2, and 3 can be obtained from **Supplemental Table 5.4**.

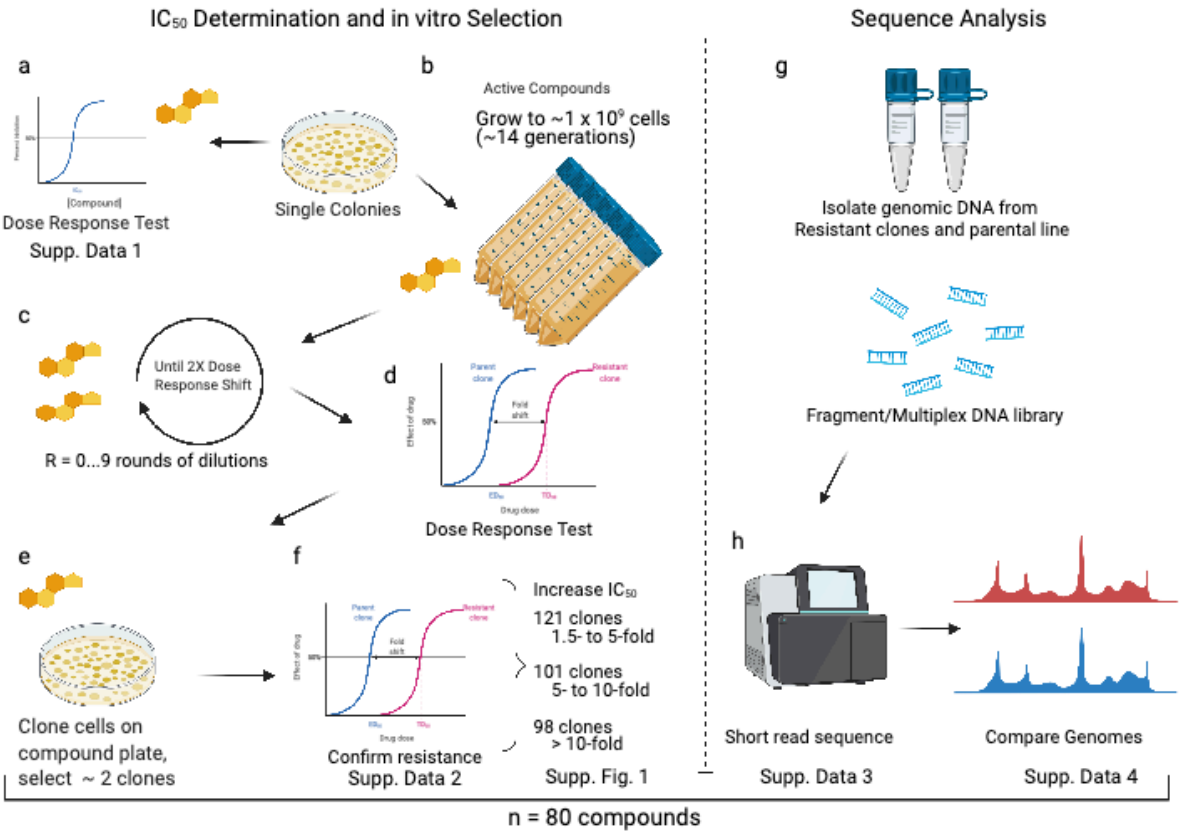

Figure 5.2. Generation of resistant yeast strains using a stepwise method of compound exposure. (A) To determine the degree of growth inhibition of small molecules, cultures derived from single colonies of the ABC$_{16}$-Green Monster strain (GM) were exposed to various drugs and the IC$_{50}$s determined. (B) For *in vitro* selections single colonies of GM were picked and grown to saturation in YPD media. 50µl cells of a saturated culture (OD$_{600}$=1) were inoculated into 50mL tubes containing 20mL of YPD media with a small molecule inhibitor and grown until saturation. The starting drug concentration was the pre-determined IC$_{50}$. (C) Upon reaching saturation cultures were diluted (1:400) into fresh media with increasing drug concentrations. (D) Development of resistance was evaluated through regular IC$_{50}$ determinations. (E) Once cultures showed at least a 2-fold shift in IC$_{50}$ single clones were generated by plating an aliquot of the resistant strain onto compound-containing YPD plates. (F) Two independent clones were picked and the IC$_{50}$ shift confirmed. IC$_{50}$ values were calculated by subtracting OD$_{600}$ nm values at time 0 hours from time 18 hours. Nonlinear regression on log([inhibitor]) vs. response with variable slope was performed using GraphPad Prism. Cycloheximide was used as a negative control. (G) DNA from clones deemed to be resistant (through a combination of fold-shift of IC$_{50}$ and p-value) was isolated and their whole genome analyzed. (H) The genomes of the drug-naïve parents and the drug-resistant clones were compared and allele differences between these two clones were determined. Data from all in *vitro* evolutions was analyzed in great detail. To further validate the potential resistance of the identified mutations allelic replacement of these SNVs into the parental line through CRISPR-Cas9 was performed. Graphics created with Biorender.com under BioRender's Academic License Terms.

Figure 5.3. Mutations observed in yeast IVIEWGA experiments. (A) Base transition. Classification of mutation based on base transition type for 1,286 SNV mutations obtained via compound selection and absence of compound selection. (B) Classification of the most common mutation types in the dataset and their occurrence in essential vs. nonessential genes. Essentiality data was imported from the *Saccharomyces* Genome Deletion Project database and proportion of essential vs. nonessential genes that contained missense, synonymous, frameshift, and stop gained mutations were calculated. (C) Mutation type. Variant classes for 1,405 mutations (INDELs and SNVs supplied from **Supplemental Table 5.4**) obtained via compound selection versus a mutation dataset from non-compound selection conditions. (D) Circos plot. Circos plot of SNVs (blue), INDELs (orange), and CNVs (cyan) identified through resistance generation, generated with BioCircos R package. (E-G). Intergenic mutations. Plot locating each coding region mutation onto the gene (grey) and intergenic mutation onto the chromosome (orange) based on the calculated distance. Mutations were mapped to their corresponding genomic location using *S. cerevisiae* S288C genome version R64-2-1. Intergenic mutations are located at no more than 500bp away from the start/end of the gene.

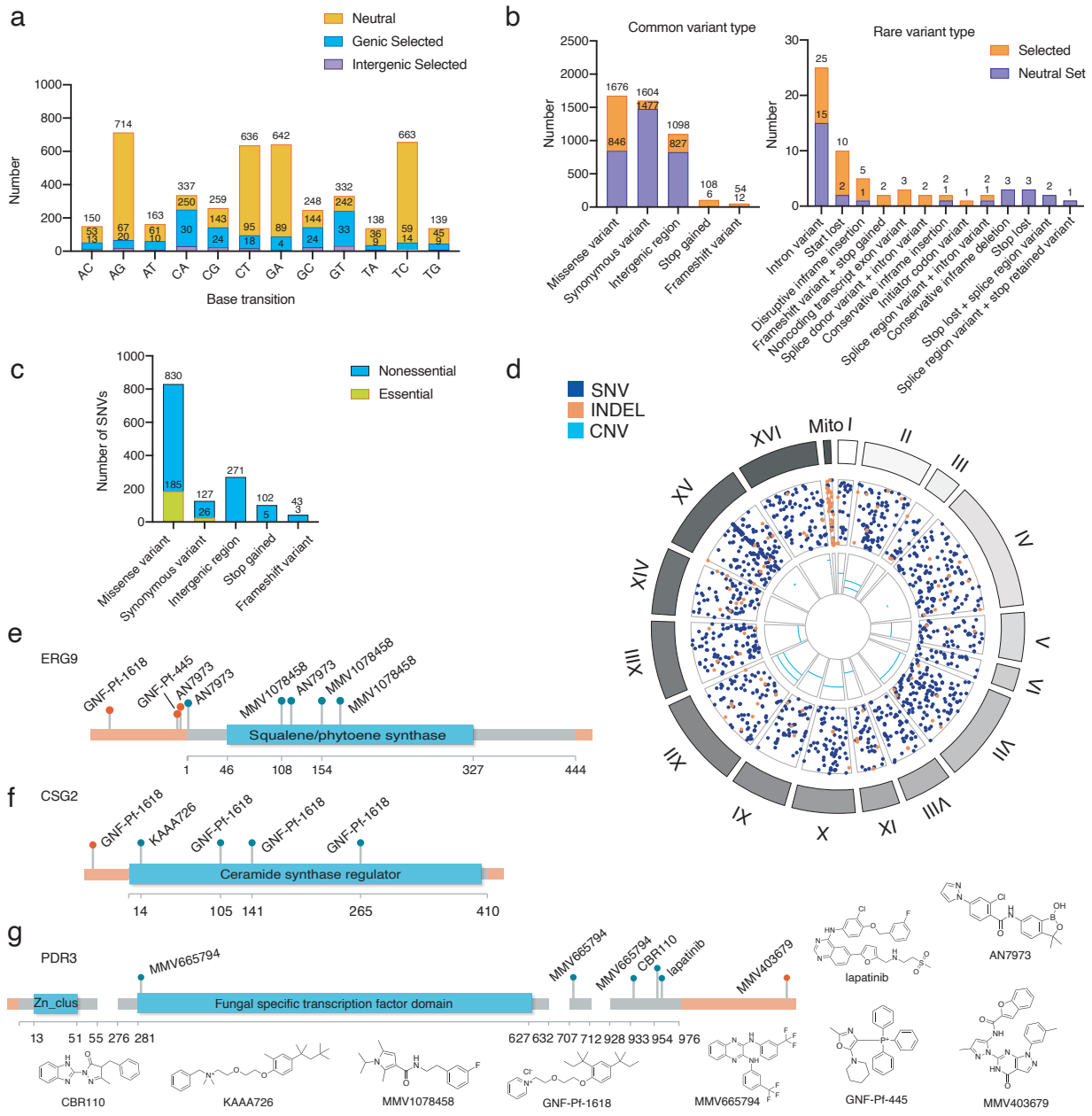
a
Neutral
Genic Selected
Intergenic Selected
Number
Base transition
AC
AG
AT
CA
CG
CT
GA
GC
GT
TA
TC
TG
b
Common variant type
Rare variant type
Selected
Neutral Set
Missense variant
Synonymous variant
Intergenic region
Stop gained
Frameshift variant
Intron variant
Start lost
Disruptive inframe insertion
Frameshift variant + stop gained
Noncoding transcript exon variant
Splice donor variant + intron variant
Conservative inframe insertion
Initiator codon variant
Splice region variant + intron variant
Conservative inframe deletion
Stop lost
Stop lost + splice region variant
Splice region variant + stop retained variant
c
Nonessential
Essential
Number of SNVs
d
SNV
INDEL
CNV
Mito I
e
ERG9
GNF-Pf-1618
GNF-Pf-445
AN7973
MMV1078458
Squalene/phytoene synthase
f
CSG2
KAAA726
Ceramide synthase regulator
g
PDR3
MMV665794
CBR110
lapatinib
MMV403679
Zn_clus
Fungal specific transcription factor domain
KAAA726
MMV1078458
GNF-Pf-1618
GNF-Pf-445

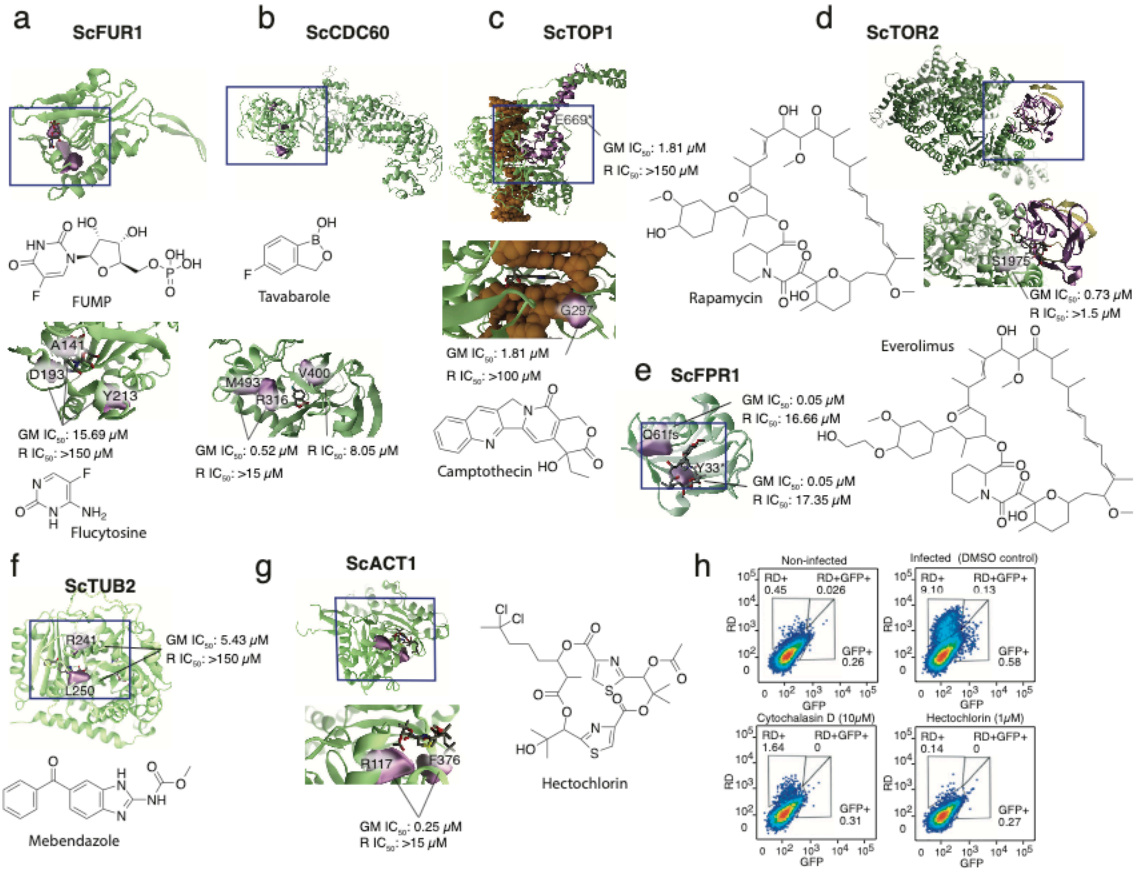

Figure 5.4. Resistance-conferring mutations in detail. Proteins and DNA are shown in green and orange, respectively. R = resistant line, GM = green monster parents. (A) Fur1 in complex with 5-FUMP. *Sc*Fur1 homology model, with a bound 5-FUMP analog (uridine monophosphate) taken from an aligned *holo Tm*Fur1 crystal structure (PDB ID: 1O5O). (B) Cdc60 model. Cdc60 homology model bound to a docked tavaborole molecule. (C) Top1 model. DNA-Top1-camptothecin complex, modelled using a *Sc*Top1 crystal structure (PDB: 1OIS), with bound camptothecin taken from an aligned *holo Hs*Top1p crystal structure (PDB: 1T8I). (D) Tor2 model. mTOR-rapamycin-Fpr1 tertiary complex model, modelled using a crystal structure of the human complex as a template (PDB ID: 4DRI). mTOR residues 1001 to 2474 are shown in green (homology model), and Fpr1 is shown in yellow (crystal structure, PDB: 1YAT). (E) Fpr1-rapamycin model. Fpr-rapamycin (crystal structure, PDB: 1YAT). (F) Tub2-nocodazol model. Tub2-nocodazol (crystal structure, PDB: 5CA1). (G) Act1 model. Act1 (crystal structure, PDB: 1YAG), bound to a docked hectochlorin molecule. Evaluation of hepatocellular traversal by *P. berghei* sporozoites using an established flow cytometry-based assay[Error! Reference source not found.]. (H) Liver cell invasion assay. Flow cytometry plots show traversal and invasion of host cells at 2 hours post-invasion by exoerythrocytic forms in Huh7.5.1 cells. The percent of rhodamine-dextran positive single cells (RD) was used to determine overall traversal frequency, controlled against cytochalasin D (positive) at 10μM and infected untreated conditions, while invasion was evaluated by exclusive GFP+ signal.

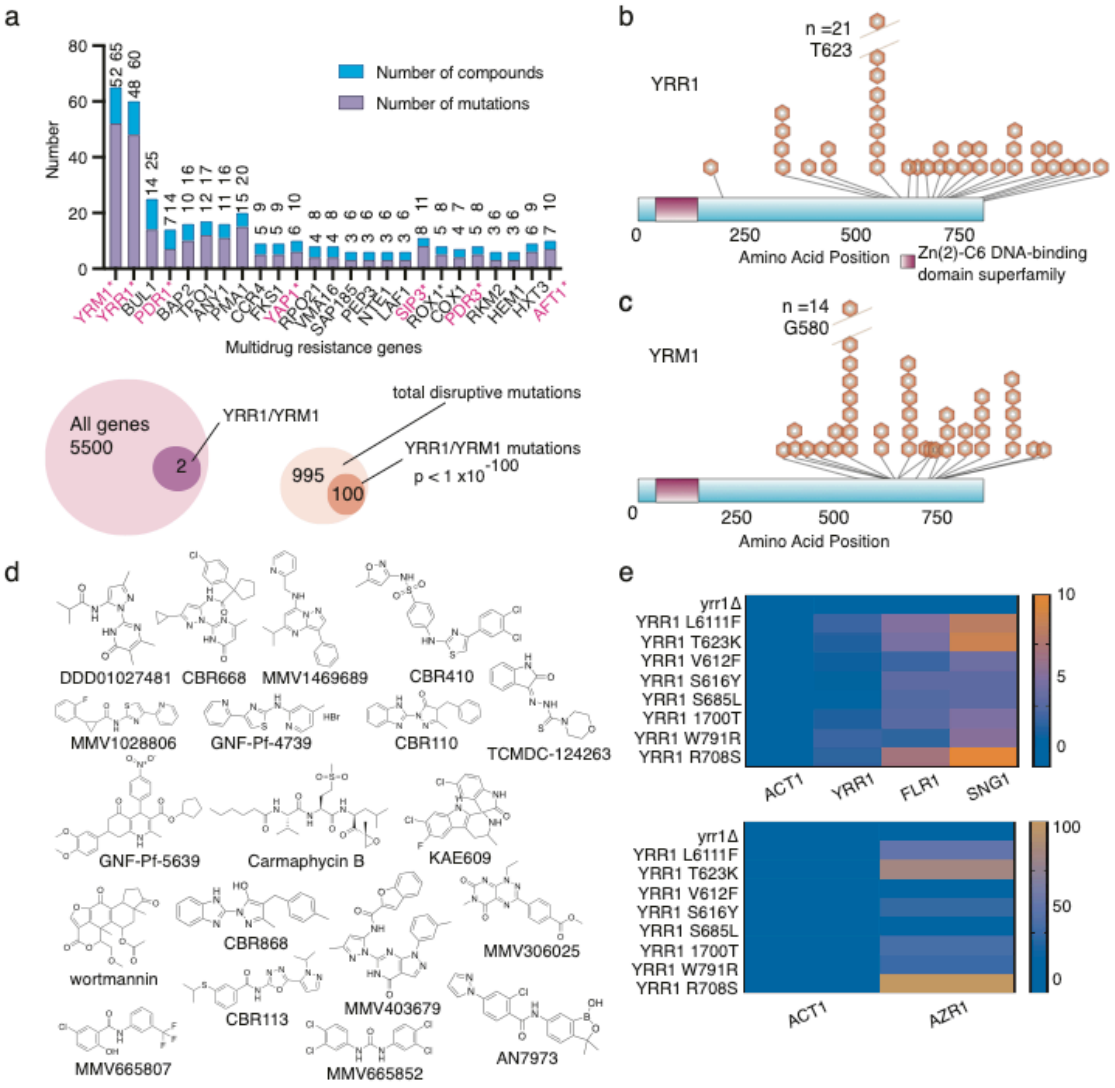

Figure 5.5. Mutations in transcription factors are over-represented. (A) Genes identified with three of more different compounds. Genes (8) with ontology GO:0140110 (transcription regulator activity) are shown in red. *YRR1* (B) and *YRM1* (C) mutation localization. Distribution of mutations in *YRR1* and *YRM1* across the amino acid sequence clustered in the C-terminal activation domain. (D) Scaffolds. Compounds used in selections resulting in *YRR1* and *YRM1* mutations. (E) *YRR1* single nucleotide mutations but not loss-of-function mutations constitutively activate transcriptional targets. RT-qPCR was utilized to monitor mRNA levels of *YRR1* and *YRR1* activated genes. Clones with *YRR1* point mutations show increases in mRNA levels of *YRR1, SNG1, FLG1*, and *AZR1* relative to the wild-type strain (GM), but the deletion mutant does not. In the absence of *YRR1*, associated genes display baseline or lower level of expression. The heatmap indicates fold change normalized to *ACT1*.

Table 5.1. Summary of statistically enriched genes identified in compound selections. 32 genes contained at least 4 independently selected coding mutations, the significance threshold for number of mutations occurring in a gene at a rate not expected by chance across the dataset. Bonferroni-corrected p-values were calculated using the hypergeometric mean function (number of successes in sample = number of times gene was identified as mutated; sample size = total number of genes mutated in dataset (731); successes in population = number of independent selections (355); population size = number of genes in yeast genome multiplied by 355) followed by Bonferroni-correction using number of independent selections. NG = number of times gene was identified as mutated in independent evolution experiments. NC = number of compounds.

Gene	Description	NG	NC	Compounds	p-value
YRM1	Zn2-Cys6 zinc finger transcription factor	52	13	See Supplemental Table 5.4	3.53×10^{-116}
YRR1	Zn2-Cys6 zinc-finger transcription factor	48	12	See Supplemental Table 5.4	2.51×10^{-105}
PMA1	Plasma membrane P2-type H+-ATPase	15	5	GNF-Pf-445, Hygromycin B, KAE609, Wortmannin, GNF-Pf-3891	3.00×10^{-24}
BUL1	Ubiquitin-binding component of the Rsp5p E3-ubiquitin ligase complex	14	11	See Supplemental Table 5.4	3.92×10^{-22}
PDE2	High-affinity cyclic AMP phosphodiesterase	13	2	MMV000570, MMV007181	4.76×10^{-20}
TPO1	Polyamine transporter of the major facilitator superfamily	12	5	GNF-Pf-4283, MMV006389, CBR410, CBR572, TCMDC-124263	5.34×10^{-18}
ANY1	Putative protein of unknown function	11	5	Amitriptyline, MMV019017, Clomipramine, MMV396736, Sertraline	5.51×10^{-16}
BAP2	High-affinity leucine permease	10	6	GNF-Pf-3703, GNF-Pf-3815, GNF-Pf-5129, GNF-Pf-5468, MMV006389	5.19×10^{-14}
SIP3	Putative sterol transfer protein	8	3	GNF-Pf-445, Lomerizine, Loratidine	3.38×10^{-10}
INP53	Polyphosphatidylinositol phosphatase	8	1	MMV000442	3.38×10^{-10}
AFT1	Transcription factor involved in iron utilization	7	3	MMV085203, MMV1007245, CBR868	2.28×10^{-8}
PDR1	Transcription factor that regulates the pleiotropic drug response	7	7	DDD01027481, Doxorubicin, MMV000442, MMV007224, MMV667491, CBR668, CBR110	2.28×10^{-8}
ERG9	Farnesyl-diphosphate farnesyl transferase	7	2	AN7973, MMV1078458	2.28×10^{-8}
YAP1	Basic leucine zipper (bZIP) transcription factor	6	4	Cycloheximide, GNF-Pf-4739, DDD01027481, MMV001246	1.34×10^{-6}
TOP2	Topoisomerase II	6	1	Etoposide	1.34×10^{-6}
HXT3	Low affinity glucose transporter of the major facilitator superfamily	6	3	Amitriptyline, DDD01035522, GNF-Pf-445	1.34×10^{-6}
ERG11	Lanosterol 14-alpha-demethylase	6	2	MMV001239, CBR499	1.34×10^{-6}
FUR1	Uracil phosphoribosyltransferase	6	1	Flucytosine	1.34×10^{-6}
CCR4	Component of the CCR4-NOT transcriptional complex	5	4	GNF-Pf-2823, GNF-Pf-4583, MMV403679, CBR868	6.76×10^{-5}
ERG3	C-5 sterol desaturase	5	2	Miconazole, Posaconazole	6.76×10^{-5}
FKS1	Catalytic subunit of 1,3-beta-D-glucan synthase	5	4	DDD01027481, CBR113, CBR668, CBR110	6.76×10^{-5}
CDC60	Cytosolic leucyl tRNA synthetase	5	2	CBR668, Tavaborole	
ROX1	Heme-dependent repressor of hypoxic genes;	5	3	Loratadine, MMV665909, TCMDC-124263	6.76×10^{-5}
PDR3	Transcriptional activator of the pleiotropic drug resistance network	5	3	Lapatinib, MMV665794, CBR110	6.76×10^{-5}
OSH3	Member of an oxysterol-binding protein family	5	1	Posaconazole	6.76×10^{-5}
CSG2	Endoplasmic reticulum membrane protein	4	2	GNF-Pf-1618, KAAA726	4.76×10^{-2}
ELO2	Fatty acid elongase	4	2	Doxorubicin, MMV667491	4.76×10^{-2}

Table 5.1. Summary of statistically enriched genes identified in compound selections, Continued.

TUP1	General repressor of transcription	4	1	Diethylstilbestrol	
RPO21	RNA polymerase II largest subunit B220	4	4	Lapatinib, MMV007181, MMV1469689, CBR110	4.76×10^{-2}
SUR2	Sphinganine C4-hydroxylase	4	1	MMV667491	4.76×10^{-2}
VMA16	Subunit c'' of the vacuolar ATPase	4	4	Lapatinib, MMV019017, MMV396736, MMV665882	4.76×10^{-2}
PAN1	Part of actin cytoskeleton-regulatory complex Pan1p-Sla1p-End3p	4	2	Hygromycin B, KAE609	4.76×10^{-2}

Chapter 6

Conclusions

The World Health Organization considers antimicrobial resistance to be one of the top 10 global health threats currently facing humanity. While this often refers to prokaryotic pathogens – namely, bacteria – eukaryotic pathogens such as parasites and fungi also exhibit an alarming propensity to evolve drug resistance in a short period of time, threatening the efficacy of available first-line treatments. Experimental evolution is one tool that has been used successfully to study this development of resistance under the tight control of a laboratory environment. Inside of a test tube, the selection forces that are applied to the organism of interest are much more clearly defined that those that exist *in vivo*. Whole genome sequencing of a lab-generated resistant microbe often very easily identifies at least one mutation responsible for driving the resistance phenotype. Evolution experiments in microorganisms are usually highly scalable and cost-effective, meaning they can be reproduced multiple times to achieve statistical confidence in the findings. This dissertation summarizes the findings of evolution experiments performed in three different microorganisms with clinical implications – *Plasmodium falciparum*, *Toxoplasma gondii*, and *Saccharomyces cerevisiae*.

Both Chapters 2 and 3 concern drug resistance development in *Plasmodium falciparum*, the causative agent of the severest form of human malaria. In Chapter 2 we investigated an individual antimalarial drug target, DHODH, and its resistance potential with the clinical candidate DSM265. Selections of *P. falciparum* with DSM265 and its analogs were performed in both the *in vitro* (tissue culture flask) and *in vivo* (mouse model) environment. We repeatedly identified the same SNVs and CNVs contributing to the resistance phenotype, highlighting that the cheaper and faster *in vitro* method was generally a good model of resistance development. Interestingly, the C276Y mutation that

was commonly identified in this study was also observed in the Phase 2a clinical trials for DSM265, showing up as a mutation in at least one mutation with a recrudescent infection following single-dose treatment[125]. While this supports the *in vitro* system as a model for understanding clinical resistance development, it is difficult to say whether the same would be true across all antimalarial drug targets and clinical candidates. A tissue culture flask simply cannot recapitulate all of the selective forces applied to the parasite, so field variants are unlikely to perfectly mirror those identified in *in vitro* studies like ours. Nonetheless, we show that the *in vitro* model can successfully identify drug targets and certain key mutations that could hold importance for further development of different drug classes. Indeed, one of the most sobering findings of our work with DHODH as an antimalarial drug target is the rapidity with which the parasite evolves resistance – a finding that is supported *in vitro*, in murine models, and patient themselves. Resistance liability is such a concern for DHODH that further DSM265 clinical development has been halted, representing almost a decade of work and millions of dollars invested in the project. In fact, the Medicines for Malaria Venture has proposed that resistance liability testing now be one of the very first steps in any antimalarial drug discovery program[357].

Chapter 3 expanded on the idea of Chapter 2 by collating a decade's worth of compound selections performed in *P. falciparum* into a single accessible repository. To our knowledge, this is the single largest dataset of its kind. In addition to providing the complete set of mutations identified across 113 individual compound selections, which is useful for determining whether certain compounds should continue to be investigated as potential next-generation antimalarials, we looked at the occurrences of certain genes and mutations across the dataset in aggregate to identify patterns in resistance

development. Perhaps not surprisingly, we observed a large abundance of mutations in known, validated multidrug resistance mechanisms which in total affected half of all compounds in the dataset. A useful finding for further study is that most mutations that occurred in validated drug targets were localized to the catalytic portion of the protein or within another relevant functional domain. This provides a starting point for assessing the entire list of variants for novel drug targets or compound-interacting molecules. Because follow-up experiments in *Plasmodium* are costly and time-consuming, it is imperative that we make informed decisions about what genes to pursue; these decisions can be aided by the dataset presented here.

Chapter 4 next explores resistance generation to the gold standard treatment for malaria, Artemisinin (ART), in both *P. falciparum* and *T. gondii*. While both parasites are classified under the same phylum Apicomplexa, the biological pathways involved in parasitism of their respective hosts are quite different. The mechanism by which ART works against the malaria parasite is not fully understood but is widely known to (1) involve the formation of free radicals which damage a large number of proteins in the parasite, and (2) involve disruption of proteasome function. Crucially, ART is activated by interactions with heme in host red blood cells (RBCs), which explains why it works against the RBC-dwelling malaria parasite but not *T. gondii*. Selections in both *Toxoplasma* and *Plasmodium* yielded no common resistance genes between the two of them, as might be expected. However, the two candidate genes identified in *T. gondii* – DegP2, a serine protease, and Ark1, a serine/threonine kinase of unknown function – are believed to be involved in the parasite stress response, which does at least partially line up with selection results in *Plasmodium*. Perhaps the key feature that is shared across both organisms is

the multigenic nature of ART resistance development. This supports the theory that ART is a promiscuous, non-specific drug and highlights the need for additional studies to comprehensively define the ART "resistome," given it is the gold standard therapy.

Finally, Chapter 5 explores fungal resistance mechanisms using the model microbe *S. cerevisiae*. Compared to both *P. falciparum* and *T. gondii*, yeast is by far the simplest organism to work with at scale. We took advantage of its easy culturing conditions to generate 355 resistant lines with 80 different small molecules spanning a collection of antimalarials, antifungals, and antitumor agents. Whole genome analysis identified that the most abundantly identified genes across the dataset were two Zn_2C_6 transcription factors, *YRR1* and *YRM1*, part of a family of transcription factors that are known only to exist in fungi. 19 structurally diverse compounds yielded mutations in at least one of these transcription factors. Given their known function in the pleiotropic drug response, this finding was perhaps not surprising. The gain-of-function mutations acquired during selection are believed to cause an increase in the transcription of drug pumps, which would lead to resistance to many compounds irrespective of their specific mechanism of action. However, it is interesting that in both of the two large selection datasets explored in this dissertation – the *P. falciparum* selection dataset in Chapter 3 and the yeast dataset explored in Chapter 5 – multidrug resistance mechanisms are abundant and affect a large proportion of compounds tested. If anything, this highlights the remarkable ability of microorganisms, no matter what biological kingdom, to evolve ways to survive environmental stressors such as the application of an inhibitor. Indeed, the most of the major resistance mechanisms in *Plasmodium* are membrane-bound

proteins involved in transport, and the major diver of resistance in yeast was found to be a set of transcription factors that mainly upregulate the activity of membrane transporters.

Altogether, this dissertation seeks to shed light on common pathways of resistance across a series of eukaryotic microorganisms with implications in human health. The genomic drivers of drug resistance are diverse and many; however, several patterns exist. The classic case of resistance mutations that occur within the binding pocket of the drug target of interest are of perhaps the most use to drug discovery and development campaigns. Indeed, both the *S. cerevisiae* and *P. falciparum* resistance generation projects were initiated as a means to identify novel drug targets for a variety of compounds with antimicrobial activity. In many cases, experimental evolution did lead to the discovery of new drug targets or lent a greater understanding of ones that already were being developed, as reviewed in Chapter 1. In the end, though, we find that multidrug resistance mechanisms make up a significant portion of the driver genes identified across both projects. Taken in tandem, these results provide a much more comprehensive understanding of how antimicrobial resistance emerges, proliferates, and hopefully, how it can be controlled and defeated. While experimental evolution is but one method of understanding the phenomenon of drug resistance, as shown here, it is a powerful one.

REFERENCES

1. White, N.J., Pukrittayakamee, S., Hien, T.T., Faiz, M.A., Mokuolu, O.A. & Dondorp, A.M. Malaria. *Lancet* **383**, 723-35 (2014).

2. Nilsson, S.K., Childs, L.M., Buckee, C. & Marti, M. Targeting Human Transmission Biology for Malaria Elimination. *PLoS Pathog* **11**, e1004871 (2015).

3. Tilley, L., Straimer, J., Gnadig, N.F., Ralph, S.A. & Fidock, D.A. Artemisinin Action and Resistance in Plasmodium falciparum. *Trends Parasitol* **32**, 682-696 (2016).

4. Blasco, B., Leroy, D. & Fidock, D.A. Antimalarial drug resistance: linking Plasmodium falciparum parasite biology to the clinic. *Nat Med* **23**, 917-928 (2017).

5. White, N.J., Pukrittayakamee, S., Phyo, A.P., Rueangweerayut, R., Nosten, F., Jittamala, P., Jeeyapant, A., Jain, J.P., Lefevre, G., Li, R., Magnusson, B., Diagana, T.T. & Leong, F.J. Spiroindolone KAE609 for falciparum and vivax malaria. *N Engl J Med* **371**, 403-10 (2014).

6. Rottmann, M., McNamara, C., Yeung, B.K., Lee, M.C., Zou, B., Russell, B., Seitz, P., Plouffe, D.M., Dharia, N.V., Tan, J., Cohen, S.B., Spencer, K.R., Gonzalez-Paez, G.E., Lakshminarayana, S.B., Goh, A., Suwanarusk, R., Jegla, T., Schmitt, E.K., Beck, H.P., Brun, R., Nosten, F., Renia, L., Dartois, V., Keller, T.H., Fidock, D.A., Winzeler, E.A. & Diagana, T.T. Spiroindolones, a potent compound class for the treatment of malaria. *Science* **329**, 1175-80 (2010).

7. Spillman, N.J., Allen, R.J., McNamara, C.W., Yeung, B.K., Winzeler, E.A., Diagana, T.T. & Kirk, K. Na(+) regulation in the malaria parasite Plasmodium falciparum involves the cation ATPase PfATP4 and is a target of the spiroindolone antimalarials. *Cell Host Microbe* **13**, 227-37 (2013).

8. Flannery, E.L., McNamara, C.W., Kim, S.W., Kato, T.S., Li, F., Teng, C.H., Gagaring, K., Manary, M.J., Barboa, R., Meister, S., Kuhen, K., Vinetz, J.M., Chatterjee, A.K. & Winzeler, E.A. Mutations in the P-type cation-transporter ATPase 4, PfATP4, mediate resistance to both aminopyrazole and spiroindolone antimalarials. *ACS Chem Biol* **10**, 413-20 (2015).

9. Ginsburg, H., Handeli, S., Friedman, S., Gorodetsky, R. & Krugliak, M. Effects of red blood cell potassium and hypertonicity on the growth of Plasmodium falciparum in culture. *Z Parasitenkd* **72**, 185-99 (1986).

10. Allman, E.L., Painter, H.J., Samra, J., Carrasquilla, M. & Llinas, M. Metabolomic Profiling of the Malaria Box Reveals Antimalarial Target Pathways. *Antimicrob Agents Chemother* **60**, 6635-6649 (2016).

11. Jimenez-Diaz, M.B., Ebert, D., Salinas, Y., Pradhan, A., Lehane, A.M., Myrand-Lapierre, M.E., O'Loughlin, K.G., Shackleford, D.M., Justino de Almeida, M., Carrillo, A.K., Clark, J.A., Dennis, A.S., Diep, J., Deng, X., Duffy, S., Endsley, A.N., Fedewa, G., Guiguemde, W.A., Gomez, M.G., Holbrook, G., Horst, J., Kim, C.C., Liu, J., Lee, M.C., Matheny, A., Martinez, M.S., Miller, G., Rodriguez-Alejandre, A., Sanz, L., Sigal, M., Spillman, N.J., Stein, P.D., Wang, Z., Zhu, F., Waterson, D., Knapp, S., Shelat, A., Avery, V.M., Fidock, D.A., Gamo, F.J., Charman, S.A., Mirsalis, J.C., Ma, H., Ferrer, S., Kirk, K., Angulo-Barturen, I., Kyle, D.E., DeRisi, J.L., Floyd, D.M. & Guy, R.K. (+)-SJ733, a clinical candidate for malaria that acts through ATP4 to induce rapid host-mediated clearance of Plasmodium. *Proc Natl Acad Sci U S A* **111**, E5455-62 (2014).

12. Vaidya, A.B., Morrisey, J.M., Zhang, Z., Das, S., Daly, T.M., Otto, T.D., Spillman, N.J., Wyvratt, M., Siegl, P., Marfurt, J., Wirjanata, G., Sebayang, B.F., Price, R.N., Chatterjee, A., Nagle, A., Stasiak, M., Charman, S.A., Angulo-Barturen, I., Ferrer, S., Belen Jimenez-Diaz, M., Martinez, M.S., Gamo, F.J., Avery, V.M., Ruecker, A., Delves, M., Kirk, K., Berriman, M., Kortagere, S., Burrows, J., Fan, E. & Bergman, L.W. Pyrazoleamide compounds are potent antimalarials that target Na+ homeostasis in intraerythrocytic Plasmodium falciparum. *Nat Commun* **5**, 5521 (2014).

13. Pham, J.S., Dawson, K.L., Jackson, K.E., Lim, E.E., Pasaje, C.F., Turner, K.E. & Ralph, S.A. Aminoacyl-tRNA synthetases as drug targets in eukaryotic parasites. *Int J Parasitol Drugs Drug Resist* **4**, 1-13 (2014).

14. Ling, J., Reynolds, N. & Ibba, M. Aminoacyl-tRNA synthesis and translational quality control. *Annu Rev Microbiol* **63**, 61-78 (2009).

15. Yadavalli, S.S. & Ibba, M. Quality control in aminoacyl-tRNA synthesis its role in translational fidelity. *Adv Protein Chem Struct Biol* **86**, 1-43 (2012).

16. Bhatt, T.K., Kapil, C., Khan, S., Jairajpuri, M.A., Sharma, V., Santoni, D., Silvestrini, F., Pizzi, E. & Sharma, A. A genomic glimpse of aminoacyl-tRNA synthetases in malaria parasite Plasmodium falciparum. *BMC Genomics* **10**, 644 (2009).

17. Sharma, A. & Sharma, A. Plasmodium falciparum mitochondria import tRNAs along with an active phenylalanyl-tRNA synthetase. *Biochem J* **465**, 459-69 (2015).

18. Istvan, E.S., Dharia, N.V., Bopp, S.E., Gluzman, I., Winzeler, E.A. & Goldberg, D.E. Validation of isoleucine utilization targets in Plasmodium falciparum. *Proc Natl Acad Sci U S A* **108**, 1627-32 (2011).

19. Kato, N., Comer, E., Sakata-Kato, T., Sharma, A., Sharma, M., Maetani, M., Bastien, J., Brancucci, N.M., Bittker, J.A., Corey, V., Clarke, D., Derbyshire, E.R.,

Dornan, G.L., Duffy, S., Eckley, S., Itoe, M.A., Koolen, K.M., Lewis, T.A., Lui, P.S., Lukens, A.K., Lund, E., March, S., Meibalan, E., Meier, B.C., McPhail, J.A., Mitasev, B., Moss, E.L., Sayes, M., Van Gessel, Y., Wawer, M.J., Yoshinaga, T., Zeeman, A.M., Avery, V.M., Bhatia, S.N., Burke, J.E., Catteruccia, F., Clardy, J.C., Clemons, P.A., Dechering, K.J., Duvall, J.R., Foley, M.A., Gusovsky, F., Kocken, C.H., Marti, M., Morningstar, M.L., Munoz, B., Neafsey, D.E., Sharma, A., Winzeler, E.A., Wirth, D.F., Scherer, C.A. & Schreiber, S.L. Diversity-oriented synthesis yields novel multistage antimalarial inhibitors. *Nature* **538**, 344-349 (2016).

20. Khan, S., Sharma, A., Jamwal, A., Sharma, V., Pole, A.K., Thakur, K.K. & Sharma, A. Uneven spread of cis- and trans-editing aminoacyl-tRNA synthetase domains within translational compartments of P. falciparum. *Sci Rep* **1**, 188 (2011).

21. Hoepfner, D., McNamara, C.W., Lim, C.S., Studer, C., Riedl, R., Aust, T., McCormack, S.L., Plouffe, D.M., Meister, S., Schuierer, S., Plikat, U., Hartmann, N., Staedtler, F., Cotesta, S., Schmitt, E.K., Petersen, F., Supek, F., Glynne, R.J., Tallarico, J.A., Porter, J.A., Fishman, M.C., Bodenreider, C., Diagana, T.T., Movva, N.R. & Winzeler, E.A. Selective and specific inhibition of the plasmodium falciparum lysyl-tRNA synthetase by the fungal secondary metabolite cladosporin. *Cell Host Microbe* **11**, 654-63 (2012).

22. Khan, S., Sharma, A., Belrhali, H., Yogavel, M. & Sharma, A. Structural basis of malaria parasite lysyl-tRNA synthetase inhibition by cladosporin. *J Struct Funct Genomics* **15**, 63-71 (2014).

23. Fang, P., Han, H., Wang, J., Chen, K., Chen, X. & Guo, M. Structural Basis for Specific Inhibition of tRNA Synthetase by an ATP Competitive Inhibitor. *Chem Biol* **22**, 734-44 (2015).

24. Hoen, R., Novoa, E.M., Lopez, A., Camacho, N., Cubells, L., Vieira, P., Santos, M., Marin-Garcia, P., Bautista, J.M., Cortes, A., Ribas de Pouplana, L. & Royo, M. Selective inhibition of an apicoplastic aminoacyl-tRNA synthetase from Plasmodium falciparum. *Chembiochem* **14**, 499-509 (2013).

25. Keller, T.L., Zocco, D., Sundrud, M.S., Hendrick, M., Edenius, M., Yum, J., Kim, Y.J., Lee, H.K., Cortese, J.F., Wirth, D.F., Dignam, J.D., Rao, A., Yeo, C.Y., Mazitschek, R. & Whitman, M. Halofuginone and other febrifugine derivatives inhibit prolyl-tRNA synthetase. *Nat Chem Biol* **8**, 311-7 (2012).

26. Herman, J.D., Pepper, L.R., Cortese, J.F., Estiu, G., Galinsky, K., Zuzarte-Luis, V., Derbyshire, E.R., Ribacke, U., Lukens, A.K., Santos, S.A., Patel, V., Clish, C.B., Sullivan, W.J., Jr., Zhou, H., Bopp, S.E., Schimmel, P., Lindquist, S., Clardy, J., Mota, M.M., Keller, T.L., Whitman, M., Wiest, O., Wirth, D.F. & Mazitschek, R. The cytoplasmic prolyl-tRNA synthetase of the malaria parasite is a dual-stage target of febrifugine and its analogs. *Sci Transl Med* **7**, 288ra77 (2015).

27. Jain, V., Yogavel, M., Kikuchi, H., Oshima, Y., Hariguchi, N., Matsumoto, M., Goel, P., Touquet, B., Jumani, R.S., Tacchini-Cottier, F., Harlos, K., Huston, C.D., Hakimi, M.A. & Sharma, A. Targeting Prolyl-tRNA Synthetase to Accelerate Drug Discovery against Malaria, Leishmaniasis, Toxoplasmosis, Cryptosporidiosis, and Coccidiosis. *Structure* **25**, 1495-1505 e6 (2017).

28. Werner, R.G., Thorpe, L.F., Reuter, W. & Nierhaus, K.H. Indolmycin inhibits prokaryotic tryptophanyl-tRNA ligase. *Eur J Biochem* **68**, 1-3 (1976).

29. Pasaje, C.F., Cheung, V., Kennedy, K., Lim, E.E., Baell, J.B., Griffin, M.D. & Ralph, S.A. Selective inhibition of apicoplast tryptophanyl-tRNA synthetase causes delayed death in Plasmodium falciparum. *Sci Rep* **6**, 27531 (2016).

30. Otoguro, K., Ui, H., Ishiyama, A., Kobayashi, M., Togashi, H., Takahashi, Y., Masuma, R., Tanaka, H., Tomoda, H., Yamada, H. & Omura, S. In vitro and in vivo antimalarial activities of a non-glycosidic 18-membered macrolide antibiotic, borrelidin, against drug-resistant strains of Plasmodia. *J Antibiot (Tokyo)* **56**, 727-9 (2003).

31. Frohler, J., Rechenmacher, A., Thomale, J., Nass, G. & Bock, A. Genetic analysis of mutations causing borrelidin resistance by overproduction of threonyl-transfer ribonucleic acid synthetase. *J Bacteriol* **143**, 1135-41 (1980).

32. Pham, J.S., Sakaguchi, R., Yeoh, L.M., De Silva, N.S., McFadden, G.I., Hou, Y.M. & Ralph, S.A. A dual-targeted aminoacyl-tRNA synthetase in Plasmodium falciparum charges cytosolic and apicoplast tRNACys. *Biochem J* **458**, 513-23 (2014).

33. Jackson, K.E., Pham, J.S., Kwek, M., De Silva, N.S., Allen, S.M., Goodman, C.D., McFadden, G.I., Ribas de Pouplana, L. & Ralph, S.A. Dual targeting of aminoacyl-tRNA synthetases to the apicoplast and cytosol in Plasmodium falciparum. *Int J Parasitol* **42**, 177-86 (2012).

34. Novoa, E.M., Camacho, N., Tor, A., Wilkinson, B., Moss, S., Marin-Garcia, P., Azcarate, I.G., Bautista, J.M., Mirando, A.C., Francklyn, C.S., Varon, S., Royo, M., Cortes, A. & Ribas de Pouplana, L. Analogs of natural aminoacyl-tRNA synthetase inhibitors clear malaria in vivo. *Proc Natl Acad Sci U S A* **111**, E5508-17 (2014).

35. Chakraborty, B., Mukherjee, R. & Sengupta, J. Structural insights into the mechanism of translational inhibition by the fungicide sordarin. *J Comput Aided Mol Des* **27**, 173-84 (2013).

36. Justice, M.C., Hsu, M.J., Tse, B., Ku, T., Balkovec, J., Schmatz, D. & Nielsen, J. Elongation factor 2 as a novel target for selective inhibition of fungal protein synthesis. *J Biol Chem* **273**, 3148-51 (1998).

37. Shastry, M., Nielsen, J., Ku, T., Hsu, M.J., Liberator, P., Anderson, J., Schmatz, D. & Justice, M.C. Species-specific inhibition of fungal protein synthesis by sordarin: identification of a sordarin-specificity region in eukaryotic elongation factor 2. *Microbiology (Reading)* **147**, 383-390 (2001).

38. Baragana, B., Hallyburton, I., Lee, M.C., Norcross, N.R., Grimaldi, R., Otto, T.D., Proto, W.R., Blagborough, A.M., Meister, S., Wirjanata, G., Ruecker, A., Upton, L.M., Abraham, T.S., Almeida, M.J., Pradhan, A., Porzelle, A., Luksch, T., Martinez, M.S., Luksch, T., Bolscher, J.M., Woodland, A., Norval, S., Zuccotto, F., Thomas, J., Simeons, F., Stojanovski, L., Osuna-Cabello, M., Brock, P.M., Churcher, T.S., Sala, K.A., Zakutansky, S.E., Jimenez-Diaz, M.B., Sanz, L.M., Riley, J., Basak, R., Campbell, M., Avery, V.M., Sauerwein, R.W., Dechering, K.J., Noviyanti, R., Campo, B., Frearson, J.A., Angulo-Barturen, I., Ferrer-Bazaga, S., Gamo, F.J., Wyatt, P.G., Leroy, D., Siegl, P., Delves, M.J., Kyle, D.E., Wittlin, S., Marfurt, J., Price, R.N., Sinden, R.E., Winzeler, E.A., Charman, S.A., Bebrevska, L., Gray, D.W., Campbell, S., Fairlamb, A.H., Willis, P.A., Rayner, J.C., Fidock, D.A., Read, K.D. & Gilbert, I.H. A novel multiple-stage antimalarial agent that inhibits protein synthesis. *Nature* **522**, 315-20 (2015).

39. Dechering, K.J., Duerr, H.P., Koolen, K.M.J., Gemert, G.V., Bousema, T., Burrows, J., Leroy, D. & Sauerwein, R.W. Modelling mosquito infection at natural parasite densities identifies drugs targeting EF2, PI4K or ATP4 as key candidates for interrupting malaria transmission. *Sci Rep* **7**, 17680 (2017).

40. Painter, H.J., Morrisey, J.M., Mather, M.W. & Vaidya, A.B. Specific role of mitochondrial electron transport in blood-stage Plasmodium falciparum. *Nature* **446**, 88-91 (2007).

41. Vaidya, A.B. & Mather, M.W. Mitochondrial evolution and functions in malaria parasites. *Annu Rev Microbiol* **63**, 249-67 (2009).

42. Phillips, M.A. & Rathod, P.K. Plasmodium dihydroorotate dehydrogenase: a promising target for novel anti-malarial chemotherapy. *Infect Disord Drug Targets* **10**, 226-39 (2010).

43. Phillips, M.A., Lotharius, J., Marsh, K., White, J., Dayan, A., White, K.L., Njoroge, J.W., El Mazouni, F., Lao, Y., Kokkonda, S., Tomchick, D.R., Deng, X., Laird, T., Bhatia, S.N., March, S., Ng, C.L., Fidock, D.A., Wittlin, S., Lafuente-Monasterio, M., Benito, F.J., Alonso, L.M., Martinez, M.S., Jimenez-Diaz, M.B., Bazaga, S.F., Angulo-Barturen, I., Haselden, J.N., Louttit, J., Cui, Y., Sridhar, A., Zeeman, A.M., Kocken, C., Sauerwein, R., Dechering, K., Avery, V.M., Duffy, S., Delves, M., Sinden, R., Ruecker, A., Wickham, K.S., Rochford, R., Gahagen, J., Iyer, L., Riccio, E., Mirsalis, J., Bathhurst, I., Rueckle, T., Ding, X., Campo, B., Leroy, D., Rogers, M.J., Rathod, P.K., Burrows, J.N. & Charman, S.A. A long-duration dihydroorotate dehydrogenase inhibitor (DSM265) for prevention and treatment of malaria. *Sci Transl Med* **7**, 296ra111 (2015).

44. McCarthy, J.S., Lotharius, J., Ruckle, T., Chalon, S., Phillips, M.A., Elliott, S., Sekuloski, S., Griffin, P., Ng, C.L., Fidock, D.A., Marquart, L., Williams, N.S., Gobeau, N., Bebrevska, L., Rosario, M., Marsh, K. & Mohrle, J.J. Safety, tolerability, pharmacokinetics, and activity of the novel long-acting antimalarial DSM265: a two-part first-in-human phase 1a/1b randomised study. *Lancet Infect Dis* **17**, 626-635 (2017).

45. Phillips, M.A., White, K.L., Kokkonda, S., Deng, X., White, J., El Mazouni, F., Marsh, K., Tomchick, D.R., Manjalanagara, K., Rudra, K.R., Wirjanata, G., Noviyanti, R., Price, R.N., Marfurt, J., Shackleford, D.M., Chiu, F.C., Campbell, M., Jimenez-Diaz, M.B., Bazaga, S.F., Angulo-Barturen, I., Martinez, M.S., Lafuente-Monasterio, M., Kaminsky, W., Silue, K., Zeeman, A.M., Kocken, C., Leroy, D., Blasco, B., Rossignol, E., Rueckle, T., Matthews, D., Burrows, J.N., Waterson, D., Palmer, M.J., Rathod, P.K. & Charman, S.A. A Triazolopyrimidine-Based Dihydroorotate Dehydrogenase Inhibitor with Improved Drug-like Properties for Treatment and Prevention of Malaria. *ACS Infect Dis* **2**, 945-957 (2016).

46. Booker, M.L., Bastos, C.M., Kramer, M.L., Barker, R.H., Jr., Skerlj, R., Sidhu, A.B., Deng, X., Celatka, C., Cortese, J.F., Guerrero Bravo, J.E., Crespo Llado, K.N., Serrano, A.E., Angulo-Barturen, I., Jimenez-Diaz, M.B., Viera, S., Garuti, H., Wittlin, S., Papastogiannidis, P., Lin, J.W., Janse, C.J., Khan, S.M., Duraisingh, M., Coleman, B., Goldsmith, E.J., Phillips, M.A., Munoz, B., Wirth, D.F., Klinger, J.D., Wiegand, R. & Sybertz, E. Novel inhibitors of Plasmodium falciparum dihydroorotate dehydrogenase with anti-malarial activity in the mouse model. *J Biol Chem* **285**, 33054-33064 (2010).

47. Azeredo, L., Coutinho, J.P., Jabor, V.A.P., Feliciano, P.R., Nonato, M.C., Kaiser, C.R., Menezes, C.M.S., Hammes, A.S.O., Caffarena, E.R., Hoelz, L.V.B., de Souza, N.B., Pereira, G.A.N., Ceravolo, I.P., Krettli, A.U. & Boechat, N. Evaluation of 7-arylaminopyrazolo[1,5-a]pyrimidines as anti-Plasmodium falciparum, antimalarial, and Pf-dihydroorotate dehydrogenase inhibitors. *Eur J Med Chem* **126**, 72-83 (2017).

48. Guler, J.L., Freeman, D.L., Ahyong, V., Patrapuvich, R., White, J., Gujjar, R., Phillips, M.A., DeRisi, J. & Rathod, P.K. Asexual populations of the human malaria parasite, Plasmodium falciparum, use a two-step genomic strategy to acquire accurate, beneficial DNA amplifications. *PLoS Pathog* **9**, e1003375 (2013).

49. Maetani, M., Kato, N., Jabor, V.A.P., Calil, F.A., Nonato, M.C., Scherer, C.A. & Schreiber, S.L. Discovery of Antimalarial Azetidine-2-carbonitriles That Inhibit P. falciparum Dihydroorotate Dehydrogenase. *ACS Med Chem Lett* **8**, 438-442 (2017).

50. Ross, L.S., Gamo, F.J., Lafuente-Monasterio, M.J., Singh, O.M., Rowland, P., Wiegand, R.C. & Wirth, D.F. In vitro resistance selections for Plasmodium falciparum dihydroorotate dehydrogenase inhibitors give mutants with multiple

point mutations in the drug-binding site and altered growth. *J Biol Chem* **289**, 17980-95 (2014).

51. Nam, T.G., McNamara, C.W., Bopp, S., Dharia, N.V., Meister, S., Bonamy, G.M., Plouffe, D.M., Kato, N., McCormack, S., Bursulaya, B., Ke, H., Vaidya, A.B., Schultz, P.G. & Winzeler, E.A. A chemical genomic analysis of decoquinate, a Plasmodium falciparum cytochrome b inhibitor. *ACS Chem Biol* **6**, 1214-22 (2011).

52. Corey, V.C., Lukens, A.K., Istvan, E.S., Lee, M.C.S., Franco, V., Magistrado, P., Coburn-Flynn, O., Sakata-Kato, T., Fuchs, O., Gnadig, N.F., Goldgof, G., Linares, M., Gomez-Lorenzo, M.G., De Cozar, C., Lafuente-Monasterio, M.J., Prats, S., Meister, S., Tanaseichuk, O., Wree, M., Zhou, Y., Willis, P.A., Gamo, F.J., Goldberg, D.E., Fidock, D.A., Wirth, D.F. & Winzeler, E.A. A broad analysis of resistance development in the malaria parasite. *Nat Commun* **7**, 11901 (2016).

53. Dong, C.K., Urgaonkar, S., Cortese, J.F., Gamo, F.J., Garcia-Bustos, J.F., Lafuente, M.J., Patel, V., Ross, L., Coleman, B.I., Derbyshire, E.R., Clish, C.B., Serrano, A.E., Cromwell, M., Barker, R.H., Jr., Dvorin, J.D., Duraisingh, M.T., Wirth, D.F., Clardy, J. & Mazitschek, R. Identification and validation of tetracyclic benzothiazepines as Plasmodium falciparum cytochrome bc1 inhibitors. *Chem Biol* **18**, 1602-10 (2011).

54. Vallieres, C., Fisher, N., Antoine, T., Al-Helal, M., Stocks, P., Berry, N.G., Lawrenson, A.S., Ward, S.A., O'Neill, P.M., Biagini, G.A. & Meunier, B. HDQ, a potent inhibitor of Plasmodium falciparum proliferation, binds to the quinone reduction site of the cytochrome bc1 complex. *Antimicrob Agents Chemother* **56**, 3739-47 (2012).

55. Capper, M.J., O'Neill, P.M., Fisher, N., Strange, R.W., Moss, D., Ward, S.A., Berry, N.G., Lawrenson, A.S., Hasnain, S.S., Biagini, G.A. & Antonyuk, S.V. Antimalarial 4(1H)-pyridones bind to the Qi site of cytochrome bc1. *Proc Natl Acad Sci U S A* **112**, 755-60 (2015).

56. Lukens, A.K., Heidebrecht, R.W., Jr., Mulrooney, C., Beaudoin, J.A., Comer, E., Duvall, J.R., Fitzgerald, M.E., Masi, D., Galinsky, K., Scherer, C.A., Palmer, M., Munoz, B., Foley, M., Schreiber, S.L., Wiegand, R.C. & Wirth, D.F. Diversity-oriented synthesis probe targets Plasmodium falciparum cytochrome b ubiquinone reduction site and synergizes with oxidation site inhibitors. *J Infect Dis* **211**, 1097-103 (2015).

57. Ivanetich, K.M. & Santi, D.V. Bifunctional thymidylate synthase-dihydrofolate reductase in protozoa. *FASEB J* **4**, 1591-7 (1990).

58. Cowell, A.N., Istvan, E.S., Lukens, A.K., Gomez-Lorenzo, M.G., Vanaerschot, M., Sakata-Kato, T., Flannery, E.L., Magistrado, P., Owen, E., Abraham, M., LaMonte, G., Painter, H.J., Williams, R.M., Franco, V., Linares, M., Arriaga, I., Bopp, S.,

Corey, V.C., Gnadig, N.F., Coburn-Flynn, O., Reimer, C., Gupta, P., Murithi, J.M., Moura, P.A., Fuchs, O., Sasaki, E., Kim, S.W., Teng, C.H., Wang, L.T., Akidil, A., Adjalley, S., Willis, P.A., Siegel, D., Tanaseichuk, O., Zhong, Y., Zhou, Y., Llinas, M., Ottilie, S., Gamo, F.J., Lee, M.C.S., Goldberg, D.E., Fidock, D.A., Wirth, D.F. & Winzeler, E.A. Mapping the malaria parasite druggable genome by using in vitro evolution and chemogenomics. *Science* **359**, 191-199 (2018).

59. Chaianantakul, N., Sirawaraporn, R. & Sirawaraporn, W. Insights into the role of the junctional region of Plasmodium falciparum dihydrofolate reductase-thymidylate synthase. *Malar J* **12**, 91 (2013).

60. Mayinger, P. Phosphoinositides and vesicular membrane traffic. *Biochim Biophys Acta* **1821**, 1104-13 (2012).

61. McNamara, C.W., Lee, M.C., Lim, C.S., Lim, S.H., Roland, J., Simon, O., Yeung, B.K., Chatterjee, A.K., McCormack, S.L., Manary, M.J., Zeeman, A.M., Dechering, K.J., Kumar, T.S., Henrich, P.P., Gagaring, K., Ibanez, M., Kato, N., Kuhen, K.L., Fischli, C., Nagle, A., Rottmann, M., Plouffe, D.M., Bursulaya, B., Meister, S., Rameh, L., Trappe, J., Haasen, D., Timmerman, M., Sauerwein, R.W., Suwanarusk, R., Russell, B., Renia, L., Nosten, F., Tully, D.C., Kocken, C.H., Glynne, R.J., Bodenreider, C., Fidock, D.A., Diagana, T.T. & Winzeler, E.A. Targeting Plasmodium PI(4)K to eliminate malaria. *Nature* **504**, 248-253 (2013).

62. Paquet, T., Le Manach, C., Cabrera, D.G., Younis, Y., Henrich, P.P., Abraham, T.S., Lee, M.C.S., Basak, R., Ghidelli-Disse, S., Lafuente-Monasterio, M.J., Bantscheff, M., Ruecker, A., Blagborough, A.M., Zakutansky, S.E., Zeeman, A.M., White, K.L., Shackleford, D.M., Mannila, J., Morizzi, J., Scheurer, C., Angulo-Barturen, I., Martinez, M.S., Ferrer, S., Sanz, L.M., Gamo, F.J., Reader, J., Botha, M., Dechering, K.J., Sauerwein, R.W., Tungtaeng, A., Vanachayangkul, P., Lim, C.S., Burrows, J., Witty, M.J., Marsh, K.C., Bodenreider, C., Rochford, R., Solapure, S.M., Jimenez-Diaz, M.B., Wittlin, S., Charman, S.A., Donini, C., Campo, B., Birkholtz, L.M., Hanson, K.K., Drewes, G., Kocken, C.H.M., Delves, M.J., Leroy, D., Fidock, D.A., Waterson, D., Street, L.J. & Chibale, K. Antimalarial efficacy of MMV390048, an inhibitor of Plasmodium phosphatidylinositol 4-kinase. *Sci Transl Med* **9**(2017).

63. Sonoiki, E., Ng, C.L., Lee, M.C., Guo, D., Zhang, Y.K., Zhou, Y., Alley, M.R., Ahyong, V., Sanz, L.M., Lafuente-Monasterio, M.J., Dong, C., Schupp, P.G., Gut, J., Legac, J., Cooper, R.A., Gamo, F.J., DeRisi, J., Freund, Y.R., Fidock, D.A. & Rosenthal, P.J. A potent antimalarial benzoxaborole targets a Plasmodium falciparum cleavage and polyadenylation specificity factor homologue. *Nat Commun* **8**, 14574 (2017).

64. Singh, A.P., Zhang, Y., No, J.H., Docampo, R., Nussenzweig, V. & Oldfield, E. Lipophilic bisphosphonates are potent inhibitors of Plasmodium liver-stage growth. *Antimicrob Agents Chemother* **54**, 2987-93 (2010).

65. Martin, M.B., Grimley, J.S., Lewis, J.C., Heath, H.T., 3rd, Bailey, B.N., Kendrick, H., Yardley, V., Caldera, A., Lira, R., Urbina, J.A., Moreno, S.N., Docampo, R., Croft, S.L. & Oldfield, E. Bisphosphonates inhibit the growth of Trypanosoma brucei, Trypanosoma cruzi, Leishmania donovani, Toxoplasma gondii, and Plasmodium falciparum: a potential route to chemotherapy. *J Med Chem* **44**, 909-16 (2001).

66. Dharia, N.V., Sidhu, A.B., Cassera, M.B., Westenberger, S.J., Bopp, S.E., Eastman, R.T., Plouffe, D., Batalov, S., Park, D.J., Volkman, S.K., Wirth, D.F., Zhou, Y., Fidock, D.A. & Winzeler, E.A. Use of high-density tiling microarrays to identify mutations globally and elucidate mechanisms of drug resistance in Plasmodium falciparum. *Genome Biol* **10**, R21 (2009).

67. Spangenberg, T., Burrows, J.N., Kowalczyk, P., McDonald, S., Wells, T.N. & Willis, P. The open access malaria box: a drug discovery catalyst for neglected diseases. *PLoS One* **8**, e62906 (2013).

68. Wu, W., Herrera, Z., Ebert, D., Baska, K., Cho, S.H., DeRisi, J.L. & Yeh, E. A chemical rescue screen identifies a Plasmodium falciparum apicoplast inhibitor targeting MEP isoprenoid precursor biosynthesis. *Antimicrob Agents Chemother* **59**, 356-64 (2015).

69. Gisselberg, J.E., Herrera, Z., Orchard, L.M., Llinas, M. & Yeh, E. Specific Inhibition of the Bifunctional Farnesyl/Geranylgeranyl Diphosphate Synthase in Malaria Parasites via a New Small-Molecule Binding Site. *Cell Chem Biol* **25**, 185-193 e5 (2018).

70. Eastman, R.T., Buckner, F.S., Yokoyama, K., Gelb, M.H. & Van Voorhis, W.C. Thematic review series: lipid posttranslational modifications. Fighting parasitic disease by blocking protein farnesylation. *J Lipid Res* **47**, 233-40 (2006).

71. Nallan, L., Bauer, K.D., Bendale, P., Rivas, K., Yokoyama, K., Horney, C.P., Pendyala, P.R., Floyd, D., Lombardo, L.J., Williams, D.K., Hamilton, A., Sebti, S., Windsor, W.T., Weber, P.C., Buckner, F.S., Chakrabarti, D., Gelb, M.H. & Van Voorhis, W.C. Protein farnesyltransferase inhibitors exhibit potent antimalarial activity. *J Med Chem* **48**, 3704-13 (2005).

72. Wiesner, J., Kettler, K., Sakowski, J., Ortmann, R., Katzin, A.M., Kimura, E.A., Silber, K., Klebe, G., Jomaa, H. & Schlitzer, M. Farnesyltransferase inhibitors inhibit the growth of malaria parasites in vitro and in vivo. *Angew Chem Int Ed Engl* **43**, 251-4 (2004).

73. Rao, S., Cunningham, D., de Gramont, A., Scheithauer, W., Smakal, M., Humblet, Y., Kourteva, G., Iveson, T., Andre, T., Dostalova, J., Illes, A., Belly, R., Perez-Ruixo, J.J., Park, Y.C. & Palmer, P.A. Phase III double-blind placebo-controlled

study of farnesyl transferase inhibitor R115777 in patients with refractory advanced colorectal cancer. *J Clin Oncol* **22**, 3950-7 (2004).

74. Doll, R.J., Kirschmeier, P. & Bishop, W.R. Farnesyltransferase inhibitors as anticancer agents: critical crossroads. *Curr Opin Drug Discov Devel* **7**, 478-86 (2004).

75. Eastman, R.T., White, J., Hucke, O., Yokoyama, K., Verlinde, C.L., Hast, M.A., Beese, L.S., Gelb, M.H., Rathod, P.K. & Van Voorhis, W.C. Resistance mutations at the lipid substrate binding site of Plasmodium falciparum protein farnesyltransferase. *Mol Biochem Parasitol* **152**, 66-71 (2007).

76. Goldgof, G.M., Durrant, J.D., Ottilie, S., Vigil, E., Allen, K.E., Gunawan, F., Kostylev, M., Henderson, K.A., Yang, J., Schenken, J., LaMonte, G.M., Manary, M.J., Murao, A., Nachon, M., Stanhope, R., Prescott, M., McNamara, C.W., Slayman, C.W., Amaro, R.E., Suzuki, Y. & Winzeler, E.A. Comparative chemical genomics reveal that the spiroindolone antimalarial KAE609 (Cipargamin) is a P-type ATPase inhibitor. *Sci Rep* **6**, 27806 (2016).

77. Bibo-Verdugo, B., Jiang, Z., Caffrey, C.R. & O'Donoghue, A.J. Targeting proteasomes in infectious organisms to combat disease. *FEBS J* **284**, 1503-1517 (2017).

78. Gandolfi, S., Laubach, J.P., Hideshima, T., Chauhan, D., Anderson, K.C. & Richardson, P.G. The proteasome and proteasome inhibitors in multiple myeloma. *Cancer Metastasis Rev* **36**, 561-584 (2017).

79. Huber, E.M. & Groll, M. Inhibitors for the immuno- and constitutive proteasome: current and future trends in drug development. *Angew Chem Int Ed Engl* **51**, 8708-20 (2012).

80. Kisselev, A.F., van der Linden, W.A. & Overkleeft, H.S. Proteasome inhibitors: an expanding army attacking a unique target. *Chem Biol* **19**, 99-115 (2012).

81. Li, H., van der Linden, W.A., Verdoes, M., Florea, B.I., McAllister, F.E., Govindaswamy, K., Elias, J.E., Bhanot, P., Overkleeft, H.S. & Bogyo, M. Assessing subunit dependency of the Plasmodium proteasome using small molecule inhibitors and active site probes. *ACS Chem Biol* **9**, 1869-76 (2014).

82. Dogovski, C., Xie, S.C., Burgio, G., Bridgford, J., Mok, S., McCaw, J.M., Chotivanich, K., Kenny, S., Gnadig, N., Straimer, J., Bozdech, Z., Fidock, D.A., Simpson, J.A., Dondorp, A.M., Foote, S., Klonis, N. & Tilley, L. Targeting the cell stress response of Plasmodium falciparum to overcome artemisinin resistance. *PLoS Biol* **13**, e1002132 (2015).

83. Li, H., O'Donoghue, A.J., van der Linden, W.A., Xie, S.C., Yoo, E., Foe, I.T., Tilley, L., Craik, C.S., da Fonseca, P.C. & Bogyo, M. Structure- and function-based design of Plasmodium-selective proteasome inhibitors. *Nature* **530**, 233-6 (2016).

84. LaMonte, G.M., Almaliti, J., Bibo-Verdugo, B., Keller, L., Zou, B.Y., Yang, J., Antonova-Koch, Y., Orjuela-Sanchez, P., Boyle, C.A., Vigil, E., Wang, L., Goldgof, G.M., Gerwick, L., O'Donoghue, A.J., Winzeler, E.A., Gerwick, W.H. & Ottilie, S. Development of a Potent Inhibitor of the Plasmodium Proteasome with Reduced Mammalian Toxicity. *J Med Chem* **60**, 6721-6732 (2017).

85. Turk, B. Targeting proteases: successes, failures and future prospects. *Nat Rev Drug Discov* **5**, 785-99 (2006).

86. Drag, M. & Salvesen, G.S. Emerging principles in protease-based drug discovery. *Nat Rev Drug Discov* **9**, 690-701 (2010).

87. da Silva, F.L., Dixon, M.W., Stack, C.M., Teuscher, F., Taran, E., Jones, M.K., Lovas, E., Tilley, L., Brown, C.L., Trenholme, K.R., Dalton, J.P., Gardiner, D.L. & Skinner-Adams, T.S. A Plasmodium falciparum S33 proline aminopeptidase is associated with changes in erythrocyte deformability. *Exp Parasitol* **169**, 13-21 (2016).

88. Yeoh, S., O'Donnell, R.A., Koussis, K., Dluzewski, A.R., Ansell, K.H., Osborne, S.A., Hackett, F., Withers-Martinez, C., Mitchell, G.H., Bannister, L.H., Bryans, J.S., Kettleborough, C.A. & Blackman, M.J. Subcellular discharge of a serine protease mediates release of invasive malaria parasites from host erythrocytes. *Cell* **131**, 1072-83 (2007).

89. Harris, P.K., Yeoh, S., Dluzewski, A.R., O'Donnell, R.A., Withers-Martinez, C., Hackett, F., Bannister, L.H., Mitchell, G.H. & Blackman, M.J. Molecular identification of a malaria merozoite surface sheddase. *PLoS Pathog* **1**, 241-51 (2005).

90. Banerjee, R., Liu, J., Beatty, W., Pelosof, L., Klemba, M. & Goldberg, D.E. Four plasmepsins are active in the Plasmodium falciparum food vacuole, including a protease with an active-site histidine. *Proc Natl Acad Sci U S A* **99**, 990-5 (2002).

91. Shenai, B.R., Sijwali, P.S., Singh, A. & Rosenthal, P.J. Characterization of native and recombinant falcipain-2, a principal trophozoite cysteine protease and essential hemoglobinase of Plasmodium falciparum. *J Biol Chem* **275**, 29000-10 (2000).

92. Singh, N., Sijwali, P.S., Pandey, K.C. & Rosenthal, P.J. Plasmodium falciparum: biochemical characterization of the cysteine protease falcipain-2'. *Exp Parasitol* **112**, 187-92 (2006).

93. Sijwali, P.S., Shenai, B.R., Gut, J., Singh, A. & Rosenthal, P.J. Expression and characterization of the Plasmodium falciparum haemoglobinase falcipain-3. *Biochem J* **360**, 481-9 (2001).

94. Tanaka, T.Q., Deu, E., Molina-Cruz, A., Ashburne, M.J., Ali, O., Suri, A., Kortagere, S., Bogyo, M. & Williamson, K.C. Plasmodium dipeptidyl aminopeptidases as malaria transmission-blocking drug targets. *Antimicrob Agents Chemother* **57**, 4645-52 (2013).

95. Eggleson, K.K., Duffin, K.L. & Goldberg, D.E. Identification and characterization of falcilysin, a metallopeptidase involved in hemoglobin catabolism within the malaria parasite Plasmodium falciparum. *J Biol Chem* **274**, 32411-7 (1999).

96. Murata, C.E. & Goldberg, D.E. Plasmodium falciparum falcilysin: a metalloprotease with dual specificity. *J Biol Chem* **278**, 38022-8 (2003).

97. Sleebs, B.E., Gazdik, M., O'Neill, M.T., Rajasekaran, P., Lopaticki, S., Lackovic, K., Lowes, K., Smith, B.J., Cowman, A.F. & Boddey, J.A. Transition state mimetics of the Plasmodium export element are potent inhibitors of Plasmepsin V from P. falciparum and P. vivax. *J Med Chem* **57**, 7644-62 (2014).

98. Hodder, A.N., Sleebs, B.E., Czabotar, P.E., Gazdik, M., Xu, Y., O'Neill, M.T., Lopaticki, S., Nebl, T., Triglia, T., Smith, B.J., Lowes, K., Boddey, J.A. & Cowman, A.F. Structural basis for plasmepsin V inhibition that blocks export of malaria proteins to human erythrocytes. *Nat Struct Mol Biol* **22**, 590-6 (2015).

99. Sleebs, B.E., Lopaticki, S., Marapana, D.S., O'Neill, M.T., Rajasekaran, P., Gazdik, M., Gunther, S., Whitehead, L.W., Lowes, K.N., Barfod, L., Hviid, L., Shaw, P.J., Hodder, A.N., Smith, B.J., Cowman, A.F. & Boddey, J.A. Inhibition of Plasmepsin V activity demonstrates its essential role in protein export, PfEMP1 display, and survival of malaria parasites. *PLoS Biol* **12**, e1001897 (2014).

100. Nasamu, A.S., Glushakova, S., Russo, I., Vaupel, B., Oksman, A., Kim, A.S., Fremont, D.H., Tolia, N., Beck, J.R., Meyers, M.J., Niles, J.C., Zimmerberg, J. & Goldberg, D.E. Plasmepsins IX and X are essential and druggable mediators of malaria parasite egress and invasion. *Science* **358**, 518-522 (2017).

101. Amberg-Johnson, K., Hari, S.B., Ganesan, S.M., Lorenzi, H.A., Sauer, R.T., Niles, J.C. & Yeh, E. Small molecule inhibition of apicomplexan FtsH1 disrupts plastid biogenesis in human pathogens. *Elife* **6**(2017).

102. Wiesner, J., Sanderbrand, S., Altincicek, B., Beck, E. & Jomaa, H. Seeking new targets for antiparasitic agents. *Trends Parasitol* **17**, 7-8 (2001).

103. Goodman, C.D. & McFadden, G.I. Ycf93 (Orf105), a small apicoplast-encoded membrane protein in the relict plastid of the malaria parasite Plasmodium falciparum that is conserved in Apicomplexa. *PLoS One* **9**, e91178 (2014).

104. Kuhen, K.L., Chatterjee, A.K., Rottmann, M., Gagaring, K., Borboa, R., Buenviaje, J., Chen, Z., Francek, C., Wu, T., Nagle, A., Barnes, S.W., Plouffe, D., Lee, M.C., Fidock, D.A., Graumans, W., van de Vegte-Bolmer, M., van Gemert, G.J., Wirjanata, G., Sebayang, B., Marfurt, J., Russell, B., Suwanarusk, R., Price, R.N., Nosten, F., Tungtaeng, A., Gettayacamin, M., Sattabongkot, J., Taylor, J., Walker, J.R., Tully, D., Patra, K.P., Flannery, E.L., Vinetz, J.M., Renia, L., Sauerwein, R.W., Winzeler, E.A., Glynne, R.J. & Diagana, T.T. KAF156 is an antimalarial clinical candidate with potential for use in prophylaxis, treatment, and prevention of disease transmission. *Antimicrob Agents Chemother* **58**, 5060-7 (2014).

105. Clyde, D.F. & Shute, G.T. Resistance of East African varieties of Plasmodium falciparum to pyrimethamine. *Trans R Soc Trop Med Hyg* **48**, 495-500 (1954).

106. Jones, S.A. Resistance of P. falciparum and P. malariae to pyrimethamine (daraprim) following mass treatment with this drug; a preliminary note. *East Afr Med J* **31**, 47-9 (1954).

107. Basco, L.K., Eldin de Pecoulas, P., Wilson, C.M., Le Bras, J. & Mazabraud, A. Point mutations in the dihydrofolate reductase-thymidylate synthase gene and pyrimethamine and cycloguanil resistance in Plasmodium falciparum. *Mol Biochem Parasitol* **69**, 135-8 (1995).

108. Wongsrichanalai, C., Pickard, A.L., Wernsdorfer, W.H. & Meshnick, S.R. Epidemiology of drug-resistant malaria. *Lancet Infect Dis* **2**, 209-18 (2002).

109. Abdul-Ghani, R., Farag, H.F. & Allam, A.F. Sulfadoxine-pyrimethamine resistance in Plasmodium falciparum: a zoomed image at the molecular level within a geographic context. *Acta Trop* **125**, 163-90 (2013).

110. Looareesuwan, S., Viravan, C., Webster, H.K., Kyle, D.E., Hutchinson, D.B. & Canfield, C.J. Clinical studies of atovaquone, alone or in combination with other antimalarial drugs, for treatment of acute uncomplicated malaria in Thailand. *Am J Trop Med Hyg* **54**, 62-6 (1996).

111. Roper, C., Pearce, R., Bredenkamp, B., Gumede, J., Drakeley, C., Mosha, F., Chandramohan, D. & Sharp, B. Antifolate antimalarial resistance in southeast Africa: a population-based analysis. *Lancet* **361**, 1174-81 (2003).

112. Luth, M.R., Gupta, P., Ottilie, S. & Winzeler, E.A. Using in Vitro Evolution and Whole Genome Analysis To Discover Next Generation Targets for Antimalarial Drug Discovery. *ACS Infect Dis* **4**, 301-314 (2018).

113. Nzila, A. & Mwai, L. In vitro selection of Plasmodium falciparum drug-resistant parasite lines. *J Antimicrob Chemother* **65**, 390-8 (2010).

114. Korsinczky, M., Chen, N., Kotecka, B., Saul, A., Rieckmann, K. & Cheng, Q. Mutations in Plasmodium falciparum cytochrome b that are associated with atovaquone resistance are located at a putative drug-binding site. *Antimicrob Agents Chemother* **44**, 2100-8 (2000).

115. Musset, L., Bouchaud, O., Matheron, S., Massias, L. & Le Bras, J. Clinical atovaquone-proguanil resistance of Plasmodium falciparum associated with cytochrome b codon 268 mutations. *Microbes Infect* **8**, 2599-604 (2006).

116. Schwobel, B., Alifrangis, M., Salanti, A. & Jelinek, T. Different mutation patterns of atovaquone resistance to Plasmodium falciparum in vitro and in vivo: rapid detection of codon 268 polymorphisms in the cytochrome b as potential in vivo resistance marker. *Malar J* **2**, 5 (2003).

117. Baldwin, J., Michnoff, C.H., Malmquist, N.A., White, J., Roth, M.G., Rathod, P.K. & Phillips, M.A. High-throughput screening for potent and selective inhibitors of Plasmodium falciparum dihydroorotate dehydrogenase. *J Biol Chem* **280**, 21847-53 (2005).

118. Pavadai, E., El Mazouni, F., Wittlin, S., de Kock, C., Phillips, M.A. & Chibale, K. Identification of New Human Malaria Parasite Plasmodium falciparum Dihydroorotate Dehydrogenase Inhibitors by Pharmacophore and Structure-Based Virtual Screening. *J Chem Inf Model* **56**, 548-62 (2016).

119. Phillips, M.A., Gujjar, R., Malmquist, N.A., White, J., El Mazouni, F., Baldwin, J. & Rathod, P.K. Triazolopyrimidine-based dihydroorotate dehydrogenase inhibitors with potent and selective activity against the malaria parasite Plasmodium falciparum. *J Med Chem* **51**, 3649-53 (2008).

120. Patel, V., Booker, M., Kramer, M., Ross, L., Celatka, C.A., Kennedy, L.M., Dvorin, J.D., Duraisingh, M.T., Sliz, P., Wirth, D.F. & Clardy, J. Identification and characterization of small molecule inhibitors of Plasmodium falciparum dihydroorotate dehydrogenase. *J Biol Chem* **283**, 35078-85 (2008).

121. Ross, L.S., Lafuente-Monasterio, M.J., Sakata-Kato, T., Mandt, R.E.K., Gamo, F.J., Wirth, D.F. & Lukens, A.K. Identification of Collateral Sensitivity to Dihydroorotate Dehydrogenase Inhibitors in Plasmodium falciparum. *ACS Infect Dis* **4**, 508-515 (2018).

122. Lukens, A.K., Ross, L.S., Heidebrecht, R., Javier Gamo, F., Lafuente-Monasterio, M.J., Booker, M.L., Hartl, D.L., Wiegand, R.C. & Wirth, D.F. Harnessing evolutionary fitness in Plasmodium falciparum for drug discovery and suppressing resistance. *Proc Natl Acad Sci U S A* **111**, 799-804 (2014).

123. Bedingfield, P.T., Cowen, D., Acklam, P., Cunningham, F., Parsons, M.R., McConkey, G.A., Fishwick, C.W. & Johnson, A.P. Factors influencing the specificity of inhibitor binding to the human and malaria parasite dihydroorotate dehydrogenases. *J Med Chem* **55**, 5841-50 (2012).

124. White, J., Dhingra, S.K., Deng, X., El Mazouni, F., Lee, M.C.S., Afanador, G.A., Lawong, A., Tomchick, D.R., Ng, C.L., Bath, J., Rathod, P.K., Fidock, D.A. & Phillips, M.A. Identification and Mechanistic Understanding of Dihydroorotate Dehydrogenase Point Mutations in Plasmodium falciparum that Confer in Vitro Resistance to the Clinical Candidate DSM265. *ACS Infect Dis* **5**, 90-101 (2019).

125. Llanos-Cuentas, A., Casapia, M., Chuquiyauri, R., Hinojosa, J.C., Kerr, N., Rosario, M., Toovey, S., Arch, R.H., Phillips, M.A., Rozenberg, F.D., Bath, J., Ng, C.L., Cowell, A.N., Winzeler, E.A., Fidock, D.A., Baker, M., Mohrle, J.J., Hooft van Huijsduijnen, R., Gobeau, N., Araeipour, N., Andenmatten, N., Ruckle, T. & Duparc, S. Antimalarial activity of single-dose DSM265, a novel plasmodium dihydroorotate dehydrogenase inhibitor, in patients with uncomplicated Plasmodium falciparum or Plasmodium vivax malaria infection: a proof-of-concept, open-label, phase 2a study. *Lancet Infect Dis* **18**, 874-883 (2018).

126. Angulo-Barturen, I., Jimenez-Diaz, M.B., Mulet, T., Rullas, J., Herreros, E., Ferrer, S., Jimenez, E., Mendoza, A., Regadera, J., Rosenthal, P.J., Bathurst, I., Pompliano, D.L., Gomez de las Heras, F. & Gargallo-Viola, D. A murine model of falciparum-malaria by in vivo selection of competent strains in non-myelodepleted mice engrafted with human erythrocytes. *PLoS One* **3**, e2252 (2008).

127. Coteron, J.M., Marco, M., Esquivias, J., Deng, X., White, K.L., White, J., Koltun, M., El Mazouni, F., Kokkonda, S., Katneni, K., Bhamidipati, R., Shackleford, D.M., Angulo-Barturen, I., Ferrer, S.B., Jimenez-Diaz, M.B., Gamo, F.J., Goldsmith, E.J., Charman, W.N., Bathurst, I., Floyd, D., Matthews, D., Burrows, J.N., Rathod, P.K., Charman, S.A. & Phillips, M.A. Structure-guided lead optimization of triazolopyrimidine-ring substituents identifies potent Plasmodium falciparum dihydroorotate dehydrogenase inhibitors with clinical candidate potential. *J Med Chem* **54**, 5540-61 (2011).

128. Barrick, J.E. & Lenski, R.E. Genome dynamics during experimental evolution. *Nat Rev Genet* **14**, 827-39 (2013).

129. Jimenez-Diaz, M.B., Mulet, T., Viera, S., Gomez, V., Garuti, H., Ibanez, J., Alvarez-Doval, A., Shultz, L.D., Martinez, A., Gargallo-Viola, D. & Angulo-Barturen, I. Improved murine model of malaria using Plasmodium falciparum competent strains and non-myelodepleted NOD-scid IL2Rgammanull mice engrafted with human erythrocytes. *Antimicrob Agents Chemother* **53**, 4533-6 (2009).

130. Goldberg, D.E., Siliciano, R.F. & Jacobs, W.R., Jr. Outwitting evolution: fighting drug-resistant TB, malaria, and HIV. *Cell* **148**, 1271-83 (2012).

131. Lambros, C. & Vanderberg, J.P. Synchronization of Plasmodium falciparum erythrocytic stages in culture. *J Parasitol* **65**, 418-20 (1979).

132. McClure, N.S. & Day, T. A theoretical examination of the relative importance of evolution management and drug development for managing resistance. *Proc Biol Sci* **281**(2014).

133. Yang, T., Ottilie, S., Istvan, E.S., Godinez-Macias, K.P., Lukens, A.K., Baragana, B., Campo, B., Walpole, C., Niles, J.C., Chibale, K., Dechering, K.J., Llinas, M., Lee, M.C.S., Kato, N., Wyllie, S., McNamara, C.W., Gamo, F.J., Burrows, J., Fidock, D.A., Goldberg, D.E., Gilbert, I.H., Wirth, D.F., Winzeler, E.A. & Malaria Drug Accelerator, C. MalDA, Accelerating Malaria Drug Discovery. *Trends Parasitol* **37**, 493-507 (2021).

134. Mandt, R.E.K., Lafuente-Monasterio, M.J., Sakata-Kato, T., Luth, M.R., Segura, D., Pablos-Tanarro, A., Viera, S., Magan, N., Ottilie, S., Winzeler, E.A., Lukens, A.K., Gamo, F.J. & Wirth, D.F. In vitro selection predicts malaria parasite resistance to dihydroorotate dehydrogenase inhibitors in a mouse infection model. *Sci Transl Med* **11**(2019).

135. Lee, M.C.S., Lindner, S.E., Lopez-Rubio, J.J. & Llinas, M. Cutting back malaria: CRISPR/Cas9 genome editing of Plasmodium. *Brief Funct Genomics* **18**, 281-289 (2019).

136. Plouffe, D., Brinker, A., McNamara, C., Henson, K., Kato, N., Kuhen, K., Nagle, A., Adrian, F., Matzen, J.T., Anderson, P., Nam, T.G., Gray, N.S., Chatterjee, A., Janes, J., Yan, S.F., Trager, R., Caldwell, J.S., Schultz, P.G., Zhou, Y. & Winzeler, E.A. In silico activity profiling reveals the mechanism of action of antimalarials discovered in a high-throughput screen. *Proc Natl Acad Sci U S A* **105**, 9059-64 (2008).

137. Swann, J., Corey, V., Scherer, C.A., Kato, N., Comer, E., Maetani, M., Antonova-Koch, Y., Reimer, C., Gagaring, K., Ibanez, M., Plouffe, D., Zeeman, A.M., Kocken, C.H., McNamara, C.W., Schreiber, S.L., Campo, B., Winzeler, E.A. & Meister, S. High-Throughput Luciferase-Based Assay for the Discovery of Therapeutics That Prevent Malaria. *ACS Infect Dis* **2**, 281-293 (2016).

138. Plouffe, D.M., Wree, M., Du, A.Y., Meister, S., Li, F., Patra, K., Lubar, A., Okitsu, S.L., Flannery, E.L., Kato, N., Tanaseichuk, O., Comer, E., Zhou, B., Kuhen, K., Zhou, Y., Leroy, D., Schreiber, S.L., Scherer, C.A., Vinetz, J. & Winzeler, E.A. High-Throughput Assay and Discovery of Small Molecules that Interrupt Malaria Transmission. *Cell Host Microbe* **19**, 114-26 (2016).

139. Antonova-Koch, Y., Meister, S., Abraham, M., Luth, M.R., Ottilie, S., Lukens, A.K., Sakata-Kato, T., Vanaerschot, M., Owen, E., Jado, J.C., Maher, S.P., Calla, J., Plouffe, D., Zhong, Y., Chen, K., Chaumeau, V., Conway, A.J., McNamara, C.W., Ibanez, M., Gagaring, K., Serrano, F.N., Eribez, K., Taggard, C.M., Cheung, A.L., Lincoln, C., Ambachew, B., Rouillier, M., Siegel, D., Nosten, F., Kyle, D.E., Gamo, F.J., Zhou, Y., Llinas, M., Fidock, D.A., Wirth, D.F., Burrows, J., Campo, B. & Winzeler, E.A. Open-source discovery of chemical leads for next-generation chemoprotective antimalarials. *Science* **362**(2018).

140. Abraham, M., Gagaring, K., Martino, M.L., Vanaerschot, M., Plouffe, D.M., Calla, J., Godinez-Macias, K.P., Du, A.Y., Wree, M., Antonova-Koch, Y., Eribez, K., Luth, M.R., Ottilie, S., Fidock, D.A., McNamara, C.W. & Winzeler, E.A. Probing the Open Global Health Chemical Diversity Library for Multistage-Active Starting Points for Next-Generation Antimalarials. *ACS Infect Dis* **6**, 613-628 (2020).

141. Rocamora, F., Zhu, L., Liong, K.Y., Dondorp, A., Miotto, O., Mok, S. & Bozdech, Z. Oxidative stress and protein damage responses mediate artemisinin resistance in malaria parasites. *PLoS Pathog* **14**, e1006930 (2018).

142. Zhang, Y.K., Plattner, J.J., Easom, E.E., Jacobs, R.T., Guo, D., Freund, Y.R., Berry, P., Ciaravino, V., Erve, J.C.L., Rosenthal, P.J., Campo, B., Gamo, F.J., Sanz, L.M. & Cao, J. Benzoxaborole Antimalarial Agents. Part 5. Lead Optimization of Novel Amide Pyrazinyloxy Benzoxaboroles and Identification of a Preclinical Candidate. *J Med Chem* **60**, 5889-5908 (2017).

143. Sindhe, K.M.V., Wu, W., Legac, J., Zhang, Y.K., Easom, E.E., Cooper, R.A., Plattner, J.J., Freund, Y.R., DeRisi, J.L. & Rosenthal, P.J. Plasmodium falciparum Resistance to a Lead Benzoxaborole Due to Blocked Compound Activation and Altered Ubiquitination or Sumoylation. *mBio* **11**(2020).

144. Lim, M.Y., LaMonte, G., Lee, M.C.S., Reimer, C., Tan, B.H., Corey, V., Tjahjadi, B.F., Chua, A., Nachon, M., Wintjens, R., Gedeck, P., Malleret, B., Renia, L., Bonamy, G.M.C., Ho, P.C., Yeung, B.K.S., Chow, E.D., Lim, L., Fidock, D.A., Diagana, T.T., Winzeler, E.A. & Bifani, P. UDP-galactose and acetyl-CoA transporters as Plasmodium multidrug resistance genes. *Nat Microbiol* **1**, 16166 (2016).

145. LaMonte, G.M., Rocamora, F., Marapana, D.S., Gnadig, N.F., Ottilie, S., Luth, M.R., Worgall, T.S., Goldgof, G.M., Mohunlal, R., Santha Kumar, T.R., Thompson, J.K., Vigil, E., Yang, J., Hutson, D., Johnson, T., Huang, J., Williams, R.M., Zou, B.Y., Cheung, A.L., Kumar, P., Egan, T.J., Lee, M.C.S., Siegel, D., Cowman, A.F., Fidock, D.A. & Winzeler, E.A. Pan-active imidazolopiperazine antimalarials target the Plasmodium falciparum intracellular secretory pathway. *Nat Commun* **11**, 1780 (2020).

146. Herman, J.D., Rice, D.P., Ribacke, U., Silterra, J., Deik, A.A., Moss, E.L., Broadbent, K.M., Neafsey, D.E., Desai, M.M., Clish, C.B., Mazitschek, R. & Wirth, D.F. A genomic and evolutionary approach reveals non-genetic drug resistance in malaria. *Genome Biol* **15**, 511 (2014).

147. Xie, S.C., Gillett, D.L., Spillman, N.J., Tsu, C., Luth, M.R., Ottilie, S., Duffy, S., Gould, A.E., Hales, P., Seager, B.A., Charron, C.L., Bruzzese, F., Yang, X., Zhao, X., Huang, S.C., Hutton, C.A., Burrows, J.N., Winzeler, E.A., Avery, V.M., Dick, L.R. & Tilley, L. Target Validation and Identification of Novel Boronate Inhibitors of the Plasmodium falciparum Proteasome. *J Med Chem* **61**, 10053-10066 (2018).

148. Schalkwijk, J., Allman, E.L., Jansen, P.A.M., de Vries, L.E., Verhoef, J.M.J., Jackowski, S., Botman, P.N.M., Beuckens-Schortinghuis, C.A., Koolen, K.M.J., Bolscher, J.M., Vos, M.W., Miller, K., Reeves, S.A., Pett, H., Trevitt, G., Wittlin, S., Scheurer, C., Sax, S., Fischli, C., Angulo-Barturen, I., Jimenez-Diaz, M.B., Josling, G., Kooij, T.W.A., Bonnert, R., Campo, B., Blaauw, R.H., Rutjes, F., Sauerwein, R.W., Llinas, M., Hermkens, P.H.H. & Dechering, K.J. Antimalarial pantothenamide metabolites target acetyl-coenzyme A biosynthesis in Plasmodium falciparum. *Sci Transl Med* **11**(2019).

149. Reader, J., van der Watt, M.E., Taylor, D., Le Manach, C., Mittal, N., Ottilie, S., Theron, A., Moyo, P., Erlank, E., Nardini, L., Venter, N., Lauterbach, S., Bezuidenhout, B., Horatscheck, A., van Heerden, A., Spillman, N.J., Cowell, A.N., Connacher, J., Opperman, D., Orchard, L.M., Llinas, M., Istvan, E.S., Goldberg, D.E., Boyle, G.A., Calvo, D., Mancama, D., Coetzer, T.L., Winzeler, E.A., Duffy, J., Koekemoer, L.L., Basarab, G., Chibale, K. & Birkholtz, L.M. Multistage and transmission-blocking targeted antimalarials discovered from the open-source MMV Pandemic Response Box. *Nat Commun* **12**, 269 (2021).

150. Tahlan, K., Wilson, R., Kastrinsky, D.B., Arora, K., Nair, V., Fischer, E., Barnes, S.W., Walker, J.R., Alland, D., Barry, C.E., 3rd & Boshoff, H.I. SQ109 targets MmpL3, a membrane transporter of trehalose monomycolate involved in mycolic acid donation to the cell wall core of Mycobacterium tuberculosis. *Antimicrob Agents Chemother* **56**, 1797-809 (2012).

151. Stokes, B.H., Yoo, E., Murithi, J.M., Luth, M.R., Afanasyev, P., da Fonseca, P.C.A., Winzeler, E.A., Ng, C.L., Bogyo, M. & Fidock, D.A. Covalent Plasmodium falciparum-selective proteasome inhibitors exhibit a low propensity for generating resistance in vitro and synergize with multiple antimalarial agents. *PLoS Pathog* **15**, e1007722 (2019).

152. Fisher, G.M., Cobbold, S.A., Jezewski, A., Carpenter, E.F., Arnold, M., Cowell, A.N., Tjhin, E.T., Saliba, K.J., Skinner-Adams, T.S., Lee, M.C.S., Odom John, A., Winzeler, E.A., McConville, M.J., Poulsen, S.A. & Andrews, K.T. The Key Glycolytic Enzyme Phosphofructokinase Is Involved in Resistance to Antiplasmodial Glycosides. *mBio* **11**(2020).

153. Ellis, K.M., Lucantoni, L., Chavchich, M., Abraham, M., De Paoli, A., Luth, M.R., Zeeman, A.M., Delves, M.J., Teran, F.S., Straschil, U., Baum, J., Kocken, C.H.M., Ralph, S.A., Winzeler, E.A., Avery, V.M., Edstein, M.D., Baell, J.B. & Creek, D.J. The Novel bis-1,2,4-Triazine MIPS-0004373 Demonstrates Rapid and Potent Activity against All Blood Stages of the Malaria Parasite. *Antimicrob Agents Chemother* **65**, e0031121 (2021).

154. Vanaerschot, M., Murithi, J.M., Pasaje, C.F.A., Ghidelli-Disse, S., Dwomoh, L., Bird, M., Spottiswoode, N., Mittal, N., Arendse, L.B., Owen, E.S., Wicht, K.J., Siciliano, G., Bosche, M., Yeo, T., Kumar, T.R.S., Mok, S., Carpenter, E.F., Giddins, M.J., Sanz, O., Ottilie, S., Alano, P., Chibale, K., Llinas, M., Uhlemann, A.C., Delves, M., Tobin, A.B., Doerig, C., Winzeler, E.A., Lee, M.C.S., Niles, J.C. & Fidock, D.A. Inhibition of Resistance-Refractory P. falciparum Kinase PKG Delivers Prophylactic, Blood Stage, and Transmission-Blocking Antiplasmodial Activity. *Cell Chem Biol* **27**, 806-816 e8 (2020).

155. Knaab, T.C., Held, J., Burckhardt, B.B., Rubiano, K., Okombo, J., Yeo, T., Mok, S., Uhlemann, A.C., Lungerich, B., Fischli, C., Pessanha de Carvalho, L., Mordmuller, B., Wittlin, S., Fidock, D.A. & Kurz, T. 3-Hydroxy-propanamidines, a New Class of Orally Active Antimalarials Targeting Plasmodium falciparum. *J Med Chem* **64**, 3035-3047 (2021).

156. Xie, S.C., Metcalfe, R.D., Dunn, E., Morton, C.J., Huang, S.C., Puhalovich, T., Du, Y., Wittlin, S., Nie, S., Luth, M.R., Ma, L., Kim, M.S., Pasaje, C.F.A., Kumpornsin, K., Giannangelo, C., Houghton, F.J., Churchyard, A., Famodimu, M.T., Barry, D.C., Gillett, D.L., Dey, S., Kosasih, C.C., Newman, W., Niles, J.C., Lee, M.C.S., Baum, J., Ottilie, S., Winzeler, E.A., Creek, D.J., Williamson, N., Parker, M.W., Brand, S., Langston, S.P., Dick, L.R., Griffin, M.D.W., Gould, A.E. & Tilley, L. Reaction hijacking of tyrosine tRNA synthetase as a new whole-of-life-cycle antimalarial strategy. *Science* **376**, 1074-1079 (2022).

157. Miles, A., Iqbal, Z., Vauterin, P., Pearson, R., Campino, S., Theron, M., Gould, K., Mead, D., Drury, E., O'Brien, J., Ruano Rubio, V., MacInnis, B., Mwangi, J., Samarakoon, U., Ranford-Cartwright, L., Ferdig, M., Hayton, K., Su, X.Z., Wellems, T., Rayner, J., McVean, G. & Kwiatkowski, D. Indels, structural variation, and recombination drive genomic diversity in Plasmodium falciparum. *Genome Res* **26**, 1288-99 (2016).

158. Schwach, F., Bushell, E., Gomes, A.R., Anar, B., Girling, G., Herd, C., Rayner, J.C. & Billker, O. PlasmoGEM, a database supporting a community resource for large-scale experimental genetics in malaria parasites. *Nucleic Acids Res* **43**, D1176-82 (2015).

159. Bushell, E., Gomes, A.R., Sanderson, T., Anar, B., Girling, G., Herd, C., Metcalf, T., Modrzynska, K., Schwach, F., Martin, R.E., Mather, M.W., McFadden, G.I., Parts, L., Rutledge, G.G., Vaidya, A.B., Wengelnik, K., Rayner, J.C. & Billker, O.

Functional Profiling of a Plasmodium Genome Reveals an Abundance of Essential Genes. *Cell* **170**, 260-272 e8 (2017).

160. Zhang, M., Wang, C., Otto, T.D., Oberstaller, J., Liao, X., Adapa, S.R., Udenze, K., Bronner, I.F., Casandra, D., Mayho, M., Brown, J., Li, S., Swanson, J., Rayner, J.C., Jiang, R.H.Y. & Adams, J.H. Uncovering the essential genes of the human malaria parasite Plasmodium falciparum by saturation mutagenesis. *Science* **360**(2018).

161. Sakharkar, K.R., Sakharkar, M.K. & Chow, V.T. A novel genomics approach for the identification of drug targets in pathogens, with special reference to Pseudomonas aeruginosa. *In Silico Biol* **4**, 355-60 (2004).

162. Doyle, M.A., Gasser, R.B., Woodcroft, B.J., Hall, R.S. & Ralph, S.A. Drug target prediction and prioritization: using orthology to predict essentiality in parasite genomes. *BMC Genomics* **11**, 222 (2010).

163. Howick, V.M., Russell, A.J.C., Andrews, T., Heaton, H., Reid, A.J., Natarajan, K., Butungi, H., Metcalf, T., Verzier, L.H., Rayner, J.C., Berriman, M., Herren, J.K., Billker, O., Hemberg, M., Talman, A.M. & Lawniczak, M.K.N. The Malaria Cell Atlas: Single parasite transcriptomes across the complete Plasmodium life cycle. *Science* **365**(2019).

164. Reid, A.J., Talman, A.M., Bennett, H.M., Gomes, A.R., Sanders, M.J., Illingworth, C.J.R., Billker, O., Berriman, M. & Lawniczak, M.K. Single-cell RNA-seq reveals hidden transcriptional variation in malaria parasites. *Elife* **7**(2018).

165. Murithi, J.M., Owen, E.S., Istvan, E.S., Lee, M.C.S., Ottilie, S., Chibale, K., Goldberg, D.E., Winzeler, E.A., Llinas, M., Fidock, D.A. & Vanaerschot, M. Combining Stage Specificity and Metabolomic Profiling to Advance Antimalarial Drug Discovery. *Cell Chem Biol* **27**, 158-171 e3 (2020).

166. Mistry, J., Chuguransky, S., Williams, L., Qureshi, M., Salazar, G.A., Sonnhammer, E.L.L., Tosatto, S.C.E., Paladin, L., Raj, S., Richardson, L.J., Finn, R.D. & Bateman, A. Pfam: The protein families database in 2021. *Nucleic Acids Res* **49**, D412-D419 (2021).

167. Hou, C., Tian, W., Kleist, T., He, K., Garcia, V., Bai, F., Hao, Y., Luan, S. & Li, L. DUF221 proteins are a family of osmosensitive calcium-permeable cation channels conserved across eukaryotes. *Cell Res* **24**, 632-5 (2014).

168. Ashburner, M., Ball, C.A., Blake, J.A., Botstein, D., Butler, H., Cherry, J.M., Davis, A.P., Dolinski, K., Dwight, S.S., Eppig, J.T., Harris, M.A., Hill, D.P., Issel-Tarver, L., Kasarskis, A., Lewis, S., Matese, J.C., Richardson, J.E., Ringwald, M., Rubin, G.M. & Sherlock, G. Gene ontology: tool for the unification of biology. The Gene Ontology Consortium. *Nat Genet* **25**, 25-9 (2000).

169. Gene Ontology, C. The Gene Ontology resource: enriching a GOld mine. *Nucleic Acids Res* **49**, D325-D334 (2021).

170. Forte, B., Ottilie, S., Plater, A., Campo, B., Dechering, K.J., Gamo, F.J., Goldberg, D.E., Istvan, E.S., Lee, M., Lukens, A.K., McNamara, C.W., Niles, J.C., Okombo, J., Pasaje, C.F.A., Siegel, M.G., Wirth, D., Wyllie, S., Fidock, D.A., Baragana, B., Winzeler, E.A. & Gilbert, I.H. Prioritization of Molecular Targets for Antimalarial Drug Discovery. *ACS Infect Dis* **7**, 2764-2776 (2021).

171. D'Arcy, P., Wang, X. & Linder, S. Deubiquitinase inhibition as a cancer therapeutic strategy. *Pharmacol Ther* **147**, 32-54 (2015).

172. Waterhouse, A., Bertoni, M., Bienert, S., Studer, G., Tauriello, G., Gumienny, R., Heer, F.T., de Beer, T.A.P., Rempfer, C., Bordoli, L., Lepore, R. & Schwede, T. SWISS-MODEL: homology modelling of protein structures and complexes. *Nucleic Acids Res* **46**, W296-W303 (2018).

173. Lee, B.H., Lee, M.J., Park, S., Oh, D.C., Elsasser, S., Chen, P.C., Gartner, C., Dimova, N., Hanna, J., Gygi, S.P., Wilson, S.M., King, R.W. & Finley, D. Enhancement of proteasome activity by a small-molecule inhibitor of USP14. *Nature* **467**, 179-84 (2010).

174. Wang, Y., Jiang, Y., Ding, S., Li, J., Song, N., Ren, Y., Hong, D., Wu, C., Li, B., Wang, F., He, W., Wang, J. & Mei, Z. Small molecule inhibitors reveal allosteric regulation of USP14 via steric blockade. *Cell Res* **28**, 1186-1194 (2018).

175. Quistgaard, E.M., Low, C., Guettou, F. & Nordlund, P. Understanding transport by the major facilitator superfamily (MFS): structures pave the way. *Nat Rev Mol Cell Biol* **17**, 123-32 (2016).

176. Alibert-Franco, S., Pradines, B., Mahamoud, A., Davin-Regli, A. & Pages, J.M. Efflux mechanism, an attractive target to combat multidrug resistant Plasmodium falciparum and Pseudomonas aeruginosa. *Curr Med Chem* **16**, 301-17 (2009).

177. Istvan, E.S., Mallari, J.P., Corey, V.C., Dharia, N.V., Marshall, G.R., Winzeler, E.A. & Goldberg, D.E. Esterase mutation is a mechanism of resistance to antimalarial compounds. *Nat Commun* **8**, 14240 (2017).

178. Reed, M.B., Saliba, K.J., Caruana, S.R., Kirk, K. & Cowman, A.F. Pgh1 modulates sensitivity and resistance to multiple antimalarials in Plasmodium falciparum. *Nature* **403**, 906-9 (2000).

179. Foote, S.J., Kyle, D.E., Martin, R.K., Oduola, A.M., Forsyth, K., Kemp, D.J. & Cowman, A.F. Several alleles of the multidrug-resistance gene are closely linked to chloroquine resistance in Plasmodium falciparum. *Nature* **345**, 255-8 (1990).

180. Wilson, C.M., Serrano, A.E., Wasley, A., Bogenschutz, M.P., Shankar, A.H. & Wirth, D.F. Amplification of a gene related to mammalian mdr genes in drug-resistant Plasmodium falciparum. *Science* **244**, 1184-6 (1989).

181. Price, R.N., Uhlemann, A.C., Brockman, A., McGready, R., Ashley, E., Phaipun, L., Patel, R., Laing, K., Looareesuwan, S., White, N.J., Nosten, F. & Krishna, S. Mefloquine resistance in Plasmodium falciparum and increased pfmdr1 gene copy number. *Lancet* **364**, 438-447 (2004).

182. Sidhu, A.B., Valderramos, S.G. & Fidock, D.A. pfmdr1 mutations contribute to quinine resistance and enhance mefloquine and artemisinin sensitivity in Plasmodium falciparum. *Mol Microbiol* **57**, 913-26 (2005).

183. Tindall, S.M., Vallieres, C., Lakhani, D.H., Islahudin, F., Ting, K.N. & Avery, S.V. Heterologous Expression of a Novel Drug Transporter from the Malaria Parasite Alters Resistance to Quinoline Antimalarials. *Sci Rep* **8**, 2464 (2018).

184. Mok, S., Liong, K.Y., Lim, E.H., Huang, X., Zhu, L., Preiser, P.R. & Bozdech, Z. Structural polymorphism in the promoter of pfmrp2 confers Plasmodium falciparum tolerance to quinoline drugs. *Mol Microbiol* **91**, 918-34 (2014).

185. Koenderink, J.B., Kavishe, R.A., Rijpma, S.R. & Russel, F.G. The ABCs of multidrug resistance in malaria. *Trends Parasitol* **26**, 440-6 (2010).

186. Kidgell, C., Volkman, S.K., Daily, J., Borevitz, J.O., Plouffe, D., Zhou, Y., Johnson, J.R., Le Roch, K., Sarr, O., Ndir, O., Mboup, S., Batalov, S., Wirth, D.F. & Winzeler, E.A. A systematic map of genetic variation in Plasmodium falciparum. *PLoS Pathog* **2**, e57 (2006).

187. Wellems, T.E., Panton, L.J., Gluzman, I.Y., do Rosario, V.E., Gwadz, R.W., Walker-Jonah, A. & Krogstad, D.J. Chloroquine resistance not linked to mdr-like genes in a Plasmodium falciparum cross. *Nature* **345**, 253-5 (1990).

188. Goodyer, I.D. & Taraschi, T.F. Plasmodium falciparum: a simple, rapid method for detecting parasite clones in microtiter plates. *Exp Parasitol* **86**, 158-60 (1997).

189. Yoo, E., Schulze, C.J., Stokes, B.H., Onguka, O., Yeo, T., Mok, S., Gnadig, N.F., Zhou, Y., Kurita, K., Foe, I.T., Terrell, S.M., Boucher, M.J., Cieplak, P., Kumpornsin, K., Lee, M.C.S., Linington, R.G., Long, J.Z., Uhlemann, A.C., Weerapana, E., Fidock, D.A. & Bogyo, M. The Antimalarial Natural Product Salinipostin A Identifies Essential alpha/beta Serine Hydrolases Involved in Lipid Metabolism in P. falciparum Parasites. *Cell Chem Biol* **27**, 143-157 e5 (2020).

190. Honma, H., Hirai, M., Nakamura, S., Hakimi, H., Kawazu, S., Palacpac, N.M., Hisaeda, H., Matsuoka, H., Kawai, S., Endo, H., Yasunaga, T., Ohashi, J., Mita,

T., Horii, T., Furusawa, M. & Tanabe, K. Generation of rodent malaria parasites with a high mutation rate by destructing proofreading activity of DNA polymerase delta. *DNA Res* **21**, 439-46 (2014).

191. Pelleau, S., Moss, E.L., Dhingra, S.K., Volney, B., Casteras, J., Gabryszewski, S.J., Volkman, S.K., Wirth, D.F., Legrand, E., Fidock, D.A., Neafsey, D.E. & Musset, L. Adaptive evolution of malaria parasites in French Guiana: Reversal of chloroquine resistance by acquisition of a mutation in pfcrt. *Proc Natl Acad Sci U S A* **112**, 11672-7 (2015).

192. Valderramos, S.G., Valderramos, J.C., Musset, L., Purcell, L.A., Mercereau-Puijalon, O., Legrand, E. & Fidock, D.A. Identification of a mutant PfCRT-mediated chloroquine tolerance phenotype in Plasmodium falciparum. *PLoS Pathog* **6**, e1000887 (2010).

193. Peterson, D.S., Walliker, D. & Wellems, T.E. Evidence that a point mutation in dihydrofolate reductase-thymidylate synthase confers resistance to pyrimethamine in falciparum malaria. *Proc Natl Acad Sci U S A* **85**, 9114-8 (1988).

194. McKenna, A., Hanna, M., Banks, E., Sivachenko, A., Cibulskis, K., Kernytsky, A., Garimella, K., Altshuler, D., Gabriel, S., Daly, M. & DePristo, M.A. The Genome Analysis Toolkit: a MapReduce framework for analyzing next-generation DNA sequencing data. *Genome Res* **20**, 1297-303 (2010).

195. Van der Auwera, G.A., Carneiro, M.O., Hartl, C., Poplin, R., Del Angel, G., Levy-Moonshine, A., Jordan, T., Shakir, K., Roazen, D., Thibault, J., Banks, E., Garimella, K.V., Altshuler, D., Gabriel, S. & DePristo, M.A. From FastQ data to high confidence variant calls: the Genome Analysis Toolkit best practices pipeline. *Curr Protoc Bioinformatics* **43**, 11 10 1-11 10 33 (2013).

196. Cingolani, P., Platts, A., Wang le, L., Coon, M., Nguyen, T., Wang, L., Land, S.J., Lu, X. & Ruden, D.M. A program for annotating and predicting the effects of single nucleotide polymorphisms, SnpEff: SNPs in the genome of Drosophila melanogaster strain w1118; iso-2; iso-3. *Fly (Austin)* **6**, 80-92 (2012).

197. Peters, J., Fowler, E., Gatton, M., Chen, N., Saul, A. & Cheng, Q. High diversity and rapid changeover of expressed var genes during the acute phase of Plasmodium falciparum infections in human volunteers. *Proc Natl Acad Sci U S A* **99**, 10689-94 (2002).

198. Bultrini, E., Brick, K., Mukherjee, S., Zhang, Y., Silvestrini, F., Alano, P. & Pizzi, E. Revisiting the Plasmodium falciparum RIFIN family: from comparative genomics to 3D-model prediction. *BMC Genomics* **10**, 445 (2009).

199. Niang, M., Yan Yam, X. & Preiser, P.R. The Plasmodium falciparum STEVOR multigene family mediates antigenic variation of the infected erythrocyte. *PLoS Pathog* **5**, e1000307 (2009).

200. Schmittgen, T.D. & Livak, K.J. Analyzing real-time PCR data by the comparative C(T) method. *Nat Protoc* **3**, 1101-8 (2008).

201. Pappas, G., Roussos, N. & Falagas, M.E. Toxoplasmosis snapshots: global status of Toxoplasma gondii seroprevalence and implications for pregnancy and congenital toxoplasmosis. *Int J Parasitol* **39**, 1385-94 (2009).

202. Montoya, J.G. & Liesenfeld, O. Toxoplasmosis. *Lancet* **363**, 1965-76 (2004).
203. Watts, E., Zhao, Y., Dhara, A., Eller, B., Patwardhan, A. & Sinai, A.P. Novel Approaches Reveal that Toxoplasma gondii Bradyzoites within Tissue Cysts Are Dynamic and Replicating Entities In Vivo. *mBio* **6**, e01155-15 (2015).

204. Israelski, D.M. & Remington, J.S. Toxoplasmosis in the non-AIDS immunocompromised host. *Curr Clin Top Infect Dis* **13**, 322-56 (1993).

205. Luft, B.J. & Remington, J.S. Toxoplasmic encephalitis in AIDS. *Clin Infect Dis* **15**, 211-22 (1992).

206. Cabral, C.M., Tuladhar, S., Dietrich, H.K., Nguyen, E., MacDonald, W.R., Trivedi, T., Devineni, A. & Koshy, A.A. Neurons are the Primary Target Cell for the Brain-Tropic Intracellular Parasite Toxoplasma gondii. *PLoS Pathog* **12**, e1005447 (2016).

207. Torgerson, P.R. & Mastroiacovo, P. The global burden of congenital toxoplasmosis: a systematic review. *Bull World Health Organ* **91**, 501-8 (2013).

208. Glasner, P.D., Silveira, C., Kruszon-Moran, D., Martins, M.C., Burnier Junior, M., Silveira, S., Camargo, M.E., Nussenblatt, R.B., Kaslow, R.A. & Belfort Junior, R. An unusually high prevalence of ocular toxoplasmosis in southern Brazil. *Am J Ophthalmol* **114**, 136-44 (1992).

209. Dunay, I.R., Gajurel, K., Dhakal, R., Liesenfeld, O. & Montoya, J.G. Treatment of Toxoplasmosis: Historical Perspective, Animal Models, and Current Clinical Practice. *Clin Microbiol Rev* **31**(2018).

210. Gajurel, K., Gomez, C.A., Dhakal, R., Vogel, H. & Montoya, J.G. Failure of primary atovaquone prophylaxis for prevention of toxoplasmosis in hematopoietic cell transplant recipients. *Transpl Infect Dis* **18**, 446-452 (2016).

211. Baatz, H., Mirshahi, A., Puchta, J., Gumbel, H. & Hattenbach, L.O. Reactivation of toxoplasma retinochoroiditis under atovaquone therapy in an immunocompetent patient. *Ocul Immunol Inflamm* **14**, 185-7 (2006).

212. Eastman, R.T. & Fidock, D.A. Artemisinin-based combination therapies: a vital tool in efforts to eliminate malaria. *Nat Rev Microbiol* **7**, 864-74 (2009).

213. Heller, L.E. & Roepe, P.D. Artemisinin-Based Antimalarial Drug Therapy: Molecular Pharmacology and Evolving Resistance. *Trop Med Infect Dis* **4**(2019).

214. Kaiser, M., Wittlin, S., Nehrbass-Stuedli, A., Dong, Y., Wang, X., Hemphill, A., Matile, H., Brun, R. & Vennerstrom, J.L. Peroxide bond-dependent antiplasmodial specificity of artemisinin and OZ277 (RBx11160). *Antimicrob Agents Chemother* **51**, 2991-3 (2007).

215. Giannangelo, C., Fowkes, F.J.I., Simpson, J.A., Charman, S.A. & Creek, D.J. Ozonide Antimalarial Activity in the Context of Artemisinin-Resistant Malaria. *Trends Parasitol* **35**, 529-543 (2019).

216. Hencken, C.P., Jones-Brando, L., Bordon, C., Stohler, R., Mott, B.T., Yolken, R., Posner, G.H. & Woodard, L.E. Thiazole, oxadiazole, and carboxamide derivatives of artemisinin are highly selective and potent inhibitors of Toxoplasma gondii. *J Med Chem* **53**, 3594-601 (2010).

217. Jones-Brando, L., D'Angelo, J., Posner, G.H. & Yolken, R. In vitro inhibition of Toxoplasma gondii by four new derivatives of artemisinin. *Antimicrob Agents Chemother* **50**, 4206-8 (2006).

218. Sarciron, M.E., Saccharin, C., Petavy, A.F. & Peyron, F. Effects of artesunate, dihydroartemisinin, and an artesunate-dihydroartemisinin combination against Toxoplasma gondii. *Am J Trop Med Hyg* **62**, 73-6 (2000).

219. Dunay, I.R., Chan, W.C., Haynes, R.K. & Sibley, L.D. Artemisone and artemiside control acute and reactivated toxoplasmosis in a murine model. *Antimicrob Agents Chemother* **53**, 4450-6 (2009).

220. Schultz, T.L., Hencken, C.P., Woodard, L.E., Posner, G.H., Yolken, R.H., Jones-Brando, L. & Carruthers, V.B. A thiazole derivative of artemisinin moderately reduces Toxoplasma gondii cyst burden in infected mice. *J Parasitol* **100**, 516-21 (2014).

221. Holfels, E., McAuley, J., Mack, D., Milhous, W.K. & McLeod, R. In vitro effects of artemisinin ether, cycloguanil hydrochloride (alone and in combination with sulfadiazine), quinine sulfate, mefloquine, primaquine phosphate, trifluoperazine hydrochloride, and verapamil on Toxoplasma gondii. *Antimicrob Agents Chemother* **38**, 1392-6 (1994).

222. Sigala, P.A. & Goldberg, D.E. The peculiarities and paradoxes of Plasmodium heme metabolism. *Annu Rev Microbiol* **68**, 259-78 (2014).

223. Klonis, N., Xie, S.C., McCaw, J.M., Crespo-Ortiz, M.P., Zaloumis, S.G., Simpson, J.A. & Tilley, L. Altered temporal response of malaria parasites determines differential sensitivity to artemisinin. *Proc Natl Acad Sci U S A* **110**, 5157-62 (2013).

224. Ismail, H.M., Barton, V., Phanchana, M., Charoensutthivarakul, S., Wong, M.H., Hemingway, J., Biagini, G.A., O'Neill, P.M. & Ward, S.A. Artemisinin activity-based probes identify multiple molecular targets within the asexual stage of the malaria parasites Plasmodium falciparum 3D7. *Proc Natl Acad Sci U S A* **113**, 2080-5 (2016).

225. Wang, J., Zhang, C.J., Chia, W.N., Loh, C.C., Li, Z., Lee, Y.M., He, Y., Yuan, L.X., Lim, T.K., Liu, M., Liew, C.X., Lee, Y.Q., Zhang, J., Lu, N., Lim, C.T., Hua, Z.C., Liu, B., Shen, H.M., Tan, K.S. & Lin, Q. Haem-activated promiscuous targeting of artemisinin in Plasmodium falciparum. *Nat Commun* **6**, 10111 (2015).

226. Witkowski, B., Amaratunga, C., Khim, N., Sreng, S., Chim, P., Kim, S., Lim, P., Mao, S., Sopha, C., Sam, B., Anderson, J.M., Duong, S., Chuor, C.M., Taylor, W.R., Suon, S., Mercereau-Puijalon, O., Fairhurst, R.M. & Menard, D. Novel phenotypic assays for the detection of artemisinin-resistant Plasmodium falciparum malaria in Cambodia: in-vitro and ex-vivo drug-response studies. *Lancet Infect Dis* **13**, 1043-9 (2013).

227. Ariey, F., Witkowski, B., Amaratunga, C., Beghain, J., Langlois, A.C., Khim, N., Kim, S., Duru, V., Bouchier, C., Ma, L., Lim, P., Leang, R., Duong, S., Sreng, S., Suon, S., Chuor, C.M., Bout, D.M., Menard, S., Rogers, W.O., Genton, B., Fandeur, T., Miotto, O., Ringwald, P., Le Bras, J., Berry, A., Barale, J.C., Fairhurst, R.M., Benoit-Vical, F., Mercereau-Puijalon, O. & Menard, D. A molecular marker of artemisinin-resistant Plasmodium falciparum malaria. *Nature* **505**, 50-5 (2014).

228. Straimer, J., Gnadig, N.F., Witkowski, B., Amaratunga, C., Duru, V., Ramadani, A.P., Dacheux, M., Khim, N., Zhang, L., Lam, S., Gregory, P.D., Urnov, F.D., Mercereau-Puijalon, O., Benoit-Vical, F., Fairhurst, R.M., Menard, D. & Fidock, D.A. Drug resistance. K13-propeller mutations confer artemisinin resistance in Plasmodium falciparum clinical isolates. *Science* **347**, 428-31 (2015).

229. Bridgford, J.L., Xie, S.C., Cobbold, S.A., Pasaje, C.F.A., Herrmann, S., Yang, T., Gillett, D.L., Dick, L.R., Ralph, S.A., Dogovski, C., Spillman, N.J. & Tilley, L. Artemisinin kills malaria parasites by damaging proteins and inhibiting the proteasome. *Nat Commun* **9**, 3801 (2018).

230. Breglio, K.F., Rahman, R.S., Sa, J.M., Hott, A., Roberts, D.J. & Wellems, T.E. Kelch Mutations in Plasmodium falciparum Protein K13 Do Not Modulate Dormancy after Artemisinin Exposure and Sorbitol Selection In Vitro. *Antimicrob Agents Chemother* **62**(2018).

231. Sutherland, C.J., Lansdell, P., Sanders, M., Muwanguzi, J., van Schalkwyk, D.A., Kaur, H., Nolder, D., Tucker, J., Bennett, H.M., Otto, T.D., Berriman, M., Patel, T.A., Lynn, R., Gkrania-Klotsas, E. & Chiodini, P.L. pfk13-Independent Treatment Failure in Four Imported Cases of Plasmodium falciparum Malaria Treated with Artemether-Lumefantrine in the United Kingdom. *Antimicrob Agents Chemother* **61**(2017).

232. Sa, J.M., Kaslow, S.R., Krause, M.A., Melendez-Muniz, V.A., Salzman, R.E., Kite, W.A., Zhang, M., Moraes Barros, R.R., Mu, J., Han, P.K., Mershon, J.P., Figan, C.E., Caleon, R.L., Rahman, R.S., Gibson, T.J., Amaratunga, C., Nishiguchi, E.P., Breglio, K.F., Engels, T.M., Velmurugan, S., Ricklefs, S., Straimer, J., Gnadig, N.F., Deng, B., Liu, A., Diouf, A., Miura, K., Tullo, G.S., Eastman, R.T., Chakravarty, S., James, E.R., Udenze, K., Li, S., Sturdevant, D.E., Gwadz, R.W., Porcella, S.F., Long, C.A., Fidock, D.A., Thomas, M.L., Fay, M.P., Sim, B.K.L., Hoffman, S.L., Adams, J.H., Fairhurst, R.M., Su, X.Z. & Wellems, T.E. Artemisinin resistance phenotypes and K13 inheritance in a Plasmodium falciparum cross and Aotus model. *Proc Natl Acad Sci U S A* **115**, 12513-12518 (2018).

233. Mbengue, A., Bhattacharjee, S., Pandharkar, T., Liu, H., Estiu, G., Stahelin, R.V., Rizk, S.S., Njimoh, D.L., Ryan, Y., Chotivanich, K., Nguon, C., Ghorbal, M., Lopez-Rubio, J.J., Pfrender, M., Emrich, S., Mohandas, N., Dondorp, A.M., Wiest, O. & Haldar, K. A molecular mechanism of artemisinin resistance in Plasmodium falciparum malaria. *Nature* **520**, 683-7 (2015).

234. Demas, A.R., Sharma, A.I., Wong, W., Early, A.M., Redmond, S., Bopp, S., Neafsey, D.E., Volkman, S.K., Hartl, D.L. & Wirth, D.F. Mutations in Plasmodium falciparum actin-binding protein coronin confer reduced artemisinin susceptibility. *Proc Natl Acad Sci U S A* **115**, 12799-12804 (2018).

235. Liu, X., Cao, J., Huang, G., Zhao, Q. & Shen, J. Biological Activities of Artemisinin Derivatives Beyond Malaria. *Curr Top Med Chem* **19**, 205-222 (2019).

236. Efferth, T. Cancer combination therapies with artemisinin-type drugs. *Biochem Pharmacol* **139**, 56-70 (2017).

237. Efferth, T. From ancient herb to modern drug: Artemisia annua and artemisinin for cancer therapy. *Semin Cancer Biol* **46**, 65-83 (2017).

238. Li, W., Mo, W., Shen, D., Sun, L., Wang, J., Lu, S., Gitschier, J.M. & Zhou, B. Yeast model uncovers dual roles of mitochondria in action of artemisinin. *PLoS Genet* **1**, e36 (2005).

239. Wang, J., Huang, L., Li, J., Fan, Q., Long, Y., Li, Y. & Zhou, B. Artemisinin directly targets malarial mitochondria through its specific mitochondrial activation. *PLoS One* **5**, e9582 (2010).

240. Lu, M., Sun, L., Zhou, J. & Yang, J. Dihydroartemisinin induces apoptosis in colorectal cancer cells through the mitochondria-dependent pathway. *Tumour Biol* **35**, 5307-14 (2014).

241. Mercer, A.E., Copple, I.M., Maggs, J.L., O'Neill, P.M. & Park, B.K. The role of heme and the mitochondrion in the chemical and molecular mechanisms of mammalian cell death induced by the artemisinin antimalarials. *J Biol Chem* **286**, 987-96 (2011).

242. Nagamune, K., Moreno, S.N. & Sibley, L.D. Artemisinin-resistant mutants of Toxoplasma gondii have altered calcium homeostasis. *Antimicrob Agents Chemother* **51**, 3816-23 (2007).

243. Radke, J.R., Striepen, B., Guerini, M.N., Jerome, M.E., Roos, D.S. & White, M.W. Defining the cell cycle for the tachyzoite stage of Toxoplasma gondii. *Mol Biochem Parasitol* **115**, 165-75 (2001).

244. Lorenzi, H., Khan, A., Behnke, M.S., Namasivayam, S., Swapna, L.S., Hadjithomas, M., Karamycheva, S., Pinney, D., Brunk, B.P., Ajioka, J.W., Ajzenberg, D., Boothroyd, J.C., Boyle, J.P., Darde, M.L., Diaz-Miranda, M.A., Dubey, J.P., Fritz, H.M., Gennari, S.M., Gregory, B.D., Kim, K., Saeij, J.P., Su, C., White, M.W., Zhu, X.Q., Howe, D.K., Rosenthal, B.M., Grigg, M.E., Parkinson, J., Liu, L., Kissinger, J.C., Roos, D.S. & Sibley, L.D. Local admixture of amplified and diversified secreted pathogenesis determinants shapes mosaic Toxoplasma gondii genomes. *Nat Commun* **7**, 10147 (2016).

245. Lentini, G., El Hajj, H., Papoin, J., Fall, G., Pfaff, A.W., Tawil, N., Braun-Breton, C. & Lebrun, M. Characterization of Toxoplasma DegP, a rhoptry serine protease crucial for lethal infection in mice. *PLoS One* **12**, e0189556 (2017).

246. Seidi, A., Muellner-Wong, L.S., Rajendran, E., Tjhin, E.T., Dagley, L.F., Aw, V.Y., Faou, P., Webb, A.I., Tonkin, C.J. & van Dooren, G.G. Elucidating the mitochondrial proteome of Toxoplasma gondii reveals the presence of a divergent cytochrome c oxidase. *Elife* **7**(2018).

247. Harding, C.R., Sidik, S.M., Petrova, B., Gnadig, N.F., Okombo, J., Herneisen, A.L., Ward, K.E., Markus, B.M., Boydston, E.A., Fidock, D.A. & Lourido, S. Genetic screens reveal a central role for heme metabolism in artemisinin susceptibility. *Nat Commun* **11**, 4813 (2020).

248. Brown, K.M., Long, S. & Sibley, L.D. Plasma Membrane Association by N-Acylation Governs PKG Function in Toxoplasma gondii. *mBio* **8**(2017).

249. Ashton, M., Hai, T.N., Sy, N.D., Huong, D.X., Van Huong, N., Nieu, N.T. & Cong, L.D. Artemisinin pharmacokinetics is time-dependent during repeated oral administration in healthy male adults. *Drug Metab Dispos* **26**, 25-7 (1998).

250. Witkowski, B., Lelievre, J., Barragan, M.J., Laurent, V., Su, X.Z., Berry, A. & Benoit-Vical, F. Increased tolerance to artemisinin in Plasmodium falciparum is mediated by a quiescence mechanism. *Antimicrob Agents Chemother* **54**, 1872-7 (2010).

251. Thomas, P.D., Campbell, M.J., Kejariwal, A., Mi, H., Karlak, B., Daverman, R., Diemer, K., Muruganujan, A. & Narechania, A. PANTHER: a library of protein families and subfamilies indexed by function. *Genome Res* **13**, 2129-41 (2003).

252. Zollman, S., Godt, D., Prive, G.G., Couderc, J.L. & Laski, F.A. The BTB domain, found primarily in zinc finger proteins, defines an evolutionarily conserved family that includes several developmentally regulated genes in Drosophila. *Proc Natl Acad Sci U S A* **91**, 10717-21 (1994).

253. Coppee, R., Jeffares, D.C., Miteva, M.A., Sabbagh, A. & Clain, J. Comparative structural and evolutionary analyses predict functional sites in the artemisinin resistance malaria protein K13. *Sci Rep* **9**, 10675 (2019).

254. Paloque, L., Coppee, R., Stokes, B.H., Gnadig, N.F., Niare, K., Augereau, J.M., Fidock, D.A., Clain, J. & Benoit-Vical, F. Mutation in the Plasmodium falciparum BTB/POZ Domain of K13 Protein Confers Artemisinin Resistance. *Antimicrob Agents Chemother* **66**, e0132021 (2022).

255. Bopp, S.E., Manary, M.J., Bright, A.T., Johnston, G.L., Dharia, N.V., Luna, F.L., McCormack, S., Plouffe, D., McNamara, C.W., Walker, J.R., Fidock, D.A., Denchi, E.L. & Winzeler, E.A. Mitotic evolution of Plasmodium falciparum shows a stable core genome but recombination in antigen families. *PLoS Genet* **9**, e1003293 (2013).

256. Farrell, A., Coleman, B.I., Benenati, B., Brown, K.M., Blader, I.J., Marth, G.T. & Gubbels, M.J. Whole genome profiling of spontaneous and chemically induced mutations in Toxoplasma gondii. *BMC Genomics* **15**, 354 (2014).

257. Good, B.H., McDonald, M.J., Barrick, J.E., Lenski, R.E. & Desai, M.M. The dynamics of molecular evolution over 60,000 generations. *Nature* **551**, 45-50 (2017).

258. Sidik, S.M., Huet, D., Ganesan, S.M., Huynh, M.H., Wang, T., Nasamu, A.S., Thiru, P., Saeij, J.P.J., Carruthers, V.B., Niles, J.C. & Lourido, S. A Genome-wide CRISPR Screen in Toxoplasma Identifies Essential Apicomplexan Genes. *Cell* **166**, 1423-1435 e12 (2016).

259. Pallen, M.J. & Wren, B.W. The HtrA family of serine proteases. *Mol Microbiol* **26**, 209-21 (1997).

260. Padmanabhan, N., Fichtner, L., Dickmanns, A., Ficner, R., Schulz, J.B. & Braus, G.H. The yeast HtrA orthologue Ynm3 is a protease with chaperone activity that aids survival under heat stress. *Mol Biol Cell* **20**, 68-77 (2009).

261. Vande Walle, L., Lamkanfi, M. & Vandenabeele, P. The mitochondrial serine protease HtrA2/Omi: an overview. *Cell Death Differ* **15**, 453-60 (2008).

262. Huynh, M.H. & Carruthers, V.B. Tagging of endogenous genes in a Toxoplasma gondii strain lacking Ku80. *Eukaryot Cell* **8**, 530-9 (2009).

263. Soldati, D. & Boothroyd, J.C. Transient transfection and expression in the obligate intracellular parasite Toxoplasma gondii. *Science* **260**, 349-52 (1993).

264. Shen, B., Brown, K.M., Lee, T.D. & Sibley, L.D. Efficient gene disruption in diverse strains of Toxoplasma gondii using CRISPR/CAS9. *mBio* **5**, e01114-14 (2014).

265. Long, S., Brown, K.M., Drewry, L.L., Anthony, B., Phan, I.Q.H. & Sibley, L.D. Calmodulin-like proteins localized to the conoid regulate motility and cell invasion by Toxoplasma gondii. *PLoS Pathog* **13**, e1006379 (2017).

266. Lourido, S., Tang, K. & Sibley, L.D. Distinct signalling pathways control Toxoplasma egress and host-cell invasion. *EMBO J* **31**, 4524-34 (2012).

267. Carr, I.M., Robinson, J.I., Dimitriou, R., Markham, A.F., Morgan, A.W. & Bonthron, D.T. Inferring relative proportions of DNA variants from sequencing electropherograms. *Bioinformatics* **25**, 3244-50 (2009).

268. Li, H. & Durbin, R. Fast and accurate short read alignment with Burrows-Wheeler transform. *Bioinformatics* **25**, 1754-60 (2009).

269. Gillet-Markowska, A., Louvel, G. & Fischer, G. bz-rates: A Web Tool to Estimate Mutation Rates from Fluctuation Analysis. *G3 (Bethesda)* **5**, 2323-7 (2015).

270. Rosche, W.A. & Foster, P.L. Determining mutation rates in bacterial populations. *Methods* **20**, 4-17 (2000).

271. Dettman, J.R., Rodrigue, N., Melnyk, A.H., Wong, A., Bailey, S.F. & Kassen, R. Evolutionary insight from whole-genome sequencing of experimentally evolved microbes. *Mol Ecol* **21**, 2058-77 (2012).

272. Barrick, J.E., Yu, D.S., Yoon, S.H., Jeong, H., Oh, T.K., Schneider, D., Lenski, R.E. & Kim, J.F. Genome evolution and adaptation in a long-term experiment with Escherichia coli. *Nature* **461**, 1243-7 (2009).

273. Lenski, R.E. & Travisano, M. Dynamics of adaptation and diversification: a 10,000-generation experiment with bacterial populations. *Proc Natl Acad Sci U S A* **91**, 6808-14 (1994).

274. Dunham, M.J., Badrane, H., Ferea, T., Adams, J., Brown, P.O., Rosenzweig, F. & Botstein, D. Characteristic genome rearrangements in experimental evolution of Saccharomyces cerevisiae. *Proc Natl Acad Sci U S A* **99**, 16144-9 (2002).

275. Araya, C.L., Payen, C., Dunham, M.J. & Fields, S. Whole-genome sequencing of a laboratory-evolved yeast strain. *BMC Genomics* **11**, 88 (2010).

276. Chang, S.L., Lai, H.Y., Tung, S.Y. & Leu, J.Y. Dynamic large-scale chromosomal rearrangements fuel rapid adaptation in yeast populations. *PLoS Genet* **9**, e1003232 (2013).

277. Albert, T.J., Dailidiene, D., Dailide, G., Norton, J.E., Kalia, A., Richmond, T.A., Molla, M., Singh, J., Green, R.D. & Berg, D.E. Mutation discovery in bacterial genomes: metronidazole resistance in Helicobacter pylori. *Nat Methods* **2**, 951-3 (2005).

278. Toprak, E., Veres, A., Michel, J.B., Chait, R., Hartl, D.L. & Kishony, R. Evolutionary paths to antibiotic resistance under dynamically sustained drug selection. *Nat Genet* **44**, 101-5 (2011).

279. Cowen, L.E., Sanglard, D., Calabrese, D., Sirjusingh, C., Anderson, J.B. & Kohn, L.M. Evolution of drug resistance in experimental populations of Candida albicans. *J Bacteriol* **182**, 1515-22 (2000).

280. Peter, J., De Chiara, M., Friedrich, A., Yue, J.X., Pflieger, D., Bergstrom, A., Sigwalt, A., Barre, B., Freel, K., Llored, A., Cruaud, C., Labadie, K., Aury, J.M., Istace, B., Lebrigand, K., Barbry, P., Engelen, S., Lemainque, A., Wincker, P., Liti, G. & Schacherer, J. Genome evolution across 1,011 Saccharomyces cerevisiae isolates. *Nature* **556**, 339-344 (2018).

281. Winzeler, E.A., Shoemaker, D.D., Astromoff, A., Liang, H., Anderson, K., Andre, B., Bangham, R., Benito, R., Boeke, J.D., Bussey, H., Chu, A.M., Connelly, C., Davis, K., Dietrich, F., Dow, S.W., El Bakkoury, M., Foury, F., Friend, S.H., Gentalen, E., Giaever, G., Hegemann, J.H., Jones, T., Laub, M., Liao, H., Liebundguth, N., Lockhart, D.J., Lucau-Danila, A., Lussier, M., M'Rabet, N., Menard, P., Mittmann, M., Pai, C., Rebischung, C., Revuelta, J.L., Riles, L., Roberts, C.J., Ross-MacDonald, P., Scherens, B., Snyder, M., Sookhai-Mahadeo, S., Storms, R.K., Veronneau, S., Voet, M., Volckaert, G., Ward, T.R., Wysocki, R., Yen, G.S., Yu, K., Zimmermann, K., Philippsen, P., Johnston, M. & Davis, R.W. Functional characterization of the S. cerevisiae genome by gene deletion and parallel analysis. *Science* **285**, 901-6 (1999).

282. Giaever, G., Chu, A.M., Ni, L., Connelly, C., Riles, L., Veronneau, S., Dow, S., Lucau-Danila, A., Anderson, K., Andre, B., Arkin, A.P., Astromoff, A., El-Bakkoury, M., Bangham, R., Benito, R., Brachat, S., Campanaro, S., Curtiss, M., Davis, K., Deutschbauer, A., Entian, K.D., Flaherty, P., Foury, F., Garfinkel, D.J., Gerstein, M., Gotte, D., Guldener, U., Hegemann, J.H., Hempel, S., Herman, Z., Jaramillo, D.F., Kelly, D.E., Kelly, S.L., Kotter, P., LaBonte, D., Lamb, D.C., Lan, N., Liang, H., Liao, H., Liu, L., Luo, C., Lussier, M., Mao, R., Menard, P., Ooi, S.L., Revuelta, J.L., Roberts, C.J., Rose, M., Ross-Macdonald, P., Scherens, B., Schimmack, G., Shafer, B., Shoemaker, D.D., Sookhai-Mahadeo, S., Storms, R.K., Strathern, J.N., Valle, G., Voet, M., Volckaert, G., Wang, C.Y., Ward, T.R., Wilhelmy, J., Winzeler, E.A., Yang, Y., Yen, G., Youngman, E., Yu, K., Bussey, H., Boeke, J.D., Snyder, M., Philippsen, P., Davis, R.W. & Johnston, M. Functional profiling of the Saccharomyces cerevisiae genome. *Nature* **418**, 387-91 (2002).

283. Hillenmeyer, M.E., Fung, E., Wildenhain, J., Pierce, S.E., Hoon, S., Lee, W., Proctor, M., St Onge, R.P., Tyers, M., Koller, D., Altman, R.B., Davis, R.W., Nislow, C. & Giaever, G. The chemical genomic portrait of yeast: uncovering a phenotype for all genes. *Science* **320**, 362-5 (2008).

284. Puddu, F., Herzog, M., Selivanova, A., Wang, S., Zhu, J., Klein-Lavi, S., Gordon, M., Meirman, R., Millan-Zambrano, G., Ayestaran, I., Salguero, I., Sharan, R., Li, R., Kupiec, M. & Jackson, S.P. Genome architecture and stability in the Saccharomyces cerevisiae knockout collection. *Nature* **573**, 416-420 (2019).

285. Behan, F.M., Iorio, F., Picco, G., Goncalves, E., Beaver, C.M., Migliardi, G., Santos, R., Rao, Y., Sassi, F., Pinnelli, M., Ansari, R., Harper, S., Jackson, D.A., McRae, R., Pooley, R., Wilkinson, P., van der Meer, D., Dow, D., Buser-Doepner, C., Bertotti, A., Trusolino, L., Stronach, E.A., Saez-Rodriguez, J., Yusa, K. & Garnett, M.J. Prioritization of cancer therapeutic targets using CRISPR-Cas9 screens. *Nature* **568**, 511-516 (2019).

286. Yang, Z. & Blenner, M. Genome editing systems across yeast species. *Curr Opin Biotechnol* **66**, 255-266 (2020).

287. Despres, P.C., Dube, A.K., Seki, M., Yachie, N. & Landry, C.R. Perturbing proteomes at single residue resolution using base editing. *Nat Commun* **11**, 1871 (2020).

288. Kuroda, K. & Ueda, M. CRISPR Nickase-Mediated Base Editing in Yeast. *Methods Mol Biol* **2196**, 27-37 (2021).

289. Blair, J.M., Webber, M.A., Baylay, A.J., Ogbolu, D.O. & Piddock, L.J. Molecular mechanisms of antibiotic resistance. *Nat Rev Microbiol* **13**, 42-51 (2015).

290. Ferrari, S., Ischer, F., Calabrese, D., Posteraro, B., Sanguinetti, M., Fadda, G., Rohde, B., Bauser, C., Bader, O. & Sanglard, D. Gain of function mutations in

CgPDR1 of Candida glabrata not only mediate antifungal resistance but also enhance virulence. *PLoS Pathog* **5**, e1000268 (2009).

291. Warner, D.M., Shafer, W.M. & Jerse, A.E. Clinically relevant mutations that cause derepression of the Neisseria gonorrhoeae MtrC-MtrD-MtrE Efflux pump system confer different levels of antimicrobial resistance and in vivo fitness. *Mol Microbiol* **70**, 462-78 (2008).

292. Corvec, S., Caroff, N., Espaze, E., Marraillac, J. & Reynaud, A. -11 Mutation in the ampC promoter increasing resistance to beta-lactams in a clinical Escherichia coli strain. *Antimicrob Agents Chemother* **46**, 3265-7 (2002).

293. Nelson, E.C. & Elisha, B.G. Molecular basis of AmpC hyperproduction in clinical isolates of Escherichia coli. *Antimicrob Agents Chemother* **43**, 957-9 (1999).

294. Suzuki, Y., Stam, J., Novotny, M., Yachie, N., Lasken, R.S. & Roth, F.P. The green monster process for the generation of yeast strains carrying multiple gene deletions. *J Vis Exp*, e4072 (2012).

295. Rocamora, F., Gupta, P., Istvan, E.S., Luth, M.R., Carpenter, E.F., Kumpornsin, K., Sasaki, E., Calla, J., Mittal, N., Carolino, K., Owen, E., Llinas, M., Ottilie, S., Goldberg, D.E., Lee, M.C.S. & Winzeler, E.A. PfMFR3: A Multidrug-Resistant Modulator in Plasmodium falciparum. *ACS Infect Dis* **7**, 811-825 (2021).

296. Ottilie, S., Goldgof, G.M., Calvet, C.M., Jennings, G.K., LaMonte, G., Schenken, J., Vigil, E., Kumar, P., McCall, L.I., Lopes, E.S., Gunawan, F., Yang, J., Suzuki, Y., Siqueira-Neto, J.L., McKerrow, J.H., Amaro, R.E., Podust, L.M., Durrant, J.D. & Winzeler, E.A. Rapid Chagas Disease Drug Target Discovery Using Directed Evolution in Drug-Sensitive Yeast. *ACS Chem Biol* **12**, 422-434 (2017).

297. Van Voorhis, W.C., Adams, J.H., Adelfio, R., Ahyong, V., Akabas, M.H., Alano, P., Alday, A., Aleman Resto, Y., Alsibaee, A., Alzualde, A., Andrews, K.T., Avery, S.V., Avery, V.M., Ayong, L., Baker, M., Baker, S., Ben Mamoun, C., Bhatia, S., Bickle, Q., Bounaadja, L., Bowling, T., Bosch, J., Boucher, L.E., Boyom, F.F., Brea, J., Brennan, M., Burton, A., Caffrey, C.R., Camarda, G., Carrasquilla, M., Carter, D., Belen Cassera, M., Chih-Chien Cheng, K., Chindaudomsate, W., Chubb, A., Colon, B.L., Colon-Lopez, D.D., Corbett, Y., Crowther, G.J., Cowan, N., D'Alessandro, S., Le Dang, N., Delves, M., DeRisi, J.L., Du, A.Y., Duffy, S., Abd El-Salam El-Sayed, S., Ferdig, M.T., Fernandez Robledo, J.A., Fidock, D.A., Florent, I., Fokou, P.V., Galstian, A., Gamo, F.J., Gokool, S., Gold, B., Golub, T., Goldgof, G.M., Guha, R., Guiguemde, W.A., Gural, N., Guy, R.K., Hansen, M.A., Hanson, K.K., Hemphill, A., Hooft van Huijsduijnen, R., Horii, T., Horrocks, P., Hughes, T.B., Huston, C., Igarashi, I., Ingram-Sieber, K., Itoe, M.A., Jadhav, A., Naranuntarat Jensen, A., Jensen, L.T., Jiang, R.H., Kaiser, A., Keiser, J., Ketas, T., Kicka, S., Kim, S., Kirk, K., Kumar, V.P., Kyle, D.E., Lafuente, M.J., Landfear, S., Lee, N., Lee, S., Lehane, A.M., Li, F., Little, D., Liu, L., Llinas, M., Loza, M.I.,

Lubar, A., Lucantoni, L., Lucet, I., Maes, L., Mancama, D., Mansour, N.R., March, S., McGowan, S., Medina Vera, I., Meister, S., Mercer, L., Mestres, J., Mfopa, A.N., Misra, R.N., Moon, S., Moore, J.P., Morais Rodrigues da Costa, F., Muller, J., Muriana, A., Nakazawa Hewitt, S., Nare, B., Nathan, C., Narraidoo, N., Nawaratna, S., Ojo, K.K., Ortiz, D., Panic, G., Papadatos, G., Parapini, S., Patra, K., Pham, N., Prats, S., Plouffe, D.M., Poulsen, S.A., Pradhan, A., Quevedo, C., Quinn, R.J., Rice, C.A., Abdo Rizk, M., Ruecker, A., St Onge, R., Salgado Ferreira, R., Samra, J., Robinett, N.G., Schlecht, U., Schmitt, M., Silva Villela, F., Silvestrini, F., Sinden, R., Smith, D.A., Soldati, T., Spitzmuller, A., Stamm, S.M., Sullivan, D.J., Sullivan, W., Suresh, S., Suzuki, B.M., Suzuki, Y., Swamidass, S.J., Taramelli, D., Tchokouaha, L.R., Theron, A., Thomas, D., Tonissen, K.F., Townson, S., Tripathi, A.K., Trofimov, V., Udenze, K.O., Ullah, I., Vallieres, C., Vigil, E., Vinetz, J.M., Voong Vinh, P., Vu, H., Watanabe, N.A., Weatherby, K., White, P.M., Wilks, A.F., Winzeler, E.A., Wojcik, E., Wree, M., Wu, W., Yokoyama, N., Zollo, P.H., Abla, N., Blasco, B., Burrows, J., Laleu, B., Leroy, D., Spangenberg, T., Wells, T. & Willis, P.A. Open Source Drug Discovery with the Malaria Box Compound Collection for Neglected Diseases and Beyond. *PLoS Pathog* **12**, e1005763 (2016).

298. Zhu, Y.O., Siegal, M.L., Hall, D.W. & Petrov, D.A. Precise estimates of mutation rate and spectrum in yeast. *Proc Natl Acad Sci U S A* **111**, E2310-8 (2014).

299. Giaever, G. & Nislow, C. The yeast deletion collection: a decade of functional genomics. *Genetics* **197**, 451-65 (2014).

300. Yona, A.H., Manor, Y.S., Herbst, R.H., Romano, G.H., Mitchell, A., Kupiec, M., Pilpel, Y. & Dahan, O. Chromosomal duplication is a transient evolutionary solution to stress. *Proc Natl Acad Sci U S A* **109**, 21010-5 (2012).

301. Jennings, S.M., Tsay, Y.H., Fisch, T.M. & Robinson, G.W. Molecular cloning and characterization of the yeast gene for squalene synthetase. *Proc Natl Acad Sci U S A* **88**, 6038-42 (1991).

302. Fegueur, M., Richard, L., Charles, A.D. & Karst, F. Isolation and primary structure of the ERG9 gene of Saccharomyces cerevisiae encoding squalene synthetase. *Curr Genet* **20**, 365-72 (1991).

303. Markovich, S., Yekutiel, A., Shalit, I., Shadkchan, Y. & Osherov, N. Genomic approach to identification of mutations affecting caspofungin susceptibility in Saccharomyces cerevisiae. *Antimicrob Agents Chemother* **48**, 3871-6 (2004).

304. Delaveau, T., Delahodde, A., Carvajal, E., Subik, J. & Jacq, C. PDR3, a new yeast regulatory gene, is homologous to PDR1 and controls the multidrug resistance phenomenon. *Mol Gen Genet* **244**, 501-11 (1994).

305. Payen, C., Sunshine, A.B., Ong, G.T., Pogachar, J.L., Zhao, W. & Dunham, M.J. High-Throughput Identification of Adaptive Mutations in Experimentally Evolved Yeast Populations. *PLoS Genet* **12**, e1006339 (2016).

306. Strathern, J., Malagon, F., Irvin, J., Gotte, D., Shafer, B., Kireeva, M., Lubkowska, L., Jin, D.J. & Kashlev, M. The fidelity of transcription: RPB1 (RPO21) mutations that increase transcriptional slippage in S. cerevisiae. *J Biol Chem* **288**, 2689-99 (2013).

307. Hope, W.W., Tabernero, L., Denning, D.W. & Anderson, M.J. Molecular mechanisms of primary resistance to flucytosine in Candida albicans. *Antimicrob Agents Chemother* **48**, 4377-86 (2004).

308. Zhao, H., Palencia, A., Seiradake, E., Ghaemi, Z., Cusack, S., Luthey-Schulten, Z. & Martinis, S. Analysis of the Resistance Mechanism of a Benzoxaborole Inhibitor Reveals Insight into the Leucyl-tRNA Synthetase Editing Mechanism. *ACS Chem Biol* **10**, 2277-85 (2015).

309. Sarkar, J., Mao, W., Lincecum, T.L., Jr., Alley, M.R. & Martinis, S.A. Characterization of benzoxaborole-based antifungal resistance mutations demonstrates that editing depends on electrostatic stabilization of the leucyl-tRNA synthetase editing cap. *FEBS Lett* **585**, 2986-91 (2011).

310. Rock, F.L., Mao, W., Yaremchuk, A., Tukalo, M., Crepin, T., Zhou, H., Zhang, Y.K., Hernandez, V., Akama, T., Baker, S.J., Plattner, J.J., Shapiro, L., Martinis, S.A., Benkovic, S.J., Cusack, S. & Alley, M.R. An antifungal agent inhibits an aminoacyl-tRNA synthetase by trapping tRNA in the editing site. *Science* **316**, 1759-61 (2007).

311. Alhossary, A., Handoko, S.D., Mu, Y. & Kwoh, C.K. Fast, accurate, and reliable molecular docking with QuickVina 2. *Bioinformatics* **31**, 2214-6 (2015).

312. Pommier, Y. DNA topoisomerase I inhibitors: chemistry, biology, and interfacial inhibition. *Chem Rev* **109**, 2894-902 (2009).

313. Miao, Z.H., Player, A., Shankavaram, U., Wang, Y.H., Zimonjic, D.B., Lorenzi, P.L., Liao, Z.Y., Liu, H., Shimura, T., Zhang, H.L., Meng, L.H., Zhang, Y.W., Kawasaki, E.S., Popescu, N.C., Aladjem, M.I., Goldstein, D.J., Weinstein, J.N. & Pommier, Y. Nonclassic functions of human topoisomerase I: genome-wide and pharmacologic analyses. *Cancer Res* **67**, 8752-61 (2007).

314. Gongora, C., Vezzio-Vie, N., Tuduri, S., Denis, V., Causse, A., Auzanneau, C., Collod-Beroud, G., Coquelle, A., Pasero, P., Pourquier, P., Martineau, P. & Del Rio, M. New Topoisomerase I mutations are associated with resistance to camptothecin. *Mol Cancer* **10**, 64 (2011).

315. Yang, J., Yan, R., Roy, A., Xu, D., Poisson, J. & Zhang, Y. The I-TASSER Suite: protein structure and function prediction. *Nat Methods* **12**, 7-8 (2015).

316. Staker, B.L., Feese, M.D., Cushman, M., Pommier, Y., Zembower, D., Stewart, L. & Burgin, A.B. Structures of three classes of anticancer agents bound to the human topoisomerase I-DNA covalent complex. *J Med Chem* **48**, 2336-45 (2005).

317. Stewart, L., Redinbo, M.R., Qiu, X., Hol, W.G. & Champoux, J.J. A model for the mechanism of human topoisomerase I. *Science* **279**, 1534-41 (1998).

318. Wride, D.A., Pourmand, N., Bray, W.M., Kosarchuk, J.J., Nisam, S.C., Quan, T.K., Berkeley, R.F., Katzman, S., Hartzog, G.A., Dobkin, C.E. & Scott Lokey, R. Confirmation of the cellular targets of benomyl and rapamycin using next-generation sequencing of resistant mutants in S. cerevisiae. *Mol Biosyst* **10**, 3179-87 (2014).

319. Schulz, J.D., Moser, W., Hurlimann, E. & Keiser, J. Preventive Chemotherapy in the Fight against Soil-Transmitted Helminthiasis: Achievements and Limitations. *Trends Parasitol* **34**, 590-602 (2018).

320. Joffe, L.S., Schneider, R., Lopes, W., Azevedo, R., Staats, C.C., Kmetzsch, L., Schrank, A., Del Poeta, M., Vainstein, M.H. & Rodrigues, M.L. The Anti-helminthic Compound Mebendazole Has Multiple Antifungal Effects against Cryptococcus neoformans. *Front Microbiol* **8**, 535 (2017).

321. Thomas, J.H., Neff, N.F. & Botstein, D. Isolation and characterization of mutations in the beta-tubulin gene of Saccharomyces cerevisiae. *Genetics* **111**, 715-34 (1985).

322. Kohler, P. The biochemical basis of anthelmintic action and resistance. *Int J Parasitol* **31**, 336-45 (2001).

323. Croft, S.L., Snowdon, D. & Yardley, V. The activities of four anticancer alkyllysophospholipids against Leishmania donovani, Trypanosoma cruzi and Trypanosoma brucei. *J Antimicrob Chemother* **38**, 1041-7 (1996).

324. Gajate, C., Matos-da-Silva, M., Dakir el, H., Fonteriz, R.I., Alvarez, J. & Mollinedo, F. Antitumor alkyl-lysophospholipid analog edelfosine induces apoptosis in pancreatic cancer by targeting endoplasmic reticulum. *Oncogene* **31**, 2627-39 (2012).

325. Soto, J., Toledo, J., Gutierrez, P., Nicholls, R.S., Padilla, J., Engel, J., Fischer, C., Voss, A. & Berman, J. Treatment of American cutaneous leishmaniasis with miltefosine, an oral agent. *Clin Infect Dis* **33**, E57-61 (2001).

326. Sundar, S., Rosenkaimer, F., Makharia, M.K., Goyal, A.K., Mandal, A.K., Voss, A., Hilgard, P. & Murray, H.W. Trial of oral miltefosine for visceral leishmaniasis. *Lancet* **352**, 1821-3 (1998).

327. Hanson, P.K., Malone, L., Birchmore, J.L. & Nichols, J.W. Lem3p is essential for the uptake and potency of alkylphosphocholine drugs, edelfosine and miltefosine. *J Biol Chem* **278**, 36041-50 (2003).

328. Pomorski, T., Lombardi, R., Riezman, H., Devaux, P.F., van Meer, G. & Holthuis, J.C. Drs2p-related P-type ATPases Dnf1p and Dnf2p are required for phospholipid translocation across the yeast plasma membrane and serve a role in endocytosis. *Mol Biol Cell* **14**, 1240-54 (2003).

329. Srivastava, S., Mishra, J., Gupta, A.K., Singh, A., Shankar, P. & Singh, S. Laboratory confirmed miltefosine resistant cases of visceral leishmaniasis from India. *Parasit Vectors* **10**, 49 (2017).

330. Dias, D.A., Urban, S. & Roessner, U. A historical overview of natural products in drug discovery. *Metabolites* **2**, 303-36 (2012).

331. Vorobiev, S., Strokopytov, B., Drubin, D.G., Frieden, C., Ono, S., Condeelis, J., Rubenstein, P.A. & Almo, S.C. The structure of nonvertebrate actin: implications for the ATP hydrolytic mechanism. *Proc Natl Acad Sci U S A* **100**, 5760-5 (2003).

332. Marquez, B.L., Watts, K.S., Yokochi, A., Roberts, M.A., Verdier-Pinard, P., Jimenez, J.I., Hamel, E., Scheuer, P.J. & Gerwick, W.H. Structure and absolute stereochemistry of hectochlorin, a potent stimulator of actin assembly. *J Nat Prod* **65**, 866-71 (2002).

333. Sinnis, P., De La Vega, P., Coppi, A., Krzych, U. & Mota, M.M. Quantification of sporozoite invasion, migration, and development by microscopy and flow cytometry. *Methods Mol Biol* **923**, 385-400 (2013).

334. Le Crom, S., Devaux, F., Marc, P., Zhang, X., Moye-Rowley, W.S. & Jacq, C. New insights into the pleiotropic drug resistance network from genome-wide characterization of the YRR1 transcription factor regulation system. *Mol Cell Biol* **22**, 2642-9 (2002).

335. Kodo, N., Matsuda, T., Doi, S. & Munakata, H. Salicylic acid resistance is conferred by a novel YRR1 mutation in Saccharomyces cerevisiae. *Biochem Biophys Res Commun* **434**, 42-7 (2013).

336. Jungwirth, H. & Kuchler, K. Yeast ABC transporters-- a tale of sex, stress, drugs and aging. *FEBS Lett* **580**, 1131-8 (2006).

337. Cui, Z., Hirata, D. & Miyakawa, T. Functional analysis of the promoter of the yeast SNQ2 gene encoding a multidrug resistance transporter that confers the resistance to 4-nitroquinoline N-oxide. *Biosci Biotechnol Biochem* **63**, 162-7 (1999).

338. Teixeira, M.C., Dias, P.J., Simoes, T. & Sa-Correia, I. Yeast adaptation to mancozeb involves the up-regulation of FLR1 under the coordinate control of Yap1, Rpn4, Pdr3, and Yrr1. *Biochem Biophys Res Commun* **367**, 249-55 (2008).

339. Zhang, X., Cui, Z., Miyakawa, T. & Moye-Rowley, W.S. Cross-talk between transcriptional regulators of multidrug resistance in Saccharomyces cerevisiae. *J Biol Chem* **276**, 8812-9 (2001).

340. Lucau-Danila, A., Delaveau, T., Lelandais, G., Devaux, F. & Jacq, C. Competitive promoter occupancy by two yeast paralogous transcription factors controlling the multidrug resistance phenomenon. *J Biol Chem* **278**, 52641-50 (2003).

341. MacPherson, S., Larochelle, M. & Turcotte, B. A fungal family of transcriptional regulators: the zinc cluster proteins. *Microbiol Mol Biol Rev* **70**, 583-604 (2006).

342. Lee, A.Y., St Onge, R.P., Proctor, M.J., Wallace, I.M., Nile, A.H., Spagnuolo, P.A., Jitkova, Y., Gronda, M., Wu, Y., Kim, M.K., Cheung-Ong, K., Torres, N.P., Spear, E.D., Han, M.K., Schlecht, U., Suresh, S., Duby, G., Heisler, L.E., Surendra, A., Fung, E., Urbanus, M.L., Gebbia, M., Lissina, E., Miranda, M., Chiang, J.H., Aparicio, A.M., Zeghouf, M., Davis, R.W., Cherfils, J., Boutry, M., Kaiser, C.A., Cummins, C.L., Trimble, W.S., Brown, G.W., Schimmer, A.D., Bankaitis, V.A., Nislow, C., Bader, G.D. & Giaever, G. Mapping the cellular response to small molecules using chemogenomic fitness signatures. *Science* **344**, 208-11 (2014).

343. Giaever, G., Shoemaker, D.D., Jones, T.W., Liang, H., Winzeler, E.A., Astromoff, A. & Davis, R.W. Genomic profiling of drug sensitivities via induced haploinsufficiency. *Nat Genet* **21**, 278-83 (1999).

344. Giaever, G., Flaherty, P., Kumm, J., Proctor, M., Nislow, C., Jaramillo, D.F., Chu, A.M., Jordan, M.I., Arkin, A.P. & Davis, R.W. Chemogenomic profiling: identifying the functional interactions of small molecules in yeast. *Proc Natl Acad Sci U S A* **101**, 793-8 (2004).

345. Ho, C.H., Magtanong, L., Barker, S.L., Gresham, D., Nishimura, S., Natarajan, P., Koh, J.L.Y., Porter, J., Gray, C.A., Andersen, R.J., Giaever, G., Nislow, C., Andrews, B., Botstein, D., Graham, T.R., Yoshida, M. & Boone, C. A molecular barcoded yeast ORF library enables mode-of-action analysis of bioactive compounds. *Nat Biotechnol* **27**, 369-77 (2009).

346. Acton, E., Lee, A.H., Zhao, P.J., Flibotte, S., Neira, M., Sinha, S., Chiang, J., Flaherty, P., Nislow, C. & Giaever, G. Comparative functional genomic screens of

three yeast deletion collections reveal unexpected effects of genotype in response to diverse stress. *Open Biol* **7**(2017).

347. Wong, L.H., Flibotte, S., Sinha, S., Chiang, J., Giaever, G. & Nislow, C. Genome-Wide Screen Reveals sec21 Mutants of Saccharomyces cerevisiae Are Methotrexate-Resistant. *G3 (Bethesda)* **7**, 1251-1257 (2017).

348. Mor, V., Rella, A., Farnoud, A.M., Singh, A., Munshi, M., Bryan, A., Naseem, S., Konopka, J.B., Ojima, I., Bullesbach, E., Ashbaugh, A., Linke, M.J., Cushion, M., Collins, M., Ananthula, H.K., Sallans, L., Desai, P.B., Wiederhold, N.P., Fothergill, A.W., Kirkpatrick, W.R., Patterson, T., Wong, L.H., Sinha, S., Giaever, G., Nislow, C., Flaherty, P., Pan, X., Cesar, G.V., de Melo Tavares, P., Frases, S., Miranda, K., Rodrigues, M.L., Luberto, C., Nimrichter, L. & Del Poeta, M. Identification of a New Class of Antifungals Targeting the Synthesis of Fungal Sphingolipids. *mBio* **6**, e00647 (2015).

349. Robbins, N., Caplan, T. & Cowen, L.E. Molecular Evolution of Antifungal Drug Resistance. *Annu Rev Microbiol* **71**, 753-775 (2017).

350. Anderson, J.B., Sirjusingh, C., Parsons, A.B., Boone, C., Wickens, C., Cowen, L.E. & Kohn, L.M. Mode of selection and experimental evolution of antifungal drug resistance in Saccharomyces cerevisiae. *Genetics* **163**, 1287-98 (2003).

351. Gallagher, J.E., Zheng, W., Rong, X., Miranda, N., Lin, Z., Dunn, B., Zhao, H. & Snyder, M.P. Divergence in a master variator generates distinct phenotypes and transcriptional responses. *Genes Dev* **28**, 409-21 (2014).

352. Cui, Z., Shiraki, T., Hirata, D. & Miyakawa, T. Yeast gene YRR1, which is required for resistance to 4-nitroquinoline N-oxide, mediates transcriptional activation of the multidrug resistance transporter gene SNQ2. *Mol Microbiol* **29**, 1307-15 (1998).

353. Chen, C. & Noble, S.M. Post-transcriptional regulation of the Sef1 transcription factor controls the virulence of Candida albicans in its mammalian host. *PLoS Pathog* **8**, e1002956 (2012).

354. Wisplinghoff, H., Ebbers, J., Geurtz, L., Stefanik, D., Major, Y., Edmond, M.B., Wenzel, R.P. & Seifert, H. Nosocomial bloodstream infections due to Candida spp. in the USA: species distribution, clinical features and antifungal susceptibilities. *Int J Antimicrob Agents* **43**, 78-81 (2014).

355. Tognini, P., Thaiss, C.A., Elinav, E. & Sassone-Corsi, P. Circadian Coordination of Antimicrobial Responses. *Cell Host Microbe* **22**, 185-192 (2017).

356. Pais, P., Costa, C., Cavalheiro, M., Romao, D. & Teixeira, M.C. Transcriptional Control of Drug Resistance, Virulence and Immune System Evasion in Pathogenic Fungi: A Cross-Species Comparison. *Front Cell Infect Microbiol* **6**, 131 (2016).

357. Duffey, M., Blasco, B., Burrows, J.N., Wells, T.N.C., Fidock, D.A. & Leroy, D. Assessing risks of Plasmodium falciparum resistance to select next-generation antimalarials. *Trends Parasitol* **37**, 709-721 (2021).

358. Fisch, K.M., Meissner, T., Gioia, L., Ducom, J.C., Carland, T.M., Loguercio, S. & Su, A.I. Omics Pipe: a community-based framework for reproducible multi-omics data analysis. *Bioinformatics* **31**, 1724-8 (2015).

359. Robinson, J.T., Thorvaldsdottir, H., Winckler, W., Guttman, M., Lander, E.S., Getz, G. & Mesirov, J.P. Integrative genomics viewer. *Nat Biotechnol* **29**, 24-6 (2011).

360. Berman, H.M., Battistuz, T., Bhat, T.N., Bluhm, W.F., Bourne, P.E., Burkhardt, K., Feng, Z., Gilliland, G.L., Iype, L., Jain, S., Fagan, P., Marvin, J., Padilla, D., Ravichandran, V., Schneider, B., Thanki, N., Weissig, H., Westbrook, J.D. & Zardecki, C. The Protein Data Bank. *Acta Crystallogr D Biol Crystallogr* **58**, 899-907 (2002).

361. Madden, T.L., Tatusov, R.L. & Zhang, J. Applications of network BLAST server. *Methods Enzymol* **266**, 131-41 (1996).

362. Ropp, P.J., Spiegel, J.O., Walker, J.L., Green, H., Morales, G.A., Milliken, K.A., Ringe, J.J. & Durrant, J.D. Gypsum-DL: an open-source program for preparing small-molecule libraries for structure-based virtual screening. *J Cheminform* **11**, 34 (2019).

363. Durrant, J.D. BlendMol: advanced macromolecular visualization in Blender. *Bioinformatics* **35**, 2323-2325 (2019).